SKB

TECHNICAL REPORT

92-14

Numerical calculations on heterogeneity of groundwater flow

Sven Follin

Department of Land and Water Resources,
Royal Institute of Technology

June 1992

NUMERICAL CALCULATIONS ON HETEROGENEITY OF
GROUNDWATER FLOW

Sven Follin

Department of Land and Water Resources,
Royal Institute of Technology

June 1992

NUMERICAL CALCULATIONS

ON HETEROGENEITY

OF GROUNDWATER FLOW

Sven Follin

Department of Land and Water Resources
Royal Institute of Technology

June 1992

PREFACE

This present study is a copy of a Ph.D. thesis, which was defended in February this year at the Department of Land and Water Resources, Royal Institute of Technology, Stockholm. The thesis can be obtained from the department, where it has the code number TRITA-KUT 92:1066. The present Technical Report is published by SKB. I am most grateful to Dr. C Peter Jackson, Harwell Lab., U.K., for his proofreading and valuable comments. I would also like express my gratitude to SKB and especially Anders Ström for giving me the opportunity to publish and distribute the thesis once more.

Stockholm, June 1992

Sven Follin

*Heterogeneity is in the geology, whereas
uncertainty is in the mind of the analyst.*

Freeze et al., 1990

ABSTRACT

The upscaling of model parameters, i.e. scale-dependent parameters, is a key issue in many research fields concerned with parameter heterogeneity. The upscaling process allows for fewer model blocks and relaxes the numerical problems caused by high contrasts in the hydraulic conductivity. The trade-offs are dependent on the object but the general drawback is an increasing uncertainty about the representativeness, i.e. the relation to the real world problem. The present study deals with numerical calculations of heterogeneity of groundwater flow and solute transport in hypothetical blocks of fractured hard rock on a "3m scale" and addresses both conceptual and practical problems in numerical simulation. Evidence that the hydraulic conductivity (K) of the rock mass between major fracture zones is highly heterogeneous on a 3m scale is provided by a large number of field investigations. The present study uses the documented heterogeneity and investigates flow and transport in a two-dimensional stochastic continuum characterized by a variance in $Y = ln(K)$ of $\sigma_Y^2 = 16$, corresponding to about 12 log_{10} cycles in K. The study considers anisotropy, channelling, non-Fickian and Fickian transport, and conditional simulation. The major conclusions are: (*i*) heterogeneity gives rise to anisotropy in the upscaling process, (*ii*) the choice of support scale is crucial for the modelling of solute transport. As a consequence of the obtained results, a two-dimensional stochastic discontinuum model is presented, which provides a tool for linking stochastic continuum models to discrete fracture network models.

CONTENTS

TABLE OF FIGURES

NOMENCLATURE AND ABBREVIATIONS

A_{11}	Longitudinal macrodispersivity, (L)
A_{22}	Transverse macrodispersivity, (L)
a_{11}	Longitudinal dispersivity, (L)
a_{22}	Transverse dispersivity, (L)
C	Solute concentration, (ML^{-3})
∇C	Concentration gradient, (ML^{-4})
$C(h)$	Covariance function, $((ln(LT^{-1}))^2)$
$\tilde{D}$	Dispersion tensor, (L^2T^{-1})
D^m	Molecular diffusion coefficient, (L^2T^{-1})
E	Euler's number, $(-)$
$E\{\}$; $<>$	Expectation operator
E_φ	Dimensionless error in φ, $(-)$
E_K	Dimensionless error in K, $(-)$
Ei	Exponential integral
g	Acceleration of gravity, (LT^{-2})
$\mathbf{h}$	Lag vector, (L)
h	Magnitude of $\mathbf{h}$, (L)
I_Y	Integral scale of $Y = ln(K)$, (L)
$\mathbf{J}$	Constant hydraulic gradient, $(-)$
$\tilde{\mathbf{K}}_{ef}$	Effective (hydraulic) conductivity tensor, (LT^{-1})
$\tilde{\mathbf{K}}_S$	Block conductivity tensor, (LT^{-1})
K	Support scale conductivity, (LT^{-1})
K_{ef}	Effective hydraulic conductivity, (LT^{-1})
K_G	Statistical (spatial) geometric mean of the local conductivities of the infinite medium, (LT^{-1})
K_g	Statistical (spatial) geometric mean of the local conductivities within a block, (LT^{-1})
K_{max}	Maximum of K_{11} and K_{22}, (LT^{-1})
K_{min}	Minimum of K_{11} and K_{22}, (LT^{-1})
K_S	Block conductivity of a continuum, (LT^{-1})
K_{th}	Block conductivity of a discontinuum, (LT^{-1})

K_{11}; K_{xx}	First diagonal component of $\tilde{K}_S$, (LT^{-1})
K_{22}; K_{yy}	Second diagonal component of $\tilde{K}_S$, (LT^{-1})
K^*	Estimated conductivity, (LT^{-1})
k	Support scale permeability, (L^2)
L	Size of flow domain, (L)
L_e	Effective average path length, (L)
ln	Natural logarithm (log_e)
log_{10}	Logarithm of base 10
MSE_φ	Mean square error in φ, (L^2)
MVN	Multivariate normal distribution
m_t	Sample mean of arrival times, (T)
m_Y	Sample mean of Y, $(ln(LT^{-1}))$
N	Statistical (or spatial) sample size, (-)
N	Normal probability density function
N_p	Number of particles, (-)
n	Effective (kinematic) porosity, (-)
OEI	Overall error index, (-)
PDF	Probability density function
p	Pressure, $(ML^{-1}T^{-2})$
ΔQ	Discharge, (L^2T^{-1})
$\mathbf{q}$	Specific discharge, (LT^{-1})
q	Magnitude of $\mathbf{q}$, (LT^{-1})
q_{WE}; q_{NS}	Directional components of $\mathbf{q}$, (LT^{-1})
R	Range of correlation, (L)
RE_h	Hydraulic relative error in K_G, (-)
RE_s	Statistical relative error in K_G, (-)
REV	Representative elementary volume
r; SR	Search radius (range), (L)
S	A finite flow domain, (L^2)
s	Distance along a streamline, (L)
s_t	Sample standard deviation of arrival times, (T)
s_Y	Sample standard deviation of Y, $(ln(LT^{-1}))$
T	Macrotortuosity, (-)
t	Time, (T)

t_{ref}	Mean transit time of fluid, (T)
$V\{\}$	Variance operator
$\mathbf{v}$	Fluid velocity (LT^{-1})
v	Magnitude of $\mathbf{v}$, (LT^{-1})
w	Width of stream tube, (L)
$\tilde{\mathbf{X}}$	Displacement covariance tensor, (L^2)
X_{11}	Longitudinal spatial variance, (L^2)
X_{22}	Transverse spatial variance, (L^2)
$\mathbf{X}_t$	Particle displacement vector, (L)
$\mathbf{x}$	Cartesian point vector, (L)
x	Horizontal Cartesian coordinate, (L)
Δx	Horizontal length of the support scale block, (L)
Y	$Y = ln(K)$, $(ln(LT^{-1}))$
y	Vertical Cartesian coordinate, (L)
y	Elevation head, (L)
Δy	Vertical length of the support scale block, (L)
$(1 - \beta)$	Confidence interval, $(-)$
$\gamma(h)$	Variogram function, $((ln(LT^{-1}))^2)$
φ	Piezometric head, (L)
$\nabla\varphi$	Hydraulic gradient, $(-)$
Ψ	Lagrange stream function, (L^2T^{-1})
$\nabla\Psi$	Stream function gradient, (LT^{-1})
Ψ_{22}	Transverse spatial variance, (L^2)
λ_Y; λ	Correlation length of $Y = ln(K)$, (L)
$\lambda_{\beta/2}$	Standardized variable with $N(0, 1)$
μ	Fluid dynamic viscosity, $(ML^{-1}T^{-1})$
μ_Y	Mean of Y, $(ln(LT^{-1}))$
ρ	Fluid density, (ML^{-3})
σ_Y; $\sigma_{ln(K)}$	Standard deviation of Y, $(ln(LT^{-1}))$
τ	Dimensionless time, $(-)$
4-00	$N = 64\times64$, $\sigma_Y = 4$, and $\lambda_Y/\Delta x = \lambda_Y/\Delta y = 0$
4-22	$N = 64\times64$, $\sigma_Y = 4$, and $\lambda_Y/\Delta x = \lambda_Y/\Delta y = 2$
4-44	$N = 64\times64$, $\sigma_Y = 4$, and $\lambda_Y/\Delta x = \lambda_Y/\Delta y = 4$
4-41	$N = 64\times64$, $\sigma_Y = 4$, and $\lambda_Y/\Delta x = 4$, $\lambda_Y/\Delta y = 1$

ACKNOWLEDGEMENTS

1   INTRODUCTION

For Sweden, as for any country with a nuclear power programme, safe final disposal of radioactive waste is an important issue. The Swedish programme for waste disposal, as outlined in KBS-3 [1983], is based on siting a repository in fractured crystalline (hard) rock, see Figure 1. The present study deals with groundwater flow and solute transport in fractured hard rock and addresses both conceptual and practical problems in numerical simulation.

1.1   Objectives

The main objectives of the study are:

(i)   *to improve the understanding of how a locally heterogeneous hydraulic conductivity affects the far field flow and transport*

(ii)   *to investigate how the characterization of the hydraulic conductivity in the field can be improved at scales appropriate to the far field flow and transport models currently in use*

These objectives are dealt with by simplifying the real world problem of three-dimensional flow and transport in a fractured hard rock to a *two-dimensional* numerical flow model of a continuum.

More specifically, uniform average flow and advective transport in a two-dimensional representation of a hypothetical realization of a rock block of random (disordered) heterogeneity are here simulated and analysed by means of stochastic continuum concepts and the dual formulation of groundwater flow. Figures 2 and 3 show schematic drawings illustrating some questions raised in conjunction with a figurative repository scenario.
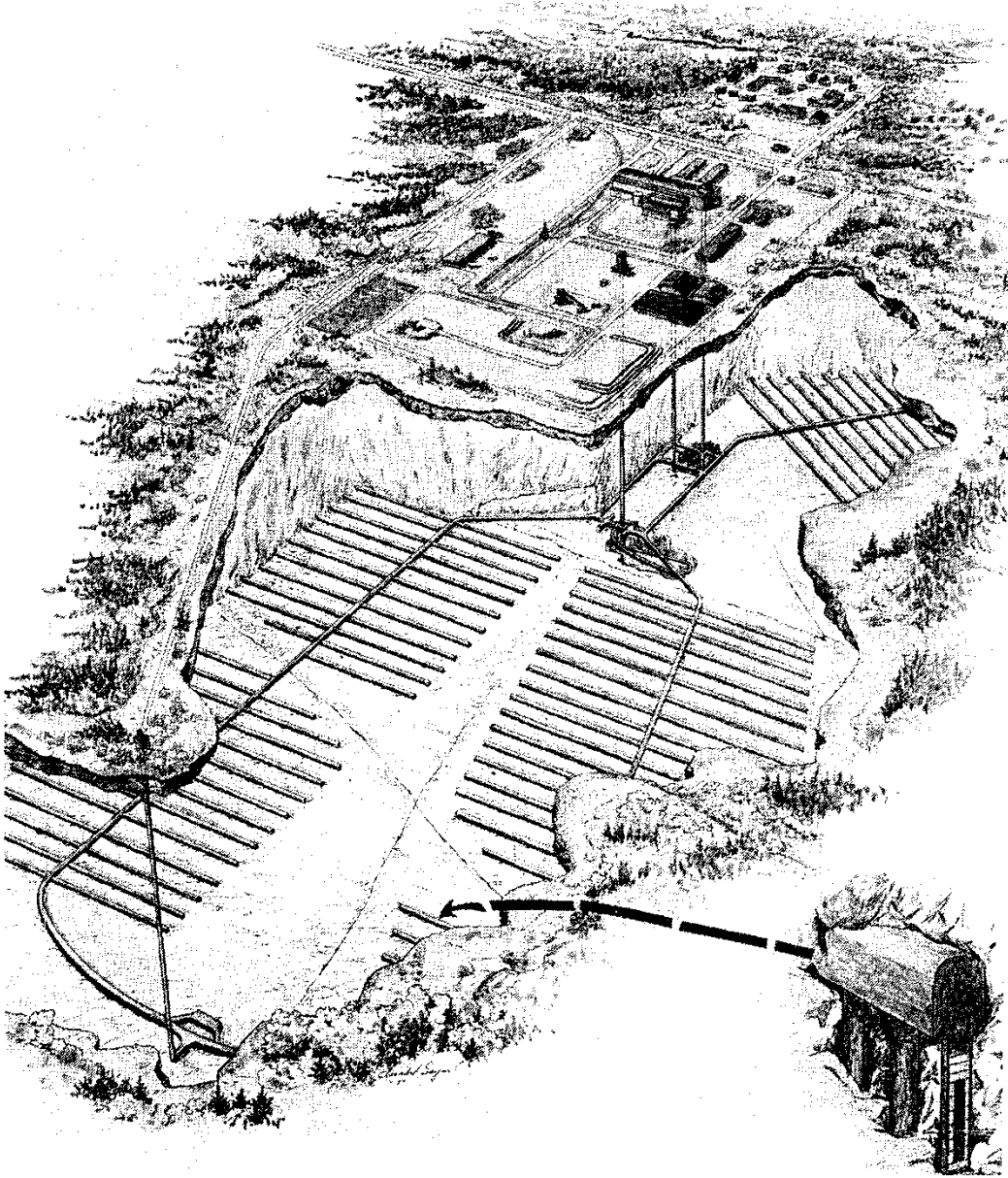
Fig. 1 Tentative outline of a repository for spent fuel according
to the KBS-3 concept [Reproduced from KBS-3, 1983].
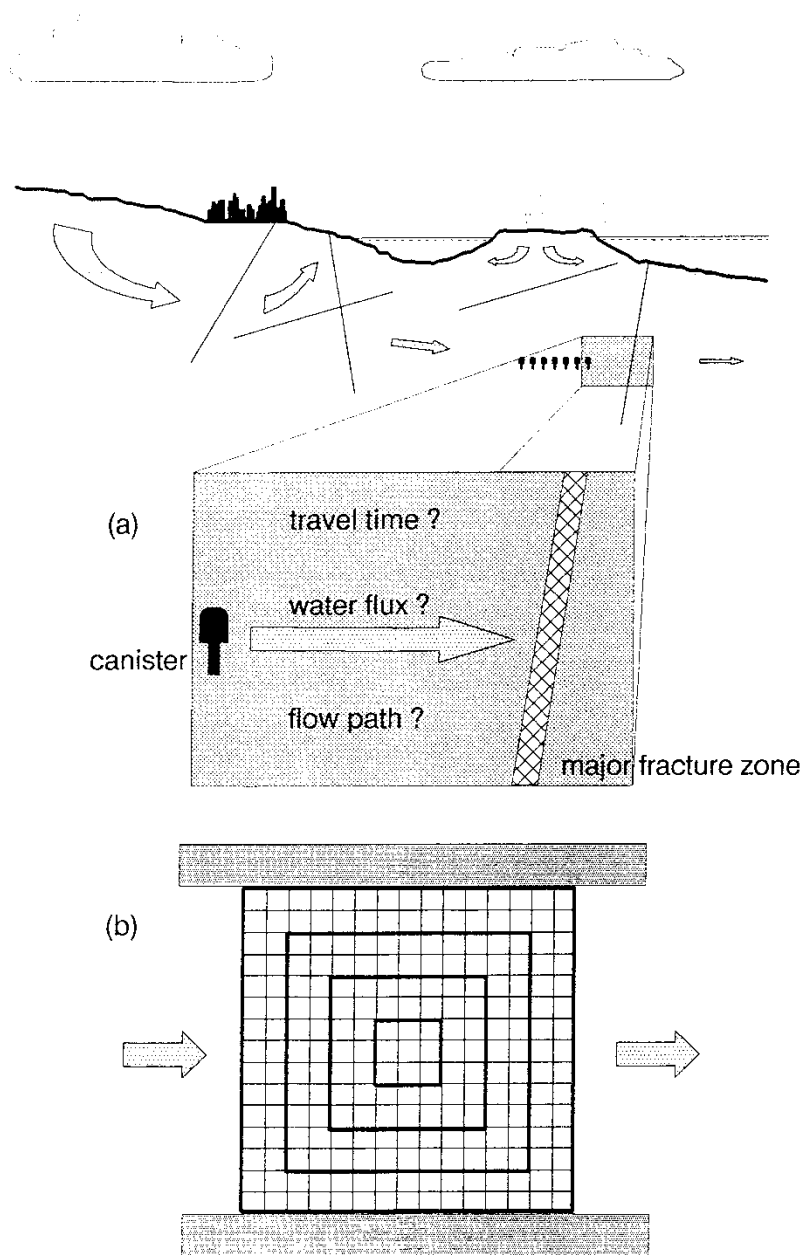
Fig. 2   Schematic view of the studied questions:

(a) Can fractured hard rock be treated as consisting of major fracture zones with intervening rock mass of random heterogeneity? (b) Can a continuum model be used for describing flow and mass transport in the rock mass, and, if so, what are the parameter values on various scales?

Fig. 3 Schematic view of the studied questions (cont.):

(c) What is the appropriate packer test interval in order to sufficiently characterize the heterogeneity in the field? (d) How are field data properly transferred to various support scales of flow models? (e) What discretization is required?

The questions raised in Figures 2 and 3 are as follows:

(a) Can fractured hard rock be treated as consisting of major fracture zones with intervening rock mass of random heterogeneity?

(b) Can a continuum model be used for describing flow and mass transport in the rock mass, and, if so, what are the parameter values on various scales?

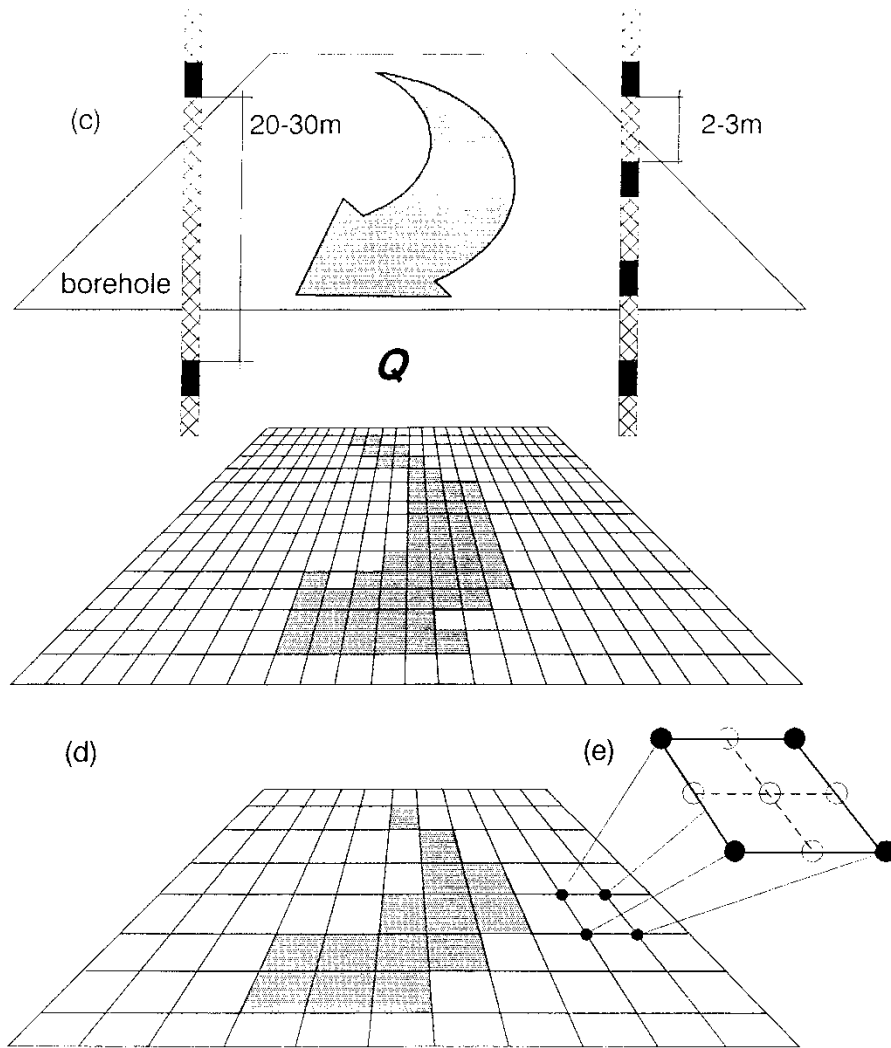(c) What is the appropriate packer test interval in order to sufficiently characterize the heterogeneity in the field?

(d) How are field data properly transferred to various support scales of flow models?

Because a numerical flow model is used, additional questions arise related to the flow model. Regardless of the choice of numerical model, a quite general question of interest is:

(e) What discretization is required?

1.2 Literature review

Unlike groundwater flow in a porous medium, groundwater flow in fractured hard rock occurs predominantly in fractures. These constitute constrained flow paths of relatively high permeability and appear with different magnitudes in their geometric characteristics (strike, dip, length, aperture, spacing, etc.) on different hierarchical scales [see, for example, Price, 1975]. The classification in hierarchical scales, however, is an approximation to the almost continuous distribution of fracture scales from large-scale faulting (major fracture zones) to small-scale fractures and joints [Nelson, 1987]. In the following, different conceptual models used to construct tentative numerical groundwater flow and solute transport models in fractured hard rock are briefly reviewed.
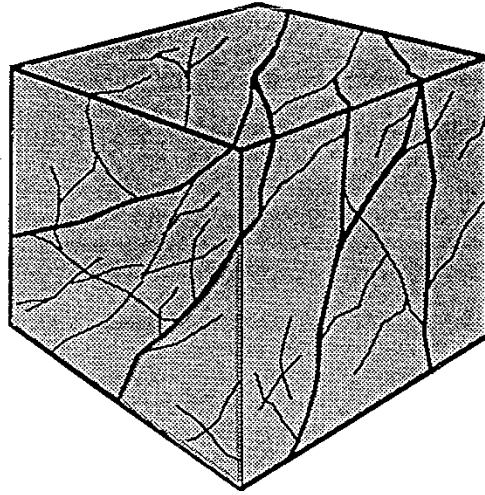
ROCK MASS
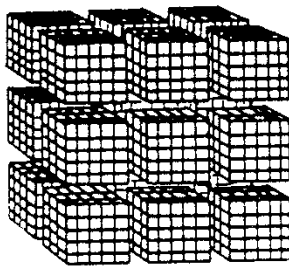
(a)
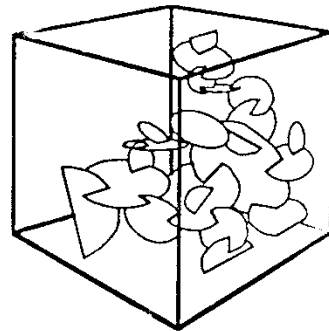
(b)
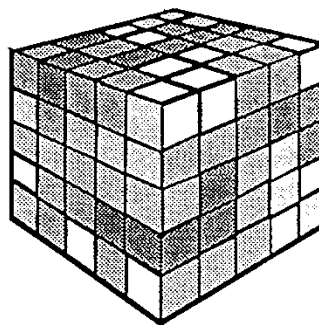
(c)

Fig. 4 Figurative drawings illustrating (a) the double porosity
approach; (b) the discrete fracture network approach; (c)
the stochastic continuum approach [After Warren & Root, 1963
and Geier & Axelsson, 1991].

From a conceptual point of view, there are no problems in studying flow and transport in fractured hard rock by adopting continuum approximations [see, e.g. Stokes, 1980; Andersson et al., 1983; Shapiro, 1987]. Two extremes may be identified. In the first case, no fractures are present. In the second case, a large number of well-connected fractures are present. Obviously, in each case a single porosity medium of constant conductivity may be assumed. An intermediate case, i.e. a case where the conductivity of a rock block is sensitive to the connectivity and other geometric charac-teristics of the fractures, e.g. the fracture density, requires a somewhat more elaborated concept. A discussion of connectivity can be found in, for example, the studies by Robinson [1984] and de Marsily [1985]. Three main approaches are described in the literature: the double porosity approach, the discrete fracture (and/or channel) network approach, and the stochastic continuum approach. The three approaches are schematically shown in Figure 4.

The *double porosity approach* [see, e.g. Barenblatt et al., 1960; Warren & Root, 1963; Boulton & Streltsova, 1977; Duguid & Lee, 1977] is the classical approach. Here, the fractures and the porous rock matrix are considered to be two overlapping continua, each with its own flow equation. The exchange between the two continua is given by a source-sink term in the two equations, whose magnitude is proportional to the local pressure difference between the two continua. Sauveplane [1984] analyses different kinds of analytical pumping test models for "fractured aquifer formations". He concludes that models based on the dual porosity approach are in general in-applicable to practical problems but of interest as research tools.

In the *discrete fracture network approach*, the efforts are focused on mapping, with as much detail as possible, the geometry of individual fractures so as to generate information about the three-dimensional network they form in a rock block. Accordingly, in order to delineate the possible flow paths useful for the evaluation of groundwater flow and solute transport, a number of assumptions are required concerning (*i*) the physics of groundwater flow and solute

transport in a single fracture, and (*ii*) the translation of deter-
ministic and/or statistical fracture geometry data so as to match
the observed hydraulic test data. Concerning the physics of ground-
water flow and solute transport in a single fracture, this subject
is often treated as a separate field of research in the literature.
The interest in details stems from the complexity of a possible re-
tardation due to chemical and physical interactions between dis-
solved constituents and the rock matrix [see, for example, Abelin,
1986]. Although this field of research is not treated here, it is
noteworthy that recent studies such as those by Moreno *et al.* [1988]
and Tsang & Tsang [1989], for example, are related to the present
study in the sense of using stochastic continuum concepts to simu-
late variable aperture and preferential flow paths (channelling).
The numerical model used by Moreno *et al.* [1988] and Tsang & Tsang
[1989], however, is considered to be a poor model of a continuum
[cf. Goode & Shapiro, 1991a]. Neither the double porosity approach
nor the discrete fracture network approach are dealt with in the
present study. However, some representative examples of the discrete
fracture network approach, which are of interest here while dis-
cussing equivalent block conductivities, include studies by Sagar &
Runchal [1982], Long *et al.* [1982], Robinson [1984], Cacas *et al.*
[1990], and Herbert & Splawski [1990].

The aforementioned *stochastic continuum approach* is adopted in
the present study, because it offers quantitative answers to several
important questions concerning the uncertainty in the input data and
the model predictions. The idea of using the stochastic continuum
theory to study groundwater flow and solute transport in fractured
media was originally proposed by Neuman [1987, 1988]. In the sto-
chastic continuum approach, which is also called the *geostatistical
approach* [see, for example, Journel & Huijbregts, 1978; de Marsily,
1986], the quantity of interest, e.g. the hydraulic conductivity, is
considered to be a *regionalized variable*, i.e. spatially disordered
variability (random heterogeneity), as it appears at different loca-
tions in space, is dealt with by using a probabilistic framework

consisting of an ensemble of realizations of equal probability, where Nature constitutes one possible realization. Substantial research activity is taking place not only to understand the effect of random heterogeneity on flow and transport in geological media but also to characterize media properties on scales appropriate to the development of subsurface flow and transport models. Much of this work depends on the development of models that statistically describe the spatial distribution of media properties and permit their numerical simulation. Neuman [1982], Dagan [1986], Gelhar [1986], Peck et al. [1988], and Freeze et al. [1990] are examples of studies that review the state of the art of these matters. Some representative examples concerning the theoretical developments of the stochastic continuum theory, which are important for the present study in terms of verification, include studies by Matheron [1967], Dagan [1979, 1982, 1984, 1987, 1988], Gelhar & Axness [1983], and Neuman et al. [1987].

The emphasis in applied hydrogeology has shifted from analytical analysis towards numerical techniques which are more flexible in their ability to deal with variable material properties and other complexities of Nature. The research in physically based distributed modelling is becoming increasingly concerned with the incorporation of stochastic elements into numerical models, particularly dealing with spatial variability and sub-grid scale effects. Some representative examples of numerical simulation of flow and transport, which are related to the outline of the present study, include studies by Warren & Price [1961], Warren & Skiba [1964], Delhomme [1978, 1979], Schwartz [1977], Smith & Freeze [1979], Smith & Schwartz [1980], Frind et al. [1987], Gómez-Hernández & Gorelick [1988], Graham & McLaughlin [1989], Rubin [1990], Rubin & Gómez-Hernández [1990], Goode [1990], Winberg et al. [1990], Desbarats [1990, 1991a, b], Desbarats & Srivastava [1991], Cacas et al. [1991], and Durlofsky [1991]. Although a number of operational models have been developed [see, for example, Javandel et al., 1984; Heijde et al., 1985; and Mangold & Tsang, 1991], fundamental difficulties still exist both on

the conceptual level and in the numerical simulation. For instance, material properties represented by parameters can probably only be regarded as representatives of the "true" material characteristics in terms of being some scale-dependent average quantities of the latter. Sagar [1978] makes the following statement:

"In numerical solutions, heterogeneities are considered, although they have to be well defined by forming blocks of known properties. Every time that the size and/or the shape of these blocks is changed in a numerical scheme these properties are to be specified afresh."

In the present study, the main sources of information on the hetero-geneity of hydraulic field data of fractured hard rock are:
- the OECD/NEA Stripa Project Technical Report Series
- the SKB Technical Report and "Arbetsrapport" Series (in particular, the studies about the Finnsjön area, SKB-91)
- the SKB Progress Report Series concerning the Äspö Hard Rock Laboratory

Together, these report series contain unique information about the heterogeneity of the conductivity of fractured hard rock on various scales. A subjective impression, based on a selective reading, is that the development of new field tests and new interpretation techniques are key issues for future modelling and site characterization. For example, the most common formula used for the computation of the conductivity from single-hole 3m double-packer tests is that of Moye [1967]. The validity of Moye's formula, however, is questioned by, for example, Doe & Remer [1982] and Braester & Thunvik [1982, 1984]. The latter authors use a numerical model so as to compare Moye's formula with an analytical solution derived by Dagan [1978]. In spite of the quantified deviations, Moye's formula is still in use, probably because of its simplicity [see, for example, Holmes, 1989; Nilsson, 1989, 1990; Andersson *et al.*, 1988,

1991]. A general presentation of the pumping test procedures and the interpretation techniques used in Sweden is found in the work by Almén *et al.* [1986]. Pickens *et al.* [1987] discuss problems associated with measurements of pressure and temperature effects in deep boreholes in low-conductivity media.

Hsieh *et al.* [1985] investigate both the *statistical* and the *hydraulic* anisotropy. Neuman [1988] concludes that the investigated rock volume in this case (a fractured granite at Oracle, Arizona) is clearly anisotropic both statistically and hydraulically although it is considered to be "homogeneously fractured". The analysis of Hsieh *et al.* [1985], however, requires cross-hole tests, which limits a further use of their methodology at other sites where only single-hole tests are possible. However, cross-hole tests are probably the most correct and efficient way to study the question of anisotropy, a conclusion pointed out already by Stokes [1980]. Doe & Geier [1990] present recent interpretation techniques for constant-pressure pumping tests in single holes based on the concept of fractional dimensions introduced by Barker [1988]. The techniques provide information about the shape, i.e. the "dimensionality", of the pressure drop away from the tested section, which is considered to be of great interest.

1.3   A few field findings

The present study focuses on the heterogeneity of the conductivity of fractured hard rock as documented in the previously mentioned report series. Concerning the theoretical assumptions behind the interpretation of packer tests as well as the subsequent use of the computed conductivities in different kinds of models, there are several key issues of interest for the present study, e.g. (*i*) the assumption of a homogeneous and isotropic continuum, (*ii*) the assumption of a spherical-radial flow regime [Moye, 1967], or even a horizontal axis-symmetric flow regime [Jacob & Lohman, 1952], and

(*iii*) the assumption of a constant volume support regardless of the conductivity being measured. None of these assumptions is free from objections [see, for example, Clark, 1979; Braester & Thunvik, 1982, 1984; Doe & Remer, 1982; Hsieh & Neuman, 1985; Hsieh *et al.*, 1985].

The present study is focused on 3m packer tests, i.e. a "3m scale" is here of main interest. A subjective selection of the information about the heterogeneity of 3m packer tests from the Äspö Hard Rock Laboratory is shown in Figures 5, 6, and 7. Beginning with Figure 5a, this figure indicates that the conductivity of fractured hard rock is log-normally distributed. The log-normal distribution of conductivity is well documented [cf. Freeze, 1975]. Figure 6 reveals the following characteristics of 3m packer tests: (*i*) the arithmetic average of the geometric means for seven boreholes is $2 \cdot 10^{-10}$ m/s, (*ii*) the average standard deviation is 2.2 in a log_{10} base, and (*iii*) the average *correlation range* of the fitted auto-covariance functions is about 12m. If this information is transferred to conventional units and measures, the average standard deviation of $ln(K)$ is 5.1, and the average *correlation length* (assuming an exponential covariance function) is less than or equal to 3m. For the Finnsjön study site, Carlsson *et al.* [1980] report an average geometric mean of about $(0.1-1) \cdot 10^{-7}$ m/s for 3m packer tests in seven boreholes. For the same data, Cvetkovic & Kung [1989] report that the average value of the standard deviation of $ln(K)$ is about 2.4, whereas the average correlation length is about 22m.

The boreholes at Finnsjön are either inclined or sub-vertical, whereas the boreholes at Äspö are essentially sub-vertical or vertical. Furthermore, both Carlsson *et al.* [1980] and Nilsson [1989, 1990] report that the lower measurement threshold of the packer test equipment generally exceeds the conductivity of the surrounding rock for about 20-75% of the 3m test sections (cf. Figure 5a). Moreover, at Finnsjön, the 3m packer tests show a decreasing trend with the depth of exploration, whereas a depth dependence at Äspö is not readily observed, cf. Figure 5b. In Figure 7, the scale dependence of the standard deviation is readily seen.
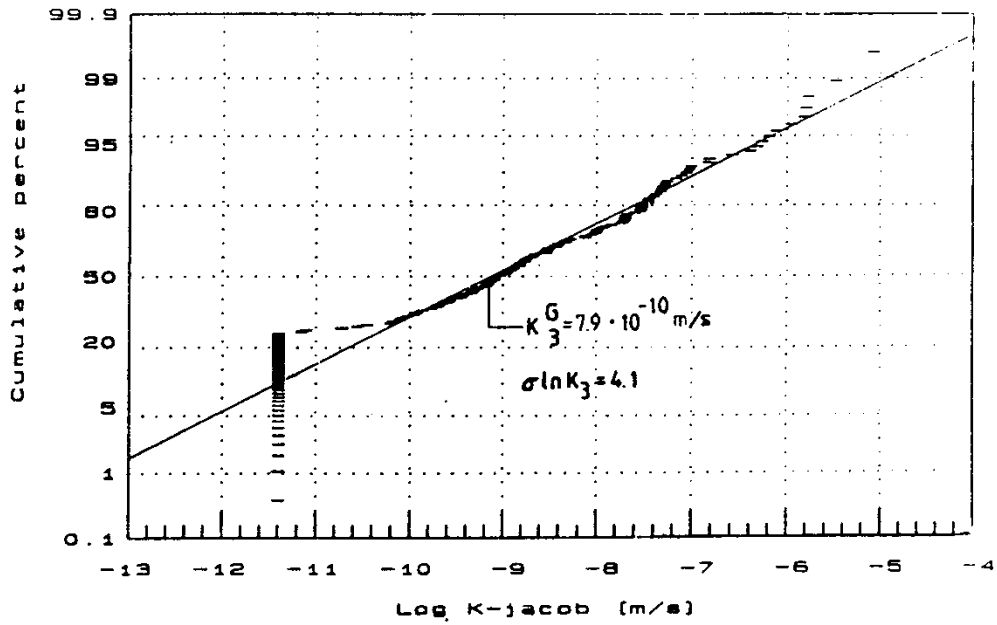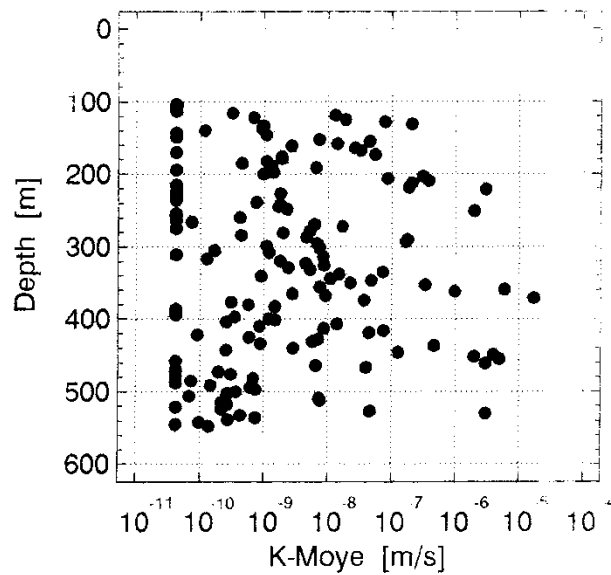
Fig. 5 (a) Normal probability plot of 3m packer tests. (b) Plot of
3m packer tests vs. depth. Borehole KAS03, Äspö Hard Rock
Laboratory, Sweden [Reproduced from Nilsson, 1989].

Borehole	Tested interval [m]	Geometric mean [log(m/s)]	Standard deviation [log(m/s)]	Correlation range [m]
KAS02	102-801	-10.8	1.70	< 27
KAS03	103-547	-9.1	1.78	< 6
KAS04	133-454	-9.1	2.30	< 3
KAS05	157-541	-10.4	2.13	< 6
KAS06	105-591	-9.3	2.70	< 6
KAS07	106-592	-9.3	2.09	< 18
KAS08	106-577	-9.8	2.78	< 21

Fig. 6   Summarized statistics of the conductivity of 3m packer tests from seven boreholes at Äspö Hard Rock Laboratory, Sweden [After Liedholm, 1991a, b].
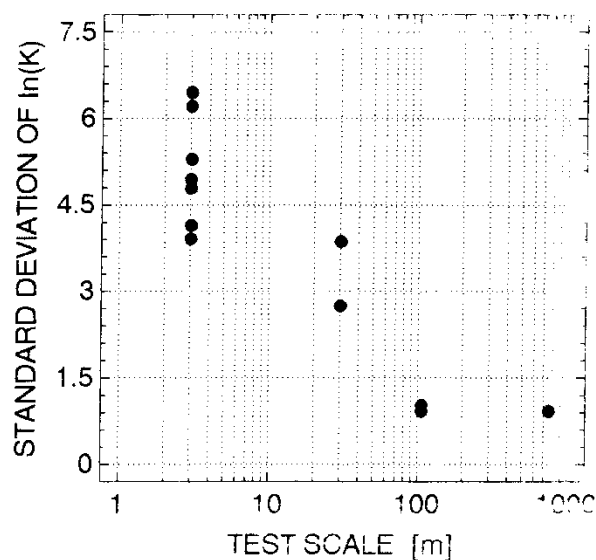

Fig. 7   Standard deviation of *ln*(*K*) vs. test scale, Äspö Hard Rock Laboratory, Sweden [After Liedholm, 1991c].

- 14 -

1.4 The support scale

Numerical simulations of flow and transport in fractured hard rock with deterministic parameters are not relevant seeing that data vary heavily between different sites as well as within a given site. A comparison of 3m packer test data from the Finnsjön study site with data from the Äspö Hard Rock Laboratory suggests that the rock mass at Finnsjön is less heterogeneous. The present study aims to be of generic interest and therefore uses an intermediate variance. The chosen parameters are shown in Figure 8.

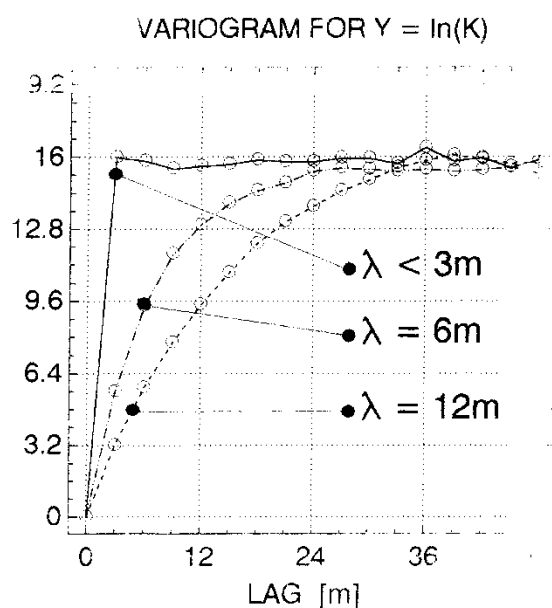|	
Size of a support block, $(\Delta x \ \Delta y)$:	$(3m)^2$
Size of the flow domain, N:	$64 \ \Delta x \times 64 \ \Delta y \ (\Rightarrow (192m)^2)$
Mean of $Y = ln(K)$, μ_Y:	$-16 \ (\Rightarrow K_G = 1.125 \cdot 10^{-7} \ m/s)$
Standard deviation, σ_Y:	$4 \ (\Rightarrow \approx 12 \ log_{10} \ cycles \ in \ K)$
Variogram function, $\gamma(h)$:	isotropic and exponential
Correlation length, λ_Y:	$(0, 6, 12)m$
Measurement threshold:	25%

Fig. 8   Chosen parameter values for the numerical simulations.

1.5 Outline of contents

The numerical calculations are divided into five experiments investigating different aspects of groundwater flow and solute transport that are of interest considering the main objectives of the study. The first experiment deals with unconditional simulation of flow (anisotropy), the second experiment deals with flow field analysis (channelling), the third experiment deals with simulation of flow on different scales of support, the fourth experiment deals with solute transport (the key issue), and the fifth experiment deals with a novel approach to numerically simulate flow and transport in a stochastic discontinuum. It is stressed that the three-dimensional real world problem is here simplified to a *two-dimensional* description. The objectives of the different experiments may be summarized as follows:

Unconditional simulation of flow: The objective is to investigate the relationship between the statistical (spatial) geometric mean of local conductivities and the numerically computed equivalent block conductivity as a function of scale, i.e. block size. The underlying hypothesis is that present statistical upscaling techniques underestimate the conductivity of finite blocks, due to their inability to take the effects of hydraulic anisotropy into account.

Flow field analysis: The objectives are (*i*) to validate the implementation of the flow model and its capability to deal with high conductivity contrasts, and (*ii*) to improve the understanding of the parameters used to characterize random heterogeneity and the impact of these parameters on the flux.

Simulation of flow on different scales: The objectives are to investigate (*i*) the validity of applying the results obtained from the unconditional simulations, and (*ii*) the differences between two scales of support.

Simulation of solute transport: The objectives are to investigate the possibility (*i*) to reproduce numerically the analytical results obtained by first-order theory, and (*ii*) to extend the numerical simulations to deal with high conductivity contrasts.

A discontinuum model: The objective is to examine briefly the differences in flow and transport between continuous and discontinuous conductivity fields.

2   REVIEW OF THEORY

The hydraulic conductivity K of an isotropic and homogeneous porous medium may be expressed as

$$K = \frac{k\,\rho\,g}{\mu} \tag{1}$$

where k is the permeability of the medium, ρ is the fluid density, g is the acceleration of gravity, and μ is the fluid dynamic viscosity. In the general case, the medium is both anisotropic and heterogeneous, which implies that the conductivity is a tensor quantity ($\tilde{K}$) whose components may vary in space. In what follows, two specific cases are reviewed in conjunction with the *two-dimensional* flow domain shown in Figure 9. The two cases are: (*i*) the dual formulation of groundwater flow in an *anisotropic* and homogeneous medium, and (*ii*) groundwater flow and solute transport in an isotropic and *heterogeneous* (stochastic) medium.
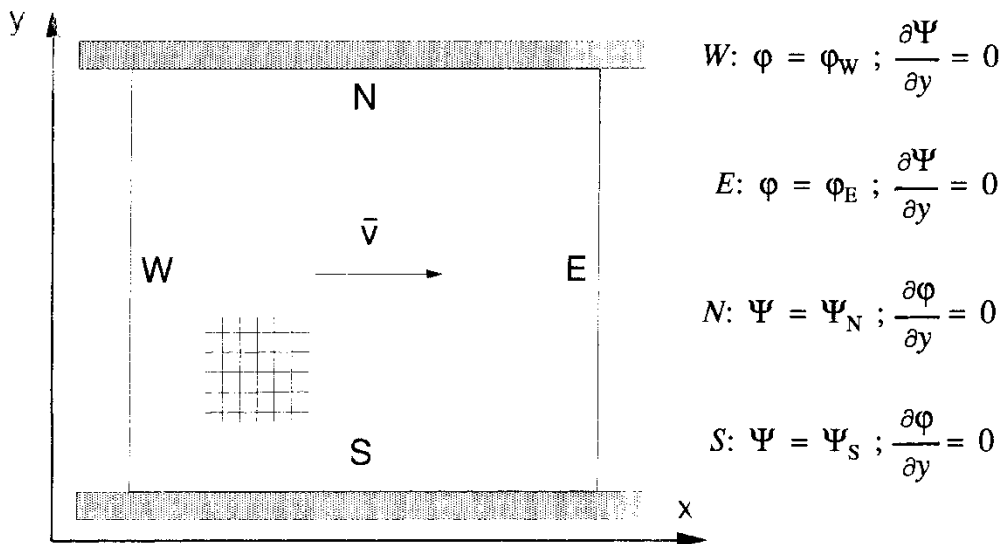

$$W:\ \varphi = \varphi_W\ ;\ \frac{\partial \Psi}{\partial y} = 0$$

$$E:\ \varphi = \varphi_E\ ;\ \frac{\partial \Psi}{\partial y} = 0$$

$$N:\ \Psi = \Psi_N\ ;\ \frac{\partial \varphi}{\partial y} = 0$$

$$S:\ \Psi = \Psi_S\ ;\ \frac{\partial \varphi}{\partial y} = 0$$

Fig. 9   Two-dimensional flow domain in a vertical x-y plane with dual boundary conditions. φ denotes the piezometric head and Ψ the Lagrange stream function [After Frind *et al.*, 1987].

Consistent presentations and complete mathematical treatments of the two cases are found in Bear [1972, 1979] and Frind & Matanga [1985] concerning the dual formulation of groundwater flow; in Matheron [1967], Gutjahr *et al.* [1978], and Dagan [1979, 1986, 1989] concerning flow in a stochastic continuum; and in Dagan [1982, 1984, 1987, 1988, 1990], Gelhar & Axness [1983] and Neuman *et al.* [1987] concerning solute transport in a stochastic continuum. Before dealing with the cases mentioned, however, the definitions of the streamline and the Lagrange stream function are reviewed.

2.1 Streamlines and the Lagrange stream function

A *streamline* is a curve that is tangent to the flux vector at every point upon it at a given instant. In other words, a streamline is an instantaneous picture of movement at various points, because the flux vector at a given point indicates the direction of motion of the fluid particle passing that point. The *pathline* of a fluid particle, however, is the trajectory as time passes, i.e. the locus of its movement. Even though the two will coincide in direction at the location of the particle, elsewhere they may be expected to diverge, because of the variation of the flux as a function of time and space. Only if the streamlines themselves do not change in form and position with time will they represent the paths actually followed by individual particles, i.e. in steady flow. Because a *streamline* is tangent to the flux vector at every point upon it at a given instant, the mathematical expression defining a streamline may be written as

$$\mathbf{q} \times d\mathbf{s} = 0 \qquad (2)$$

where $\mathbf{q}$ is the flux vector, i.e. the specific discharge, and $d\mathbf{s}$ is an element of arc along a streamline. Eq. (2) may be written more usefully in terms of displacements in a Cartesian coordinate system

$$dx = q_x \, dt \qquad dy = q_y \, dt \qquad dz = q_z \, dt \qquad (3)$$

which at any instant t_0 permits the differential equation of the streamline to be written as

$$\frac{dx}{q_x(x, y, z, t_0)} = \frac{dy}{q_y(x, y, z, t_0)} = \frac{dz}{q_z(x, y, z, t_0)} \qquad (4)$$

Thus, the differential equation of the streamline describes its form at a given instant. The differential equation of the pathline, however, involves the passage of time, i.e. t is now a variable and

$$\frac{dx}{q_x(x, y, z, t)} = \frac{dy}{q_y(x, y, z, t)} = \frac{dz}{q_z(x, y, z, t)} = dt \qquad (5)$$

The final solution to (5) has the form $x = x(x_0, y_0, z_0, t)$, etc., where $x = x_0$, $y = y_0$, and $z = z_0$ at $t = t_0$ are the initial conditions.

Lagrange (1736-1813) was the first to solve the differential equation of the streamline for *two-dimensional flow*. For the flow domain in Figure 9, the differential equation is

$$\frac{dx}{q_x} = \frac{dy}{q_y} \qquad (6)$$

Lagrange recognized the fact that the corresponding equation of continuity for an incompressible fluid in a non-deformable medium

$$\frac{\partial q_x}{\partial x} + \frac{\partial q_y}{\partial y} = 0 \qquad (7)$$

represents the analytic condition under which $q_x \, dy - q_y \, dx$ will be an exact differential, which he denoted $d\Psi$. The function $\Psi = \Psi(x, y)$ is called the *Lagrange stream function*. From the equality

$$d\Psi = \frac{\partial \Psi}{\partial x} \, dx + \frac{\partial \Psi}{\partial y} \, dy = q_x \, dy - q_y \, dx \tag{8}$$

Lagrange arrived at the following significant relationships for the two flux components,

$$q_x = \frac{\partial \Psi}{\partial y} \qquad q_y = - \frac{\partial \Psi}{\partial x} \tag{9}$$

Since along any streamline $d\Psi = 0$, constant values of the stream function evidently correspond to the equations of individual streamlines.

A stream tube is by definition bounded by two adjacent streamlines, say Ψ_a and $\Psi_b = \Psi_a + \Delta\Psi$. Considering the flux between two points a and b located on Ψ_a and Ψ_b, respectively, with $w = |b - a|$ being the width of the stream tube, integration yields

$$\int_a^b d\Psi = \int_a^b (q_x \, dy - q_y \, dx) = \Delta Q \tag{10}$$

where ΔQ is the discharge (rate of flow) passing through the stream tube. Subsequently, the discharge of a stream tube is equal to the numerical difference between two bounding streamlines

$$\Delta Q = \Psi_b - \Psi_a = \Delta\Psi \tag{11}$$

In the present study, a systematic flow pattern is obtained by plotting a series of streamlines differing by a constant increment.

2.2 The dual formulation of groundwater flow

Besides assuming a non-deformable medium and an incompressible fluid, the medium in Figure 9 is here assumed to be *anisotropic* and homogeneous. Furthermore, the flow system is assumed to be steady in a vertical x-y plane and the dual boundary conditions are either of the Dirichlet type or the Neumann type. The Dirichlet boundary conditions are of the form:

$$\Psi = \Psi_0(\mathbf{x}) \qquad \mathbf{x} \in N; \ S \tag{12a}$$

$$\varphi = \varphi_0(\mathbf{x}) \qquad \mathbf{x} \in W; \ E \tag{12b}$$

where Ψ_0 and φ_0 are specified values of the Lagrange stream function (Ψ) and piezometric head (φ), respectively, and Γ_1 and Γ_2 represent the corresponding segments of the boundary. $\varphi = p/\rho g + y$, with p being the pressure, ρ is the fluid density, g is the acceleration of gravity, and y the elevation head. The Neumann boundary conditions are of the form:

$$\frac{\partial \Psi}{\partial y} = 0 \tag{13a}$$

$$\frac{\partial \varphi}{\partial y} = 0 \tag{13b}$$

In Figure 9, the piezometric head and the stream function vary within the flow domain, i.e. $\varphi = \varphi(\mathbf{x})$ and $\Psi = \Psi(\mathbf{x})$, with $\mathbf{x} = \mathbf{x}(x, y)$ being a Cartesian point vector in two dimensions. The Darcy equation for an anisotropic and homogeneous medium may be written as

$$\mathbf{q} = - \tilde{\mathbf{K}} \ \nabla \varphi \tag{14}$$

where $\mathbf{q}$ is the specific discharge vector, $\nabla \varphi$ is the piezometric gradient, and $\tilde{\mathbf{K}}$ is a tensor of four components. The relationships between $\mathbf{q}$, $\nabla \varphi$, and $\nabla \Psi$ may be identified from a combination of (9) and (14), namely

$$q_x = -K_{xx} \frac{\partial \varphi}{\partial x} = \frac{\partial \Psi}{\partial y} \qquad (15a)$$

$$q_y = -K_{yy} \frac{\partial \varphi}{\partial y} = -\frac{\partial \Psi}{\partial x} \qquad (15b)$$

where it is assumed that the coordinate axes of the x-y plane coincide with the principal directions of conductivity, i.e. $\tilde{K}$ is in a diagonal form. Under steady flow, in absence of recharge, the continuity equation may be expressed as

$$\nabla \cdot \mathbf{q} = 0 \qquad (16)$$

By substitution of (14), the governing equation becomes

$$\nabla \cdot (\tilde{K} \, \nabla \varphi) = 0 \qquad (17)$$

An alternative formulation of (17) may be obtained by considering the fact that under the given conditions stated previously the piezometric gradient field satisfies

$$\nabla \times (- \nabla \varphi) = \nabla \times (\tilde{K}^{-1} \, \mathbf{q}) = \nabla \cdot (|\tilde{K}|^{-1} \, \tilde{K} \, \nabla \Psi) = 0 \qquad (18)$$

When the coordinate axes are parallel with the principal directions of permeability, equations (17) and (18) can be written as

$$\frac{\partial}{\partial x} \left[K_{xx} \frac{\partial \varphi}{\partial x} \right] + \frac{\partial}{\partial y} \left[K_{yy} \frac{\partial \varphi}{\partial y} \right] = 0 \qquad (19a)$$

$$\frac{\partial}{\partial x} \left[K_{yy}^{-1} \frac{\partial \Psi}{\partial x} \right] + \frac{\partial}{\partial y} \left[K_{xx}^{-1} \frac{\partial \Psi}{\partial y} \right] = 0 \qquad (19b)$$

where K_{xx}^{-1} and K_{yy}^{-1} are the resistivity components of the medium. For an anisotropic medium, the equipotentials $\varphi = $ const and the streamlines $\Psi = $ const are *not* orthogonal, although (15) is valid. In the

case of an isotropic and *heterogeneous* medium, however, the curves φ = const and Ψ = const cross one another at right angles.

It follows from (11), and the magnitude of the average velocity $v = |v(x, y)| = |q/n|$, with n being the effective (kinematic) porosity, that the distance Δs travelled by a fluid particle along any streamline s during a time interval Δt is readily derived as

$$\Delta s = v \; \Delta t = \frac{q}{n} \Delta t = \frac{\Delta \Psi}{n \; w} \Delta t \qquad (20)$$

Because the width (w) of a stream tube may very well vary in space, i.e. $w = w(s)$, the travel time corresponding to some distance Δs is obtained by integration of (12)

$$t = \frac{n}{\Delta \Psi} \int_{\Delta s} w \; ds \qquad (21)$$

2.3 The stochastic continuum

Field measurements provide a way of characterizing the spatial variability (heterogeneity) of a medium for any medium *property* of interest (see, e.g. Beran, 1968). In the classical equations for groundwater flow and solute transport, the relevant parameters, e.g. the hydraulic conductivity and the dispersivities, are considered to be constant-valued. The stochastic continuum theory, however, elaboates the parameter heterogeneity in the context of a statistical (probabilistic) framework. In what follows, a spatially varying isotropic conductivity K, or more precisely, its natural logarithmic transformation (log-conductivity), is regarded as a *statistically stationary random field* (random space function, stochastic process) $Y(x) = ln(K(x))$, with x being a Cartesian point vector in two dimensions, $x = x(x, y)$.

- 25 -

The population parameters used to characterize the spatial variability of Y are generally expressed under the hypothesis of a *multivariate normal distribution* (*MVN*). Under this simplification, the entire statistical structure of the stationary $Y(\mathbf{x})$ is completely defined with the aid of μ_Y and $\sigma_{ij} = C_Y(\mathbf{x}_i, \mathbf{x}_j)$, where μ_Y denotes the mean and C_Y the two-point covariance. Thus, we may write

$$Y(\mathbf{x}) = ln(K(\mathbf{x})) \in N(\mu_Y, \sigma_Y, \lambda_Y \text{ (or } I_Y)) \tag{22}$$

with μ_Y, σ_Y, and λ_Y (or I_Y) being the mean, the standard deviation, and the correlation length (or the integral scale), respectively, and $N()$ denotes the normal (*Gaussian*) distribution.

The assumption of stationarity implies that the moments (mathematical expectations, designated with angle brackets < >) of the log-conductivity field are invariant under translation. Usually only the assumption of *weak stationarity* (*second-order stationarity*) is made about Y, and field data are employed to derive the probability density function (*PDF*) of $Y(\mathbf{x})$ and its two-point covariance. The correlation length and the integral scale are both measures of the distance between two points beyond which $Y(\mathbf{x}_i)$ and $Y(\mathbf{x}_j)$ cease to be correlated. In this study, a *statistically isotropic* exponential covariance function in two dimensions is used

$$C(h) = \sigma_Y^2 \left[exp(-\frac{h}{\lambda_Y}) \right] \tag{23}$$

with $\mathbf{h} = \mathbf{x}_i - \mathbf{x}_j$ being the distance vector of separation (lag) between the two points, and $h = |\mathbf{h}|$. The correlation length λ_Y is defined as the distance at which the correlation between two points is reduced by a factor of e. The integral scale I_Y is defined as the area between $C(h)$ and the abscissa. For the exponential covariance function in (23), the correlation of two points three and four correlation lengths apart is approximately 5% and 0%, respectively. Furthermore, for (23) I_Y is numerically identical to λ_Y, i.e.

$$I_Y = \sigma_Y^{-2} \int_0^\infty C_Y(\mathbf{h}) \, dh = \int_0^\infty \left[exp(-\frac{h}{\lambda_Y}) \right] dh = \lambda_Y \qquad (24)$$

In some cases the experimental variance of Y increases with the size of the study area under consideration. To make the statistical framework operational, a less stringent hypothesis has to be used, called the *intrinsic hypothesis* [see, e.g. de Marsily, 1986]. It is based on the assumption that (*i*) the first-order increments of Y, i.e. $(Y(\mathbf{x} + \mathbf{h}) - Y(\mathbf{x}))$, are of finite variance, and (*ii*) these increments are themselves weakly stationary. Thus,

$$E\{(Y(\mathbf{x} + \mathbf{h}) - Y(\mathbf{x}))\} = m(\mathbf{h}) \qquad (25)$$

$$V\{(Y(\mathbf{x} + \mathbf{h}) - Y(\mathbf{x}))\} = 2\gamma(\mathbf{h}) \qquad (26)$$

The variance of the increment defines the *variogram* (*semi-variogram*) $\gamma(\mathbf{h})$, which, in concrete terms, is the mean of the square of the increment of Y as a function of the lag $\mathbf{h}$:

$$\gamma(\mathbf{h}) = \frac{1}{2} E\{(Y(\mathbf{x} + \mathbf{h}) - Y(\mathbf{x}))^2\} \qquad (27)$$

In the stationary hypothesis, both the covariance and the variogram exist, i.e.

$$\gamma(\mathbf{h}) = \sigma_Y^2 - C_Y(\mathbf{h}) \qquad (28)$$

or after substitution of (23)

$$\gamma(h) = \sigma_Y^2 \left[1 - exp(-\frac{h}{\lambda_Y}) \right] \qquad (29)$$

The variogram plays a fundamental part in geostatistical methods such as *ordinary kriging* [see, for example, Istok & Flint, 1991].

In order to replace ensemble statistics by spatial statistics, *ergodicity* must be assumed. Ergodicity implies that all states of the ensemble are available in each realization. Accordingly, the question which the classical ergodic theory seeks to answer is: When does the asymptotic behaviour of a space average of a stochastic process reach the ensemble (probabilistic) average? Whether or not ergodicity is an appropriate assumption is often discussed in the literature. Dagan [1989] concludes that it is only in the case when the size (L) of the flow domain is much larger than the integral scale of the log-conductivity field, i.e. $L/I_Y \gg 1$, that one can invoke ergodicity and employ stationarity in order to infer the statistical parameters of Y from a single realization. Cushman [1983] makes the following statement concerning ergodicity:

> "It is the existence of the averaging volume which replaces
> the ergodic hypothesis. That is, when one relates volume
> averaging techniques to probabilistic averaging techniques
> the question of ergodicity is an inappropriate question."

The parameters in (22) implicitly refer to a *support scale* for the log-conductivity field, where the flow system is treated as a *continuum*. Turning to the local (formation) scale, for example, the governing equation for the flow point variables $q(x)$ and $\varphi(x)$, which in the case of steady flow satisfy the Darcy and the continuity equations in (14) and (16), results from an averaging over a volume which is small in comparison with the regional scale of heterogeneity. In this context, the *representative elementary volume* concept (*REV*) [see, e.g. Hubbert, 1956; Bear, 1972, 1979] is often referred to in the literature, although no quantitative assessment of the size of the required averaging volume is provided by using the *REV* [see, for example, Sagar, 1978; de Marsily, 1986; Dagan, 1986; Neuman, 1990]. Hence, the spatial variability of a medium presents a problem for the specification of even the macroscopic properties of the support scale.

If a medium on some scale can be regarded as an isotropic continuum whose properties are continuous functions of the position vector only but not of the direction, the conditions are concordant with a major assumption made at present in the stochastic continuum theory. Dagan [1979] states:

"Physically speaking, these are the properties of a sample which is large compared to the pore scale but small compared to the formation scale, extracted from the aquifer at x. The sample permeability is regarded as a scalar; i.e., pore-scale anisotropy is disregarded, since it has a negligible influence in comparison with formation anisotropy."

In other words, the stochastic continuum theory assumes that the *statistical anisotropy* on the local scale is more important than the *hydraulic anisotropy* for the characterization of flow and transport on a regional scale. The assumption of local (hydraulic) isotropy is perhaps relevant for a granular porous medium. However, in order to validate this assumption in fractured hard rock, the processes of interest must take place on a scale which is of much larger extent than the heterogeneity of the support scale. Given the observed statistics of 3m packer tests, some problems are difficult to solve even if this support scale should be found to be locally isotropic considering the finite volume of the existing rock being modelled [cf. Long *et al.*, 1982; Sagar & Runchal, 1982].

The main objective of the stochastic continuum theory of groundwater flow and solute transport in heterogeneous media is to derive the equations satisfied by *macroscopic variables*. In this process, the uncertainties due to the inherent variabilities of the local log-conductivity field are smoothed out, and the macroscopic equations for the flow and transport on the regional scale resemble those of an *equivalent homogeneous medium*. Formulation of flow problems in

random media, however, results in stochastic field equations. For instance, averaging over the continuity equation in (16) yields for the mathematical expectation of the specific discharge

$$\nabla \cdot <q> = 0 \qquad (30)$$

The solution of (30) is a stochastic function with a probability density function (*PDF*) defined over the ensemble of solutions. Sagar [1978] makes the following statement in this matter:

"It is implied that certain statistical properties of the solution in the random medium will correspond to proper-ties of the solution in the real world complex medium, provided that the random medium adequately describes the real world."

In what follows, a few theoretical results are reviewed, which are used here for verification of the numerical experiments. The main question of interest is the scale problem and two questions are treated: (*i*) the problem of spatial averaging of conductivity (upscaling), and (*ii*) the scale problem associated with non-Fickian and (presumably) Fickian flow regimes in solute transport problems. The review is limited to deal with (*i*) *uniform average flow*, and (*ii*) *transport from non-point sources*. The quoted results are given without any deeper presentation of the underlying theories. Hence, for a complete presentation and better understanding, the reader is referred to the aforementioned main references.

Uniform average flow implies that the boundary conditions are such that for a heterogeneous porous medium the exact solution is a uniform flow of constant gradient and constant flux (specific discharge). In this study, it is assumed that the boundary conditions for the finite flow domain in Figure 9 are in accordance with this condition. Transport from non-point sources implies that the area of

- 30 -

solute input to groundwater has a transverse dimension much larger than the conductivity heterogeneity scale (λ_Y), i.e. the solute body has transverse dimensions such that ergodicity prevails. Furthermore, it is also necessary that the solute body travels a distance much larger than the conductivity heterogeneity scale. In order to meet these conditions, the simulations of solute transport are here accomplished by an instantaneous injection of "fluid particles", representing a conservative inert solute, over the entire upstream boundary. Moreover, the flow domain is a square, and molecular diffusion as well as hydrodynamic dispersion within the support blocks are discarded. Hence, only advective transport is considered on the local scale.

For the specific case of uniform average flow in an *unbounded* (infinite) domain, the averaging of the Darcy equation, see (14), yields a linear equation of the same type as (30), i.e. $\nabla<\varphi>$ and $<q>$ are constant and given by [cf. Dagan, 1989]

$$<\varphi(x)> = - \mathbf{J} \cdot \mathbf{x} \qquad <\mathbf{q}(x)> = - \tilde{\mathbf{K}}_{ef} \nabla<\varphi(x)> \qquad (31)$$

where $\mathbf{J}$ is a constant gradient in the mean direction of flow and $\tilde{\mathbf{K}}_{ef}$ denotes the *effective conductivity tensor*. $\tilde{\mathbf{K}}_{ef}$ represents a macroscopic property of the medium and is found to be positive definite, invertible, and symmetric. Hence, it can be reduced to a diagonal matrix with positive principal values in orthogonal directions. Furthermore, for an isotropic covariance function, see (23), it can effectively be reduced to a scalar, i.e. a diagonal matrix where the principal values are identical. The range of $\tilde{\mathbf{K}}_{ef}$ in (31) is bounded between the harmonic and the arithmetic means of the local conductivities, regardless of the dimensionality of the flow domain, the distribu-tion of the local conductivities, and the spatial correlation of the local conductivities. Furthermore, if the *PDF* of the local conductivities is *log-normal* and the spatial correlation is *invariant to rotation*, that is to say statistically isotropic,

and the flow domain is *two-dimensional*, the effective conductivity is exactly equal to the statistical (spatial) *geometric mean* of the local conductivities. In other words, $\tilde{K}_{ef}$ is a scalar entity, with

$$K_{ef} = K_G = exp(\mu_Y) \tag{32}$$

Because $\tilde{K}_{ef}$ is defined over the ensemble of solutions, the *equivalent homogeneous medium* given by (31) represents the average flow pattern, i.e. parallel streamlines, and (32) implies that the equivalent conductivity is completely defined by a single parameter, i.e. the statistical (spatial) geometric mean of the infinitely large realization. Being a macroscopic property of an unbounded domain, however, both (31) and (32) are devoid of any notion of scale. In a previous study by Follin [1989, 1990], an attempt was made to define the size of the infinite case in terms of confidence limits for the relative error in the point estimator corresponding to (32), namely $K_g = exp(m_Y)$, where m_Y is the sample mean defined by

$$m_Y = \frac{1}{N} \sum_{i=1}^{N} Y_i \tag{33}$$

with N being the sample size, i.e. the *number* of local conductivities. In classical statistics, the confidence interval for an *independent random variable* provides an estimate of the error in the point estimator. Due to the exponential function, however, the confidence interval is not symmetric in this case. If the sample size is large, Taylor's theorem for $exp(x)$ provides an approximate $(1 - \beta)$ symmetric confidence interval for the *relative error* in K_g [cf. Follin, 1990]. Conversely, the approximate confidence interval suggests that the minimum sample size needed for the relative error in K_g to be less than a specified amount ε with $(1 - \beta)$ confidence must satisfy the expression in (34), where $\lambda_{\beta/2}$ denotes the value of a standardized normally distributed random variable. Thus,

$$N \geq \left(\frac{\lambda_{B/2} \; \sigma_Y}{\varepsilon} \right)^2 \qquad (34)$$

(34) can be used to compute the expected relative error in K_g for a given sample size. For example, if $\beta = 0.05$ and a square of 64×64 support blocks is considered with $(3m)^2$/block and $\sigma_Y = 4$, the conductivity of the $(192m)^2$ square differs from the equivalent homogeneous medium value in two dimensions by a minimum of 12.5% with 95% confidence. (34) is valid only for a purely random medium due to the requirement of statistical independence. The corresponding value for a correlated field is larger, though.

Cushman [1986] concludes that $\tilde{K}_{ef}$ is a constitutive variable, which is defined in the context of a specific numerical flow experiment. Following this conclusion, the present study focuses on uniform average flow in a *finite* conductivity field, see Figure 9. The study deals with the question of whether the conductivity on a fine support scale can be scaled up to a coarser support scale without losing important features concerning the physics of the problem. Journel & Huijbregts [1978] and Vanmarke [1983] treat the scaling up process (*regularization*), but not within a hydraulic context. The determination of the *block conductivity* of finite rock blocks of a heterogeneous fractured rock is important in far field flow and transport studies because the scaling up process allows for (*i*) the use of fewer grid blocks, and (*ii*) smaller contrasts in the conductivity field, which relax the computational constraints [see, for example, Durlofsky, 1991]. In particular, the present study focuses on a finite flow domain (S) composed of a local conductivities on a fine scale, called the *original support scale*. The flow domain is then gridded on a coarser scale, called the *block scale*. The blocks are, one by one, separated from the flow domain and subjected to a flow test experiment with boundary conditions as shown in Figure 9. That is to say, each block is assigned a *block conductivity*, denoted K_S, which is determined from the flow test value using the original support scale data within the block.

The present study is so far following a line shared by many re-search workers. Warren & Price [1961], Smith & Freeze [1979], Rubin & Gómez-Hernández [1990], and Desbarats [1991b], for example, studied the block conductivity concept for statistically stationary fields. Using numerical simulations, they all conclude, under the conditions stated previously in conjunction with (32), that the up-scaled value, i.e. the finite block conductivity, is well approximated by the spatial geometric mean of the local conductivity values within it. In addition, Rubin & Gómez-Hernández [1990] and Desbarats [1991b] presented upscaling "rules" based on either (*i*) a "second-order theory", i.e. a second-order approximation of a small pertur-bation of the log-conductivity field [cf. Rubin & Gómez-Hernández, 1990], or (*ii*) a reformulation of the statistical derivations of Matheron [1967] where spatial averages rather than ensemble expecta-tions are used [cf. Desbarats, 1991b]. The study by Desbarats [1991b] is of special interest here, because it uses the concept of the Lagrange stream function.

None of the studies mentioned, however, consider extreme con-ductivity contrasts. The largest value used for the variance of the log-conductivity field is $\sigma_Y^2 \approx 2$ [Rubin & Gómez-Hernández, 1990]. Secondly, they all use a finite-difference scheme (five-point or seven-point), which inherently decreases the contrasts [see, for example, Kinzelbach, 1987a; Cacas *et al.*, 1991]. That is to say, the mass balance between two adjacent nodes is based on, for example, the harmonic mean of the corresponding local values. Strictly speak-ing, using the harmonic mean, or any other mean, instead of using the local values as such, implies that an additional correlation is implemented more or less unconsciously. Thirdly, no attempts are made to study the importance of (hydraulic) anisotropy due to sta-tistical anisotropy in the upscaling process. Discussions of aniso-tropy in conjunction with scale are found in, e.g. Long *et al.* [1982], Sagar & Runchal [1982], White & Horne [1987], Herbert & Splawski [1990], and Durlofsky [1991]. Fourthly, a comparison of uncorrelated and correlated conductivity fields is lacking.

The conclusion that the upscaled value, i.e. the block conductivity, is well approximated by the spatial geometric mean of the local conductivity values within it [cf. Rubin & Gómez-Hernández, 1990; Desbarats, 1991b] is here questioned. Strictly speaking, the assumption of a multivariate normal and ergodic distribution for Y in conjunction with (32) is valid only for the statistically stationary and isotropic *infinite* case [cf. Matheron, 1967]. Although an extrapolation of this assumption to finite fields is not warranted, this is exactly the assumption made in the statistical upscaling discussed in the literature, i.e. (*i*) the scaled fields are assumed to be statistically isotropic, and (*ii*) their multivariate spatial distributions to be identical. A heuristic argument against statistical and hydraulic isotropy can be formulated as follows:

1. Consider (*i*) an infinitely large log-conductivity field (Y), which is *statistically stationary and isotropic* (see (22)), and (*ii*) a large number of realizations of finite blocks, all with boundary conditions according to Figure 9; uniform average flow is defined. Under these circumstances, the block conductivity (K_S) and the spatial geometric mean (K_g) of each block size (S) become stochastic variables with characteristic *PDF*'s defined over the ensemble of finite blocks of the same size.

2. It is important to note that if the boundary conditions in Figure 9 are rotated $90°$, for example, then a different value of K_S can be obtained. That is to say, unless the spatial structure of the local conductivities within a block is invariant to rotation, a hydraulic anisotropy will arise analogous to the deterministic laws of arithmetic and harmonic composition [cf. de Marsily, 1986]. To simplify the reasoning, the two orthogonal values of K_S are denoted K_{11} and K_{22}, respectively.

3. Two extreme cases can be identified. At the upper extreme, where the block is infinite, the expected values of K_{11}, K_{22} and K_g,

are completely defined by the spatial geometric mean given by (32), i.e. $\langle K_{11}\rangle = \langle K_{22}\rangle = \langle K_g\rangle = K_G$. At the lower extreme, where a block is identical to the size of the original support scale, the expected values of K_{11}, K_{22} and K_g are completely defined by the log-normal distribution given by (22), i.e. $\langle K_{11}\rangle = \langle K_{22}\rangle = \langle K_g\rangle = K_A = K_G\ exp(\sigma_Y^2)$. Hence, as S decreases from being an infinite block to a finite block composed of a single conductivity value, the second moments of K_{11}, K_{22} and K_g go from zero to $(K_G^2 exp(\sigma_Y^2)(exp(\sigma_Y^2) - 1))$ [cf. Ababou & Wood, 1990]. By the same reasoning, the *PDF*'s of K_{11}, K_{22} and K_g change from being uniform to become log-normal.

4. The block size (L) required to obtain a statistical isotropy is dependent on the correlation length (λ_Y) or the range (R) of correlation. For an isotropic and exponential variogram, see (29) and Figure 9, $R \simeq 4\ \lambda_Y$. It is noteworthy that for $L = R$, all data within the block are more or less correlated under a maximum of spatial variability, i.e. uncertainty, as expressed by the definition of the sill. In other words, statistical isotropy is not warranted, unless for $L \simeq 0$ and $L \simeq \infty$.

5. Due to the nature of the log-normal distribution, the geometric mean is identical to the median. The latter divides by defini-tion the *PDF* into two parts of equal probability. Thus, whereas K_g is equal to the median, K_S, or better, K_{11} and K_{22} are scat-tered around the median. Depending on whether the spatial struc-ture of the block is invariant by rotation or not, the hydraulic components will be equal or different. The bounds for K_S are given by the relation $K_h \leq K_S \leq K_a$, with K_h and K_a being the harmonic and arithmetic means, respectively, of the local conductivities within the block [see, for example, Dagan, 1979; de Marsily, 1986; Journel *et al.*, 1986]. Hence, in order for K_g to be a representative conductivity value for an upscaled block, even for an anisotropic block, one could argue that $K_g = exp(m_Y)$

should at least be equal to the hydraulic geometric mean, i.e.

$$K_g = \sqrt{K_{11} \ K_{22}} \tag{35}$$

However, (35) is equivalent to $m_Y = 0.5 \ ln(K_{11} \ K_{22})$, which represents a particular kind of anisotropy only, i.e. it is not certain that K_g is the most representative conductivity value.

In the following, the second question of interest is dealt with, i.e. the scale problem associated with non-Fickian and (presumably) Fickian transport. The scale dependence is well documented in the literature, see, for example, Pickens & Grisak [1981], Beims [1983], and Gelhar [1986]. This means that a Fickian diffusion process represented by constant dispersivities from the onset of a solute injection is not an adequate description of the hydrodynamic dispersion phenomenon on all scales, see Figure 10. Therefore, the relevance of using the advection-dispersion equation to describe solute transport in heterogeneous media is questioned.
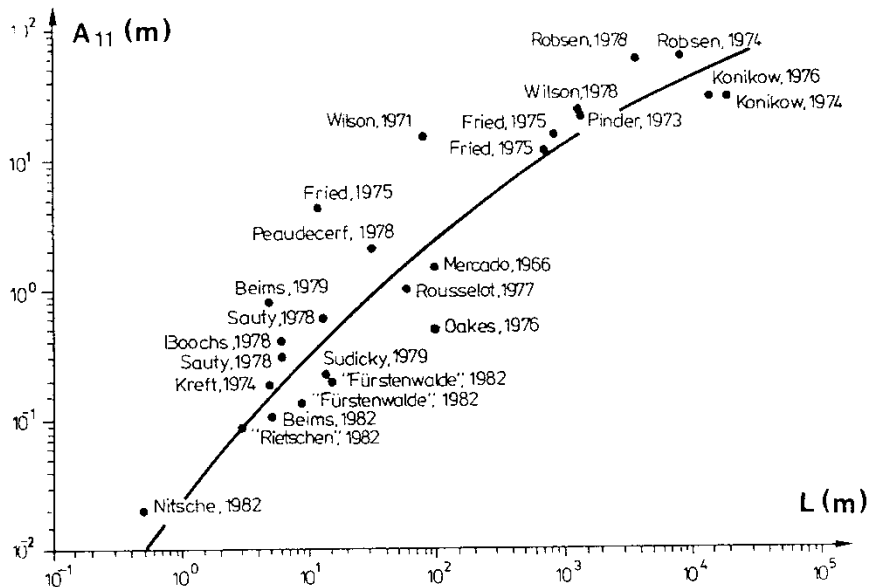
Fig. 10   Scale dependence of longitudinal dispersivity [Reproduced from Kinzelbach, 1987a, who refers to Beims, 1983].

The classical advection-dispersion equation for modelling the transport of an inert solute in a homogeneous porous medium is based on laboratory experiments and may be written as

$$\frac{\partial C}{\partial t} + \mathbf{v} \cdot \nabla C = \nabla \cdot (\tilde{\mathbf{D}} \ \nabla C) \tag{36}$$

where the solute concentration C a is function of the Cartesian space coordinates and the time, i.e. $C(\mathbf{x}, t)$. The dispersion tensor $\tilde{\mathbf{D}}$ governs the spreading of the solute around the centroid of the moving plume. $\tilde{\mathbf{D}}$ can be derived with the aid of dimensional analysis and of the requirement of tensorial invariance [see, e.g. Bear, 1972]. For uniform flow in a two-dimensional, homogeneous and isotropic medium, $\mathbf{v} = (v_x, v_y)$ with $v = v_x = |\mathbf{q}| \ / \ n$ and $v_y = 0$. For the specific case shown in Figure 9, where the x-axis coincides with the mean direction of flow, $\tilde{\mathbf{D}}$ is in a diagonal form. The dispersion coefficients are often written as linear functions of the velocity (v) and some characteristic length scales called dispersivities, which are considered to be constant-valued [Scheidegger, 1961],

$$D_{11} = a_{11} \ v + D^m \tag{37a}$$

$$D_{22} = a_{22} \ v + D^m \tag{37b}$$

In (37), a_{11} and a_{22} denote the longitudinal and transverse dispersivities, respectively, and D^m is the molecular diffusion coefficient. The common approach to modelling solute transport in natural media is to assume that (36) holds also on a large scale. At large distances, however, the spreading due to the molecular diffusion and the pore-scale dispersion are negligible in comparison with the spreading caused by the heterogeneity in the conductivity field. Conversely, if the correlation scale of the conductivity field is small compared to the size of the solute spreading, the velocity

field will become uncorrelated and a Gaussian plume shape is established provided that ergodicity is achieved. By the same reasoning, constant-valued *macrodispersivities*, designated A_{11} and A_{22}, respectively, may be considered [see, for example, Kinzelbach, 1987a; Bear & Verruijt, 1987],

$$D_{11} = A_{11} \, v \tag{38a}$$

$$D_{22} = A_{22} \, v \tag{38b}$$

Dagan [1984] notes that in numerical simulations of solute transport in finite problems, ergodicity can be achieved only if the area of the solute input to groundwater has a transverse dimension much larger than the conductivity heterogeneity scale (λ_Y).

In recent years, the stochastic continuum theory has been increasingly used to study the scale dependence of $\tilde{D}$. Because $\tilde{D}$ governs the solute spreading, i.e. the variance, different approaches may be taken to describe the non-Fickian regime in solute transport problems. In principle, two alternative Lagrangian approaches can be taken. The first approach analyses the *spatial moments* of particle positions as a function of time [Dagan, 1982, 1984, 1987, 1988], whereas the second approach describes the solute movement in terms of the *temporal moments* of particle arrival at a fixed location [see, e.g. Shapiro & Cvetkovic, 1988]. The theoretical developments of the "particle position analysis", are extensive and taken to an almost operational stage [see, e.g. Figure 2 in Dagan, 1984]. The "particle arrival time analysis", however, has received less treatment in the literature, although it deserves much attention, because it circumvents a few inherent limitations of the particle position analysis. For instance, the mapping of the particle positions at different times, as required by the position analysis, becomes quite difficult both in reality and in numerical models. Another difference between the position analysis and the

arrival time analysis, is that the former inherently defines a *volume-averaged* (*resident*) concentration, whereas the latter defines a *flux-averaged* concentration. The distinction between the two concentration averages in relation to a diffusion process is discussed by Kreft & Zuber [1978] and Parker & van Genuchten [1984]. In short, the choice of analysis method essentially depends on the method of detection. For instance, for the breakthrough problem over a given boundary, perpendicular to the mean direction of flow, Shapiro & Cvetkovic [1988] consider the arrival time analysis and the flux-averaged concentration to be the most appropriate description. Hence, the arrival time analysis is not only an alternative but also a complementary analysis method.

The present study follows the Lagrangian approach as outlined by Dagan [1984]. The theoretical assumptions made in relation to (31) and (32) are basically also made in the position analysis. A few additional assumptions are required. They may be summarized as follows: (*i*) a first-order approximation of a small perturbation of the log-conductivity field, which limits the application of theoretical results to $\sigma_Y^2 \leq 1$, (*ii*) a large Peclet number, which in this study is achieved by discarding both the molecular diffusion and the hydrodynamic dispersion, (*iii*) a constant-valued porosity field (n), (*iv*) an isotropic exponential covariance, see (23), and (*v*) an instantaneous (pulse) injection.

A Gaussian plume shape implies that the particle displacements $X_t = X_t(t; x_0, t_0)$ are also normally distributed. Smith & Schwartz [1980] and Dagan [1984], following Taylor [1921], showed that the particle displacement covariance tensor $\tilde{X}$ is directly related to the dispersion coefficients and that the *PDF* of the solute particle displacements is defined by $<X_t>$ and $\tilde{X}$. In the derivation of the solutions for $\tilde{X}$, Dagan [1984] circumvents the difficulties in relating the particle Lagrangian displacement covariance to the Eulerian velocity field by approximating the particle's tortuous path in space by its mean, i.e. X_t is approximated by $<X_t>$.

The analytical solution for two-dimensional isotropic conductivity fields is given by (39), where $\tilde{X}$ is made dimensionless by division of λ_Y^2 [cf. Eq. (4.5) and (4.6) in Dagan, 1984; or Eq. (25) and (39) in Dagan, 1988]

$$X_{11}(\tau) = \sigma_Y^2 \left[2\tau + 3 \left(\frac{1}{2} - ln(\tau) - E + Ei(-\tau) + \frac{e^{-\tau}(1 + \tau) - 1}{\tau^2} \right) \right] \qquad (39a)$$

$$X_{22}(\tau) = \sigma_Y^2 \left[ln(\tau) - \frac{3}{2} + E - Ei(-\tau) + 3 \left(\frac{1 - e^{-\tau}(1 + \tau)}{t^2} \right) \right] \qquad (39b)$$

$$X_{12} = X_{21} = 0 \qquad (39c)$$

where τ is a dimensionless time defined as $\tau = v\, t\, /\, \lambda_Y$, X_{11} and X_{22} are the longitudinal and transverse spatial variances of the ensemble mean particle displacements, respectively, E is the Euler number ($-0.57721..$), and Ei is the exponential integral. Eq. (39) demonstrates that the second-central moments of the spatial distribution of the particle displacements are non-linear functions of time in the vicinity of the solute injection. The non-Fickian macrodispersivities, for uniform average flow parallel to one of the coordinate axes in a two-dimensional flow field, are denoted $A_{11}(\tau)$ and $A_{22}(\tau)$, respectively, and are computed as

$$A_{11}(\tau) = \frac{X_{11}(\tau)\ \lambda_Y}{2\ \tau} \qquad (40a)$$

$$A_{22}(\tau) = \frac{X_{22}(\tau)\ \lambda_Y}{2\ \tau} \qquad (40b)$$

Transport may take place over large distances with respect to the correlation length (λ_Y). Eventually it becomes dominated by the asymptotic values of the displacement covariances. Dagan [1984] and Shapiro & Cvetkovic [1988] conclude that for a second-order statio-

nary log-conductivity field with an exponential covariance, solute transport becomes asymptotically analogous to a diffusion process due to a finite correlation in the advective velocity, i.e. a finite correlation in the conductivity field. The prerequisites for considering the solute transport to be asymptotically analogous to a diffusion process are also discussed by, for example, Gelhar & Axness [1983], Neuman *et al.* [1987], and Naff [1990]. The latter author concludes:

> "...a classical Fickian description, with constant coefficients...should generally be reasonable, provided that prediction of the mean concentration is at distances from the source equivalent to at least 20 length scales λ of the hydraulic conductivity process. Within 20 λ of the source, two deviations from the classical Fickian description will occur: (1) the second moment of the plume will be overestimated significantly and (2) the plume shape will be platykurtic."

Naff [1990] suggests that the non-Fickian behaviour can be corrected by adopting a Fickian description with time-dependent coefficients. This approach was adopted by Kinzelbach [1987b] who simulated non-Fickian *random-walks* by adding a state variable memorizing the travel distance of each particle. The actual dispersivity can be calculated by a given formulation of the dispersivity in function of the travel time. This is an interesting way to deal with the scale problem, particularly in applied problems.

Gelhar & Axness [1983] and Neuman *et al.* [1987] computed the asymptotic values of the macrodispersivities given by (40), although without analysing the preasymptotic, transient regime, from the onset of a solute injection. In spite of a few significant differences, the works of Dagan [1982, 1984, 1987, 1988], Gelhar & Axness [1983], and Neuman *et al.* [1987] agree in principle. For uniform flow in a statistically isotropic two-dimensional field with no

pore-scale dispersivities and no molecular diffusion, the asymptotic values of the longitudinal and transverse macrodispersivities become [cf. Dagan, 1984, 1987, 1988; Neuman *et al.*, 1987]

$$A_{11} = \lambda_Y \, \sigma_Y^2 \qquad\qquad (41a)$$

$$A_{22} = 0 \qquad\qquad (41b)$$

The conclusion by Naff [1990], that a classical Fickian description with constant coefficients should generally be reasonable provided that the prediction of the mean concentration is at distances from the source equivalent to at least 20 λ_Y, is here examined by comparing the results obtained by the non-Fickian position analysis of Dagan [1984] with the results obtained by a Fickian arrival time analysis. Kreft & Zuber [1978] provide different expressions for computing the longitudinal dispersivity for a one-dimensional form of (36) in relation to a diffusion process and the two concentration averages discussed previously. For a flux-weighted pulse injection and a flux-weighted detection [cf. Shapiro & Cvetkovic, 1988], Kreft & Zuber [1978] give the following expression for the longitudinal dispersivity A_{11}

$$A_{11}(x) = \frac{x}{2} \left(\frac{s_t}{m_t} \right)^2 \qquad\qquad (42a)$$

where x is the displacement distance in the mean direction of flow and $(s_t \, / \, m_t)$ is the coefficient of variation of the *residence-time distribution* [cf. Kreft & Zuber, 1978]. (42a) has previously been used by Desbarats [1990, 1991a] and Desbarats & Srivastava [1991], although without an accompanying experimental non-Fickian analysis. Furthermore, the numerical model used by these authors does not simulate a truly advective solute transport. In fact, there are reasons to question whether their model actually describes a continuum [cf. Goode & Shapiro, 1991b].

- 43 -

The displacement covariances derived by the position analysis provide expressions for determining both A_{11} and A_{22}, whereas the arrival time analysis, which is based on the *temporal moments* of particle arrival at a fixed location, is difficult to interpret in a transverse direction to the mean direction of flow. Dagan [1984], however, concludes that the dispersivity inferred from a common interpretation of a field test, "the breakthrough curve", is approximately equal to (40a). For the sake of comparison, an estimate of A_{22} is here obtained by computing the spatial variance of the lateral displacements of particles over a given boundary, perpendicular to the mean direction of flow. In this case the dual formulation of flow provides a means for computing the transverse dispersivity, because it is only the positions on the boundary that are of interest and not the arrival times. The computed spatial variance is designated Ψ_{22} so as to stress the difference in relation to X_{22} as well as to indicate that the dual formulation of flow is used to determine the lateral displacements. However, the suggested *mixing* of temporal and spatial variances is not warranted, and has to be regarded as a working hypothesis. Analogous to (40), the expression suggested here for A_{22} becomes

$$A_{22}(x) = \frac{\Psi_{22}}{2\,x} \qquad (42b)$$

where x is the displacement distance in the mean direction of flow and Ψ_{22} is the transverse spatial variance of the ensemble mean particle displacements over a given boundary as determined by the dual formulation of flow.

Smith & Schwartz [1980], Frind *et al.* [1987], Graham & McLaughlin [1989], and Rubin [1990] are examples of studies where numerical methods were used to compute the spatial moments of the particle positions. Smith & Schwartz [1980], in addition, also computed arrival time distributions. One of the first studies to discuss the

arrival time analysis, however, was that of Warren & Skiba [1964]. They also demonstrated the strong effect of conductivity variations on tracer particles moving through hypothetical media. This was also observed by Schwartz [1977] and Smith & Schwartz [1980]. Davis [1986] claims that because it is a physical property of the medium, dispersivity does not vary with scales bigger than the microscopic level, and that it is possible that investigators have attached too much importance to dispersivity by assigning it such large values in their models, while the contribution of advective mass transport to dispersion has been underestimated.

Following the results of the aforementioned pioneering work of Smith & Schwartz [1980], several recent studies tend to deviate from the classical context associated with the advection-dispersion paradigm and focus their interest on what may be recognized as *preferential flow paths* (*channels*). For example, the presence of channels of preferred flow within two-dimensional conductivity fields is studied by Tsang & Tsang [1989]. They argue that understanding the preferred paths of flow in heterogeneous fields is critical to our understanding of mass transport in the subsurface. Another example is the study by Silliman & Wright [1988], who analysed the structures in discretized conductivity fields in *three dimensions* for paths along which the conductivity is everywhere greater than the effective conductivity of the medium. Although Silliman & Wright [1988] did not solve the flow equations, their work implies that paths will exist within the subsurface along which the resistance to flow is everywhere less than the average as compared to the medium as a unit. Desbarats & Srivastava [1991] modelled a very large two-dimensional flow system with high conductivity paths. They showed that these paths may provide potential extreme flow routes along which contaminants may rapidly be transported.

The present study is more or less related to all the studies mentioned above, in particular to the studies by Smith & Schwartz [1980] and Frind *et al.* [1987]. However, there are four significant

aspects, which distinguish the present study from the ones mentioned here:

(1) None of the studies mentioned consider conductivity contrasts characteristic to fractured hard rock on a "3m scale", i.e. $\sigma_Y^2 = 16$. The closest value used previously is (perhaps) that of Smith & Schwartz [1980] who investigated $\sigma_Y^2 = 2.8$.

(2) The present study considers only truly advective transport, whereas comparable studies, more or less tacitly, include local dispersivities as well, thus introducing additional numerical difficulties into the particle tracking schemes as recognized by the Courant criterion and the Neumann criterion [cf. Kinzelbach, 1987a].

(3) Both non-Fickian and Fickian descriptions are used in this study to investigate the advective solute transport. Furthermore, the comparison is undertaken for both uncorrelated and correlated conductivity fields.

(4) The present study develops an alternative approach to accomplish flux-weighted injection for the onset of solute injection in conjunction with particle tracking schemes. The conventional approach to accomplish a flux-weighted injection is to select a large number of uniformly distributed injection points, and then to inject a flux-weighted number of particles at the selected points. For instance, it is quite common to take the positions of the grid nodes in a regular mesh of finite elements or finite difference cells as injection points. The adopted injection technique in the present study uses the equidistant contour level positions of the stream function at the upstream boundary. Thus, only one particle per streamline needs to be injected to infer the statistics required by the position analysis.

3   NUMERICAL CALCULATIONS

The main question of interest in the numerical calculations undertaken is the scale problem. The upscaling of model parameters, i.e. scale-dependent parameters, is a key issue in many research fields concerned with parameter heterogeneity, because the upscaling process allows for fewer model blocks and relaxes the numerical problems caused by high contrasts in the conductivity. In other words, the upscaling process implies less heterogeneity, which benefits the numerical modelling.

Spatial variability calls for graphical presentations so as to visualize the impact of the heterogeneity on flow and transport. The graphical presentations in this chapter are numerous. For editorial reasons, all figures related to a specific experiment are placed at the end of the corresponding section. The numerical calculations consist of five experiments with different objectives. They are summarized as follows:

Unconditional simulation of flow: The objective is to investigate the relationship between the statistical (spatial) geometric mean of local conductivities and the numerically computed equivalent block conductivity as a function of scale, i.e. block size.

Flow field analysis: The objectives are (*i*) to validate the implementation of the flow model and its capability to deal with high conductivity contrasts, and (*ii*) to improve the understanding of the parameters used to characterize random heterogeneity and the impact of these parameters on the flux.

Simulation of flow on different scales: The objectives are to investigate (*i*) the validity of applying the results obtained from the unconditional simulations, and (*ii*) the differences between two scales of support.

Simulation of solute transport: The objectives are to investigate the possibility (*i*) to reproduce numerically the analytical results obtained by first-order theory, and (*ii*) to extend the numerical simulations to deal with high conductivity contrasts.

A discontinuum model: The objective is to examine briefly the differences in flow and transport between continuous and discontinuous conductivity fields.

3.1 The flow model

Uniform average flow in a two-dimensional flow field is discussed in Chapter 2. The corresponding governing equations for the dual formulation of flow are given by (19) and the Dirichlet and Neumann boundary conditions for a finite block are shown in Figure 9. In what follows, the numerical model used for the flow and transport studies and the procedure used for computing the effective *block conductivity tensor* ($\tilde{\mathbf{K}}_S$) are described.

A variety of numerical procedures could be used to solve the governing equations for uniform flow in two dimensions. Because the scale problem is the key issue in the present study, it is essential that the numerical method is capable of (*i*) representing the local conductivities, i.e. the support scale conductivities, and (*ii*) providing a continuous flux between adjacent model blocks of different conductivities, seeing that the determination of the conductivity tensor of an upscaled block ($\tilde{\mathbf{K}}_S$) involves integration of the flux. A common motive for choosing a finite element method rather than a finite difference method is that the former can resolve complex geometries. For the studied cases, however, such an argument is of no consequence since the support scale is represented by squares. In the literature, the five-point finite difference method is often used for studying the scale problem because it is readily imple-

mented and permits large models to be investigated and solved [see, for example, Rubin & Gómez-Hernández, 1990; Winberg et al., 1990; Desbarats & Srivastava, 1991]. In the present study, the motive for not choosing a finite-difference method is that in such a method the mass balance between two adjacent nodes is based on some average of the local conductivities involved, e.g. the harmonic mean [cf. Kinzelbach, 1987a; Cacas et al., 1991], which means that the conductivity field used by the flow equations is numerically smoother and more correlated, i.e. less heterogeneous, than the original conductivity field.

The standard *Galerkin* finite-element procedure [see, for example, Istok, 1989], which is used here, is considered to be superior because it takes full account for the heterogeneity on the support scale. The bi-linear basis functions of the linear 4-node rectangle element used here yield a second-order accurate solution for the piezometric head (ϕ), whereas the flux (the specific discharge, q) obtained by taking the gradient of the solution of ϕ is only first-order accurate. That is to say, the flux between two adjacent elements is not continuous. There are several ways to circumvent or overcome this drawback. For instance, (*i*) to use mixed or non-conforming finite elements [cf. Durlofsky, 1991], (*ii*) to intensify the discretization, or (*iii*) to choose interpolation functions of higher order. Although interpolation functions, which have continuous derivatives at the element boundaries, provide a continuous flux field, it is important to note that they may not necessarily lead to higher accuracy as they often require numerical integration [cf. Kinzelbach, 1987a]. However, for the linear 4-node rectangle element, which is used here, the integration can be made analytically [see, for example, Frind & Matanga, 1985]. Considering the vast variability in the conductivity field, which is about 12 log_{10} cycles in K on a "3m scale", it may be concluded that most methods will have problems in reproducing an accurate and continuous flux field.

Figure 12 illustrates a discrete representation of a finite two-dimensional stochastic continuum. In the flow experiments discussed below, the y-axis is considered vertical with y being the elevation head. In Figure 12, the support scale, denoted N, consists of 256 conductivity values, i.e. $N = 16 \times 16$. The 256 conductivity values were generated by means of a random number generator. The values of the most significant input parameters to the random number generator are given in the second heading, i.e. $\sigma_{\ln(K)} = 4$ and $\lambda/\Delta x = \lambda/\Delta y = 2$. These data can be regarded as characteristic of 3m packer tests in fractured hard rocks [see, e.g. Liedholm, 1991a, b, c]. For Figure 12, the physical dimensions of the stochastic continuum are $(48m)^2$, i.e. $\Delta x = \Delta y = 3m$, and the correlation length of the isotropic and exponential variogram (see (29)) is $\lambda_Y = 6m$. It should be noted that $\sigma_{\ln(K)}$ and λ are synonymous with σ_Y and λ_Y, respectively.

Two different random number generators are used: (i) a *Turning Bands* generator [Mantoglou & Wilson, 1982] is used to generate correlated conductivity fields, and (ii) an ordinary random number generator [Schrage, 1969] is used to generate uncorrelated conductivity fields. Strictly speaking, it is impossible to generate a truly random field seeing that all points within a support block are perfectly correlated. In what follows, however, $\lambda/\Delta x = \lambda/\Delta y = 0$ is used to denote an uncorrelated conductivity field. In Figure 12, the raster graphics is divided into 8 percentiles representing the variability of the generated conductivity field. For the case shown, the median, i.e. the spatial geometric mean of the local conductivities, is $K_g = 5.86 \cdot 10^{-8}$ m/s and the minimum and maximum values are $5.04 \cdot 10^{-14}$ m/s and $2.67 \cdot 10^{-4}$ m/s, respectively. Moreover, 50% of the data fall between $3.49 \cdot 10^{-09}$ m/s and $9.78 \cdot 10^{-07}$ m/s.

The numerical procedure used here for the determination of $\tilde{K}_S$ is the same as that described by, for example, Durlofsky [1991]. It is a simple procedure which solves the governing equations given by (19) subjected to the Dirichlet and Neumann boundary conditions of (12) and (13). A graphical representation of the Dirichlet boundary conditions defining uniform average flow in a finite heterogeneous

medium is shown in Figure 13. Upon solution, if the side length (L) of the square is set to unity, the fluxes through the vertical faces (W/E-flow) and the horizontal faces (N/S-flow) of the block are calculated and give

$$K_{11} = q_{WE} \qquad\qquad (43a)$$

$$K_{22} = q_{NS} \qquad\qquad (43b)$$

However, the cross terms of $\tilde{K}_S$, i.e. K_{12} and K_{21}, cannot be determined by using this procedure. In spite of this limitation, Durlofsky [1991] concludes that the approach outlined in Figure 13 continues to be used under the tacit assumption that the diagonal terms of the $\tilde{K}_S$ computed in this manner are correct, and that the cross terms are unimportant. It should be noted that K_{11} and K_{22} in the present study are synonymous with K_{xx} and K_{yy}, respectively.

The errors associated with using the linear rectangle element are here investigated by means of three experiments: (i) the numerical solution is compared with an analytical solution, namely the deterministic laws of harmonic and arithmetic composition [cf. de Marsily, 1986], (ii) the solutions for different discretizations of Figure 12 are compared, i.e. each support block is discretized into 1, 4, 16, or 64 linear rectangle elements, and (iii) the solutions for two different interpolation functions are compared, that is to say the linear rectangle element using analytical (exact) integration is compared with a 9-node Lagrangian element with 9 Gauss integration points. The first case is shown in Figure 14, where it is demonstrated that a high conductivity contrast as such causes very few problems if the element sides are aligned with respect to the boundary conditions. The second case is shown in Figures 15-19. In these figures, the solutions of the piezometric head (φ) and the Lagrange stream function (Ψ) for four different discretizations of the $(48m)^2$ block in Figure 12 are shown. The contour lines in Figures 16-19 are computed by means of fitting

splines to the original solutions. Visual comparison of the solutions shows that a finer grid provides a more accurate definition of the flow field, particularly near high contrasts in the conductivity field, i.e. high conductivity contrasts act almost as discontinuities [cf. Goode, 1990]. In Figure 20, the corresponding differences in $\tilde{K}_S$ in relation to the spatial geometric mean of the support block conductivities are shown as functions of the discretization. Two values of σ_Y are examined, namely 1 and 4, which demonstrate: (*i*) the effect of discretization for different contrasts in the conductivity field, and (*ii*) the differences in anisotropy. In the third experiment, a block of $N = 4\times4$ is examined, see Figure 21. In this experiment, the solution of φ for W/E-flow using 256 4-node linear rectangle elements is compared with that using 64 9-node Lagrangian elements with nine Gauss integration points. Thus, the number of nodes is the same in the two cases, whereas the linear solution requires four times as many elements. Figure 21 shows that the shown solutions for φ are "identical", which makes the 9-node Lagrangian element attractive from a computer memory point of view. The disadvantage of using a numerical integration rather than an analytical integration is to some extent shown in see Figure 11.

Case	No. of elements per K-value	Upstream q $[n\cdot10^{-9}\ m/s]$	Downstream q $[n\cdot10^{-9}\ m/s]$
4N	1	7.885	7.885
4N	4	7.387	7.387
4N	16	7.118	7.118
9N	16	7.028	6.940
4N	64	6.986	6.986

Fig. 11   Comparison of flux for the problem shown in Figure 21.
(4N): 4-node linear rectangle element; (9N): 9-node Lagrangian element with 9 Gauss integration points.

2-D HYDRAULIC CONDUCTIVITY FIELD

No. of blocks: 16 × 16

$\sigma_{\ln(K)} = 4.00 \qquad \lambda/\Delta x = 2.0 \qquad \lambda/\Delta y = 2.0$

RASTER LEGEND (dim[K]=m/s)

12.5 %	12.5 %	12.5 %	12.5 %
+5.04E-14	+7.02E-10	+3.49E-09	+1.73E-08
			+5.86E-08

12.5 %	12.5 %	12.5 %	12.5 %
+5.86E-08	+2.62E-07	+9.78E-07	+3.50E-06
			+2.67E-04
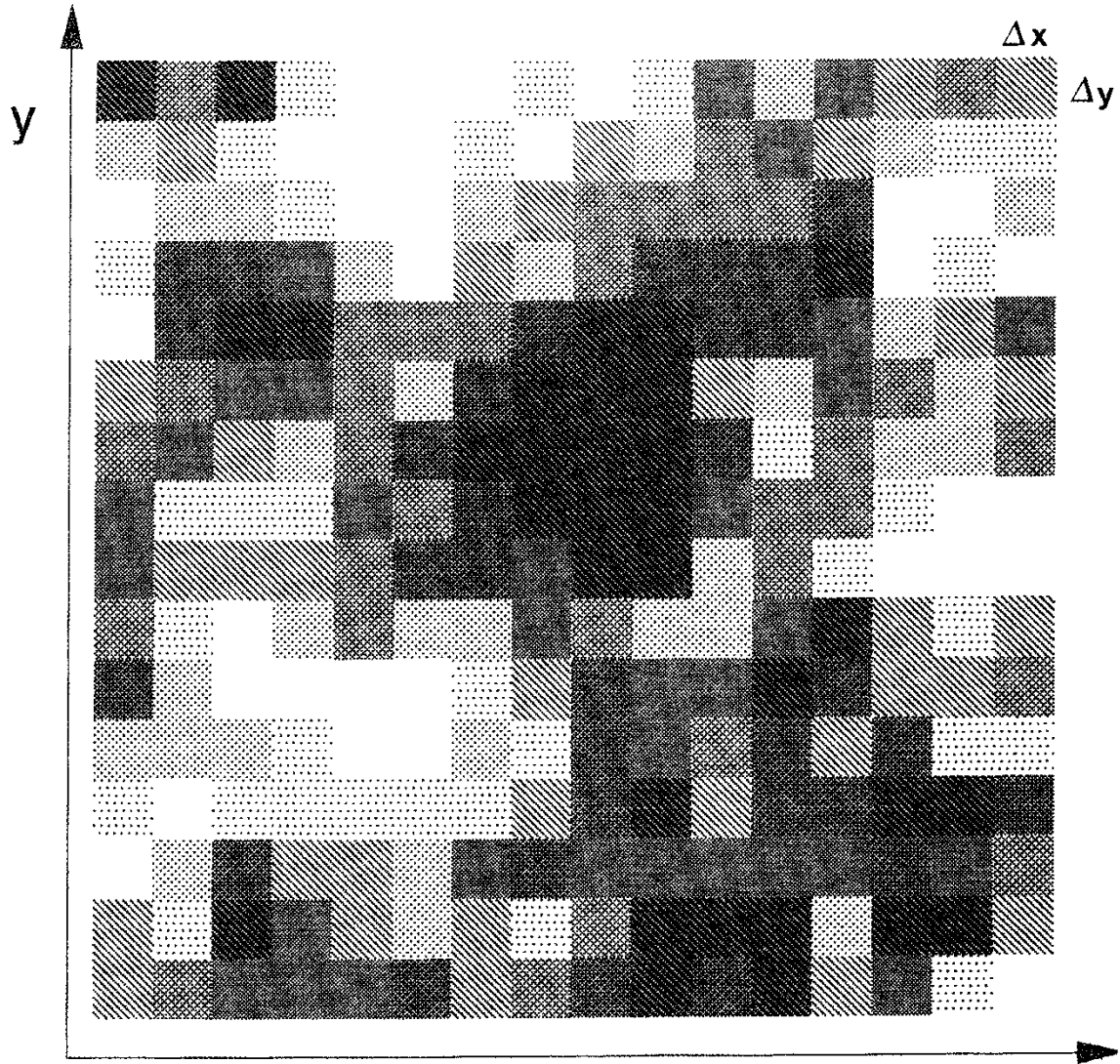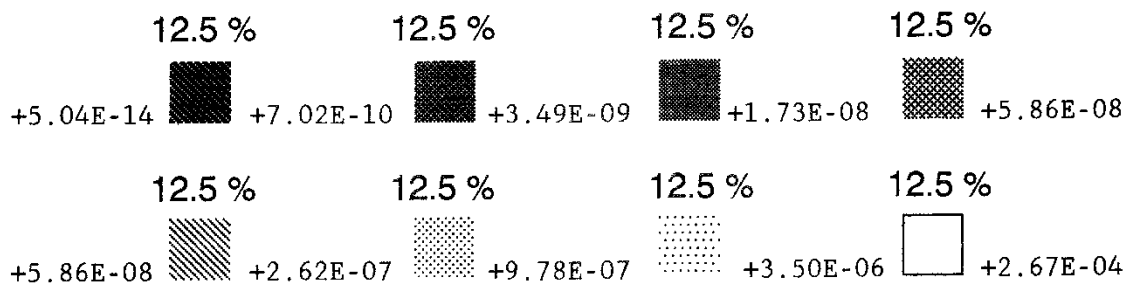
Fig. 12   Graphical representation of a hypothetical heterogeneous medium in 2-D . The number of blocks of the support scale is N = (16 x 16) .
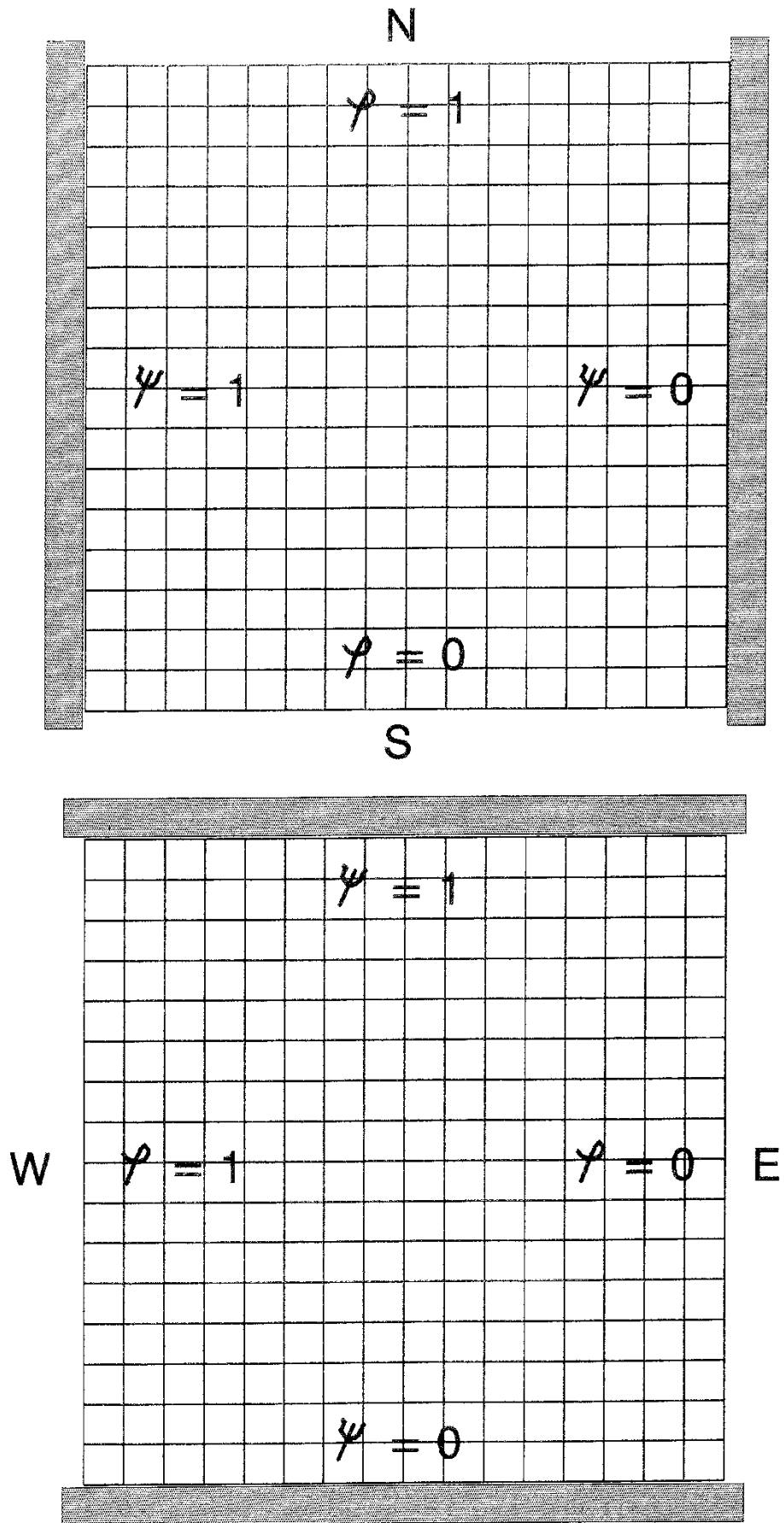
Fig. 13 Dirichlet boundary conditions for a heterogeneous medium such that the exact solution is a uniform flow of constant head gradient and constant specific discharge.

N

$3 \cdot 10^{-7}$

$3 \cdot 10^{-9}$

$3 \cdot 10^{-5}$

$3 \cdot 10^{-11}$

$3 \cdot 10^{-3}$

$3 \cdot 10^{-13}$

$3 \cdot 10^{-1}$

$3 \cdot 10^{-15}$

S

$K_H = 8 / \Sigma (1/K_i)$

$K_H = 2.376 \cdot 10^{-14}$

$K_{yy} \approx 2.37597434... \cdot 10^{-14}$

$RE_H \approx -0.0011 \%$

(a)

y

x

W

$3 \cdot 10^{-7}$

$3 \cdot 10^{-9}$

$3 \cdot 10^{-5}$

$3 \cdot 10^{-11}$

$3 \cdot 10^{-3}$

$3 \cdot 10^{-13}$

$3 \cdot 10^{-1}$

$3 \cdot 10^{-15}$

E

$K_A = \Sigma K_i / 8$

$K_A \approx 3.78787878... \cdot 10^{-2}$

$K_{xx} \approx 3.78787878... \cdot 10^{-2}$

$RE_A = 0 \%$

(b)
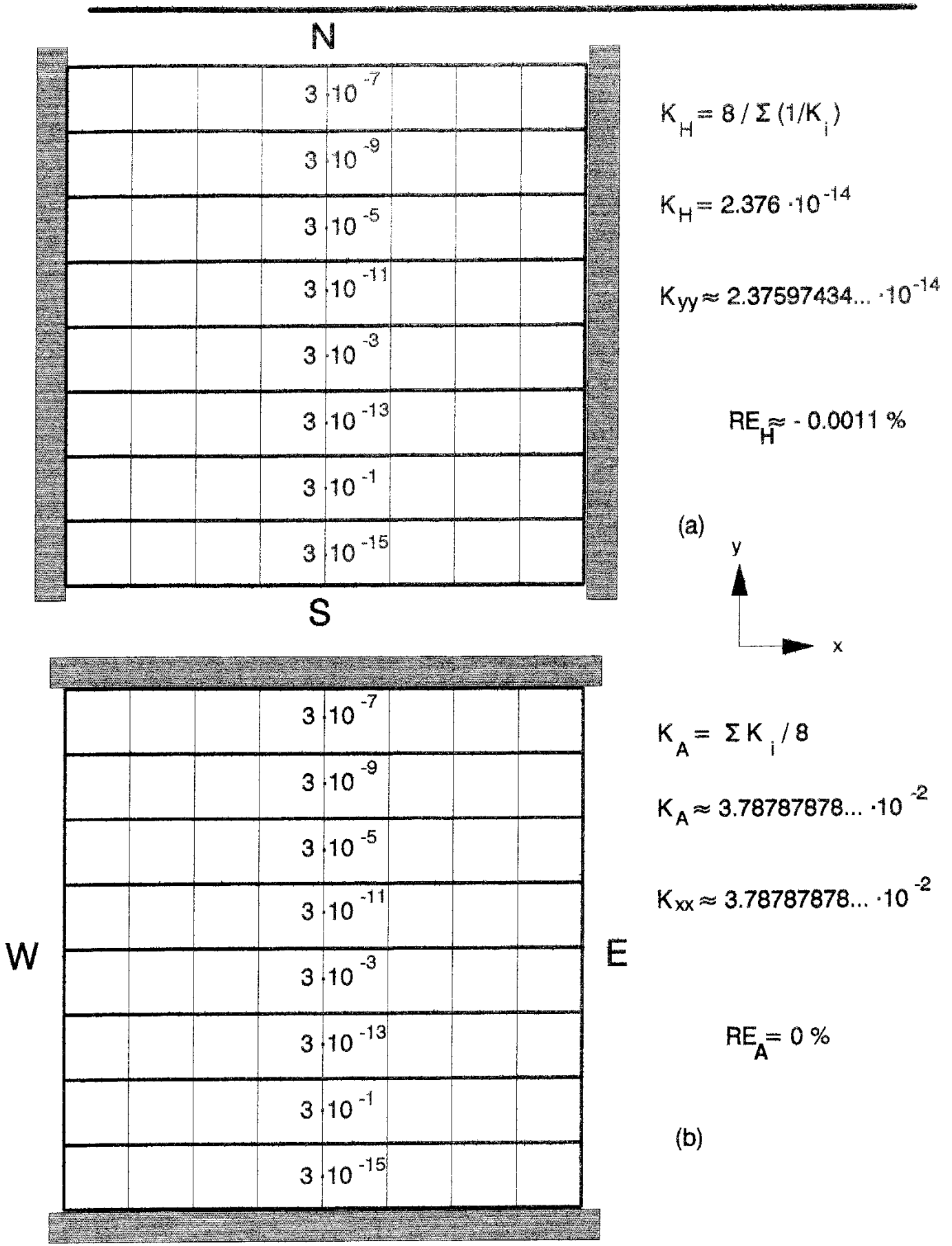
Fig. 14   Flow through 8 layers in series (a) and in parallel (b) .

The layers are of uniform thickness, but differ in conductivity (m/s).

Each layer is discretized by 8 linear rectangle elements.
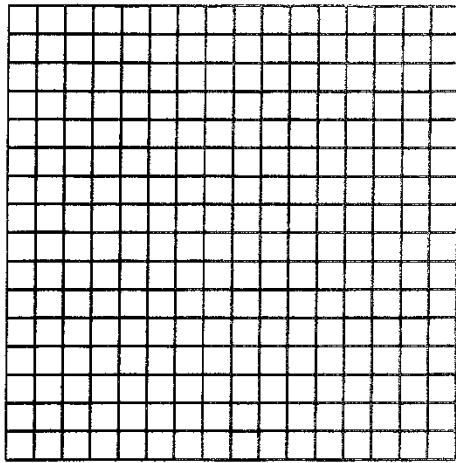
(a)
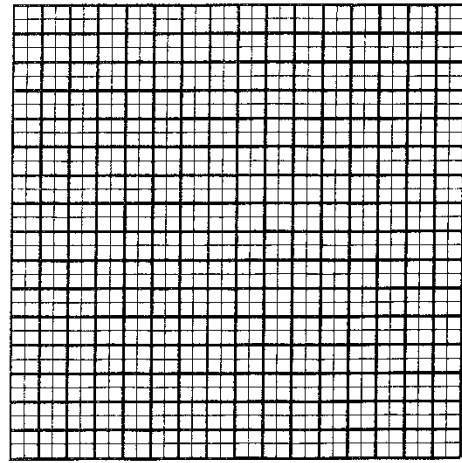
(b)
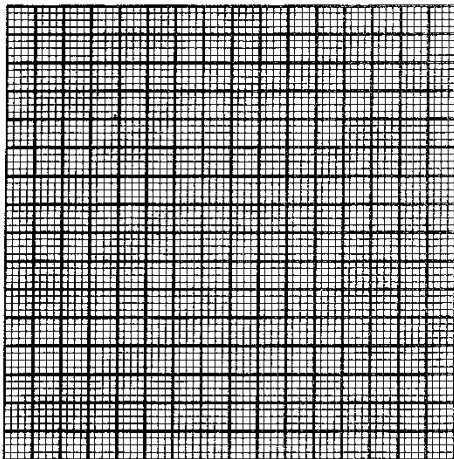
(c)
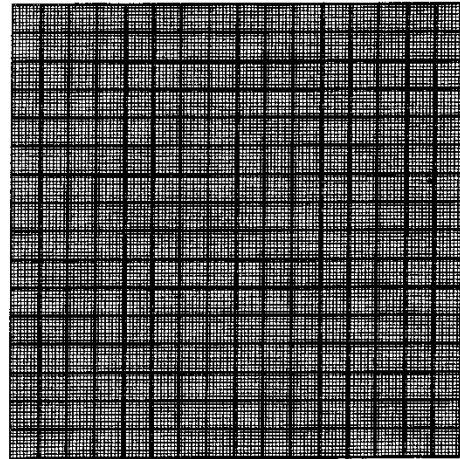
(d)

(a) 1 element/block

(b) 4 elements/block

(c) 16 elements/block

(d) 64 elements/block

Fig. 15   Four different finite element discretizations for N = (16x16) .
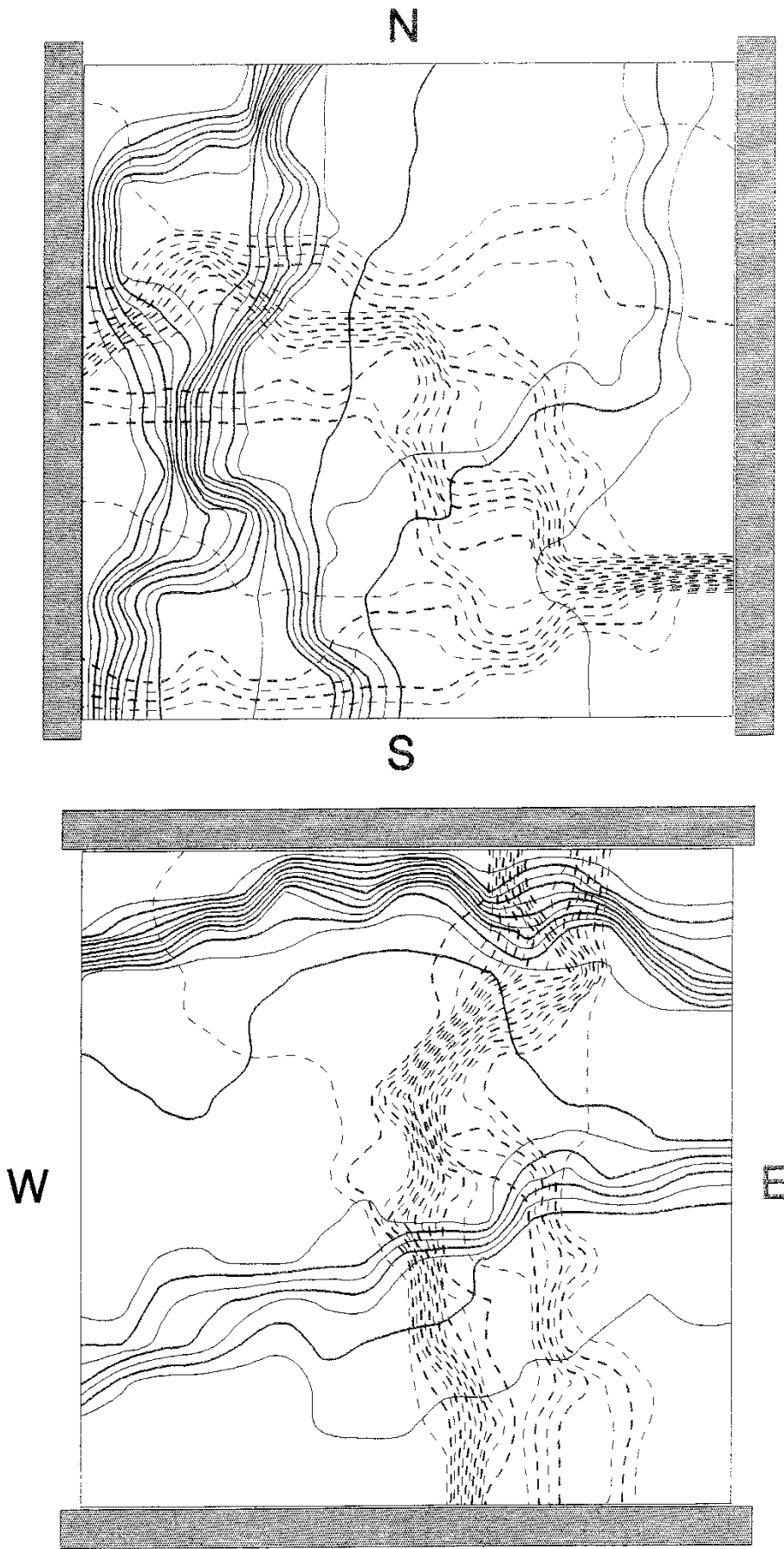
Fig. 16   Flow nets for N/S and W/E flow respectively. N = (16x16) . Each

block is discretized by 1 element. Piezometric head (dashed) and

stream function levels (solid) are in 5% increments between 0 and 1 .
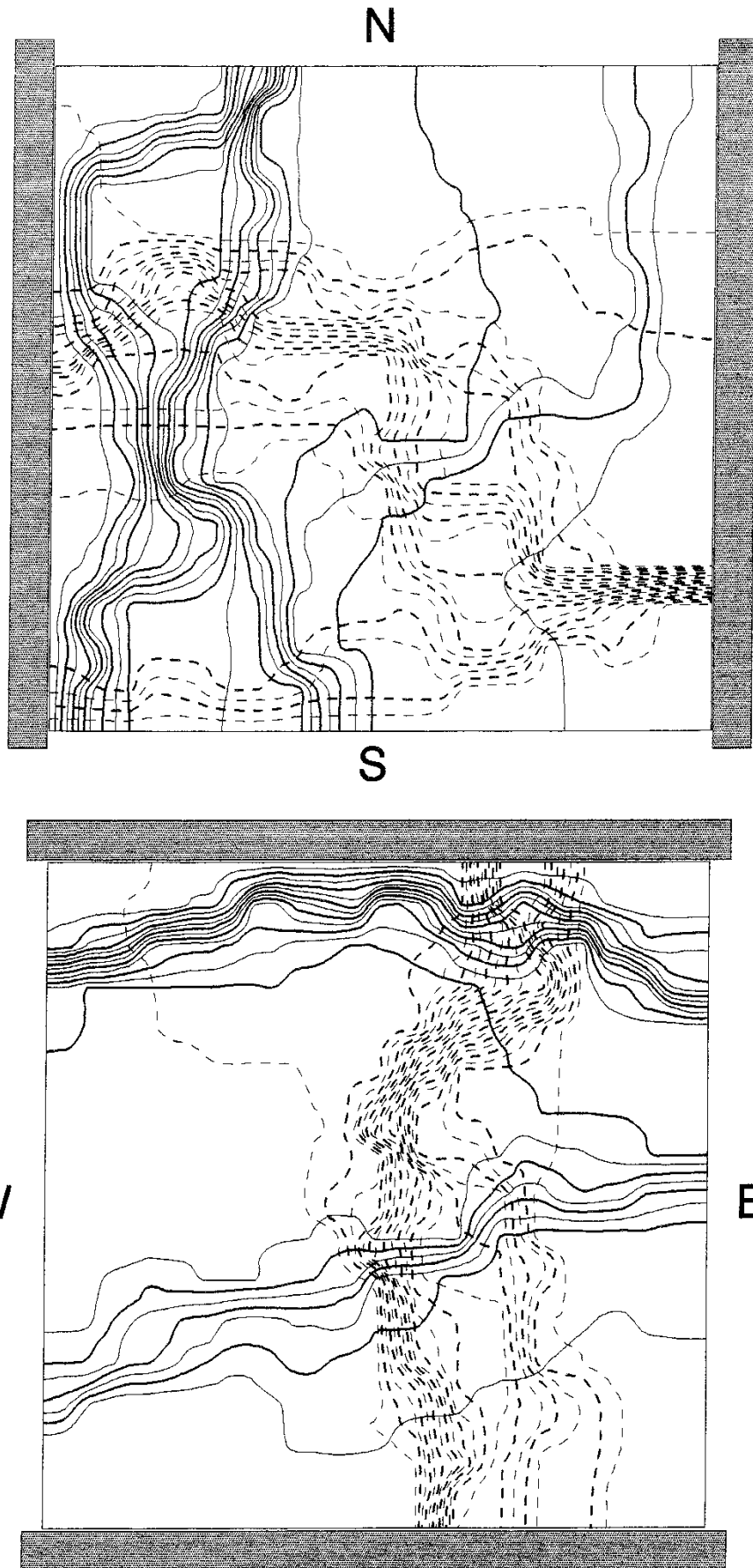
Fig. 17   Flow nets for N/S and W/E flow respectively. N = (16x16) . Each

block is discretized by 4 elements. Piezometric head (dashed) and

stream function levels (solid) are in 5% increments between 0 and 1 .
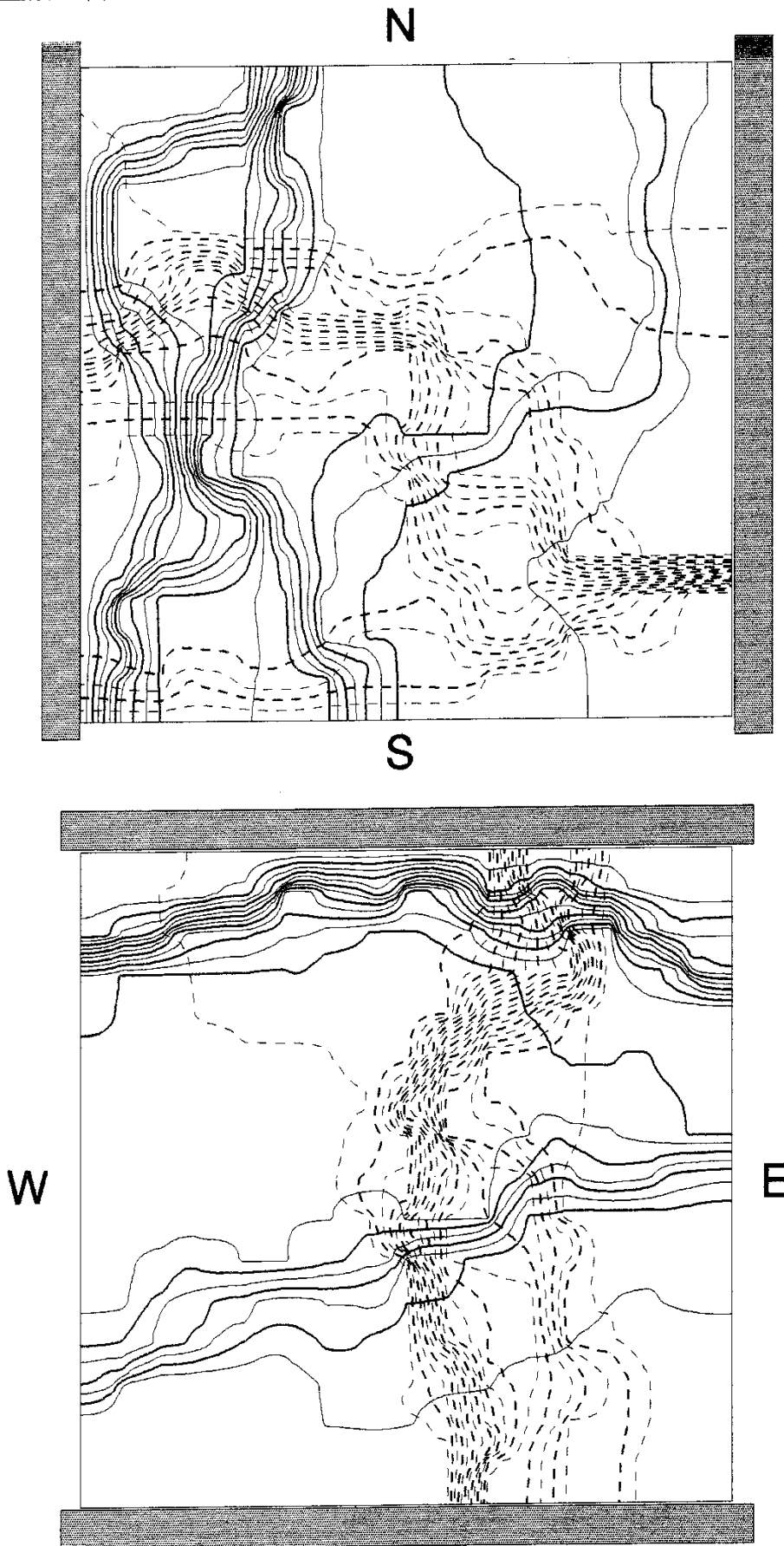
Fig. 18   Flow nets for N/S and W/E flow respectively. N = (16 x 16) . Each
block is discretized by 16 elements. Piezometric head (dashed) and
stream function levels (solid) are in 5% increments between 0 and 1 .
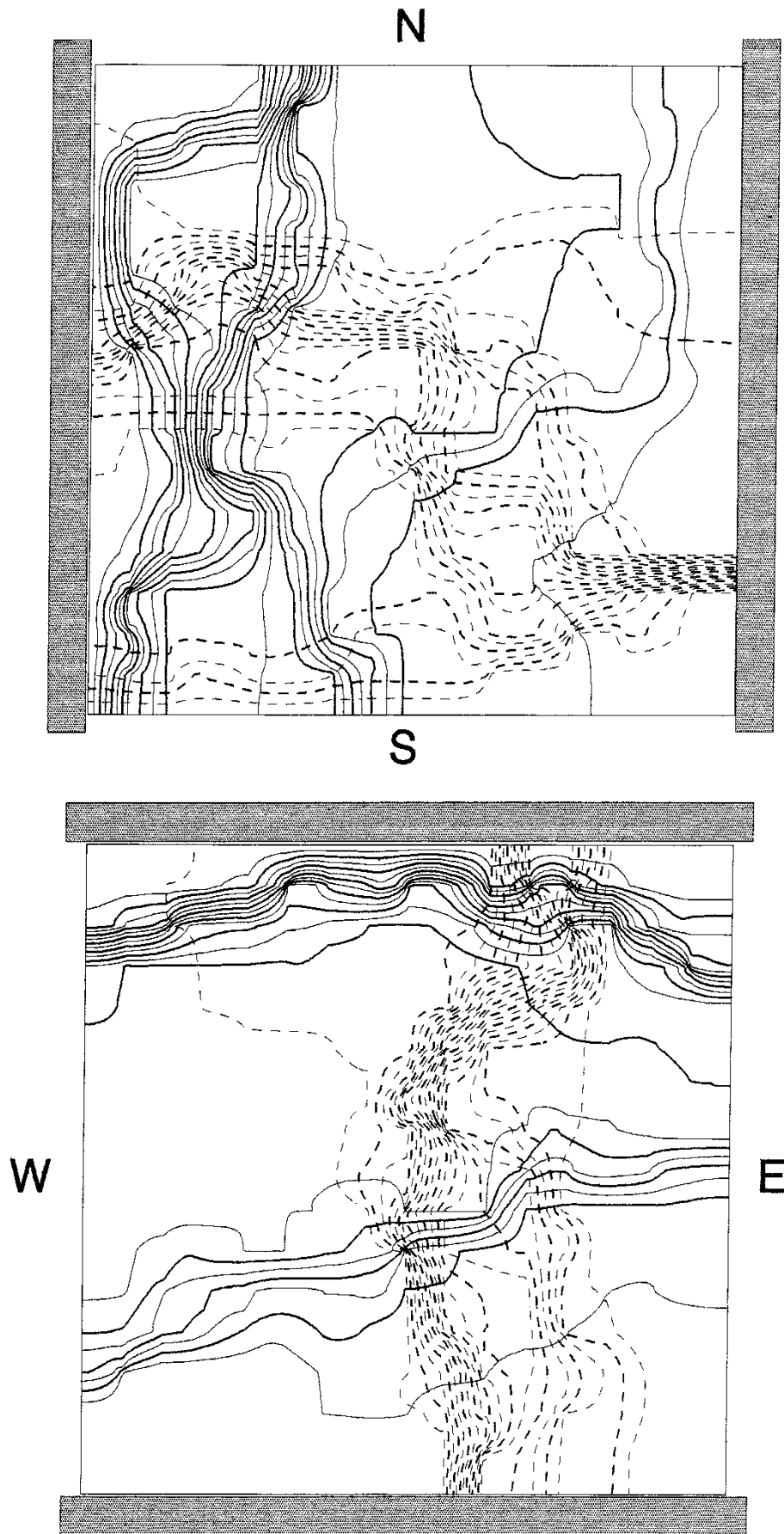
Fig. 19   Flow nets for N/S and W/E flow respectively.   N = (16 x 16) .   Each

block is discretized by 64 elements. Piezometric head (dashed) and

stream function levels (solid) are in 5% increments between 0 and 1 .
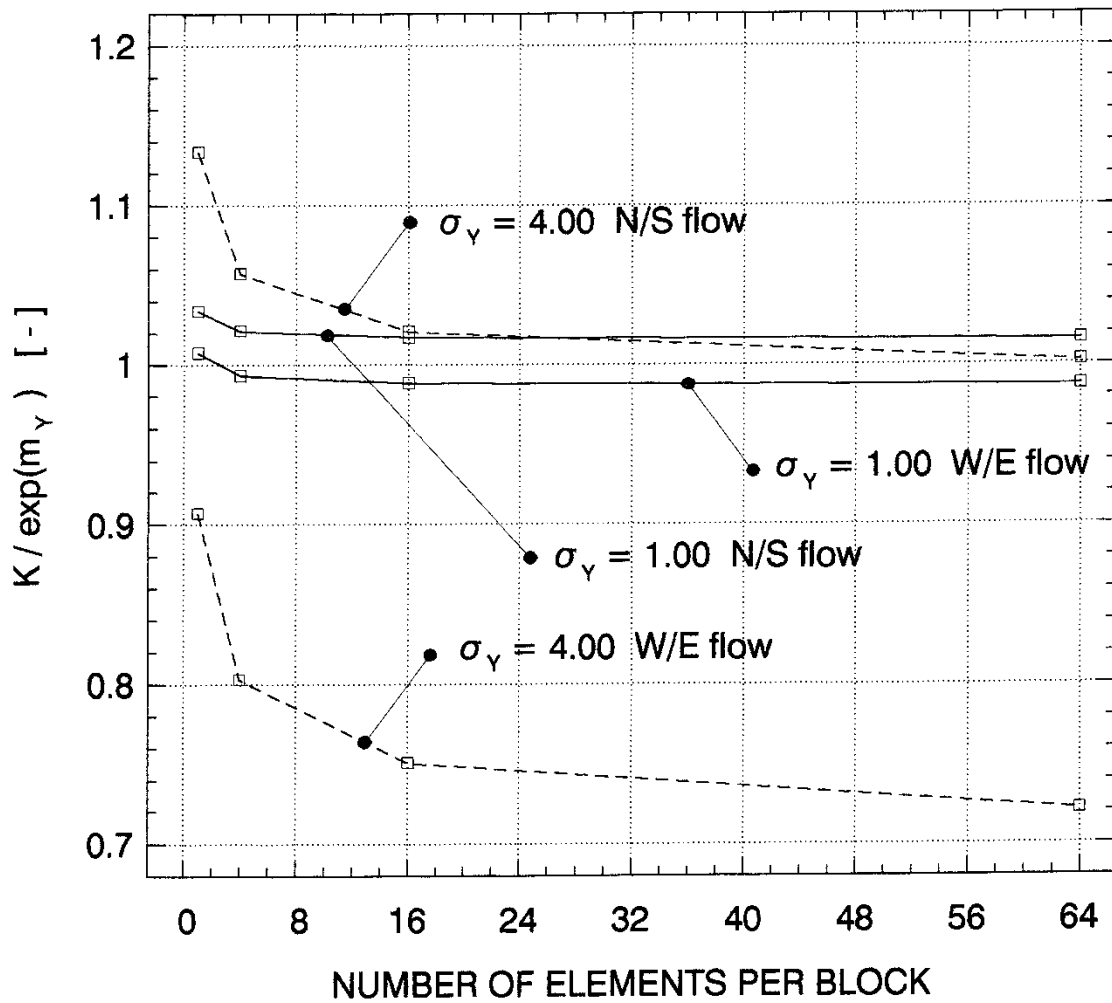
Fig. 20   The effect of different discretizations on the computed value of

K for uniform average flow through a finite heterogeneous

medium in 2-D. N = (16 x 16) and $\lambda/\Delta x = \lambda/\Delta y = 2$.
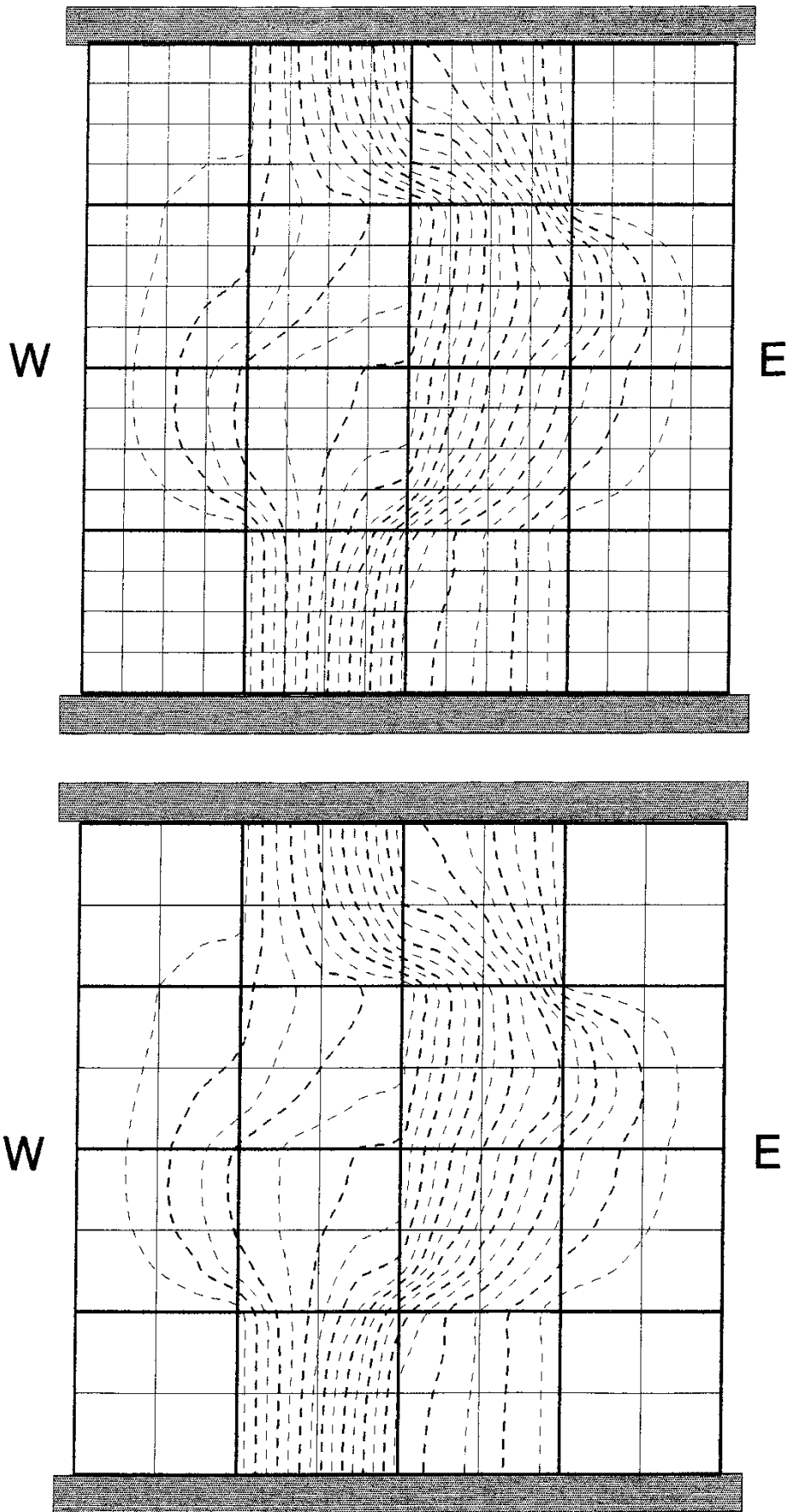
Fig. 21   Comparison of the solutions of the piezometric head (dashed lines)

for N = (4 x 4) between 256 4-node linear rectangles (above) and

64 9-node Lagrangian elements with 9 Gauss points (below).

3.2 Unconditional simulation of block conductivity

The objective of unconditional simulation of block conductivity in this study is to investigate the relationship between the statistical (spatial) geometric mean (K_g) of the local conductivities within a block and the numerically computed block conductivity tensor $(\tilde{K}_S)$ as a function of scale, i.e. block size. The hypothesis is that present statistical upscaling techniques underestimate the conductivity of finite blocks, due to their inability to take the effects of anisotropy into account. The unconditional simulations are divided into two parts: (i) a *bracketing* study and (ii) a *Monte Carlo* study. A general description of such studies is provided by, e.g. Peck *et al.* [1988] and Freeze *et al.* [1990].

The aim of the bracketing study used here is to identify the main differences between statistical and hydraulic averaging over the range of variability of the log-conductivity field $(Y(x))$ so as to optimize the subsequent Monte Carlo study. In Figure 22, the chart used in the bracketing study is shown. Two performance measures are used, namely the *statistical relative error* in K_G and the *hydraulic relative error* in K_G, denoted RE_s and RE_h, respectively. RE_s and RE_h are defined as

$$RE_s = \frac{(K_g - K_G)}{K_G} \tag{44a}$$

$$RE_h = \frac{(K_{ii} - K_G)}{K_G} \qquad i = 1,2 \tag{44b}$$

The behaviour of the spatial geometric point mean as a point estimator for K_G, i.e. $K_g = exp(m_Y)$, is discussed in Chapter 2. Figures 23 and 24 graphically demonstrate the behaviour of RE_s for different values of σ_Y, λ_Y, and N. The *PDF*s are clearly skewed for small values of N which suggest that $<K_g> \geq K_G$ for finite blocks.

- 63 -

The bracketing study comprises nine cases of hypothetical realizations where N = 64×64 and $Y(x) \in N(-16, \sigma_Y, \lambda_Y)$. One subset of the nine cases differs in the correlation length, i.e. $\lambda_Y/\Delta x = \lambda_Y/\Delta y = \{0, 2, 4\}$, whereas a second subset differs in the standard deviation, i.e. $\sigma_Y = \{0.25, 1, 4\}$. The three values of σ_Y correspond to (*i*) an approximately homogeneous medium, (*ii*) the upper limit of the first-order approximation of $Y(x)$ [see, e.g. Gutjahr *et al.*, 1978], and (*iii*) the observed spatial variability of $ln(K)$ for 3m packer tests, respectively. Each of the nine cases is investigated by means of ten realizations. The realizations are subjectively chosen so that they spread evenly about RE_s = 0 for σ_Y = 0.25. The results are shown in Figures 25 and 26. Beginning with Figure 25, it is noteworthy that the uncorrelated cases show a constant offset while keeping the unit slope. This effect is interpreted as an artifact of the first-order accurate flux solution [cf. Durlofsky, 1991]. The same observation is made by Cacas *et al.* [1991] who also make a similar comparison for a finite difference method. For the correlated cases, however, the limitation of using linear rectangles is less significant. The explanation is that a correlation in the conductivity field implies less contrasts between adjacent model blocks thus a better flux solution. For σ_Y = 4, the spreading in RE_h around the unit slope increases drastically, i.e. an increasing anisotropy is observed. At the same time there appears to be a shift in RE_s to the right.

The approach behind Figure 26 is somewhat unusual and calls for an explanation. Ten realizations of equal probability are generated but only *one* of them is of interest in terms of conductivity values, i.e. the data of the considered realization are conditioned upon the spatial structures of the remaining nine realizations by comparing the probability density functions (*PDF*'s). In this way ten equally probable realizations are obtained that differ in the spatial variability but not in the conductivities. The results in Figure 26 demonstrate that for N = 64×64 ((192m)^2) and σ_Y = 4, the spatial variability is important for the block conductivity.

In the Monte Carlo study, the relationship between the block conductivity and the statistical (spatial) geometric mean of the local conductivities within a block is investigated thoroughly. Six quadratic block sizes are studied. These are symmetrically delineated around the centre of a synthetically generated realization of random (disordered) heterogeneity. The realization consists of $N = 64\times64$ (4,096) local conductivity values defining the scale of support. The six block sizes are $N = \{2\times2, 4\times4, 8\times8, 16\times16, 32\times32, 64\times64\}$. Each block size is studied by a Monte Carlo approach consisting of 800 realizations. All realizations are considered to be finite replicates of the infinite medium defined by (32).

The mean and standard deviation of the infinite medium are set to $\mu_Y = -16$ and $\sigma_Y = 4$, respectively. Three different correlation lengths are studied, i.e. $\lambda_Y/\Delta x = \lambda_Y/\Delta y = \{0, 2, 4\}$. An exponential variogram is assumed for the latter cases (see (29)). These parameter values are characteristic of the statistics of 3m packer tests down to depths of about 500m in Swedish fractured hard rock. For each realization and each block size, both the spatial geometric mean of the local conductivity values and the conductivity in two orthogonal directions are computed. The results from the Monte Carlo study are shown in Figures 27-36 and are summarized as follows:

The 18 scatter plots shown in Figures 27-29 reveal that the principal relation between K_g and the two orthogonal components of $\tilde{K}_S$, denoted K_{xx} and K_{yy} (or K_{11} and K_{22}), respectively, is basically linear although the spreading about the unit slope is highly dependent on both the block size and the correlation length. Hence, K_g, K_{xx} and K_{yy} are all random variables [cf. Sagar, 1978].

Figure 30 demonstrates that $<K_g>/K_G$ decreases with an increasing block size, and reinforces the aforementioned impression that the limits of $<K_g>$ for finite blocks are governed by the arithmetic and geometric means, respectively, of the underlying probability density function of the local conductivity values.

Figures 31-33 show the expected value of the ratio between the block conductivity and the corresponding spatial geometric mean for the three correlations, i.e. $\lambda_Y/\Delta x = \lambda_Y/\Delta y = \{0, 2, 4\}$. In spite of the numerical problems caused by using linear rectangles, it is demonstrated that the ratio between $K_{max} = max(K_{11}, K_{22})$ and K_g is on *average* greater than or equal to unity, i.e. $<K_{max}/K_g> \geq 1$, and that the ratio between $K_{min} = min(K_{11}, K_{22})$ and K_g is on *average* less than or equal to unity, i.e. $<K_{min}/K_g> \leq 1$.

Figures 32 and 33 demonstrate that the maximum ratio of $<K_{max}/K_g>$, for $\lambda_Y/\Delta x = \lambda_Y/\Delta y = \{0, 2, 4\}$, is obtained for a block size that is approximately equal to the range of the correlation. For the exponential variogram used here, $R \simeq 4 \lambda_Y$ and the maximum values occur at 24m and 48m, respectively.

The effect of increasing the discretization is shown in Figure 34. A major improvement is obtained with four linear elements per block, and further slight improvement is obtained with increasing discretization.

Figure 35 shows the expected value of the ratio between the two orthogonal components of the block conductivity for $\lambda_Y/\Delta x = \lambda_Y/\Delta y = \{0, 2, 4\}$. It is demonstrated that the ratio K_{11}/K_{22} is on *average* equal to the ratio K_{22}/K_{11} and that these ratios are on *average* greater than or equal to unity, i.e. $<K_{11}/K_{22}> = <K_{22}/K_{11}> \geq 1$. Furthermore, the maximum value is obtained for a block size that is approximately equal to the range of the correlation. It should be noted that the results in Figure 35 are found to be *independent* of the discretization.

Figure 36 shows the expected value of the log-conductivity standard deviation. For $\lambda_Y/\Delta x = \lambda_Y/\Delta y = 4$, it is found that the decrease in uncertainty with the block size mimics the reported field findings shown in Figure 7.
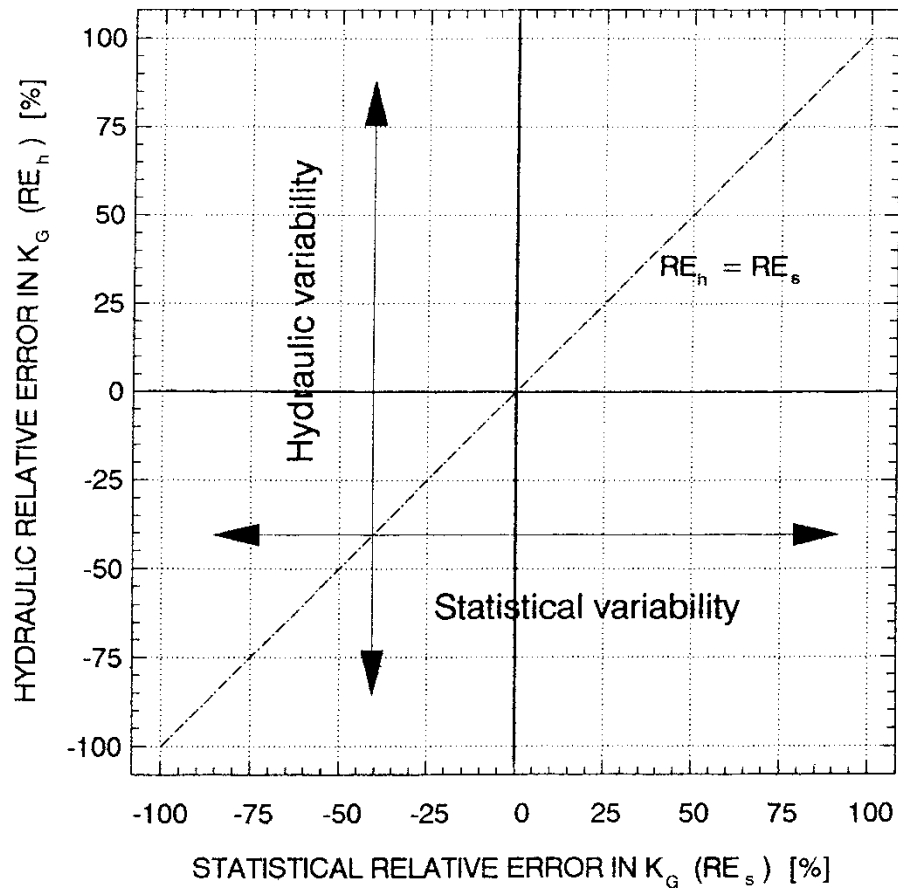
Fig. 22 Chart for comparing statistical (RE_s) and hydraulic (RE_h) relative errors in K_G for different realizations of uniform average flow through a finite heterogeneous medium in 2-D.
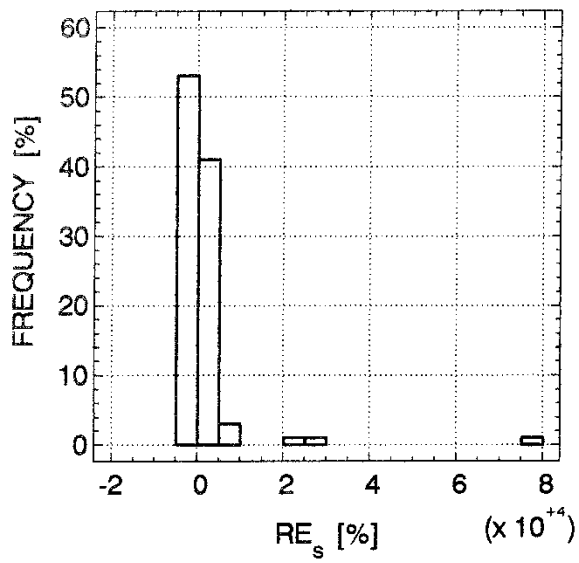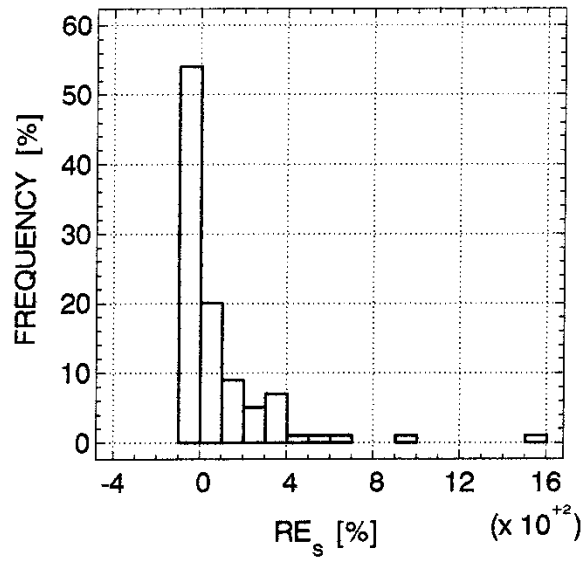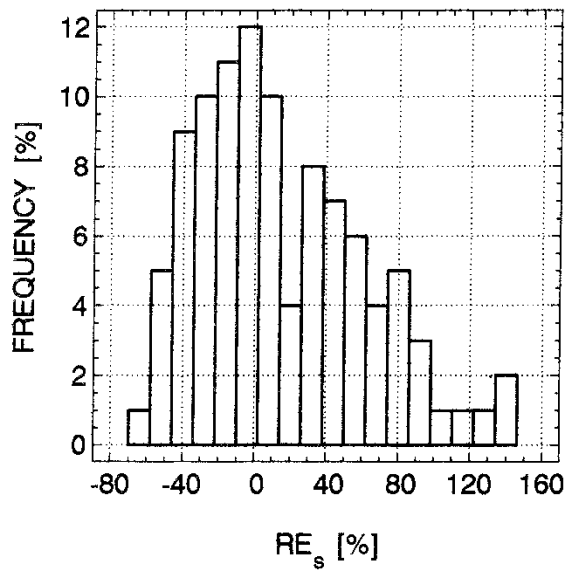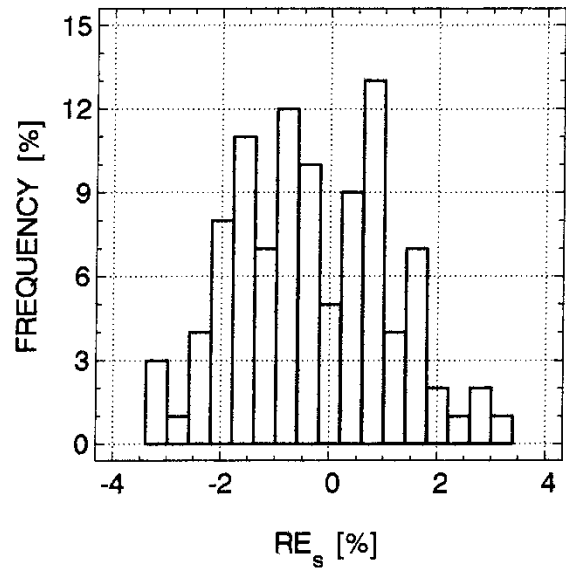
Fig. 23 Histograms of the statistical relative error in K_G (RE_s) for

100 realizations of $\lambda/\Delta x = \lambda/\Delta y = 2$ and $\sigma_Y = 4.00$.

$N = (4\text{x}4 , 16\text{x}16 , 64\text{x}64 , 256\text{x}256)$.
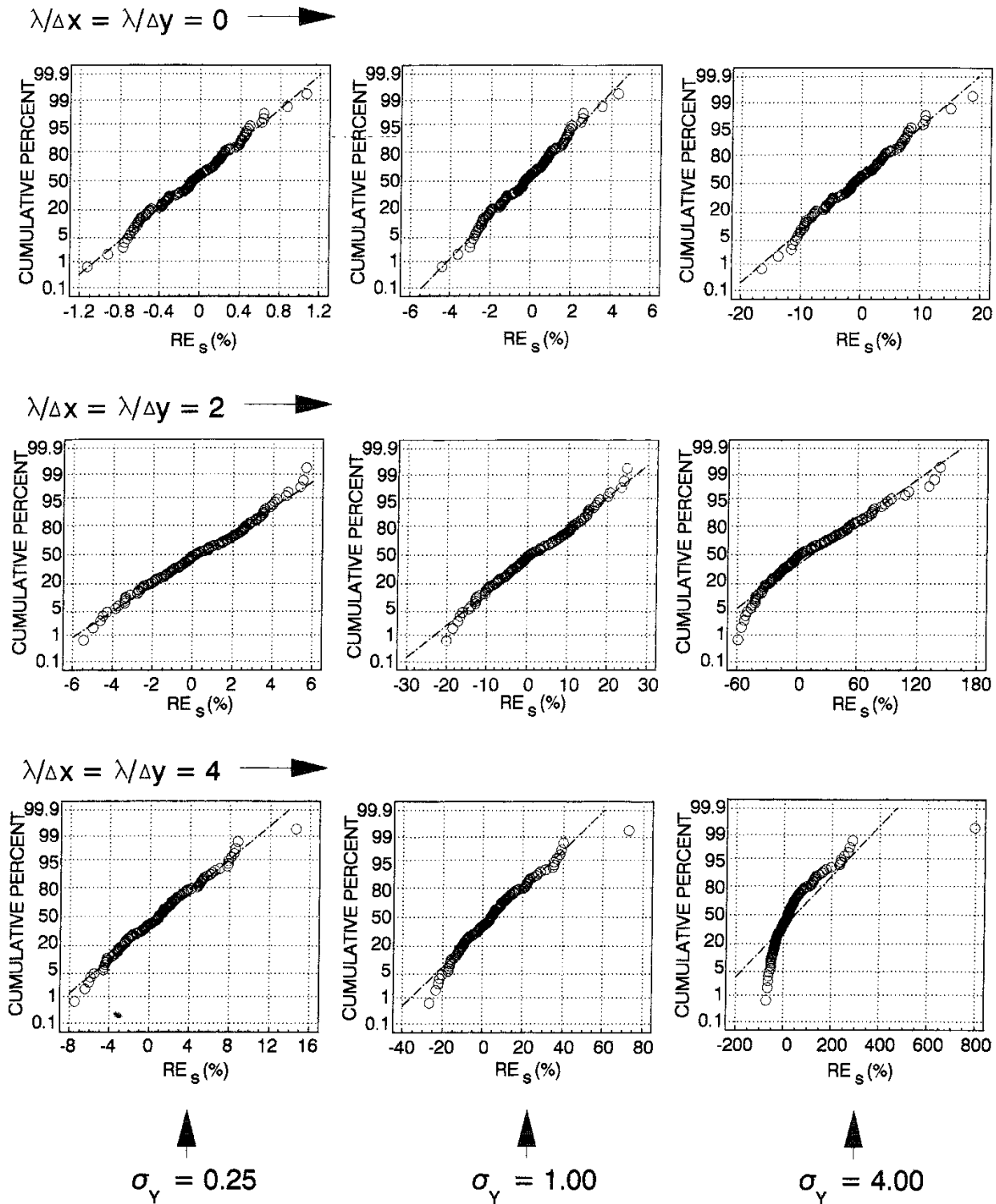
Fig. 24 Normal probability plots of the statistical relative error in K_G (RE_s) for 100 realizations of $N = (64 \times 64)$.
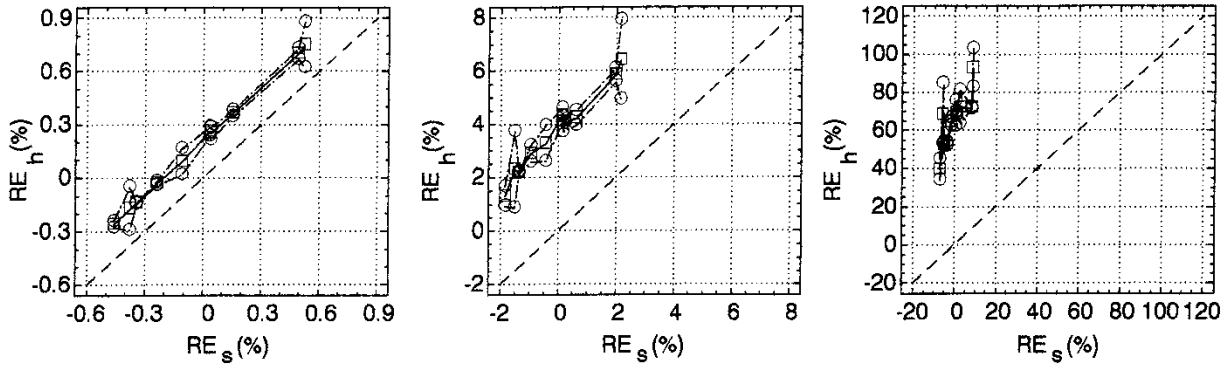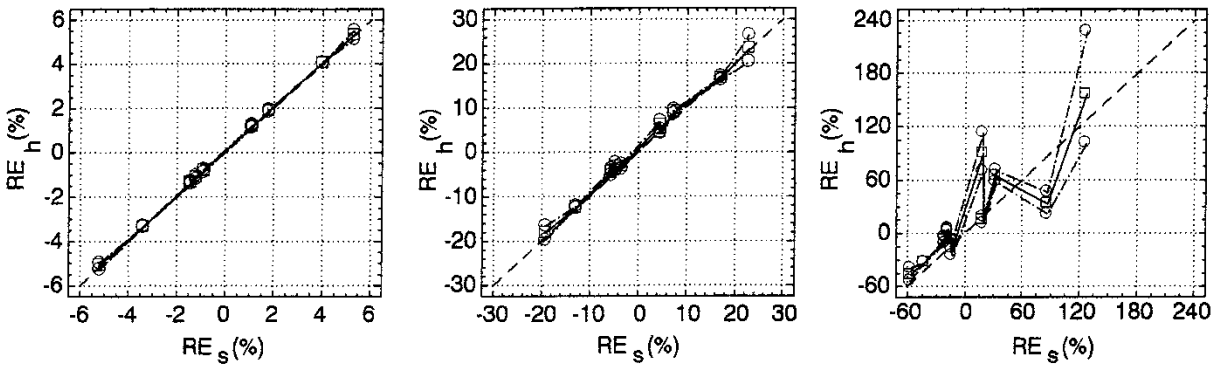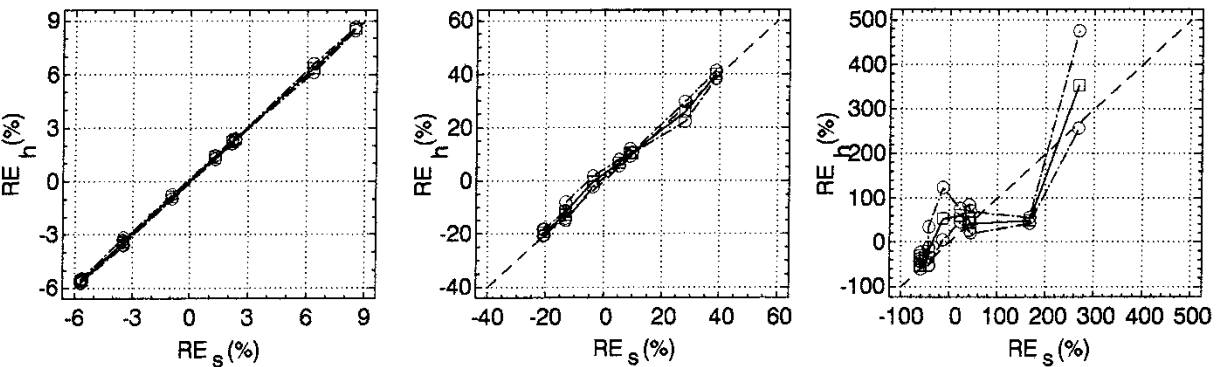
Fig. 25 Hydraulic relative errors in K_G (RE_h) versus statistical relative errors in K_G (RE_s) for ten realizations of uniform average flow through a finite heterogeneous medium in 2-D. N = (64 x 64).
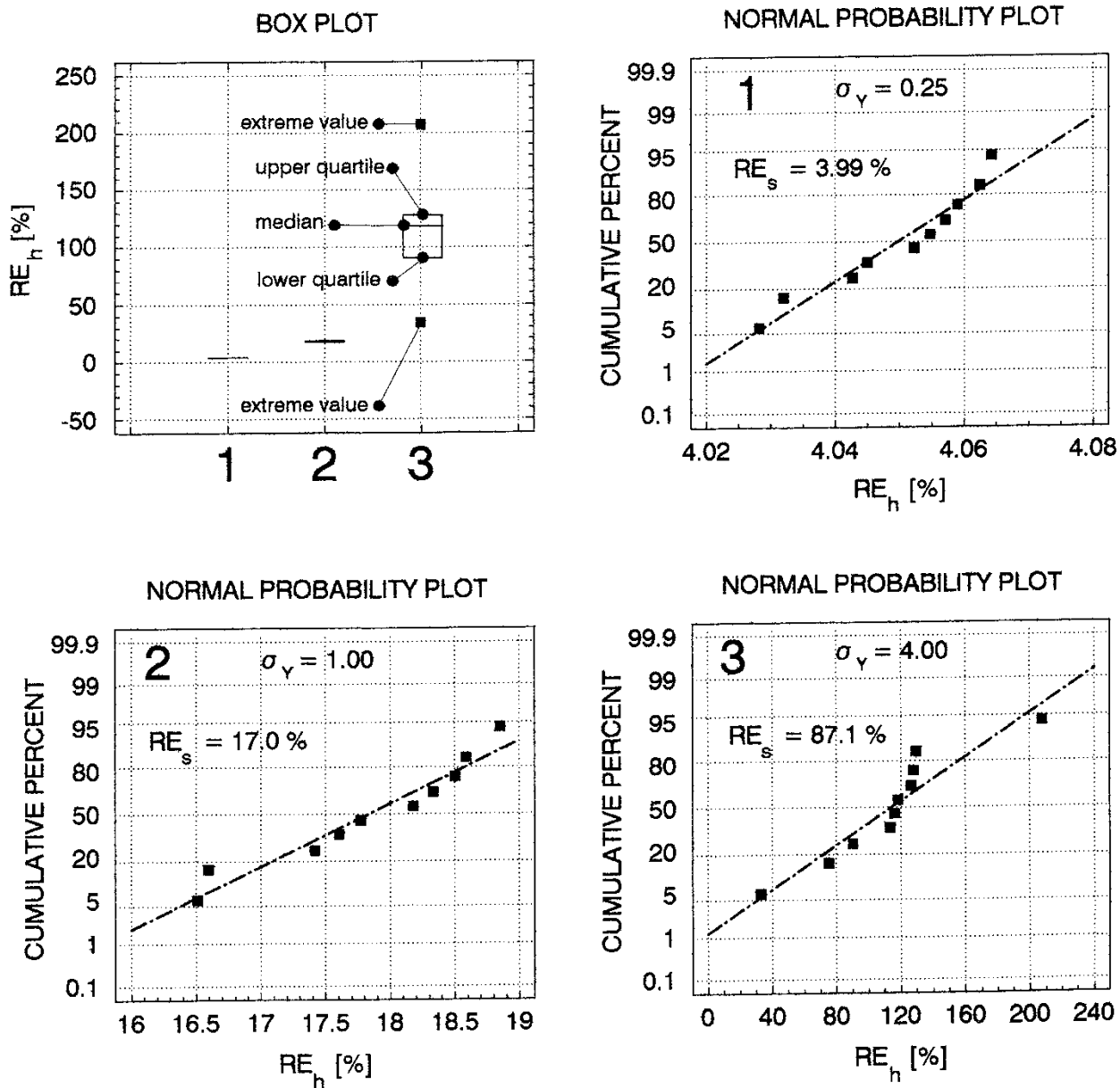
Fig. 26 Observed variability in the hydraulic relative error in K_G (RE_h) for uniform average flow through ten equally probable spatial distributions of a single realization of a finite heterogeneous medium in 2-D. N = (64 x 64) and $\lambda/\Delta x = \lambda/\Delta y = 2$.

$$RE_h = (\sqrt{(K_{xx} K_{yy})} - K_G) / K_G .$$
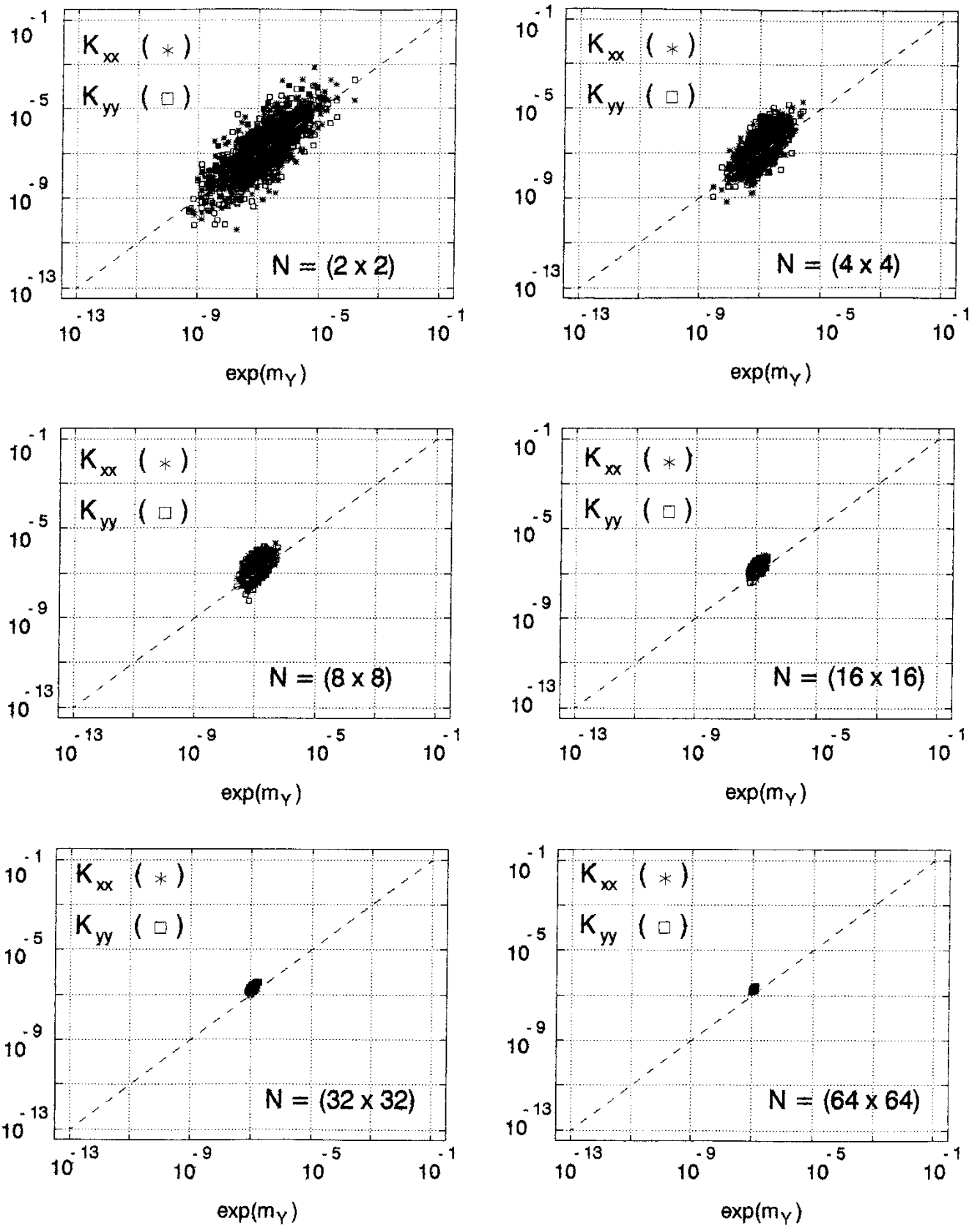
Fig. 27 Scatter plots of K vs. exp(m_Y) for 800 realizations of $\lambda/\Delta x = \lambda/\Delta y = 0$. $\sigma_Y = 4.00$.
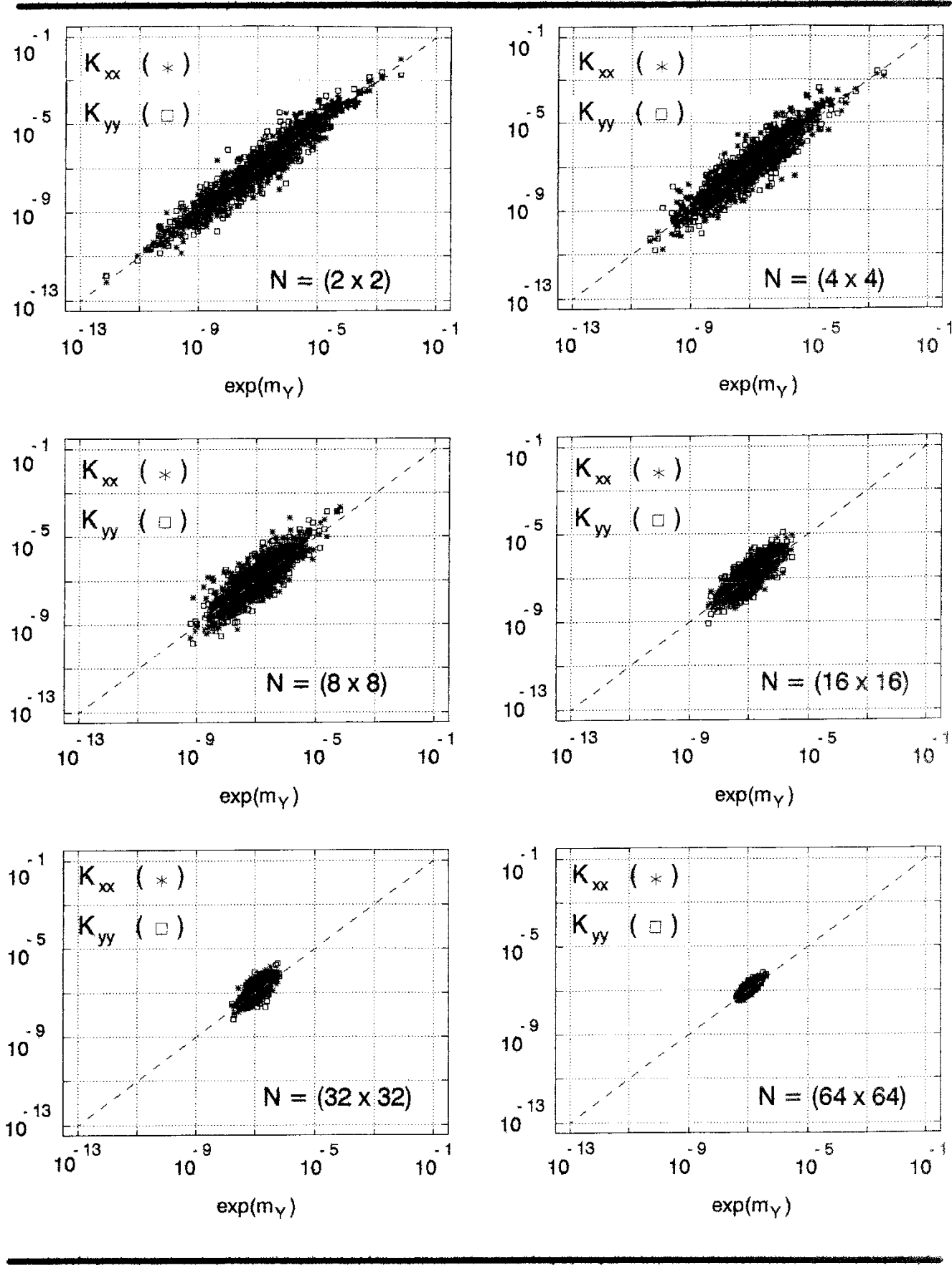
Fig. 28 Scatter plots of K vs. $\exp(m_Y)$ for 800 realizations of $\lambda/\Delta x = \lambda/\Delta y = 2$. $\sigma_Y = 4.00$.
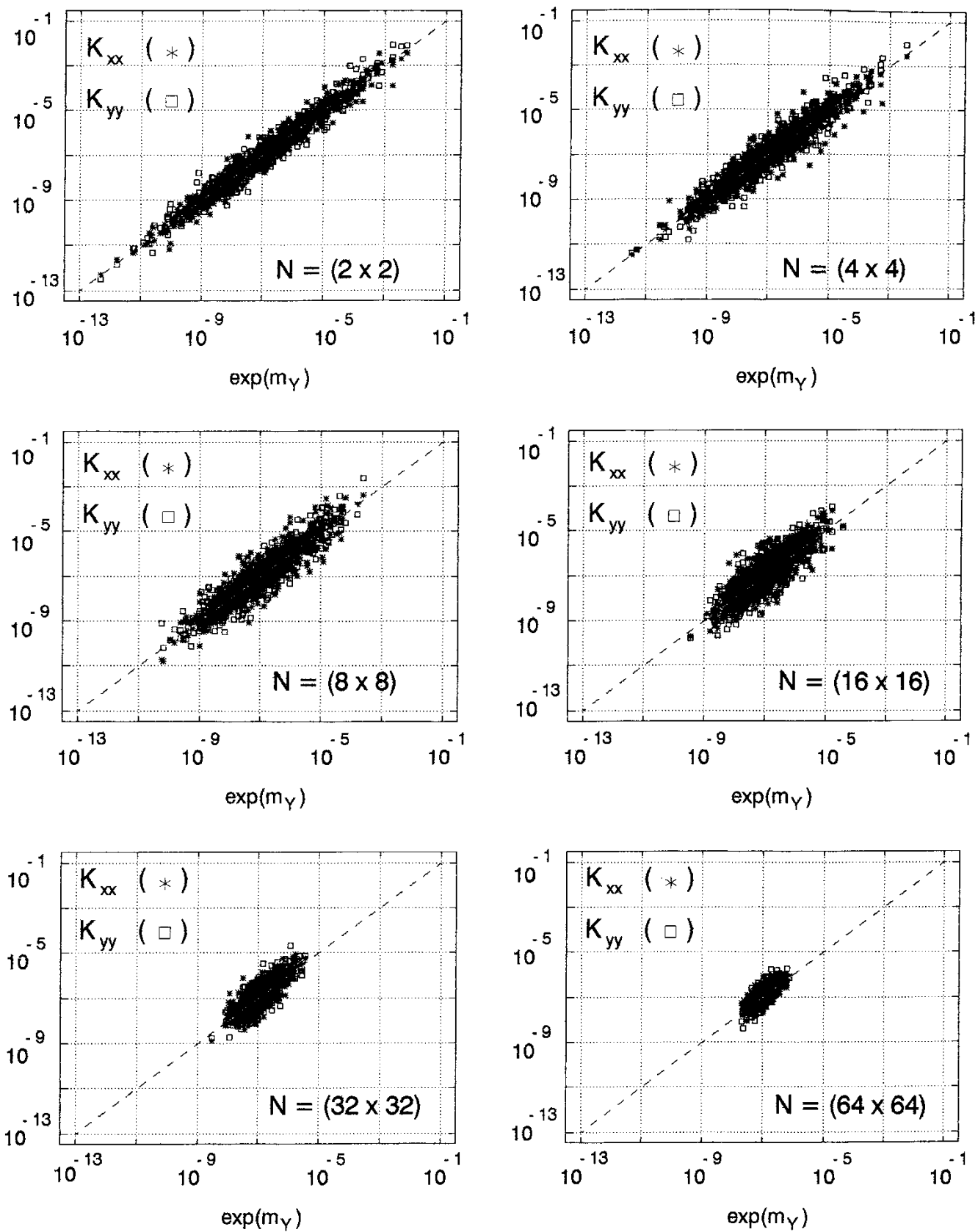
Fig. 29   Scatter plots of K vs. exp(m$_Y$) for 800 realizations of
$\lambda/\Delta x = \lambda/\Delta y = 4$. $\sigma_Y = 4.00$.
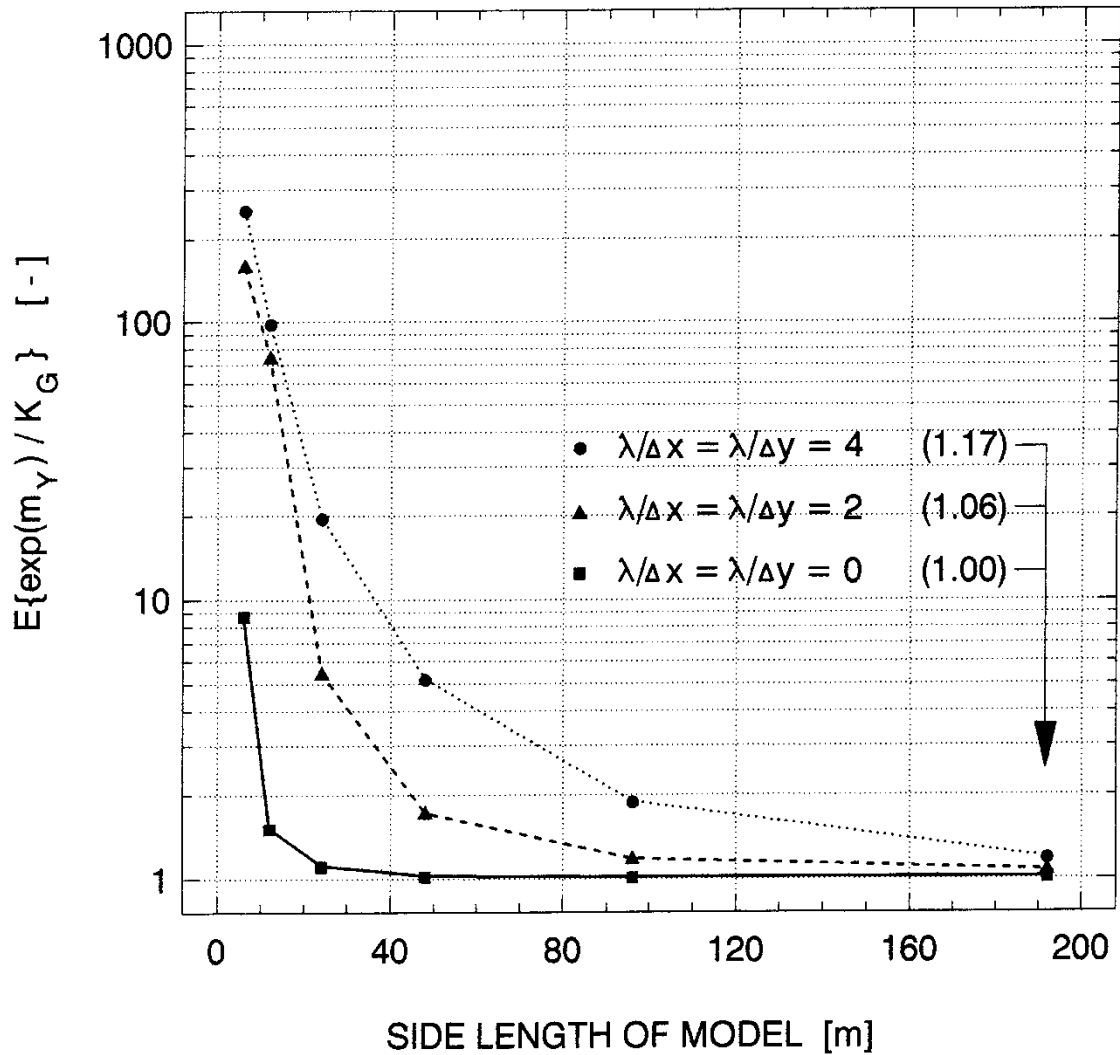
Fig. 30 E{exp(m$_Y$) / K$_G$} vs. model size. σ_Y = 4.00.

800 realizations of N = (2x2, 4x4, 8x8, 16x16, 32x32, 64x64).

$\Delta x = \Delta y$ = 3m.

(a) 1 element/block

(b) 4 elements/block

Fig. 31 E{K / exp(m$_Y$)} vs. model size. σ_Y = 4.00 . $\lambda/\Delta x = \lambda/\Delta y = 0$.

800 realizations of N = (2x2, 4x4, 8x8, 16x16, 32x32, 64x64).

$\Delta x = \Delta y = 3m$.

(a) 1 element/block

(b) 4 elements/block

Fig. 32 E{K / exp(m$_Y$)} vs. model size. σ_Y = 4.00 . $\lambda/\Delta x = \lambda/\Delta y = 2$.

800 realizations of N = (2x2, 4x4, 8x8, 16x16, 32x32, 64x64).

$\Delta x = \Delta y = 3m$.

(a) 1 element/block

(b) 4 elements/block

Fig. 33 $E\{K / \exp(m_Y)\}$ vs. model size. $\sigma_Y = 4.00$. $\lambda/\Delta x = \lambda/\Delta y = 4$.

800 realizations of $N = (2\times2, 4\times4, 8\times8, 16\times16, 32\times32, 64\times64)$.

$\Delta x = \Delta y = 3m$.
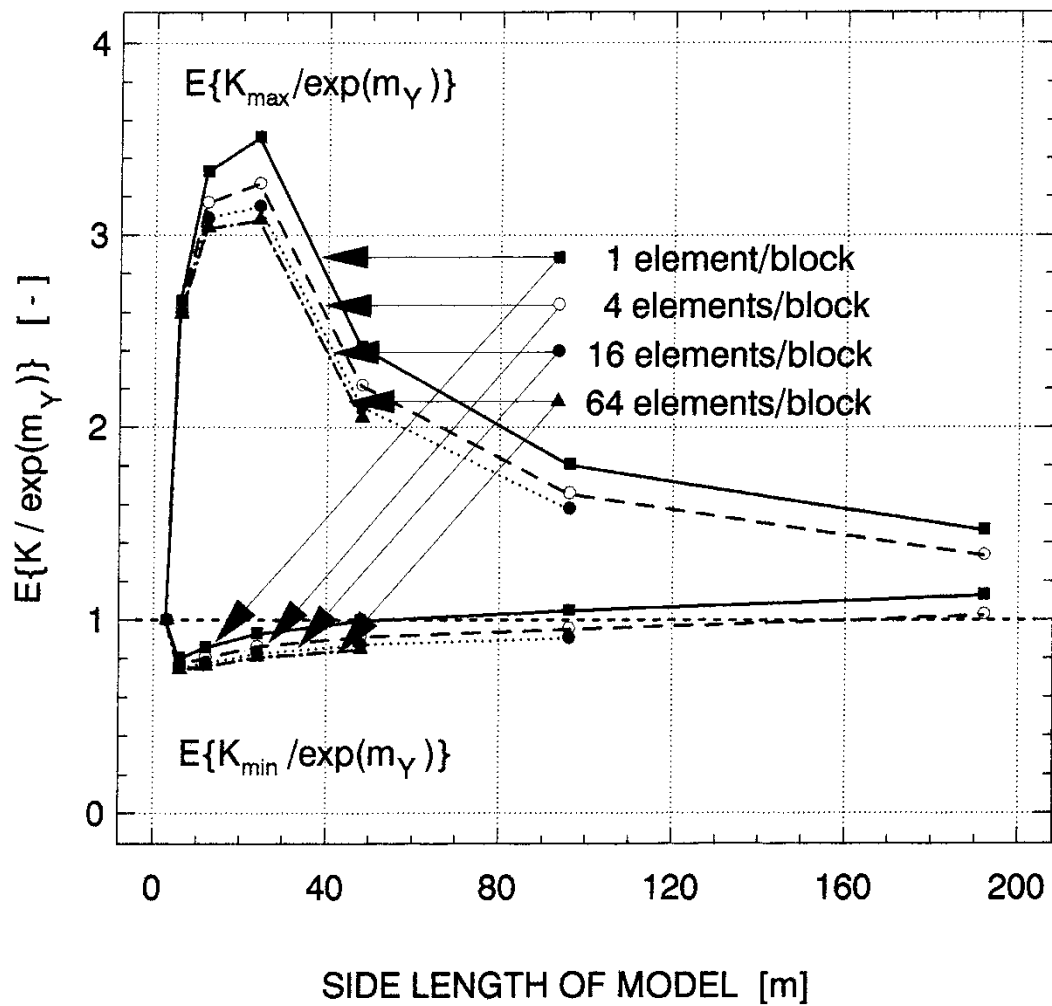
Fig. 34 $E\{K / \exp(m_Y)\}$ vs. model size. $\sigma_Y = 4.00$. $\lambda/\Delta x = \lambda/\Delta y = 2$.

800 realizations of $N = (2x2, 4x4, 8x8, 16x16, 32x32, 64x64)$.
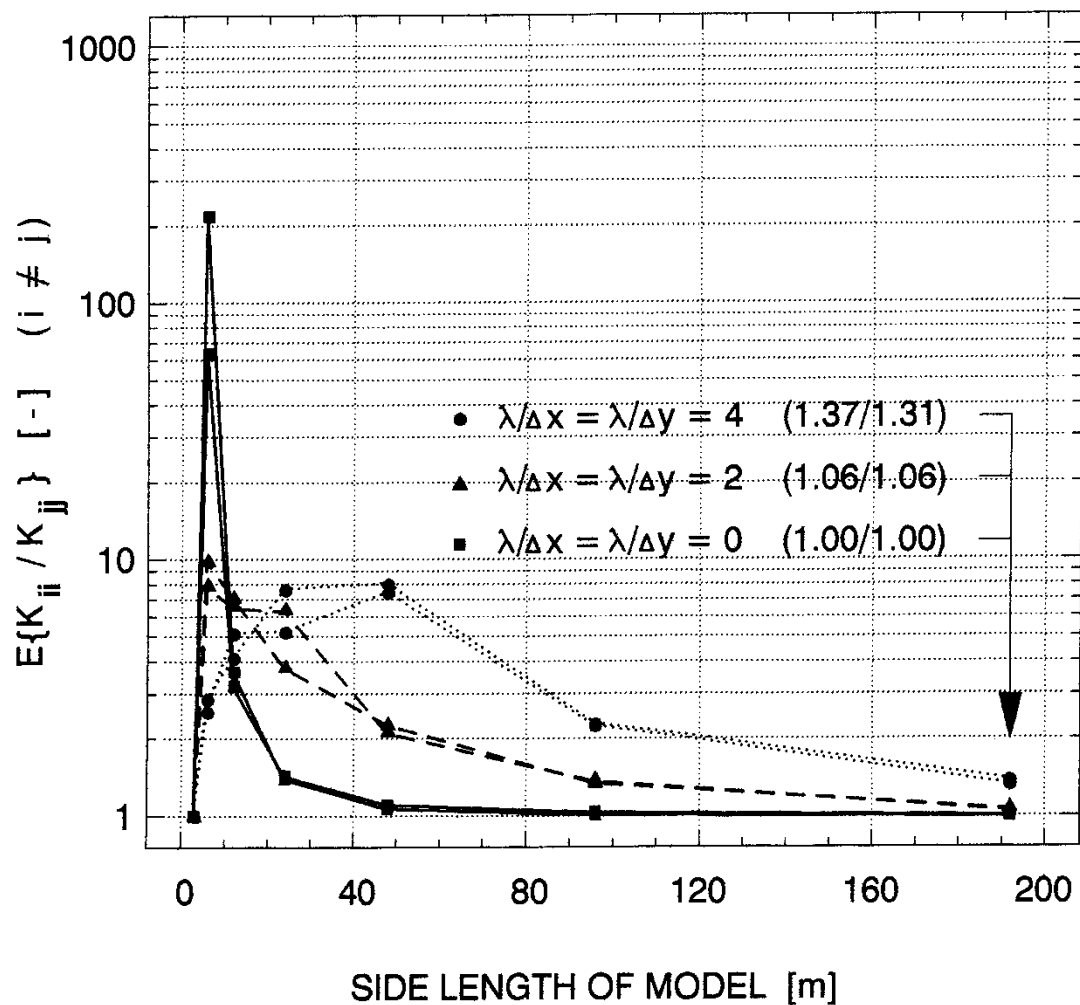
$\Delta x = \Delta y = 3m$.

Fig. 35 $E\{K_{ii} / K_{jj}\}$ $(i \neq j)$ vs. model size. $\sigma_Y = 4.00$.

The finite element discretization is 4 elements/block .

800 realizations of N = (2x2, 4x4, 8x8, 16x16, 32x32, 64x64).
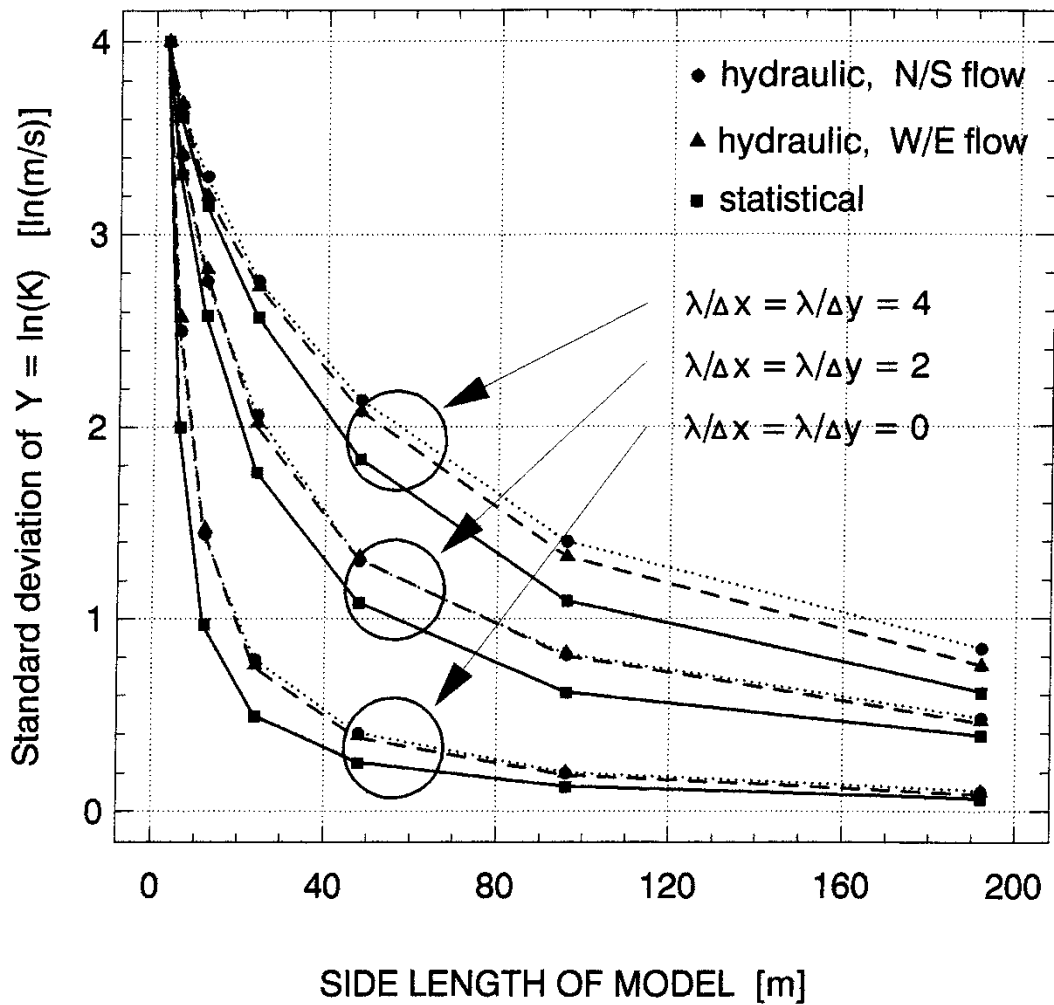
$\Delta x = \Delta y = 3m$.

Fig. 36 Standard deviation of Y = ln(K) vs. model size. σ_Y = 4.00 .

The finite element discretization is 4 elements/block .

800 realizations of N = (2x2, 4x4, 8x8, 16x16, 32x32, 64x64).

$\Delta x = \Delta y$ = 3m .

It is important to have good understanding of the flow field prior to any numerical simulation of solute transport in a heterogeneous conductivity field. The present study adopts the dual formulation of flow for steady flow in two dimensions to compute flow patterns for a few different cases of random heterogeneity. Frind & Matanga [1985] conclude that the stream function (Ψ) solution can give superior accuracy in the definition of the velocity field required for transport simulations. The objectives of the experiments undertaken here are (*i*) to validate the implementation of the flow model to allow for high conductivity contrasts, and (*ii*) to improve the understanding of the interaction between σ_Y and λ_Y and their impact on the spatial variability of the flux field, i.e. the specific discharge (q).

Because the conductivity is a random function, the specific discharge is a random vector function. It is considered that a Gaussian plume shape is established when the velocity field is uncorrelated provided that ergodicity is achieved [see, for example, Dagan, 1984; Shapiro & Cvetkovic, 1988; Naff, 1990]. Therefore, each flow pattern computed here is accompanied by a brief statistical analysis of the correlation structure of the flux field. It is stressed that these analyses are neither intended nor valid for any inference about the statistics of the ensemble.

Nine different realizations of $N = 64 \times 64$ and $N(-16, \sigma_Y, \lambda_Y)$ are generated and analysed. One subset of the nine realizations differs in the correlation length, i.e. $\lambda_Y/\Delta x = \lambda_Y/\Delta y = \{0, 2, 4\}$, whereas a second subset differs in the standard deviation, i.e. $\sigma_Y = \{0.25, 1, 4\}$. The three values of σ_Y correspond to (*i*) an approximately homogeneous medium, (*ii*) the upper limit of the first-order approximation of $Y(x)$, and (*iii*) the observed spatial variability of $ln(K)$ for 3m packer tests, respectively. On basis of the results obtained previously, each support block of the flow model is discretized with four linear rectangles, which gives a total of 16,384 elements and

16,641 nodes, see Figure 38. In addition to the common assumption of a homogeneous effective (kinematic) porosity n for the computation of the (transport) velocity $v(x)$, the case of a heterogeneous porosity $n(x)$ is also studied, although under the limiting assumption of a positive linear correlation, that is to say $ln(n(x)) \propto ln(K(x))$. In other words, upon application of the advection-dispersion equation (36), it is implicitly assumed that n is uniform. If n is a non-uniform, Dagan [1989] gives the following equation

$$\frac{\partial C}{\partial t} + v \cdot \nabla C = \frac{1}{n}\nabla \cdot (n \; \tilde{D} \; \nabla C) \qquad (45)$$

According to, for example, Gelhar et al. [1979] and Matheron & de Marsily [1980] the spatial variability in n may be neglected in most circumstances for porous media. Smith & Schwartz [1981] investigated numerically the effects of various correlations between the effective porosity and the spatial variability in the conductivity. They concluded that the influence of spatial variability in n on the solute exit location and the breakthrough curve is marginal. Cvetkovic & Shapiro [1989] studied a positively correlated porosity field in relation to a layered medium. They concluded that a variability in n delays the arrival time and increases the peak of the breakthrough curve in comparison with a uniform effective porosity. In the present study, the relationship given by (46) is adopted in those experiments where n is a random variable [cf. Carlsson & Olsson, 1981; Winberg et al., 1990]

$$ln(n(x)) = 0.34 \; ln(K(x)) \qquad (46)$$

In the following, a number of figures are shown. In short, Figures 39-54 deal with $\lambda_Y/\Delta x = \lambda_Y/\Delta y = 2$, Figures 55-59 with $\lambda_Y/\Delta x = \lambda_Y/\Delta y = 0$, and Figures 60-64 with $\lambda_Y/\Delta x = \lambda_Y/\Delta y = 4$. The study focuses on $\sigma_Y = 4$, and the corresponding realizations are denoted 4-22, 4-00, and 4-44, respectively. The statistical analyses

of the flux fields are carried out predominantly for the (natural) logarithm of the magnitude of the resultant flux vector, i.e. $ln(q(\mathbf{x}))$, where $q(\mathbf{x}) = |\mathbf{q}(\mathbf{x})|$. In one case, however, the analysis is also done for the natural value of the resultant flux vector as well as for its directional components. It is important to note that because the finite-element model used is implemented with linear rectangle elements, i.e. bi-linear interpolation functions, the computations of the longitudinal and transverse components of the flux correspond to a point that coincides with the *centroid* of each element. The flux components are obtained by computing the gradients of the piezometric head (φ) in two orthogonal directions and using Darcy's law, see (14).

Beginning with Figures 39, 55, and 60, the conductivity fields in these figures correspond to the three realizations 4-22, 4-00, and 4-44, respectively. An explanation of the information in these figures has previously been given in relation to Figure 12. Figures 40-45 show the magnitude of the specific discharge field for $\lambda_Y/\Delta x = \lambda_Y/\Delta y = 2$ and $\sigma_Y = \{0.25, 1, 4\}$ in terms of raster graphics and equidistant streamlines. Figures 46-48 show the equidistant streamlines separated from the raster graphics. The discharge between two adjacent streamlines is given by $\Delta Q = \Delta\Psi$ (see (10) and (11)). In this case, ΔQ is chosen to represent 5% of the total discharge. This value of ΔQ applies to Figures 56-58 and Figures 61-63 as well. In Figures 52, 59, and 64, the statistical analyses of $ln(q(\mathbf{x}))$ for 4-22, 4-00, and 4-44, respectively, are shown. In Figures 49-51, the statistical analysis for realization (case) 4-22 is extended to deal with the natural value of the resultant flux vector as well as its directional components parallel and perpendicular to the mean direction of flow. Finally, Figures 53-54 show the differences between uniform and positively correlated porosity fields. The following results are obtained in the qualitative analyses of the different flow patterns and the statistical analyses of the flux fields:

Figures 39, 44, and 45 demonstrate that the patches of low conductivity generally correspond to patches of low flow, whereas the patches of high conductivity do not necessarily correspond to patches of high flow. Accordingly, the phenomenon of preferential flow paths (channelling) appears to be related to the correlation structure of the low conductivity patches.

Figures 48, 58, and 63 show that the number of channels and their relative strength, i.e. streamline density, differ markedly between uncorrelated and correlated conductivity fields. It is observed that an uncorrelated field contains several minor channels of weak intensity, whereas a correlated field contains one or a few major channels of great intensity depending on the correlation length (λ_Y). For instance, it is demonstrated in Figures 48 and 63 that about 50% of the flux flows through less than 2% of the total width of the available flow domain at certain passages.

An interesting effect is the back flow phenomenon, i.e. segments of streamlines where the flow direction is oppositely directed to the mean direction of flow (see, e.g. Figures 44, 45, and 48). It is stressed here that a pronounced back flow behaviour is believed to be a two-dimensional artifact. Figure 37 gives some data of the back flow phenomenon for cases 4-00, 4-22, and 4-44. Figure 49 shows the spatial distribution of the observed back flow for N/S-flow in case 4-22.

Case	Back flow N/S [%]	Back flow W/E [%]
4-00	2.8	2.6
4-22	5.0	5.5
4-44	6.5	6.0

Fig. 37   Relative number of elements with a back flow gradient.

For N/S-flow in case 4-22, it is observed that the probability density function (PDF) of the transverse component of the flux is symmetric, i.e. normal, whereas the PDF of the longitudinal distribution is skewed, being approximately log-normal provided that the back flow is discarded (see Figures 49-51). The variograms in the x and y directions of the transverse component reveal that this component is poorly correlated. The correlation is, however, somewhat better in a direction perpendicular to the mean direction of flow. The variograms of the longitudinal component show the opposite situation. This component is well correlated, especially in a direction parallel to the mean direction of flow. Accordingly, the PDF and the variograms of the resultant flux vector are dominated by the statistics of the longitudinal component of the flux. Furthermore, it is found that the sills of the variograms of the resultant flux vector equal the sums of the corresponding sills of the variograms of its longitudinal and transverse components. This additive variance relationship suggests a poor cross correlation between the two orthogonal components of the flux. The observation is further confirmed by checking their cross variogram (not shown here, however), which shows a pure nugget effect, i.e. a constant-valued variogram, of $\gamma(h) \simeq 8.5 \cdot 10^{-14}$ $(m/s)^2$ for $h \geq 0$.

In order to compare more readily the PDF and the variogram of $ln(q(x))$ with the corresponding statistics of $Y(x) = ln(K(x))$, the directional dependence of $q(x)$ is discarded by taking the magnitude of the resultant flux vector $q(x) = |q(x)|$. Figures 52, 59, and 64 demonstrate that the PDF of the log-flux is basically symmetric. However, the symmetric shape is distorted at high flux, and the distortion increases with increasing value of the correlation length. Hence, the qualitative observation that patches of high conductivity do not necessarily correspond to patches of high flow is here verified. Furthermore, the spatial correlation is statistically anisotropic and the range is longer than for the log-conductivity field.

Figures 53 and 54 show that a positive linear correlation between the porosity and the conductivity in the log-space counteracts the previously discussed effects of a spatially varying conductivity field. That is to say, the *PDF* of $ln(|\mathbf{v(x)}|)$ is more symmetric and has a smaller variance, and its variograms are more statistically isotro-pic than the corresponding statistics of the log-flux.

All realizations discussed so far assume statistically isotropic conductivity fields. One case of *statistical anisotropy* in the con-ductivity field was investigated as well. This case will not be discussed further here. Figures A1-A7 in the appendix at the end of this study demonstrate the flow patterns and the statistics for the statistically anisotropic case studied.
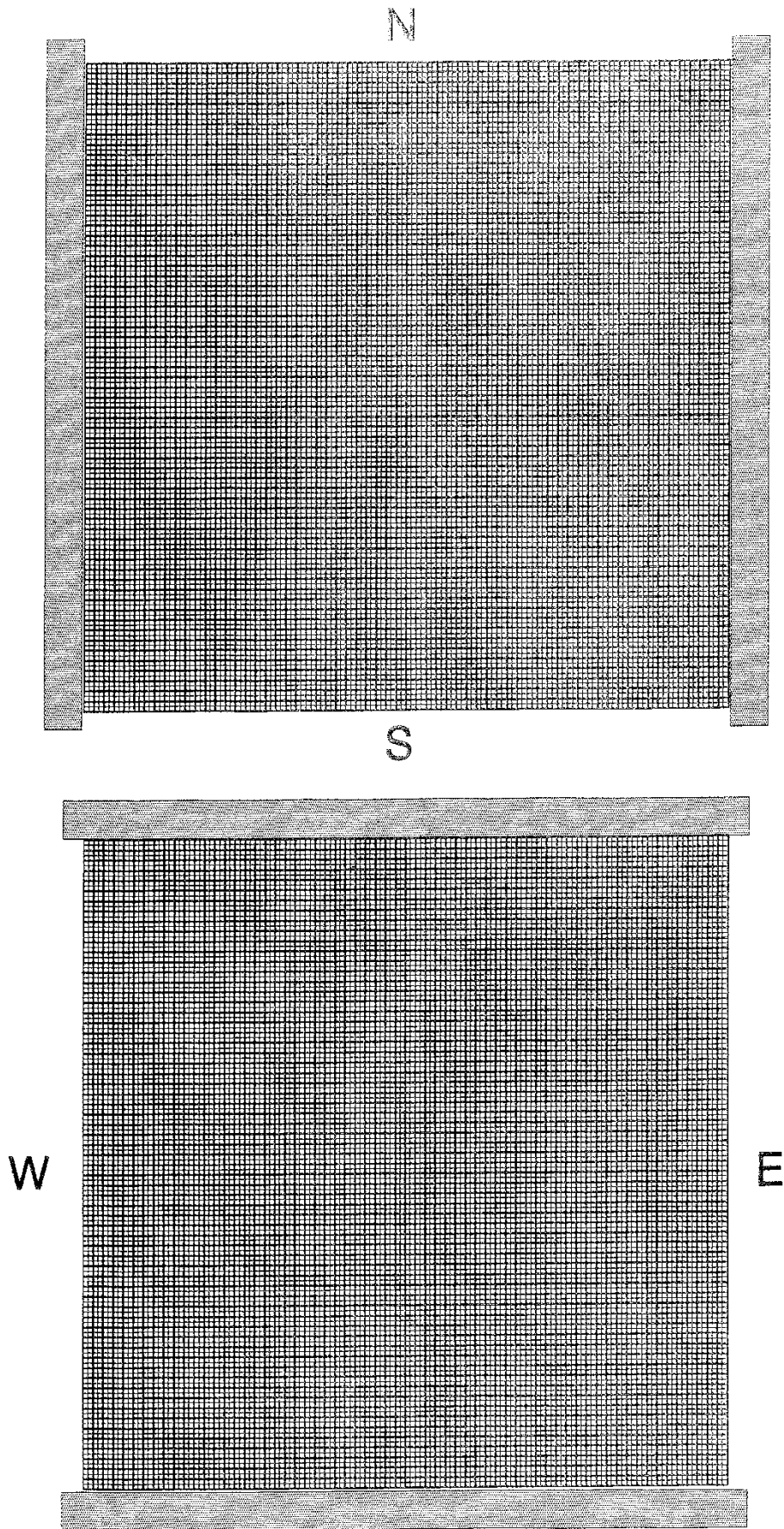
Fig. 38 Chosen finite element discretization for the flow and travel time

calculations, i.e. 4 elements/block . $N = (64 \times 64)$ and $N_e = 16{,}384$.

2-D HYDRAULIC CONDUCTIVITY FIELD

No. of blocks: 64 × 64

$\sigma_{\ln(K)} = 4.00 \qquad \lambda/\Delta x = 2.0 \qquad \lambda/\Delta y = 2.0$

RASTER LEGEND (dim[K]=m/s)

+5.04E-14	+2.56E-09	+1.49E-08	+5.90E-08	+2.11E-07
+2.11E-07	+7.19E-07	+3.04E-06	+1.89E-05	+9.42E-02
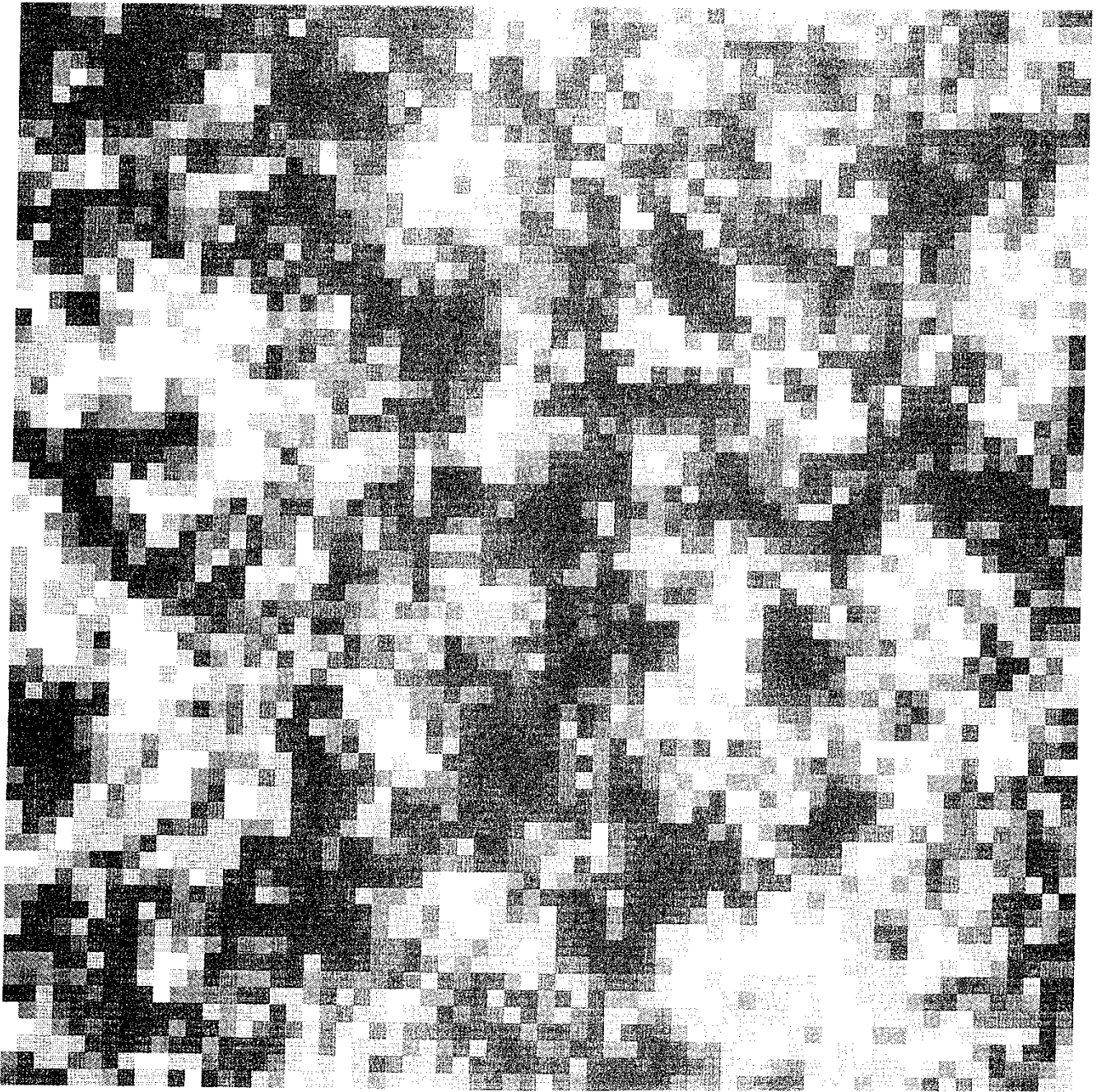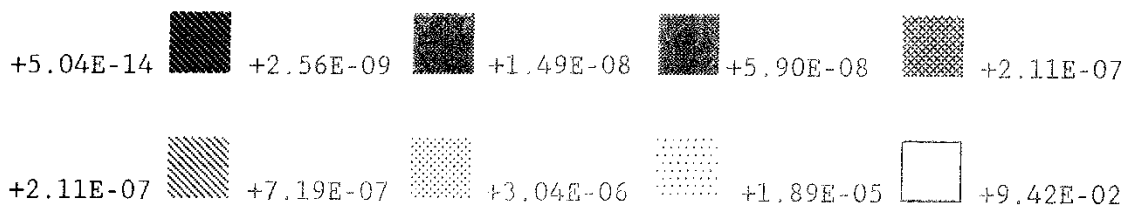
Fig. 39 Case 4-22: $\sigma_Y = 4$ and $\lambda/\Delta x = \lambda/\Delta y = 2$.

2-D SPECIFIC DISCHARGE FIELD
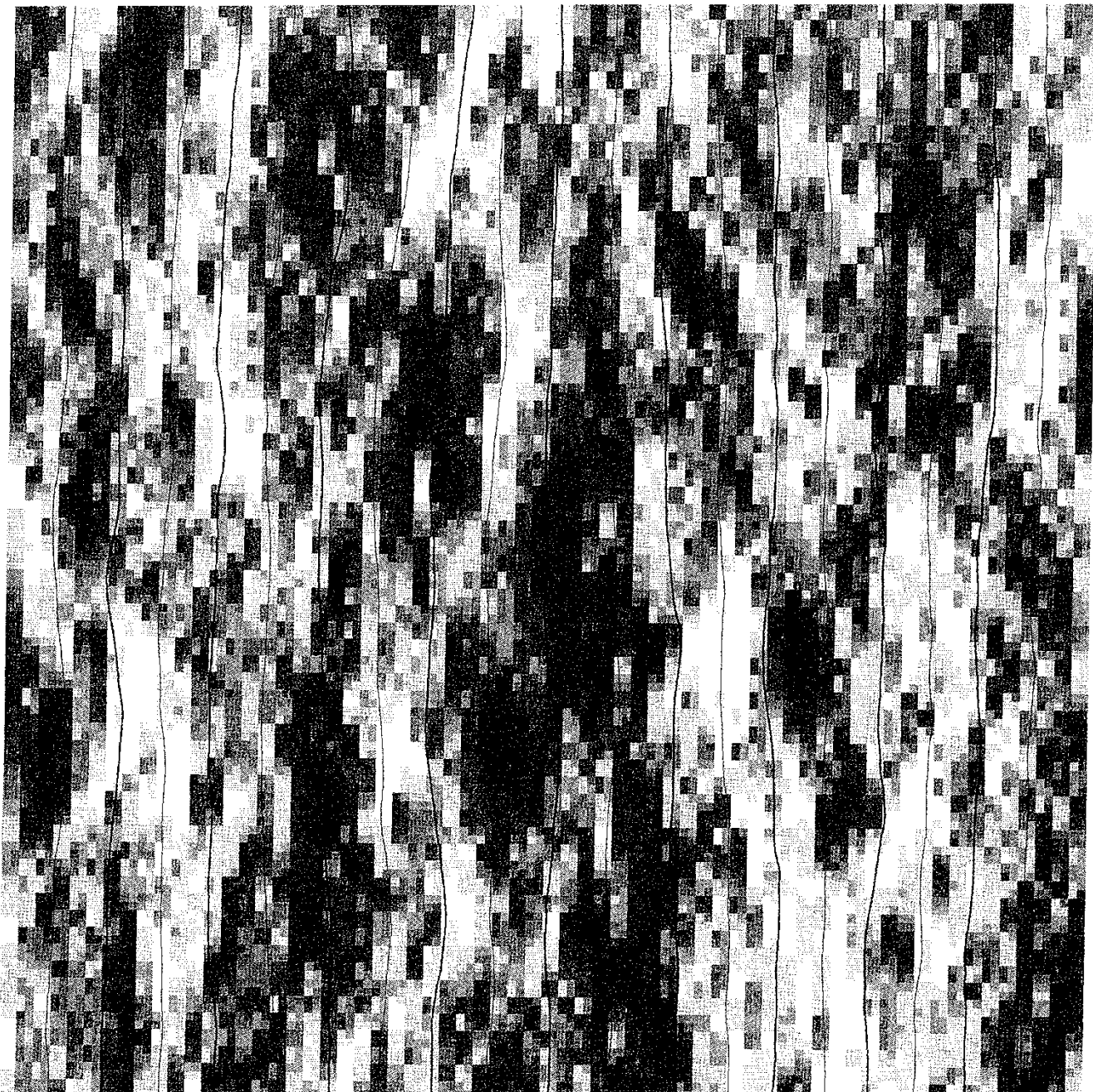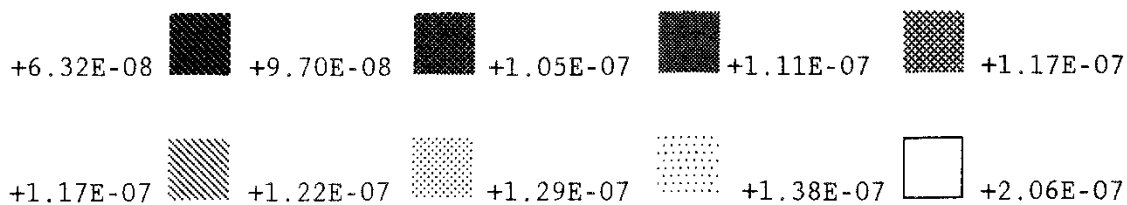
No. of blocks: 64 × 64

$\sigma_{\ln(K)}$ = 0.25 $\lambda/\Delta x$ = 2.0 $\lambda/\Delta y$ = 2.0

RASTER LEGEND (dim[q]=m/s)

+6.32E-08   +9.70E-08   +1.05E-07   +1.11E-07   +1.17E-07

+1.17E-07   +1.22E-07   +1.29E-07   +1.38E-07   +2.06E-07

Fig. 40 N/S-flow: σ_Y= 0.25 and $\lambda/\Delta x$ = $\lambda/\Delta y$ = 2 .

2-D SPECIFIC DISCHARGE FIELD

No. of blocks: 64 × 64

$\sigma_{\ln(K)} = 0.25 \qquad \lambda/\Delta x = 2.0 \qquad \lambda/\Delta y = 2.0$

RASTER LEGEND (dim[q]=m/s)

+6.29E-08	+9.67E-08	+1.05E-07	+1.11E-07	+1.17E-07
+1.17E-07	+1.22E-07	+1.29E-07	+1.39E-07	+2.04E-07
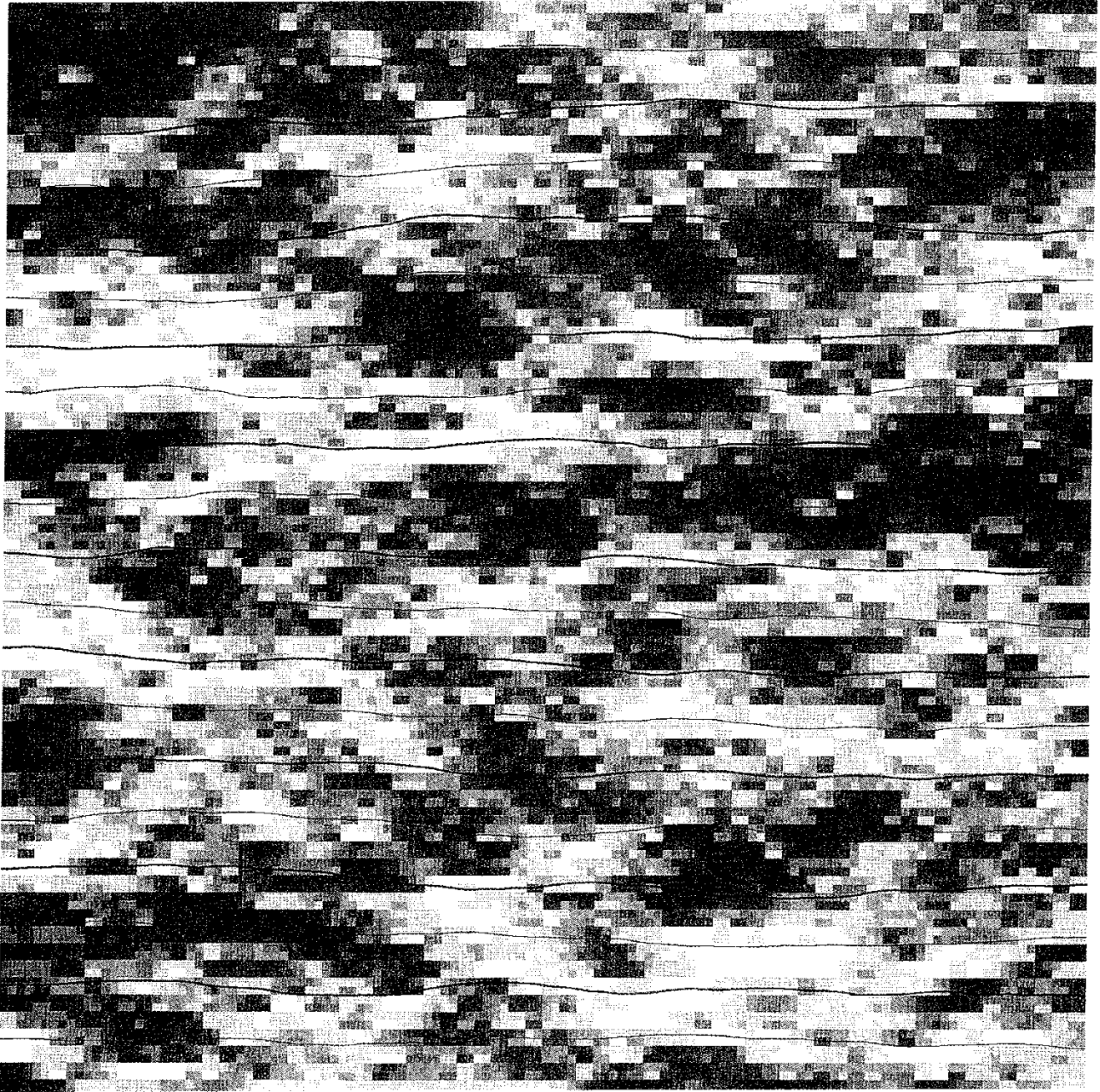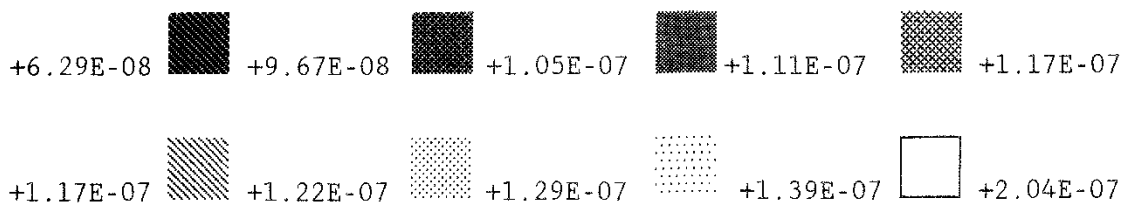
Fig. 41 W/E-flow: $\sigma_Y = 0.25$ and $\lambda/\Delta x = \lambda/\Delta y = 2$.

2-D SPECIFIC DISCHARGE FIELD

No. of blocks: 64 × 64

$\sigma_{\ln(K)} = 1.00 \qquad \lambda/\Delta x = 2.0 \qquad \lambda/\Delta y = 2.0$

RASTER LEGEND (dim[q]=m/s)

+7.76E-09 ■ +5.67E-08	■ +7.85E-08	■ +9.92E-08	▩ +1.19E-07
+1.19E-07 ▨ +1.43E-07	▦ +1.75E-07	▧ +2.28E-07	☐ +1.05E-06

Fig. 42 N/S-flow: $\sigma_Y = 1$ and $\lambda/\Delta x = \lambda/\Delta y = 2$.

2-D SPECIFIC DISCHARGE FIELD

No. of blocks: 64 × 64

$\sigma_{\ln(K)} = 1.00 \qquad \lambda/\Delta x = 2.0 \qquad \lambda/\Delta y = 2.0$

RASTER LEGEND (dim[q]=m/s)

+7.07E-09	+5.56E-08	+7.88E-08	+9.88E-08	+1.20E-07
+1.20E-07	+1.46E-07	+1.80E-07	+2.31E-07	+1.09E-06

Fig. 43 W/E-flow: $\sigma_Y = 1$ and $\lambda/\Delta x = \lambda/\Delta y = 2$.

2-D SPECIFIC DISCHARGE FIELD

No. of blocks: 64 × 64

$\sigma_{\ln(K)} = 4.00 \qquad \lambda/\Delta x = 2.0 \qquad \lambda/\Delta y = 2.0$

RASTER LEGEND (dim[q]=m/s)

+3.59E-13	+1.87E-09	+7.72E-09	+2.11E-08	+4.65E-08
+4.65E-08	+8.97E-08	+1.82E-07	+4.24E-07	+7.75E-06

Fig. 44 N/S-flow: $\sigma_Y = 4$ and $\lambda/\Delta x = \lambda/\Delta y = 2$.

2-D SPECIFIC DISCHARGE FIELD

No. of blocks: 64 × 64

$$\sigma_{\ln(K)} = 4.00 \qquad \lambda/\Delta x = 2.0 \qquad \lambda/\Delta y = 2.0$$

RASTER LEGEND (dim[q]=m/s)

+2.50E-13	+1.86E-09	+7.93E-09	+2.50E-08	+5.62E-08
+5.62E-08	+1.25E-07	+2.51E-07	+5.49E-07	+1.49E-05
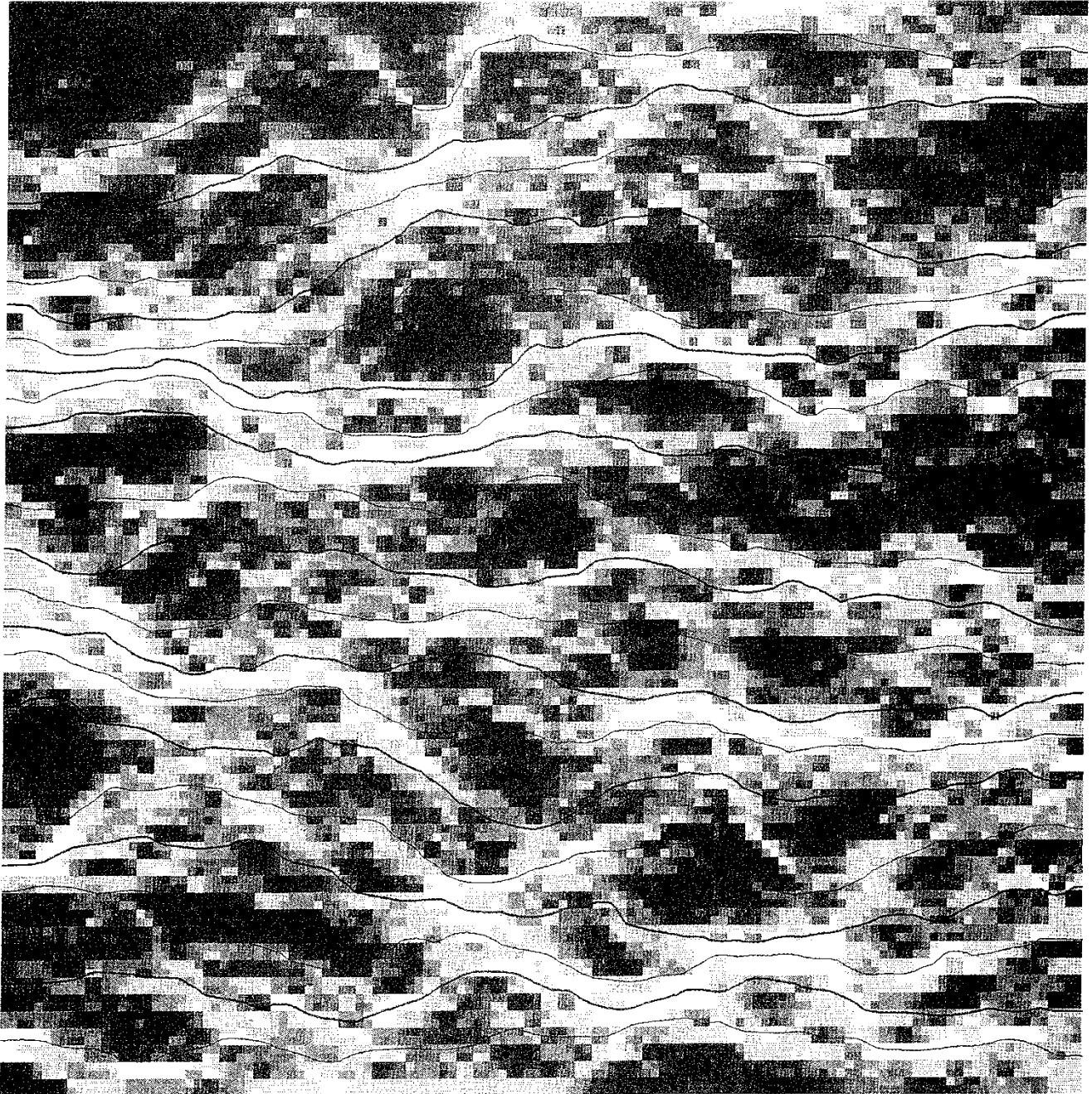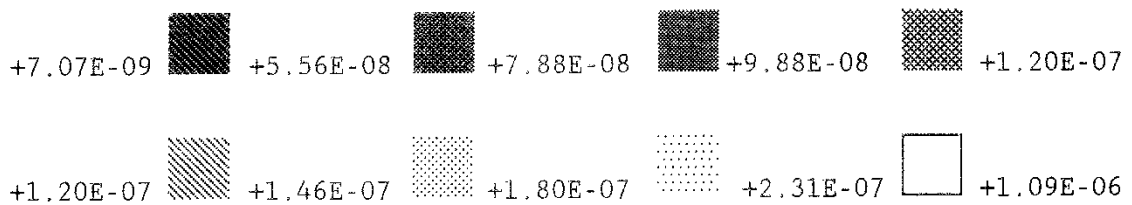
Fig. 45 W/E-flow: $\sigma_Y = 4$ and $\lambda/\Delta x = \lambda/\Delta y = 2$.

Fig. 46 Flow nets for N/S and W/E flow respectively. N = (64 x 64),

$\lambda/\Delta x = \lambda/\Delta y = 2$ and $\sigma_{\ln(K)} = 0.25$. Piezometric head (dashed) and

stream function levels (solid) are in 5% increments between 0 and 1.
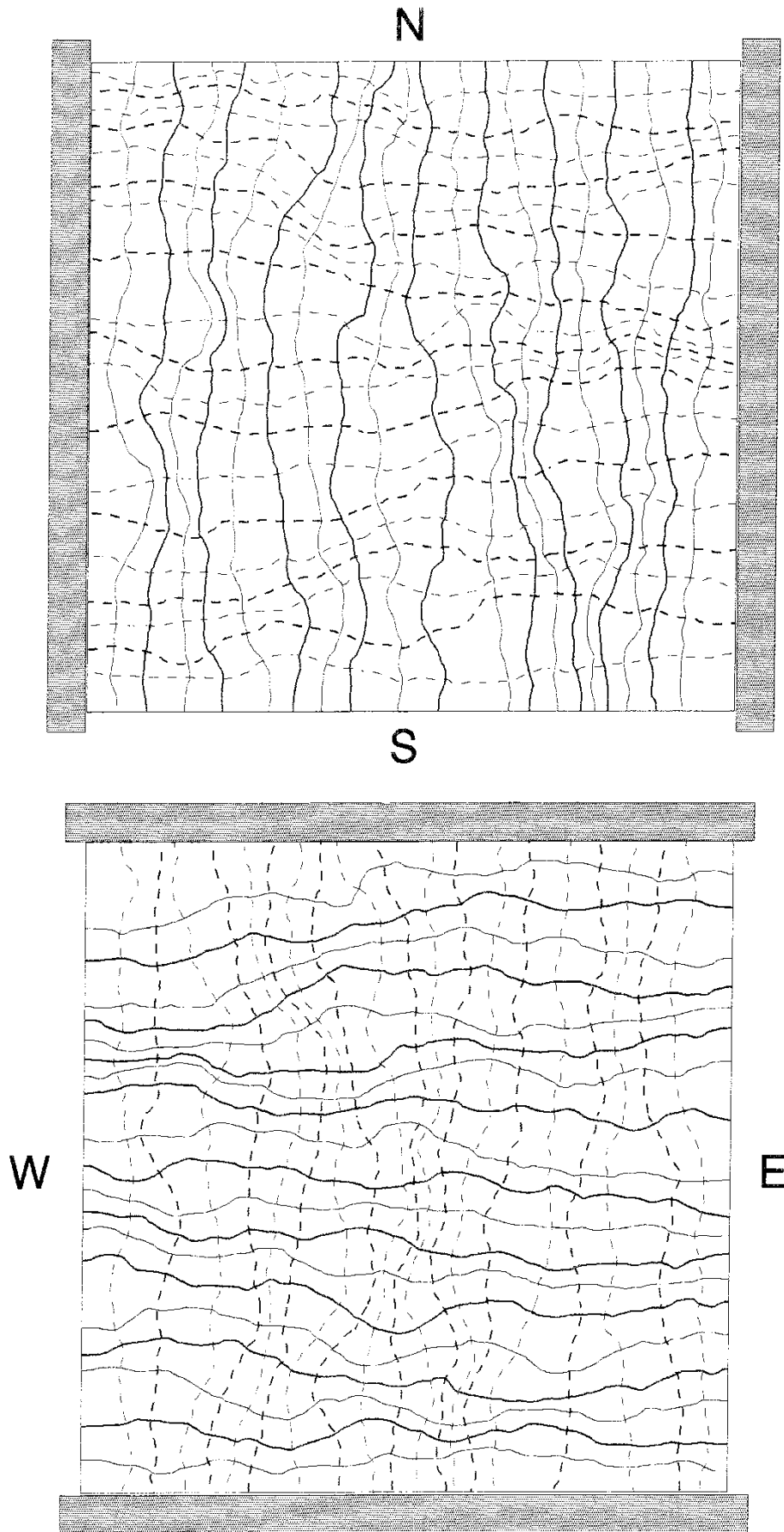
Fig. 47 Flow nets for N/S and W/E flow respectively. N = (64 x 64),

$\lambda/\Delta x = \lambda/\Delta y = 2$ and $\sigma_{\ln(K)} = 1.00$. Piezometric head (dashed) and

stream function levels (solid) are in 5% increments between 0 and 1.
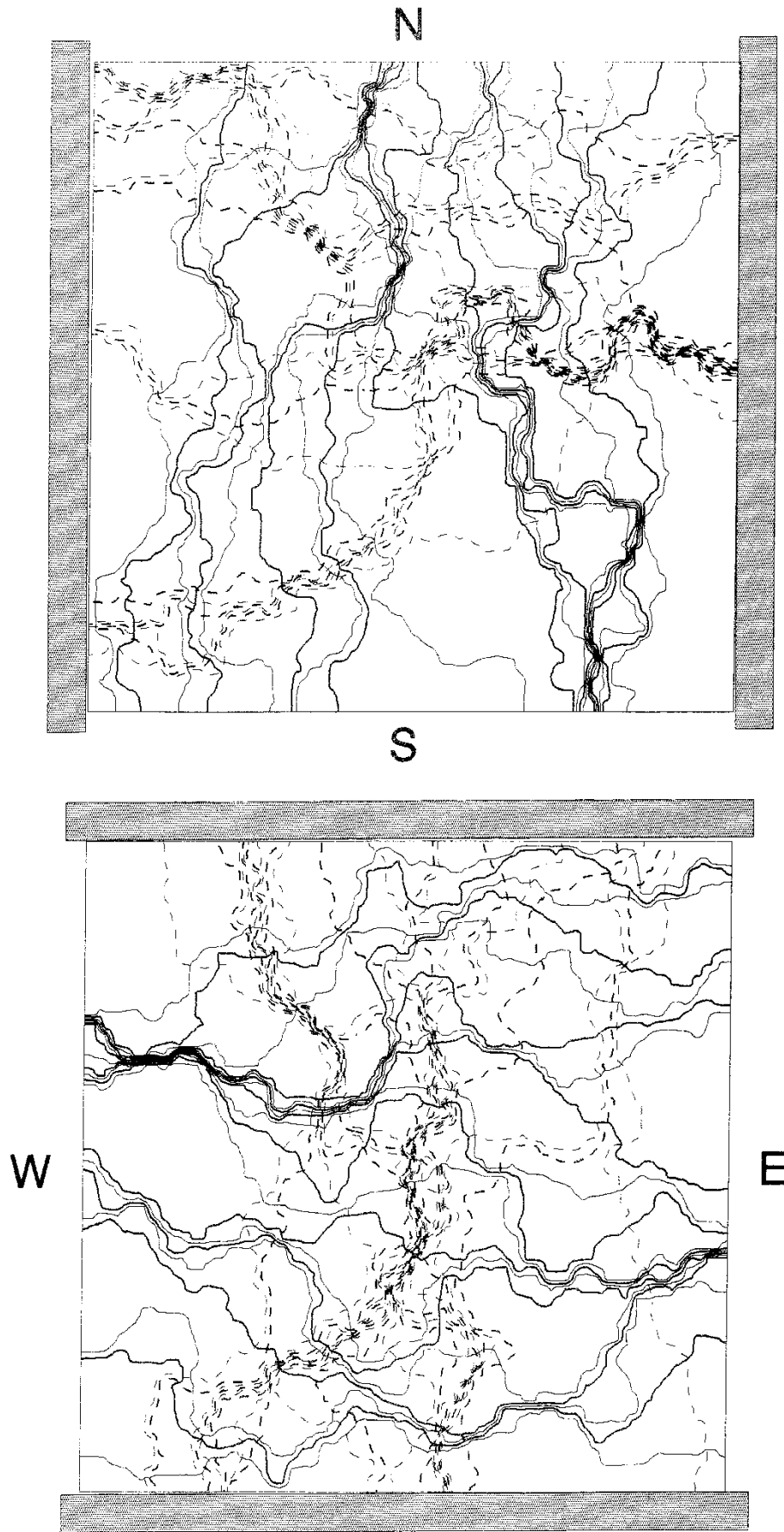
Fig. 48 Flow nets for N/S and W/E flow respectively. N = (64 x 64),

$\lambda / \Delta x = \lambda / \Delta y = 2$ and $\sigma_{\ln(K)} = 4.00$. Piezometric head (dashed) and

stream function levels (solid) are in 5% increments between 0 and 1.

2-D SPECIFIC DISCHARGE FIELD

No. of blocks: 64 × 64
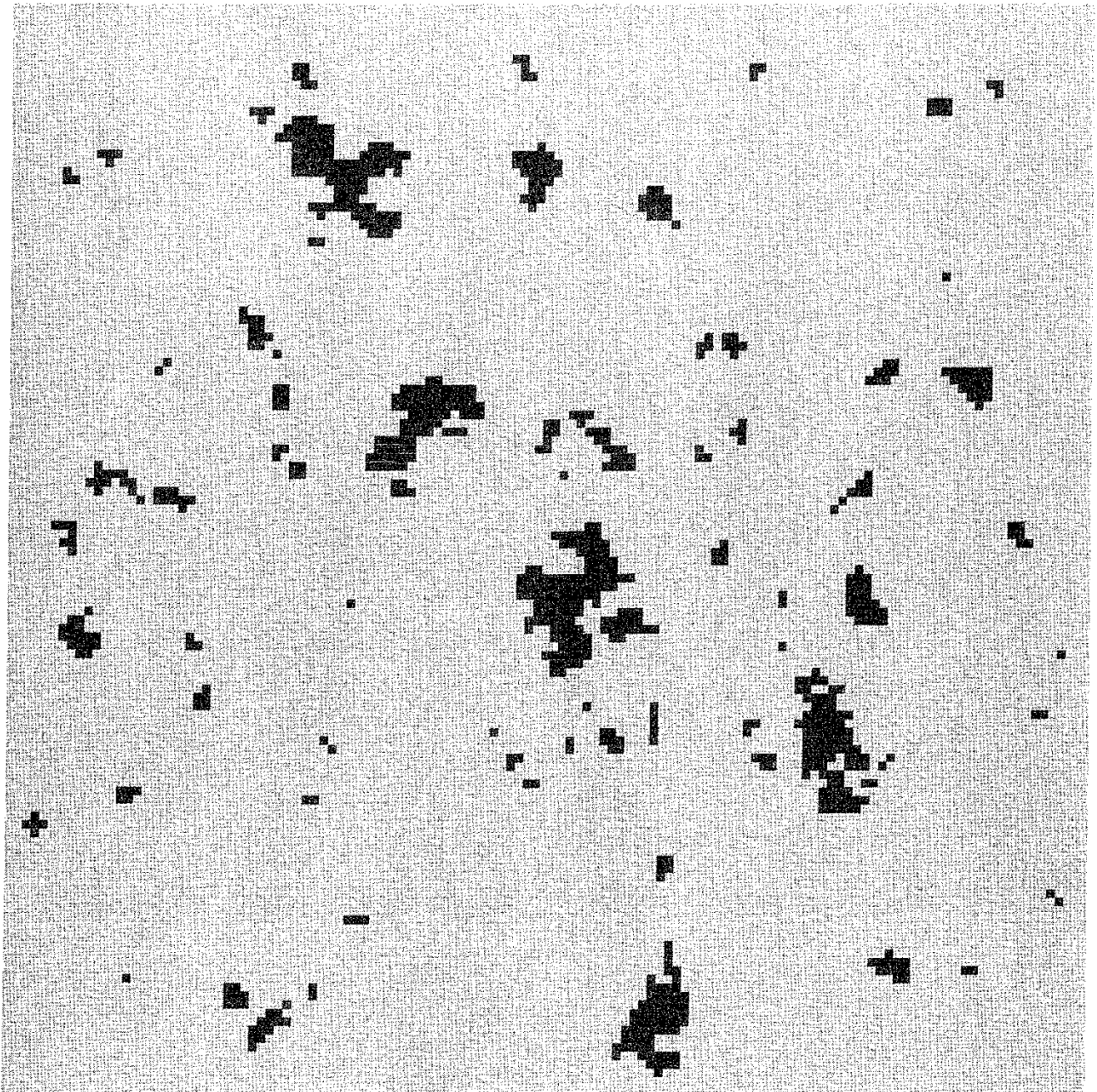
$\sigma_{\ln(K)} = 4.00 \qquad \lambda/\Delta x = 2.0 \qquad \lambda/\Delta y = 2.0$

RASTER LEGEND FOR q-long (q_y)

NORTH ■ 5%   SOUTH ▦ 95%

Fig. 49   Spatial distribution of the longitudinal specific discharge component. Case 4-22 and N/S-flow.

2-D SPECIFIC DISCHARGE FIELD

No. of blocks: 64 × 64

$\sigma_{\ln(K)} = 4.00 \qquad \lambda/\Delta x = 2.0 \qquad \lambda/\Delta y = 2.0$
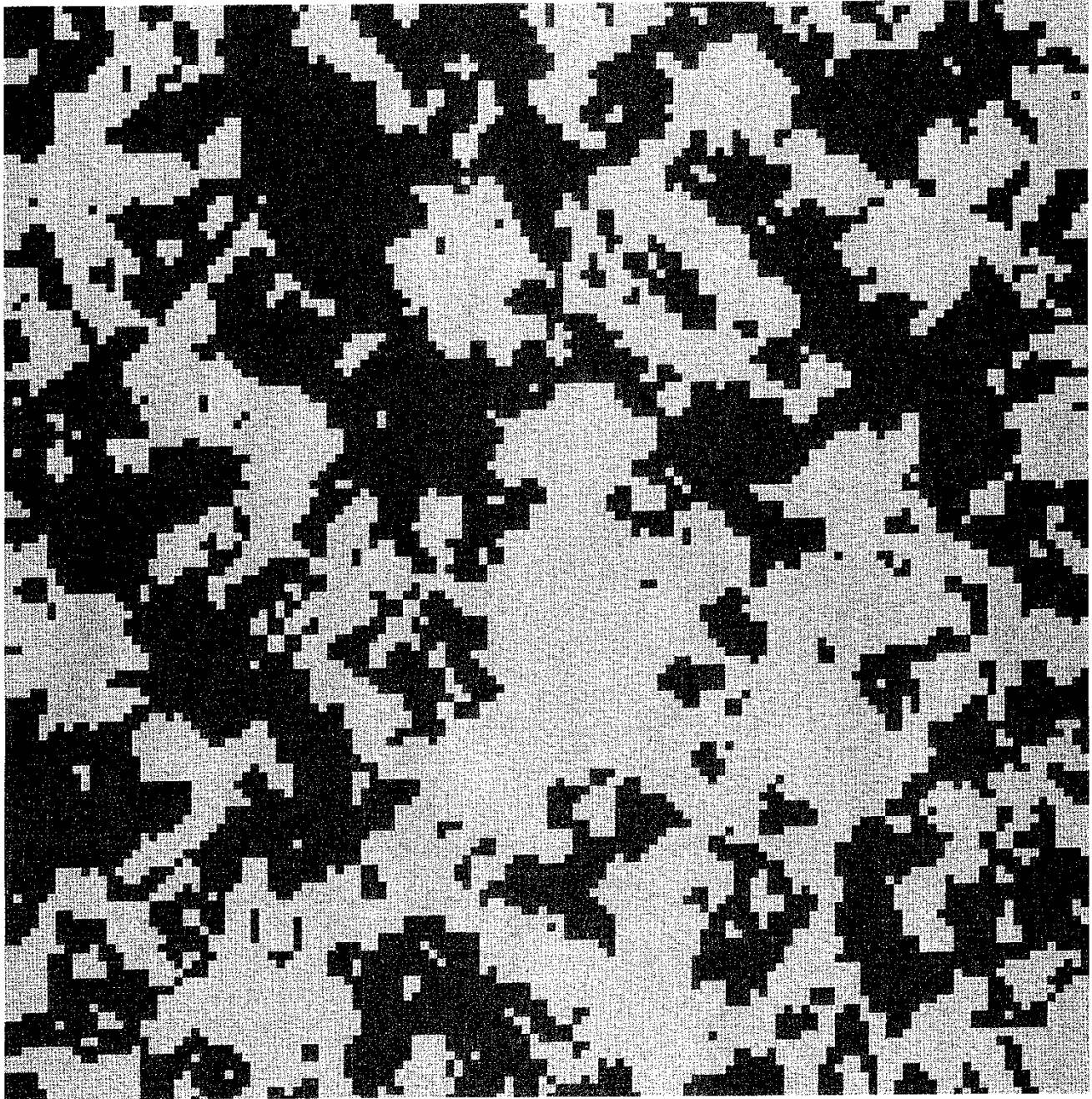
RASTER LEGEND FOR q-trans (q_x)

← WEST ■ 49 %   ▦ EAST → 51 %

Fig. 50 Spatial distribution of the transverse specific discharge component. Case 4-22 and N/S-flow .
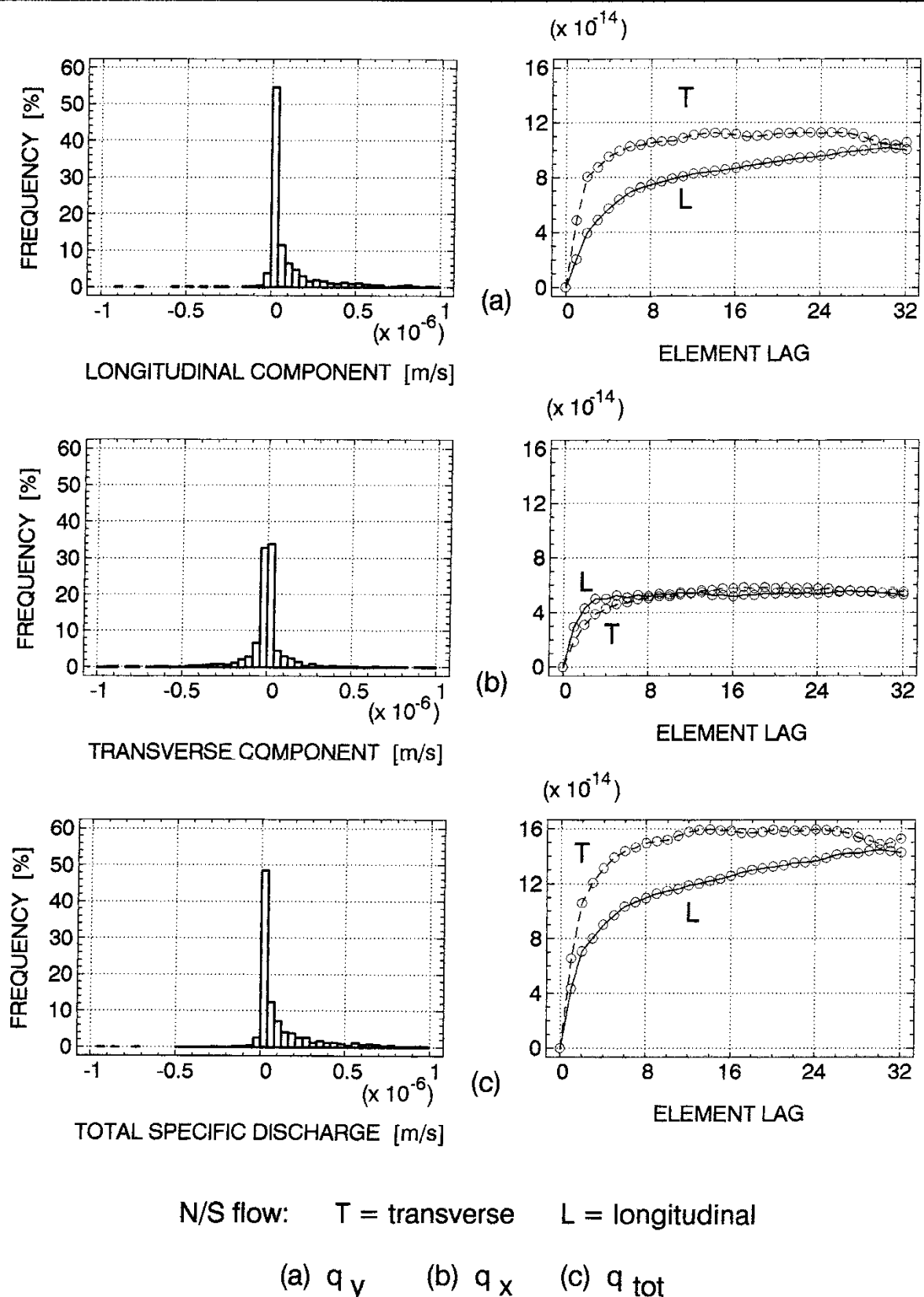
Fig. 51 Histograms and variograms of q_y, q_x and q_{tot} for case 4-22.
$\lambda/\Delta x = \lambda/\Delta y = 2$ and $\sigma_{ln(K)} = 4.00$. N/S flow.
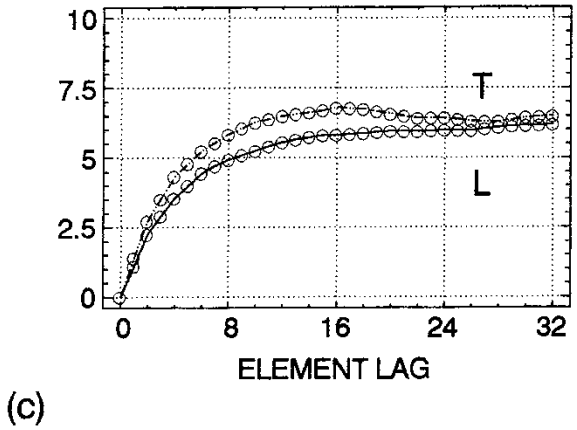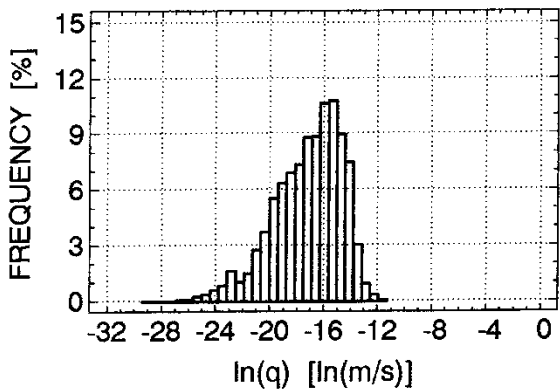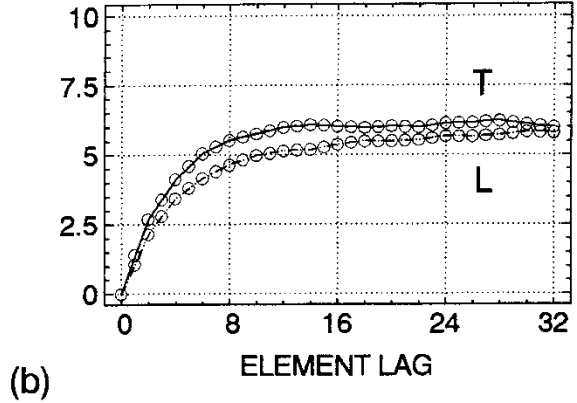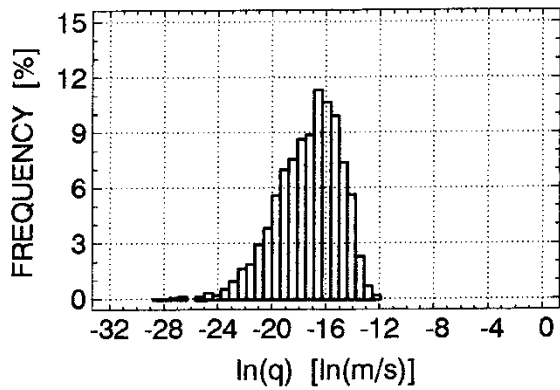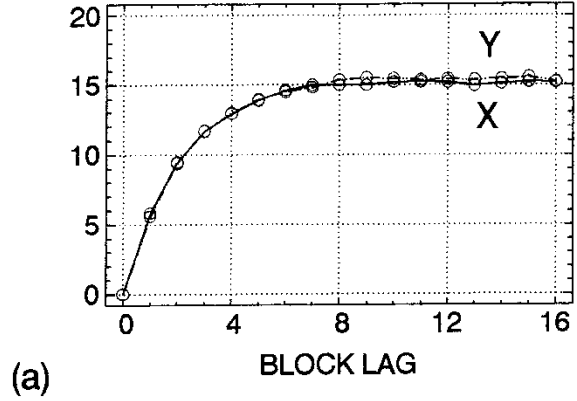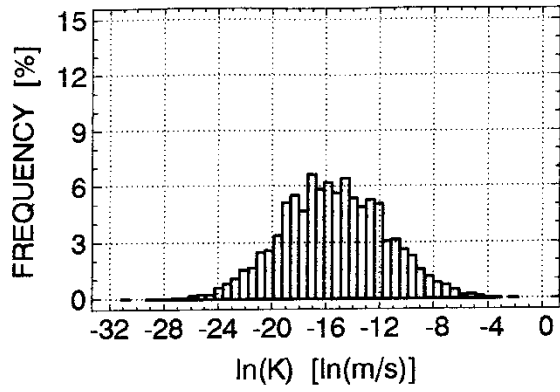
Fig. 52 Histograms and variograms of ln(K) and ln(q) for case 4-22.

$\lambda/\Delta x = \lambda/\Delta y = 2$ and $\sigma_{\ln(K)} = 4.00$.

Fig. 53 Histograms and variograms of ln(v) for case 4-22 (N/S-flow) .
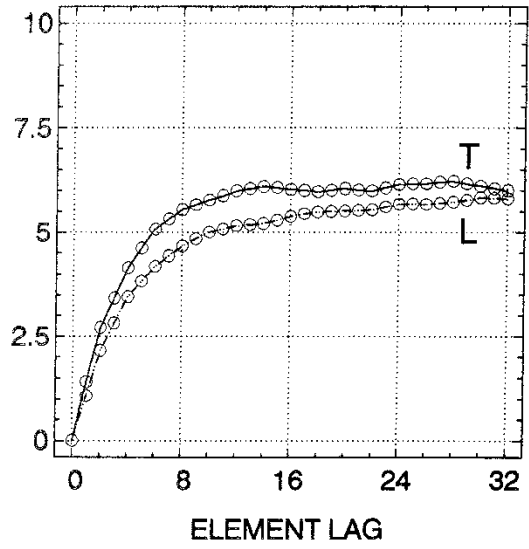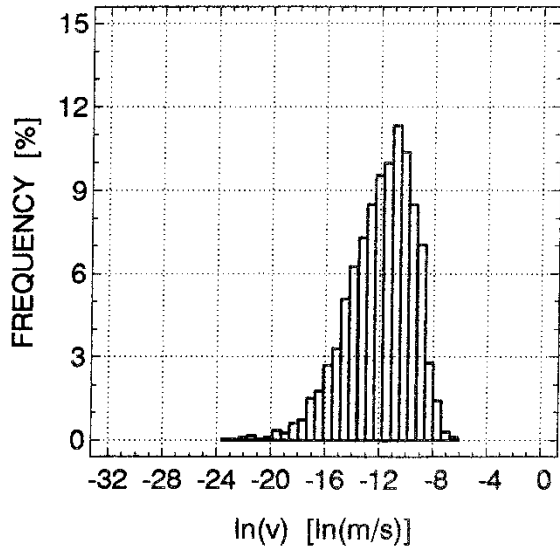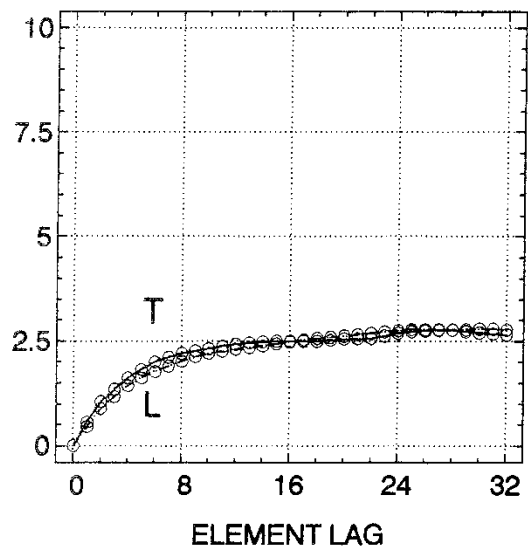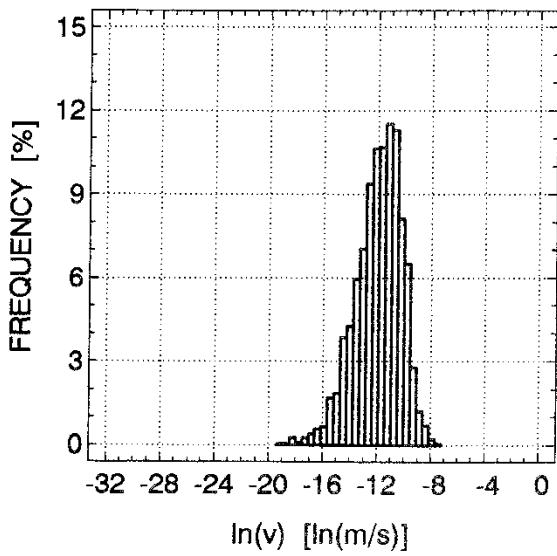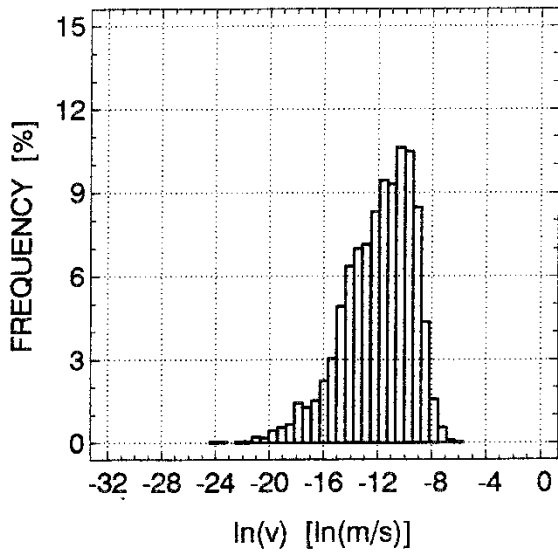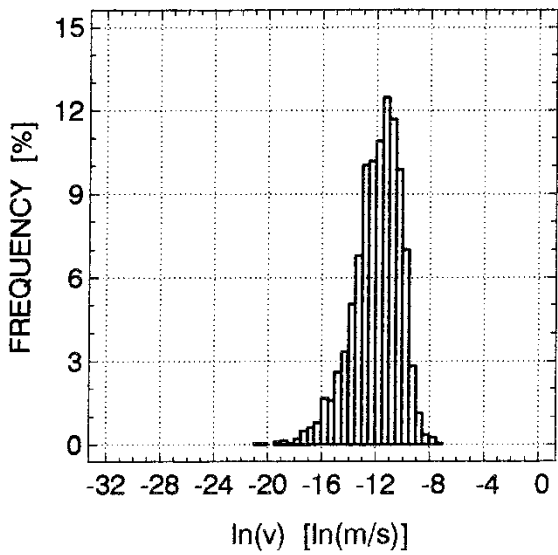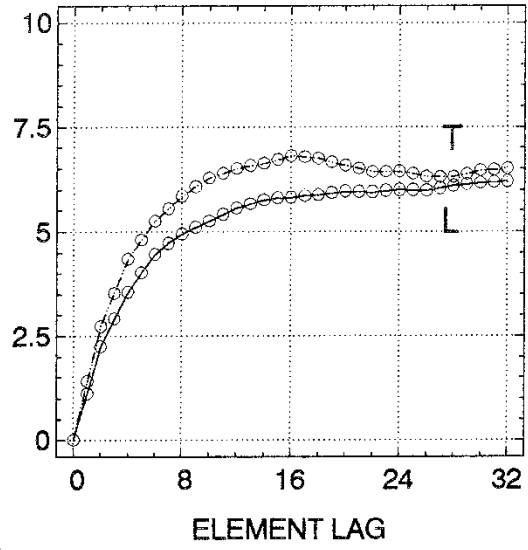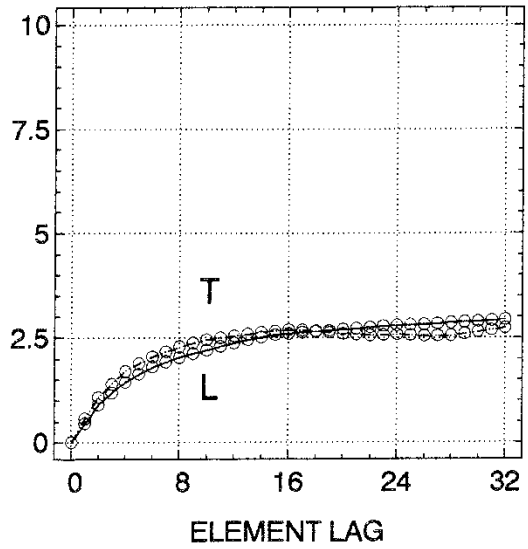
T = transverse   L = longitudinal

(a) uniform porosity   (b) variable porosity

Fig. 54 Histograms and variograms of ln(v) for case 4-22 (W/E-flow) .

2-D HYDRAULIC CONDUCTIVITY FIELD

No. of blocks: 64 × 64

$\sigma_{\ln(K)} = 4.00$ $\lambda/\triangle x = 0.0$ $\lambda/\triangle y = 0.0$

RASTER LEGEND (dim[K]=m/s)

+4.75E-14   +1.26E-09   +7.69E-09   +3.11E-08   +1.07E-07

+1.07E-07   +4.06E-07   +1.52E-06   +1.21E-05   +1.02E-01
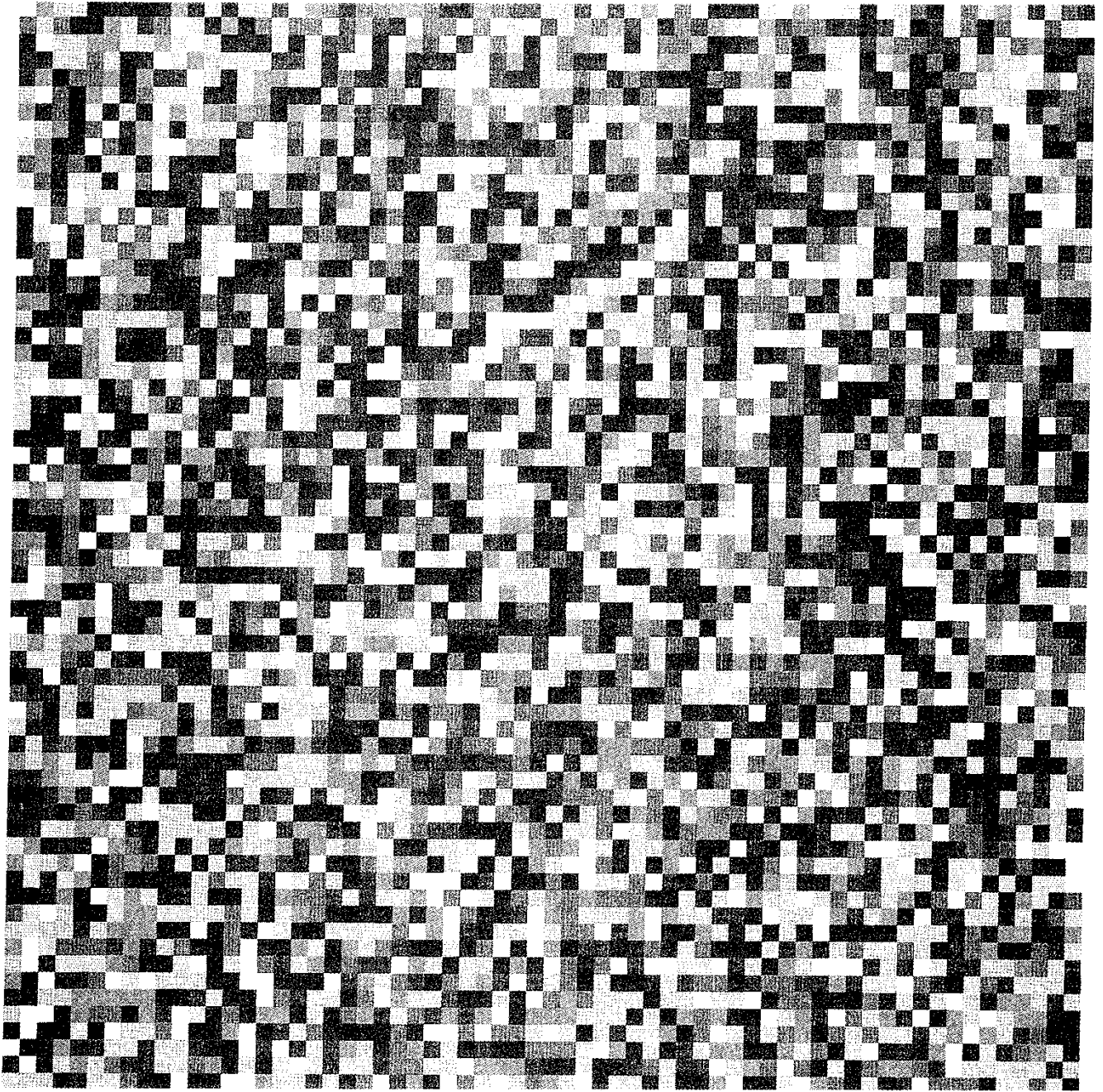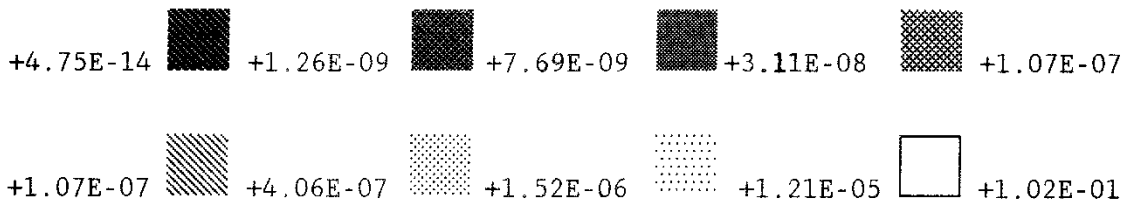
Fig. 55 Case 4-00: $\sigma_Y = 4$ and $\lambda/\triangle x = \lambda/\triangle y = 0$.
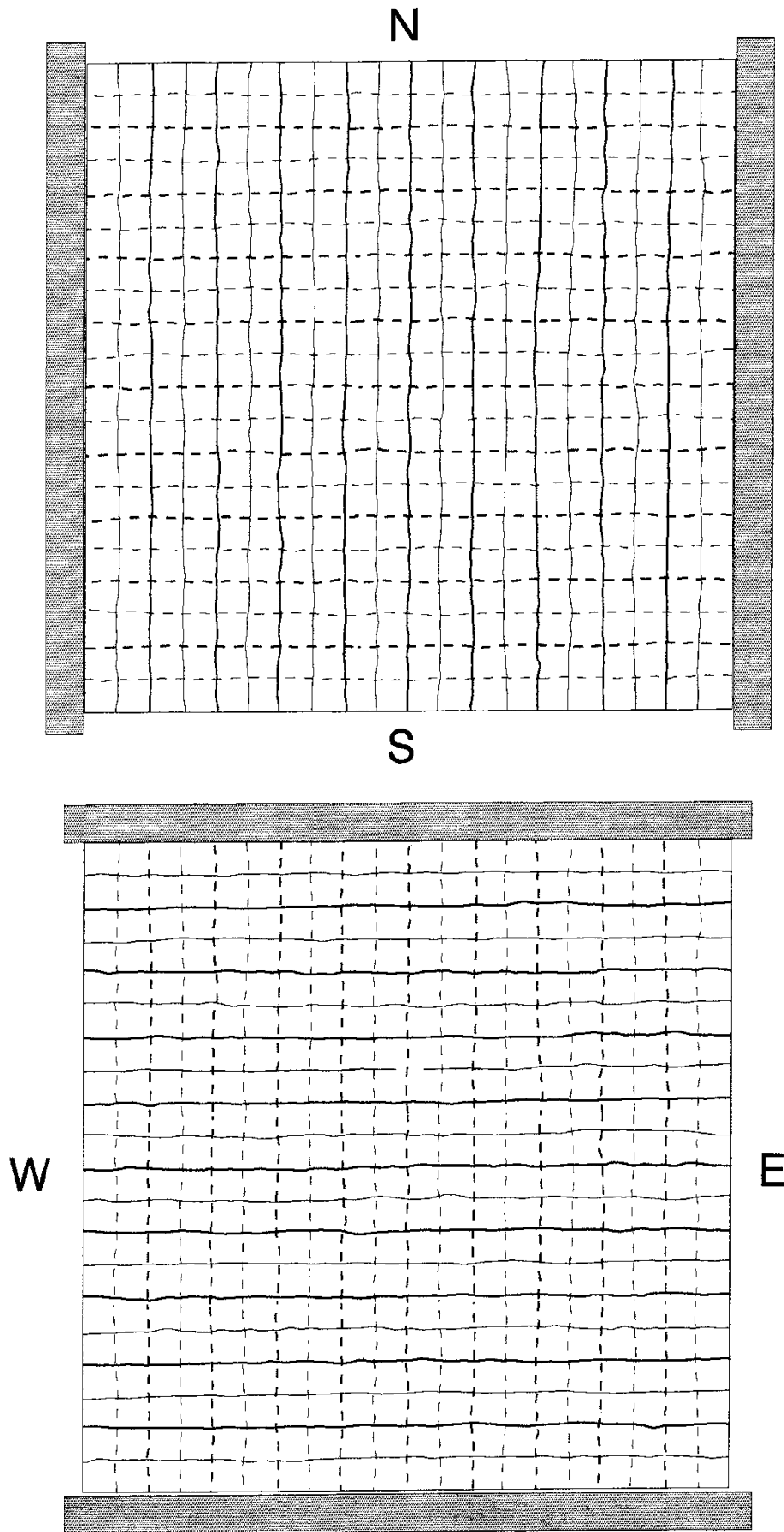
Fig. 56 Flow nets for N/S and W/E flow respectively. N = (64 x 64),

$\lambda/\Delta x = \lambda/\Delta y = 0$ and $\sigma_{\ln(K)} = 0.25$. Piezometric head (dashed) and

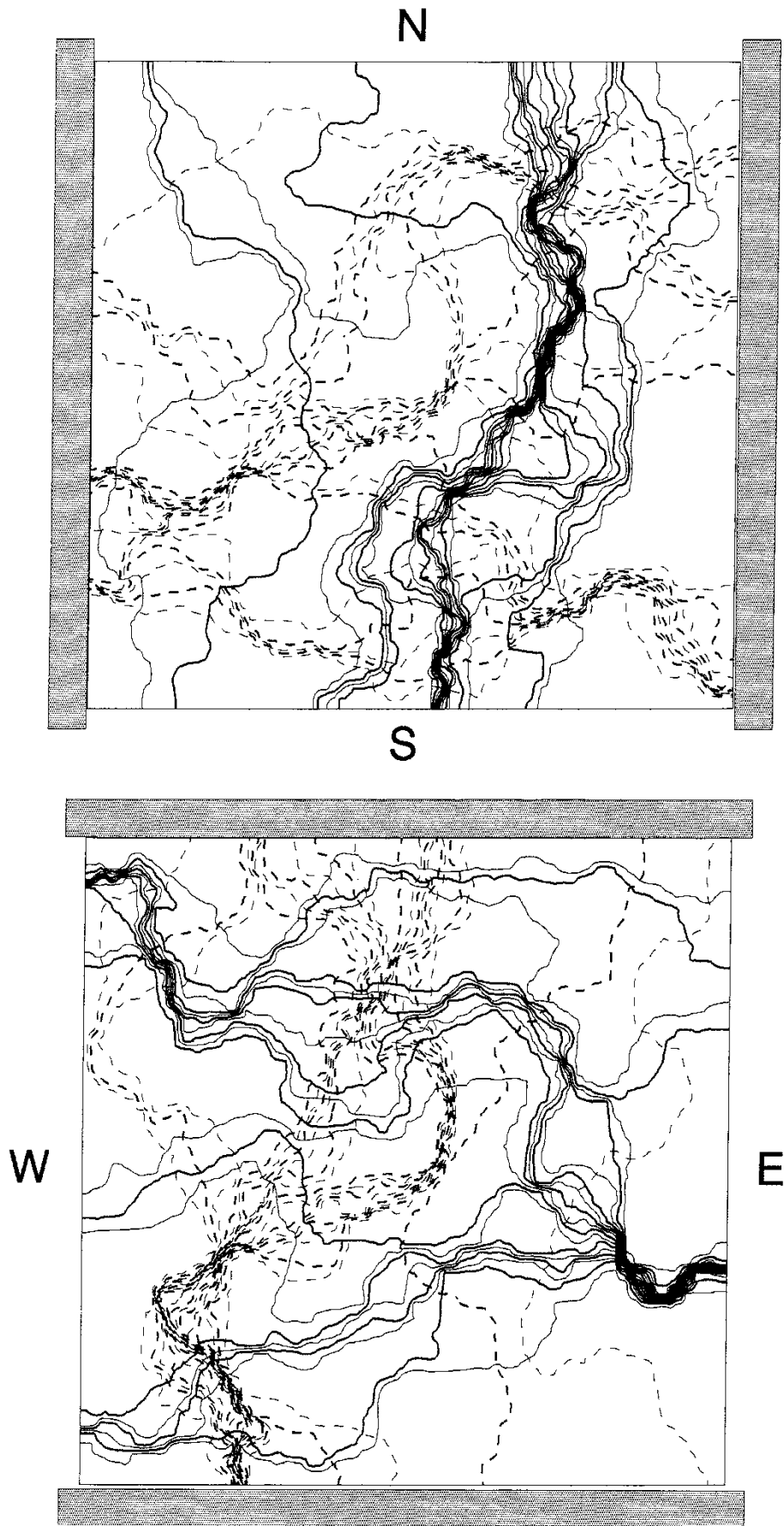stream function levels (solid) are in 5% increments between 0 and 1.
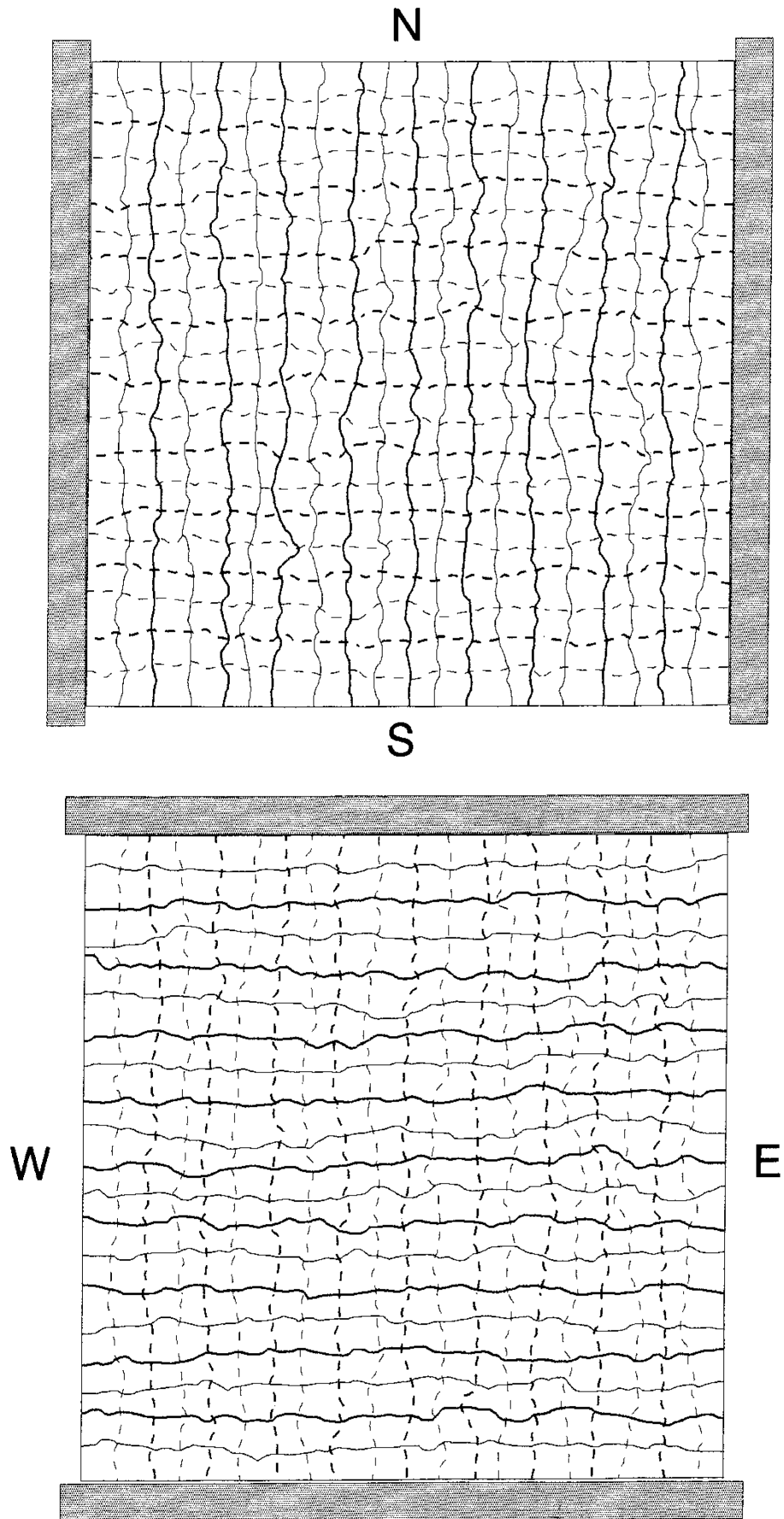
Fig. 57 Flow nets for N/S and W/E flow respectively. N = (64 x 64),

$\lambda/\Delta x = \lambda/\Delta y = 0$ and $\sigma_{\ln(K)} = 1.00$. Piezometric head (dashed) and stream function levels (solid) are in 5% increments between 0 and 1.
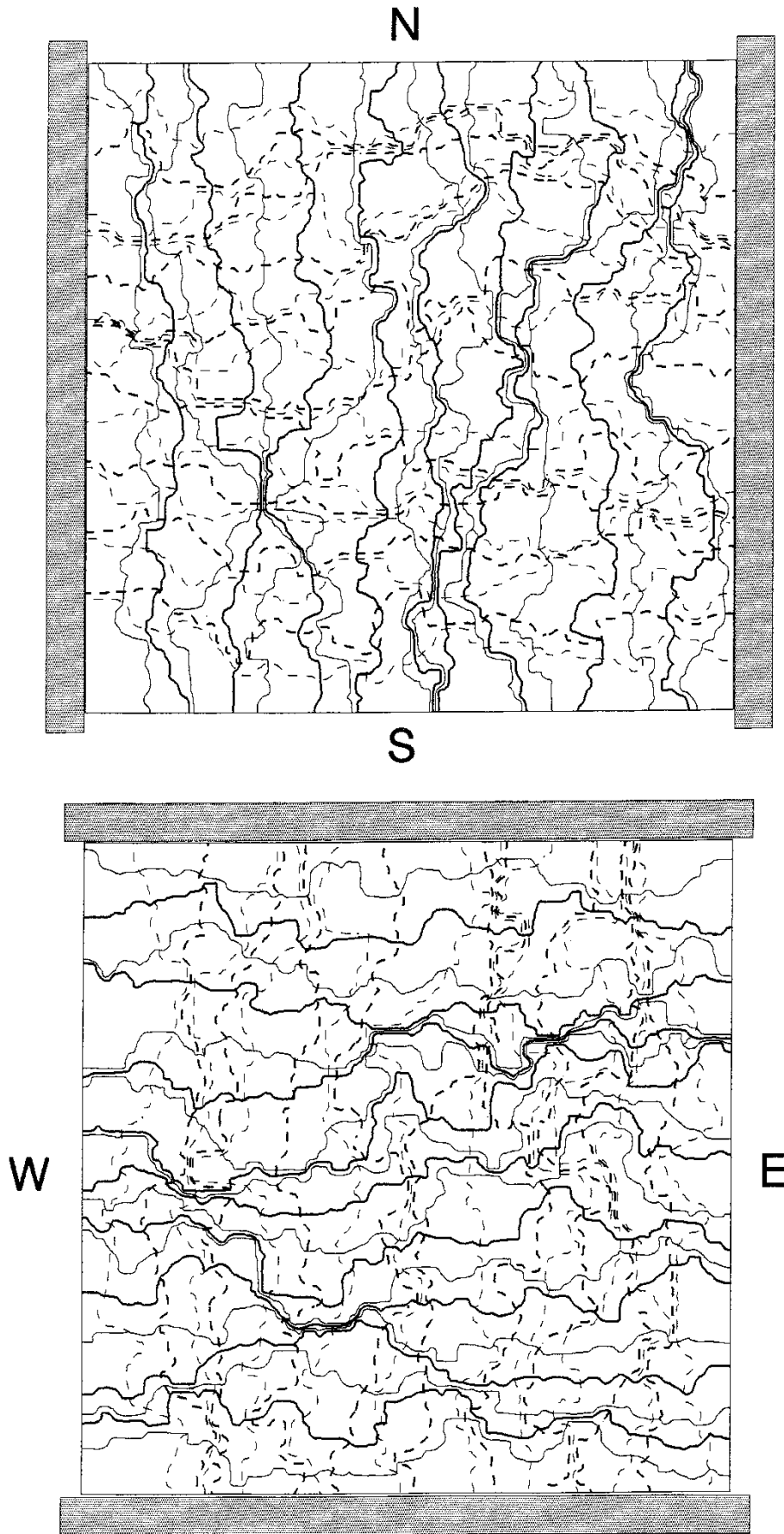
Fig. 58 Flow nets for N/S and W/E flow respectively. N = (64 x 64),

$\lambda/\Delta x = \lambda/\Delta y = 0$ and $\sigma_{\ln(K)} = 4.00$. Piezometric head (dashed) and

stream function levels (solid) are in 5% increments between 0 and 1.
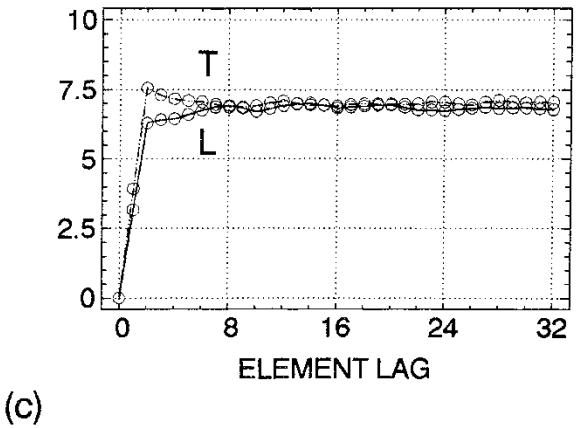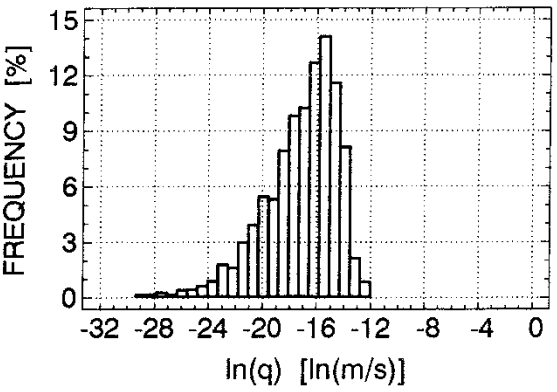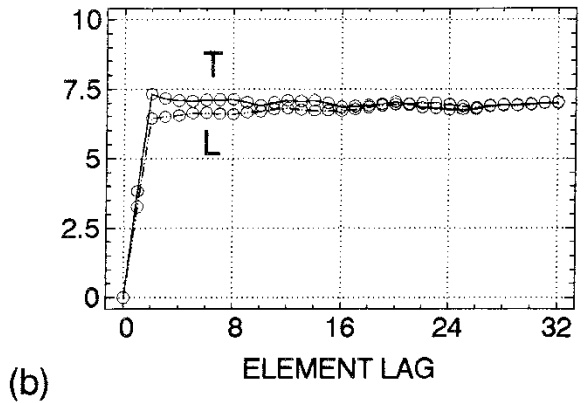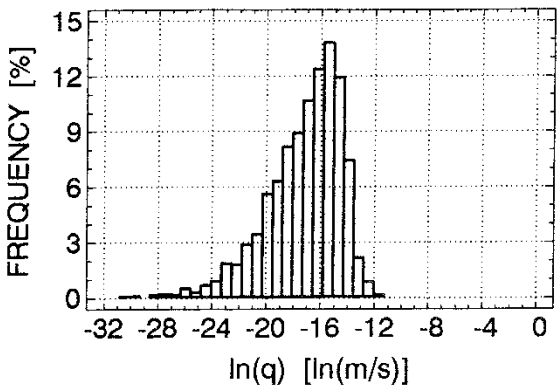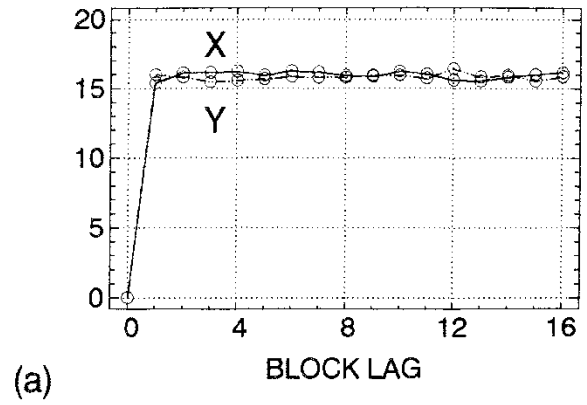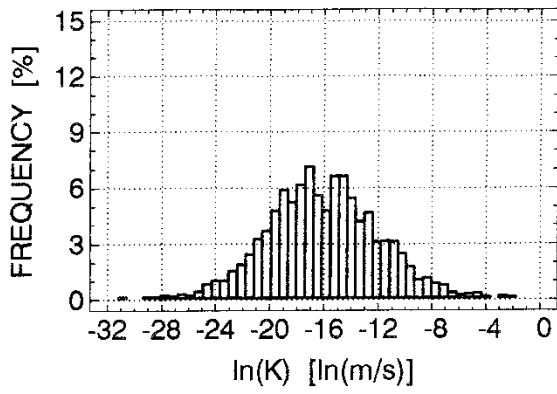
T = transverse   L = longitudinal

(a) ln(K)   (b) ln(q) N/S flow   (c) ln(q) W/E flow

Fig. 59 Histograms and variograms of ln(K) and ln(q) for case 4-00 .

$\lambda/\Delta x = \lambda/\Delta y = 0$ and $\sigma_{\ln(K)} = 4.00$.

2-D HYDRAULIC CONDUCTIVITY FIELD

No. of blocks: 64 × 64

$\sigma_{\ln(K)} = 4.00 \qquad \lambda/\Delta x = 4.0 \qquad \lambda/\Delta y = 4.0$

RASTER LEGEND (dim[K]=m/s)

+1.14E-12   +5.26E-09   +3.33E-08   +1.31E-07   +4.26E-07

+4.26E-07   +1.32E-06   +5.29E-06   +3.17E-05   +1.19E-01
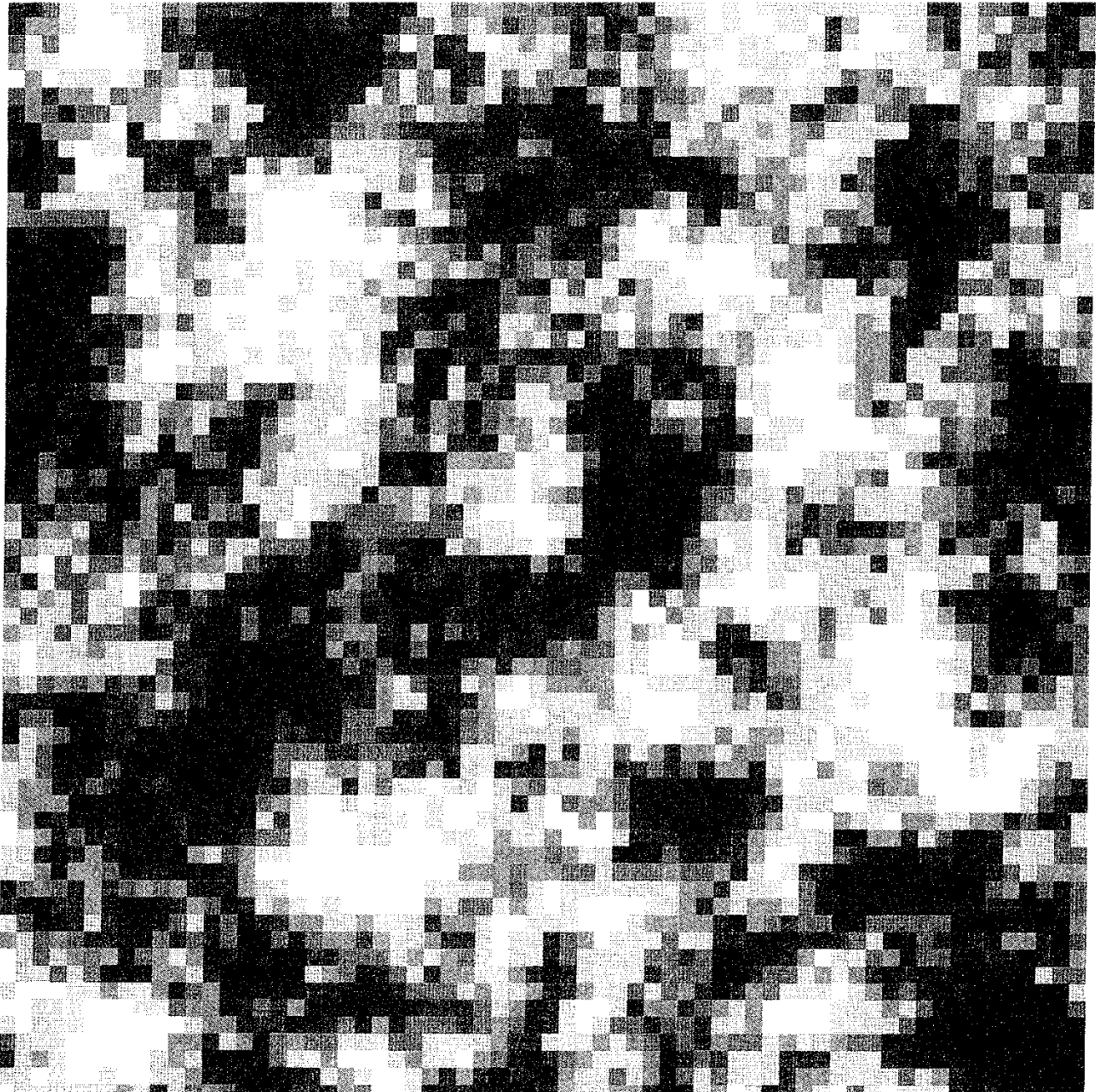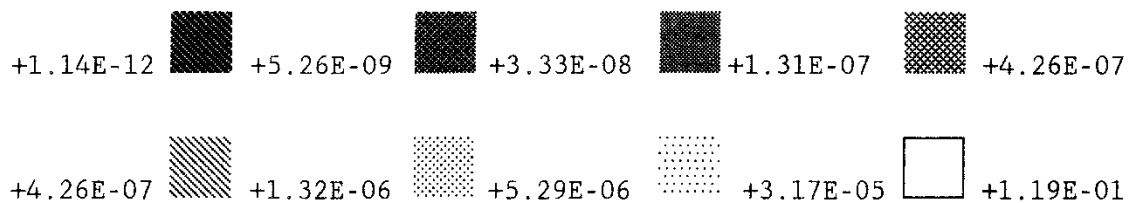
Fig. 60 Case 4-44: $\sigma_Y = 4$ and $\lambda/\Delta x = \lambda/\Delta y = 4$.
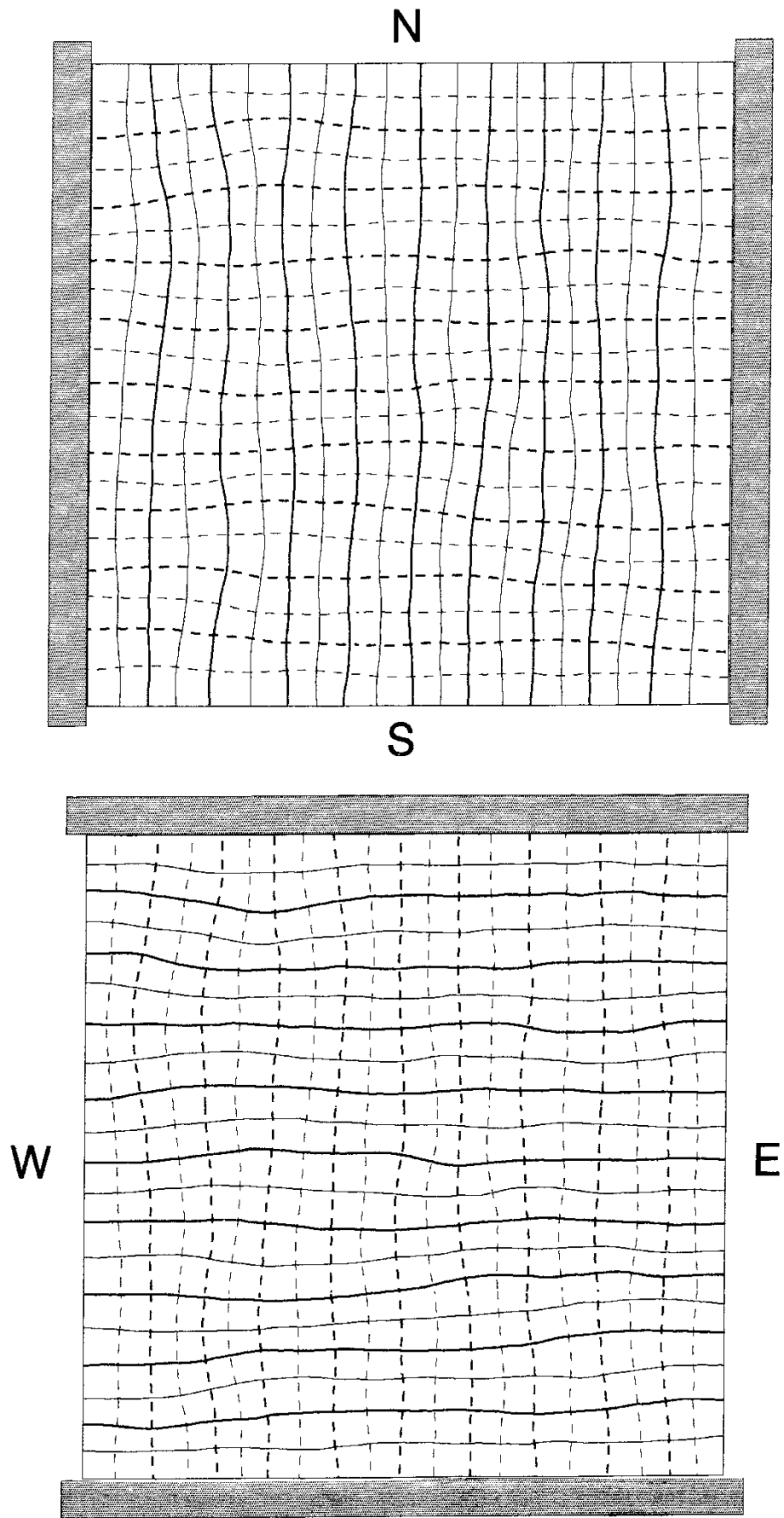
Fig. 61 Flow nets for N/S and W/E flow respectively. N = (64 x 64),

$\lambda/\Delta x = \lambda/\Delta y = 4$ and $\sigma_{\ln(K)} = 0.25$. Piezometric head (dashed) and stream function levels (solid) are in 5% increments between 0 and 1.
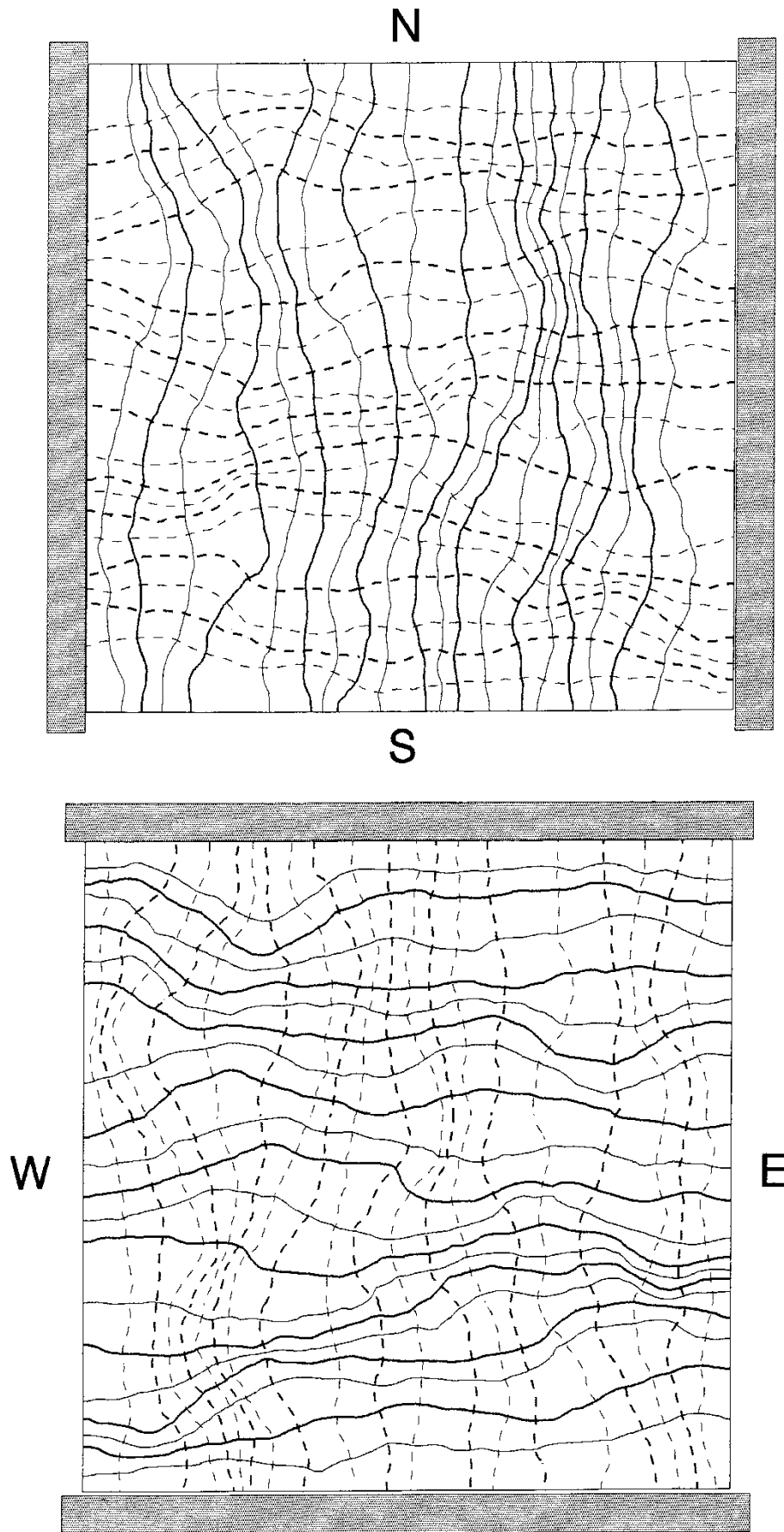
Fig. 62 Flow nets for N/S and W/E flow respectively. N = (64 x 64),

$\lambda/\Delta x = \lambda/\Delta y = 4$ and $\sigma_{\ln(K)} = 1.00$. Piezometric head (dashed) and

stream function levels (solid) are in 5% increments between 0 and 1.

Fig. 63 Flow nets for N/S and W/E flow respectively. N = (64 x 64),

$\lambda/\Delta x = \lambda/\Delta y = 4$ and $\sigma_{\ln(K)} = 4.00$. Piezometric head (dashed) and

stream function levels (solid) are in 5% increments between 0 and 1.
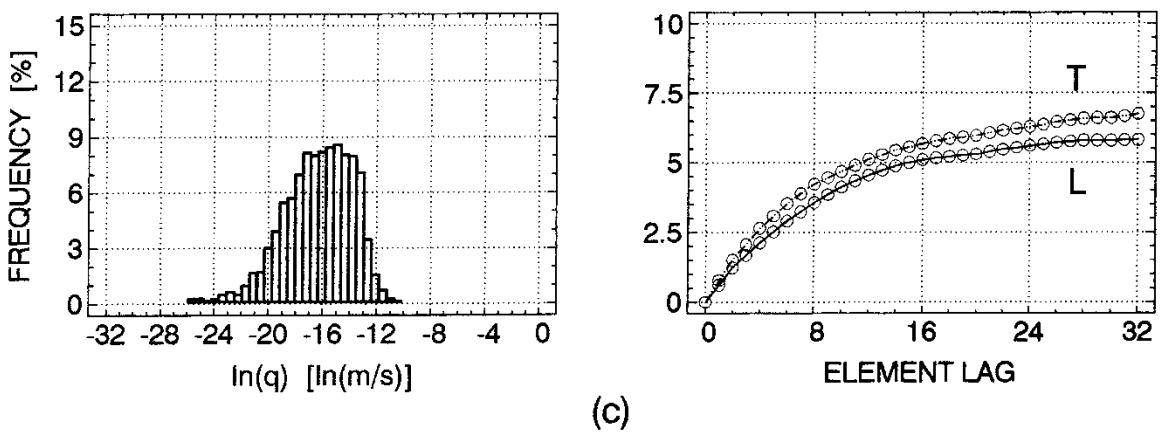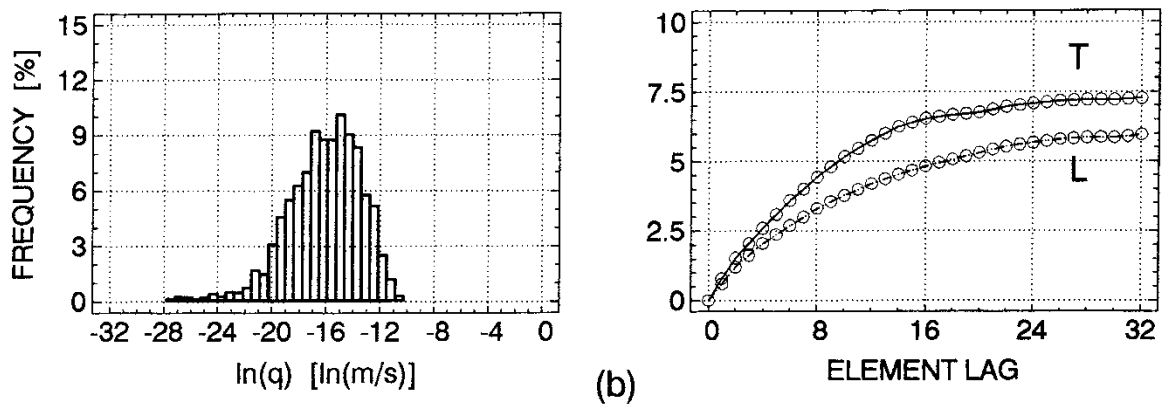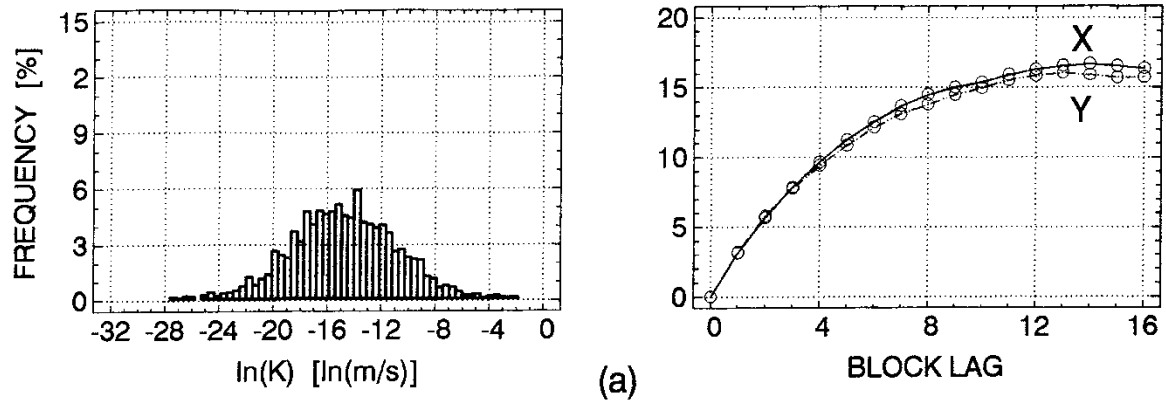
T = transverse   L = longitudinal

(a) ln(K)   (b) ln(q) N/S flow   (c) ln(q) W/E flow

Fig. 64 Histograms and variograms of ln(K) and ln(q) for case 4-44 .

$\lambda/\Delta x = \lambda/\Delta y = 4$ and $\sigma_{\ln(K)} = 4.00$.

3.4 Simulation of flow on different scales

In conditional simulation, measurements are honoured while generating a realization with a given spatial variability. For the flow problem, the measurements may represent flux, conductivity or head, or any combination of these. In this study, individual conditional realizations are not studied. Instead, the kriged conductivity field corresponding to the average look of all possible conditional realizations for a given set of data is studied. Under conditions of uniform average flow, the average hydraulic behaviour of all possible realizations is expected to correspond to the hydraulic behaviour of the average conductivity field [cf. Peck *et al.*, 1988]. In this study, the conditioning on conductivity data is addressed. The use of head data is not considered here because of the difficulties and uncertainties associated with its determination in deep boreholes in fractured hard rock [see, e.g. Almén *et al.*, 1986]. Flux data, if they exist, are more valuable for model calibration or as performance measures.

In the real world, conductivity data are obtained from interpretations of pumping tests, e.g. single-hole double-packer tests and interference tests. The information from interference tests is not readily included in a conditioning process because of the difficulties in determining the representative scales. Therefore, in the experiments presented below, only single-hole packer tests data are discussed. However, it is important to note that although the expression 'packer test data' is used below, the corresponding values are derived numerically. For instance, the block conductivity value used on a, for example, 24m scale, does not come from 'a true' packer test using a 24m straddle interval. Instead, it is replaced by a numerically derived conductivity value for a $(24m)^2$ block. There are several reasons for this simplification. The two major reasons are (*i*) it is a simple and straightforward way to control the radius of influence, i.e. to maintain a unique *point support* of each scale, and (*ii*) it provides a possibility to study the effects

of (hydraulic) anisotropy. The anisotropy is approximately addressed by doing each numerical flow experiment in two fixed orthogonal directions. The working hypothesis is made that the two directions are parallel to the principal directions of anisotropy of conductivity, i.e. it is assumed that the conductivity tensor ($\tilde{K}_S$) is in a diagonal form regardless of the block size.

Two cases of conditioning are studied: (i) the conductivity field is totally determined (deterministic case), and (ii) the conductivity field is only partially determined (stochastic case). In the latter case the remaining (unknown) values have to be estimated. There are several estimation methods in common use [see, for example, Warrick et al., 1990; Istok & Flint, 1991]. The ones compared here are the inverse distance method and ordinary kriging. The latter method takes the correlation into account, whereas the former method does not.

The differences in the hydraulic behaviour between the deterministic and the stochastic simulations are studied with respect to the hydraulic behaviour of an a priori case representing an assumed known realization of the flow domain. The chosen a priori case is characterized by $\lambda_Y/\Delta x = \lambda_Y/\Delta y = 2$, $\sigma_Y = 4$, and $N = 64\times64$, i.e. case 4-22. The a priori case is shown in Figure 70. For $\Delta x = \Delta y = 3m$, the a priori case corresponds to a hypothetical rock block of $(192m)^2$ and $\lambda_Y = 6m$. The hydraulic behaviour of the a priori case is of course completely known, see Figure 78. The interest here is focused on investigating the possibility of simulating the a priori behaviour on a different scale, or even on the same scale as the a priori case but with only a limited amount of data for conditioning.

Two support scales are studied; a "24m scale" and a "3m scale". In what follows, the a priori case is compared with various realizations using block conductivities on these two scales. On the 24m scale, the flow domain is represented by 64 $(24m)^2$ blocks, whereas on the 3m scale it is represented by 4,096 $(3m)^2$ blocks, see Figure 66. The objectives are to investigate (i) the validity of applying the results obtained from the unconditional simulations of

flow in single blocks to flow in an aggregate of blocks, and (ii) the differences between two scales of support. It is hypothesized that anisotropy is important for the upscaling process.

The degree of disagreement between the simulation experiments (being deterministic or stochastic; on the 3m scale or on the 24m scale) and the a priori case is expressed in terms of an *overall error index* (*OEI*). This index is here defined as the sum of four dimensionless errors. Two of these errors concern the differences in flux on a homogenized "192m scale", whereas the other two concern the differences in head at more than 16,000 interior nodes. The hydraulic behaviour is studied in two orthogonal directions. A low value of the *OEI* indicates a good experimental fit.

The dimensionless error of the flux is equivalent to that of the block conductivity (see relation (43)). For flow in direction i the dimensionless error is denoted E_K^i and defined as

$$E_K^i = \left| \frac{(K_{ii} - K_{ii}^{ap})}{K_{ii}^{ap}} \right| \qquad i = 1,2 \qquad (47a)$$

with K_{ii}^{ap} being the block conductivity of the a priori case for flow in direction i. The dimensionless error in the head solution for flow in the ith direction is denoted E_φ^i and defined as [cf. Loague & Green, 1990]

$$E_\varphi^i = \frac{MSE_\varphi^i}{(\sigma_\varphi^{aP_i})^2} \qquad i = 1,2 \qquad (47b)$$

with MSE_φ^i being the *mean square error* in φ for flow in direction i,

$$MSE_\varphi^i = \frac{1}{N} \sum_{j=1}^{N} (\varphi_j^i - \varphi_j^{aP_i})^2 \qquad i = 1,2 \qquad (47c)$$

$(\sigma_\varphi^{a\,p_i})^2$ in (47b) denotes the *mean square deviation* (variance) in φ of the a priori case in direction i. Consequently, the overall error index (OEI) may be written as

$$OEI = \sum_{i=1}^{2} E_K^i + E_\varphi^i \qquad (47d)$$

In what follows, nine different numerical experiments, denoted A-I, are carried out. Three experiments address the issue of interpolation and conditioning, and six experiments address statistical and hydraulic upscaling, see Figure 65.

A	Inverse distance, 2 λ_Y	$K = f(r^{-2})$	3m → 3m
B	Ordinary kriging, 2 λ_Y	$K = f(\gamma_2(h))$	3m → 3m
C	Ordinary kriging, 4 λ_Y	$K = f(\gamma_4(h))$	3m → 3m
D	Stat. geometric mean	$K = exp(m_Y)$	3m → 24m
E	Ordinary kriging, 2 λ_Y	$K = f(\gamma_2(h))$	3m → 24m
F	Ordinary kriging, 4 λ_Y	$K = f(\gamma_4(h))$	3m → 24m
G	Both components	$K_{11} = K_{xx}$ & $K_{22} = K_{yy}$	3m → 24m
H	Hydr. geometric mean	$K = \sqrt{(K_{xx}\,K_{yy})}$	3m → 24m
I	One component	$K = K_{xx}$ or $K = K_{yy}$	3m → 24m

Fig. 65 The nine experiments used here to study interpolation and conditioning (A-C) and upscaling (D-I).

As shown in Figure 65, three cases are studied using 3m blocks: (A) the inverse distance method with a search radius of $r = 2\,\lambda_Y$, (B) ordinary kriging with $r = 2\,\lambda_Y$, and (C) ordinary kriging with $r = 4\,\lambda_Y$. In each case, the equations are conditioned upon 512 "3m packer tests" (conductivity values) using eight equidistant bore-

holes, which means that 3,584 values are unknown and have to be estimated (K^*). Each borehole provides 64 conductivity values on the 3m scale and the borehole spacing is 24m, see Figure 67a. Upon kriging, the variogram of the a priori case is used here rather than the experimental variograms. According to Warrick et al. [1990], the accuracy of ordinary kriging is more influenced by the sample on which the interpolations are made than by the exact model.

Figures 68 and 69 show some statistics for the three cases A, B, and C, as well as for the a priori case 4-22. Figures 71-73 show the estimated conductivities using raster graphics. Figures 74 and 75 show the estimation errors (see also the statistics for the estimation error in Figure 68). The flow nets for the three cases are shown in Figures 79-81.

Figure 67b shows the 64 24m blocks used in this study. The 64 block conductivities are obtained either *deterministically* or *stochastically*. The deterministic way is here represented by the three cases denoted G, H, and I, see Figure 65. In these three cases, the block conductivity for each one of the 64 24m blocks is estimated by running the flow model for that particular block, i.e. the blocks are separated one by one using the conductivity values of the underlying a priori case. Furthermore, in order to investigate the role of hydraulic anisotropy, the flow model is run in two orthogonal directions for each block. The values obtained in this manner are conceptually regarded as representing 24m packer tests using the eight boreholes mentioned previously. That is to say, each borehole provides eight block conductivities on the 24m scale.

The stochastic way on the 24m scale is here represented by the two cases denoted E and F in Figure 65. In these two cases, the 64 block conductivities are estimated by computing the geometric mean of the previously kriged conductivities in conjunction with cases B and C. It should be noted that there are other more sophisticated ways to accomplish such *block estimates* [see, for example, Journel & Huijbregts, 1978; de Marsily, 1986; Peck et al., 1988].

The last experiment to be discussed here is case D in Figure 65. In this case, the conductivity of a block on the 24m scale is obtained by computing the geometric mean of all 3m data within it, i.e. the estimate is in this case fully conditioned. Figure 76 shows a raster graphics representation of case D. In Figure 77, the covariances for cases D and I are shown. Figures 82-88 show the flow nets for cases D-I. In Figures 89 and 90, the results of all the calculations are presented. In words, the results from the nine experiments are interpreted as follows:

Ordinary kriging (B) (Figures 72 and 80) yields a better result than the inverse distance method (A) (Figures 71 and 79), but is not as good as ordinary kriging (C) (Figures 73 and 81). The search radius $r = 4\ \lambda_Y$ gives full credit to the range of correlation of the log-conductivity field. The search radius $r = 2\ \lambda_Y$ is only half the range of correlation. In the inverse distance method, the correlation is irrelevant, which makes this method is of interest whenever correlation is absent, i.e. $\lambda_Y \to 0$.

Ordinary kriging (C) (Figures 73 and 81) on the 3m scale yields a better result than using only one of the two components (I) of $\tilde{K}_S$ on the 24m scale (Figures 87 and 88).

The statistical (spatial) geometric mean (D) (Figures 76 and 82) yields a better result than ordinary kriging (E) and (F) (Figures 83 and 84). The spatial geometric mean may in this case be regarded as the optimal block estimator on the 24m scale.

A use of both components of $\tilde{K}_S$ (G) (Figure 85) yields the best result. It is far better than using only one component (I) (Figures 87 and 88). Moreover, it is also better than using the *hydraulic geometric mean* (H) (Figure 86), or the statistical (spatial) geometric mean (D) (Figures 76 and 82). It is noteworthy that the flow net in Figure 85 is not locally orthogonal [cf. Bear, 1972]. In other

words, the gradient of φ is not necessarily parallel to the direction of flow in an anisotropic conductivity field.

The covariance functions on the 24m scale (see Figure 77), as inferred by analysing the block conductivities in (D) and (I), suggest that (i) the initial exponential form of the covariance function on the 3m scale is preserved on the 24m scale, and (ii) the changes in λ_Y and σ_Y appear to follow the principle of *conservation of uncertainty* [cf. Vanmarke, 1983]. These results are somewhat in contradiction to the study by Rubin & Gómez-Hernández [1990].

The results obtained here are of course only valid for the nine experiments in Figure 65 under the prevailing conditions described previously. It is important to note that the present study is dependent on two assumptions, namely that (i) the conductivity tensor on the 24m scale is in a diagonal form, and (ii) the principal components of this tensor are equal to the conductivities in two fixed orthogonal directions. Strictly speaking, both these assumptions are physically incorrect, at least for small and moderate block sizes. On the other hand, it is demonstrated in the present study that these assumptions are probably more appropriate than the usual statistical assumption of hydraulic isotropy. In spite of the tremendous progress in subsurface hydrology owing to the developments in stochastic continuum theory, it must not be forgotten that physics is an experimental science, and the numerical experiments presented here have shown that hydraulic anisotropy deserves much more attention in the upscaling process.

The theory of regionalized variables and ordinary kriging constitute cornerstones of geostatistics. For example, Warrick *et al.* [1990] and Istok & Flint [1991] discuss important constraints of traditional geostatistics. So does also Gómez-Hernández [1991] who questions the use of Gaussian generators, which he claimes to neglect the impact of high connectivity between the exterme values.
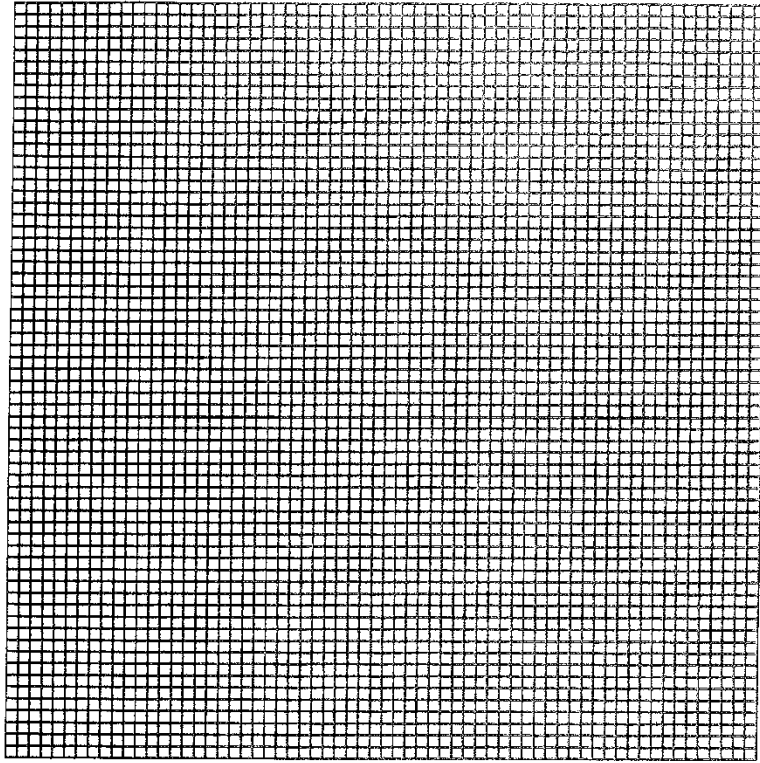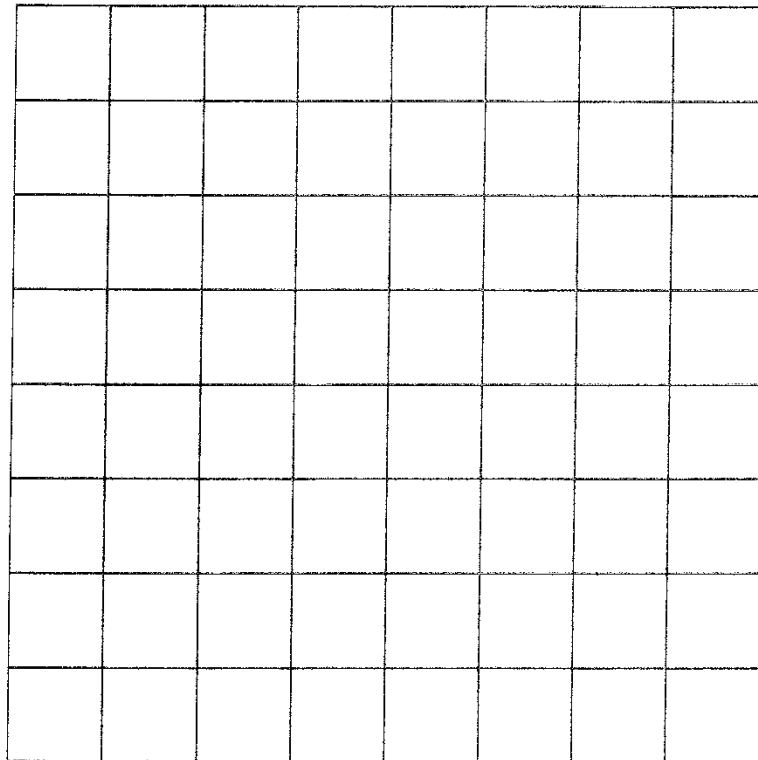
Fig. 66 Two different support scales representing the same medium:

(a) N = (64 x 64) Δx = Δy = 3m   (b) N = (8 x 8) Δx = Δy = 24m.

BH1 BH2 BH3 BH4 BH5 BH6 BH7 BH8
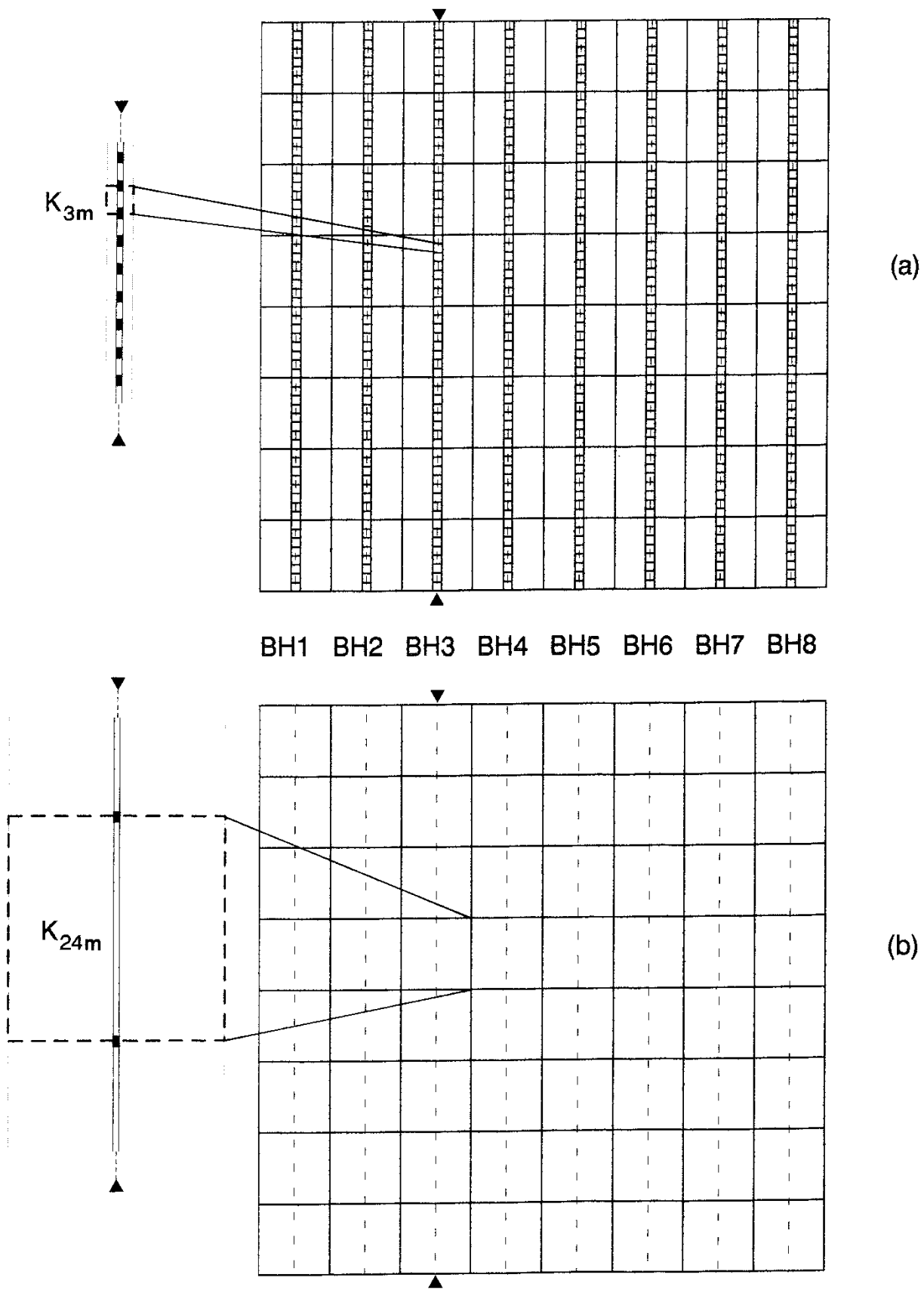
Fig. 67 Schematic view of the differences in "point support" for 8 boreholes:

(a) 512 3m-packer tests and (b) 64 24m-packer tests .
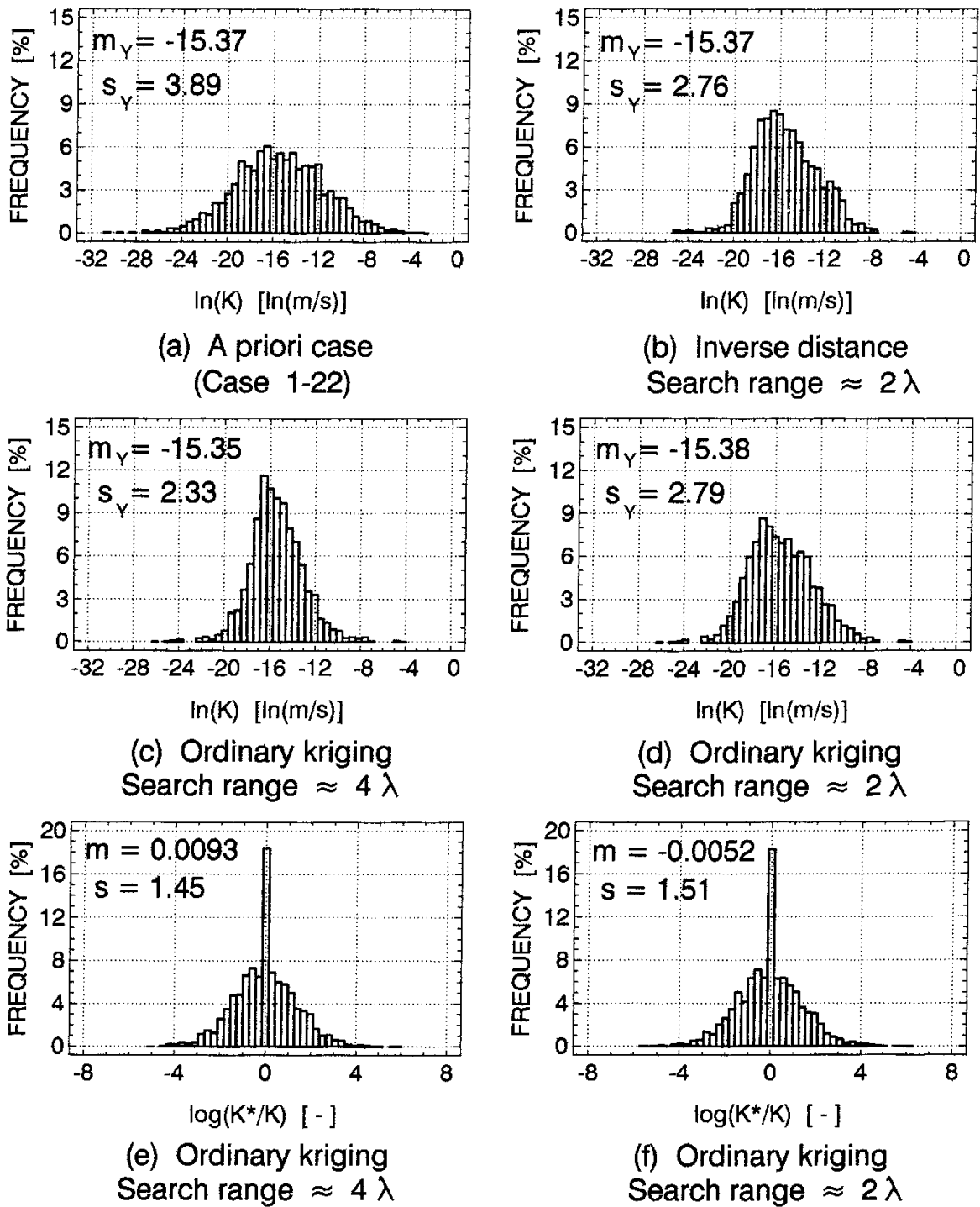
Fig. 68 Histograms for three estimates of the hydraulic conductivity of the support scale (b, c and d). The histogram for the a priori case is shown in (a) . In (e) and (f) error histograms for the two kriging estimates (K*) are shown.
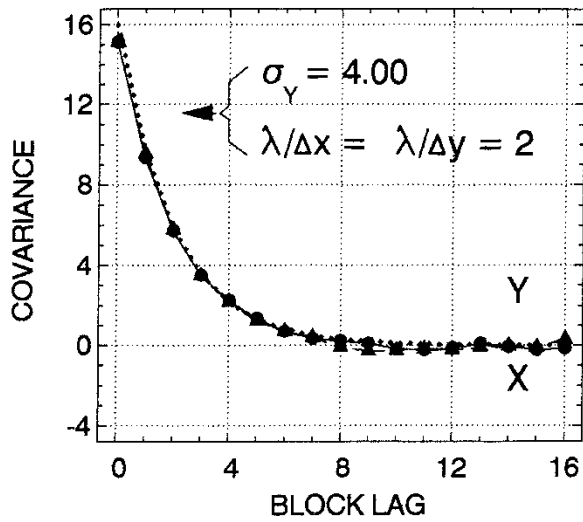
A priori case: $s_Y = 3.89$

(Case 4-22)
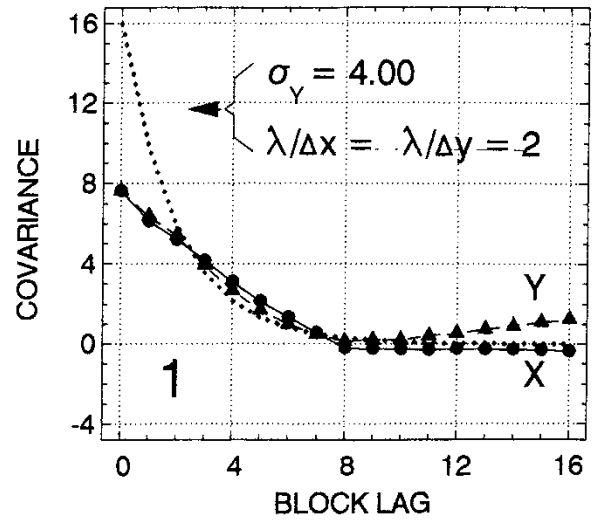
Inverse distance: $s_Y = 2.76$

Search range $\approx 2\lambda$
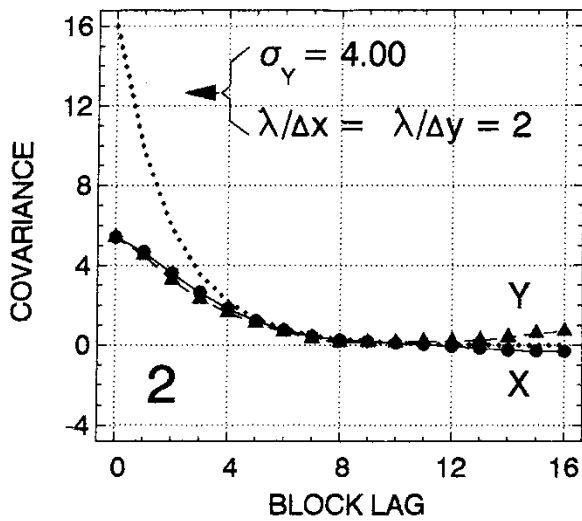
Ordinary kriging: $s_Y = 2.33$

Search range $\approx 4\lambda$
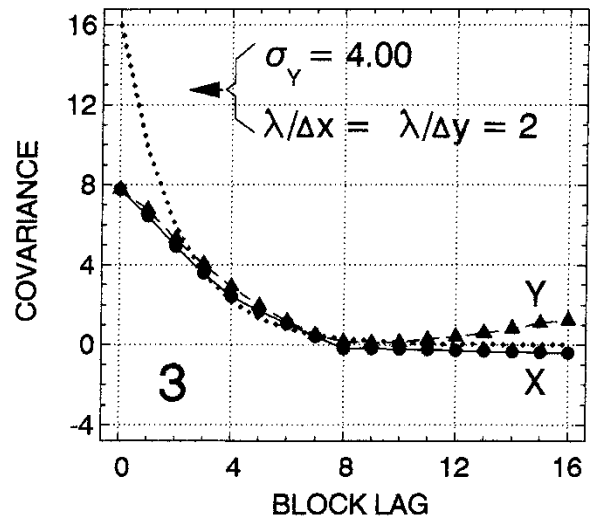
Ordinary kriging: $s_Y = 2.79$

Search range $\approx 2\lambda$

Fig. 69 Covariances for three estimates of the hydraulic conductivity
of the support scale . The a priori case is shown top left .

2-D HYDRAULIC CONDUCTIVITY FIELD

No. of blocks: 64 × 64   A priori case

$s_{\ln(K)}$ = 3.89 $\lambda/\Delta x$ = 2.0 $\lambda/\Delta y$ = 2.0

RASTER LEGEND (dim[K]=m/s)

12.5 %	12.5 %	12.5 %	12.5 %
+5.04E-14 ▨ +2.56E-09	■ +1.49E-08	■ +5.90E-08	▦ +2.11E-07
+2.11E-07 ▧ +7.19E-07	▒ +3.04E-06	⋮ +1.89E-05	□ +9.42E-02
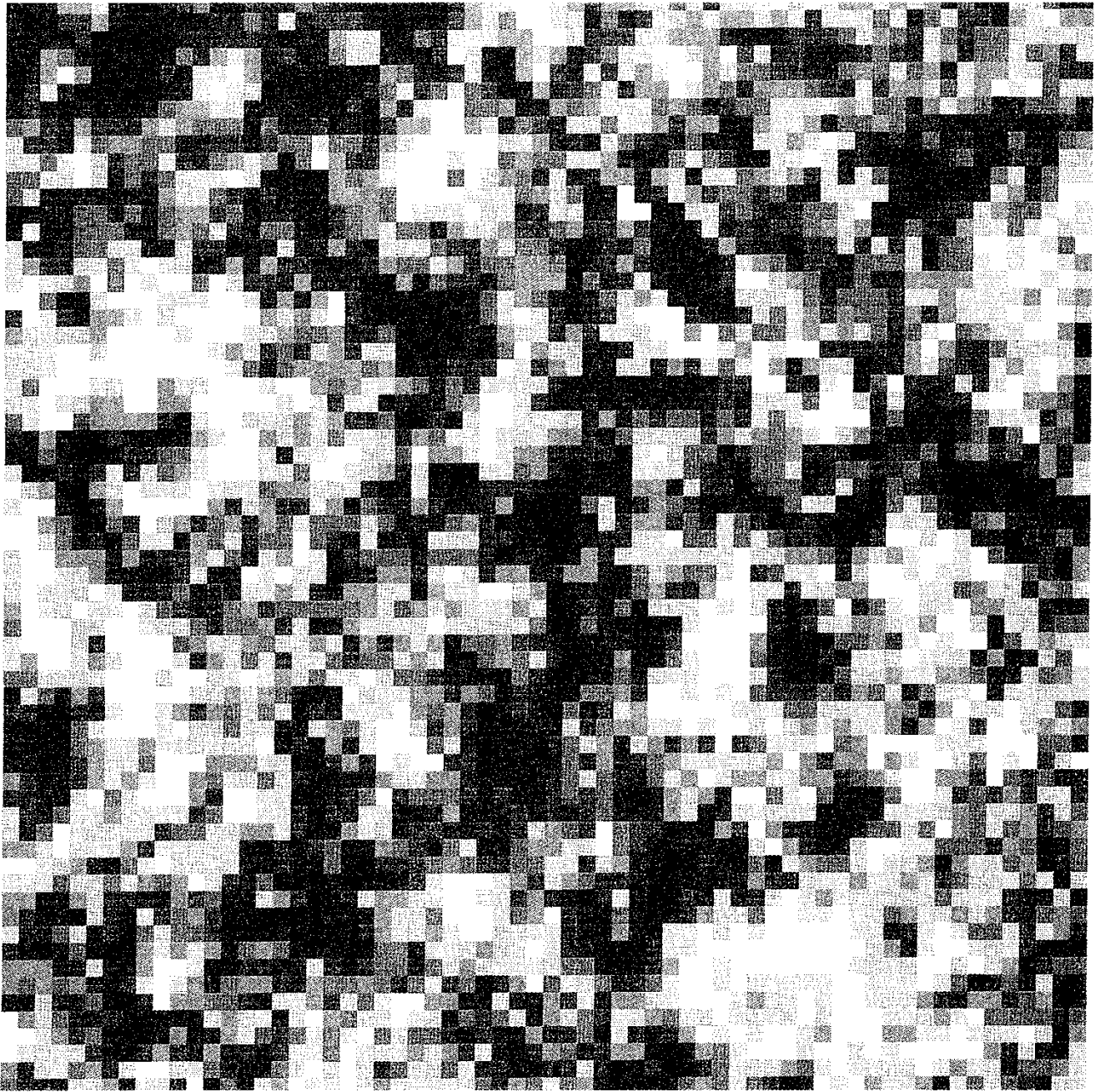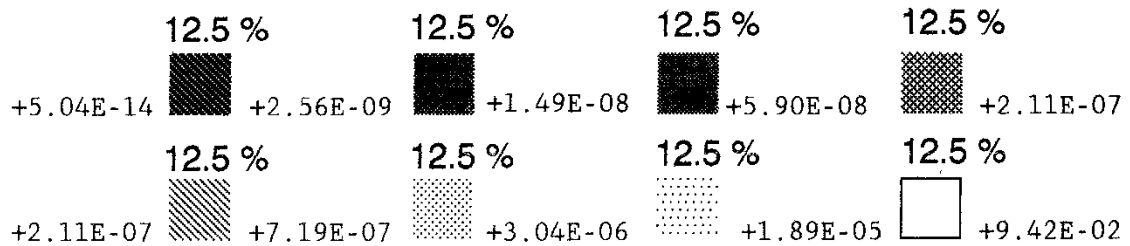
Fig. 70 The a priori case, i.e. case 4-22.

2-D HYDRAULIC CONDUCTIVITY FIELD

No. of blocks: 64 × 64   Inverse distance

$s_{ln(K)} = 2.76$ Search radius $= 2\lambda$

RASTER LEGEND (dim[K]=m/s)

3.4 %	13.0 %	17.9 %	19.1 %
+4.57E-12	+2.56E-09	+1.49E-08	+5.90E-08

+2.11E-07

15.7 %	12.6 %	12.1 %	6.2 %
+2.11E-07	+7.19E-07	+3.04E-06	+1.89E-05

+1.21E-02

Fig. 71 Case A: inverse distance, SR ≈ 2λ.

2-D HYDRAULIC CONDUCTIVITY FIELD

No. of blocks: 64 × 64   Ordinary kriging

$s_{\ln(K)}$ = 2.79   Search radius = 2λ

RASTER LEGEND (dim[K]=m/s)

4.3 %	12.7 %	17.8 %	17.8 %
+4.57E-12	+2.56E-09	+1.49E-08	+5.90E-08 +2.11E-07

15.4 %	15.3 %	10.4 %	6.3 %
+2.11E-07	+7.19E-07	+3.04E-06	+1.89E-05 +1.21E-02

Fig. 72 Case B: ordinary kriging, SR ≈ 2λ.

2-D HYDRAULIC CONDUCTIVITY FIELD

No. of blocks: 64 × 64   Ordinary kriging

$s_{ln(K)}$ = 2.33   Search radius = 4λ

RASTER LEGEND (dim[K]=m/s)

2.6 %	7.5 %	16.8 %	25.2 %
+4.57E-12 ▨ +2.56E-09	▨ +1.49E-08	▨ +5.90E-08	▨ +2.11E-07

20.9 %	15.8 %	7.6 %	3.6 %
+2.11E-07 ▨ +7.19E-07	▨ +3.04E-06	+1.89E-05	☐ +1.21E-02

Fig. 73 Case C: ordinary kriging, SR ≈ 4λ.

log(K*/K)

No. of blocks: 64 × 64   Ordinary kriging

$s_{\ln(K)} = 2.79$ Search radius = 2λ

RASTER LEGEND FOR log(K*/K)

- 5.47	■	- 3	■	- 2	■	- 1	▦	+ 0
+ 0	▧	+ 1	▒	+ 2	░	+ 3	□	+ 6.06

⊠
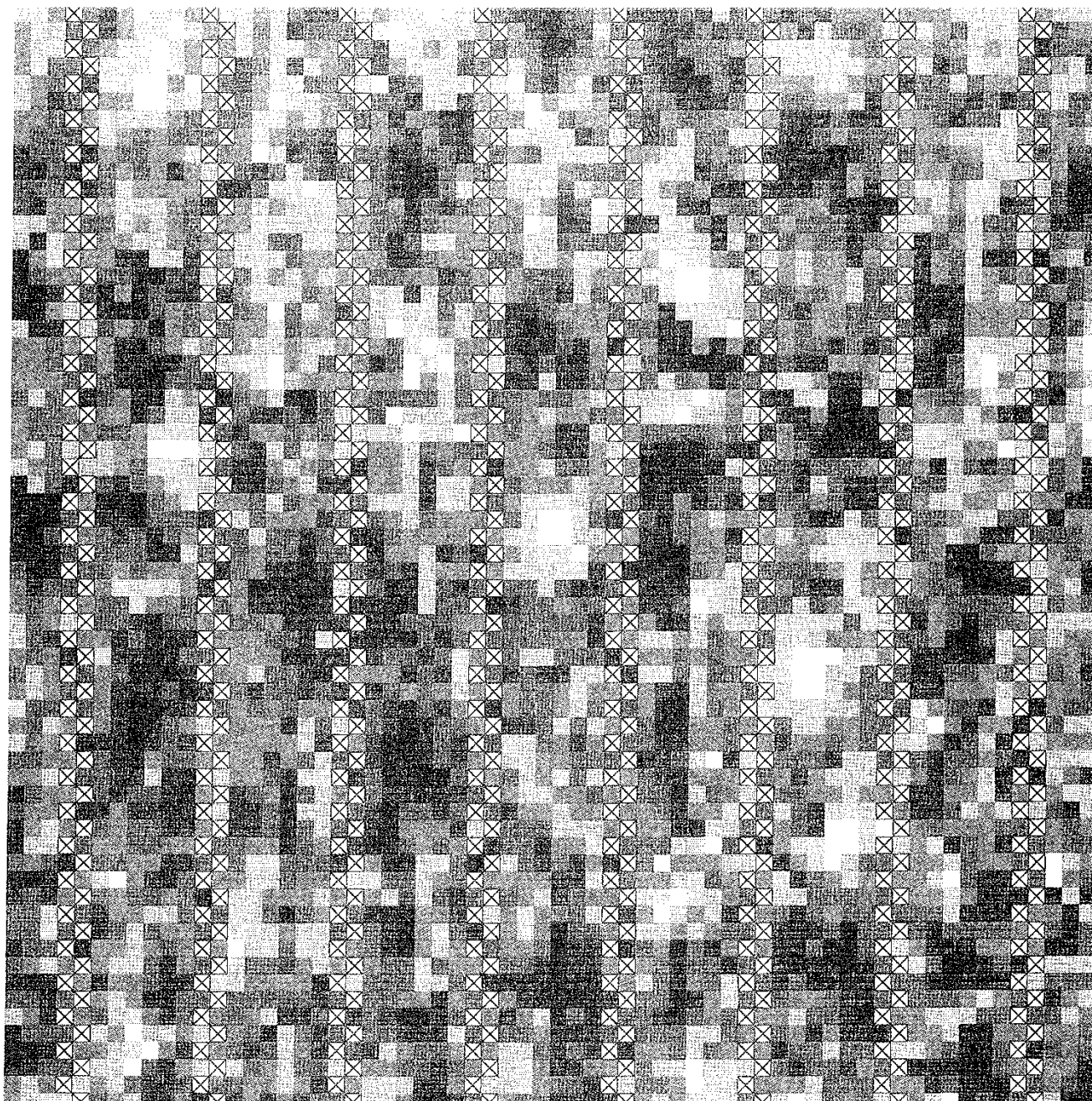
BOREHOLE DATA

Fig. 74 Kriging error for case B .

log(K*/K)

No. of blocks: 64 × 64   Ordinary kriging

$s_{\ln(K)}$ = 2.79   Search radius = 4λ

RASTER LEGEND FOR log(K*/K)

- 5.02   - 3   - 2   - 1   + 0

+ 0   + 1   + 2   + 3   + 6.01
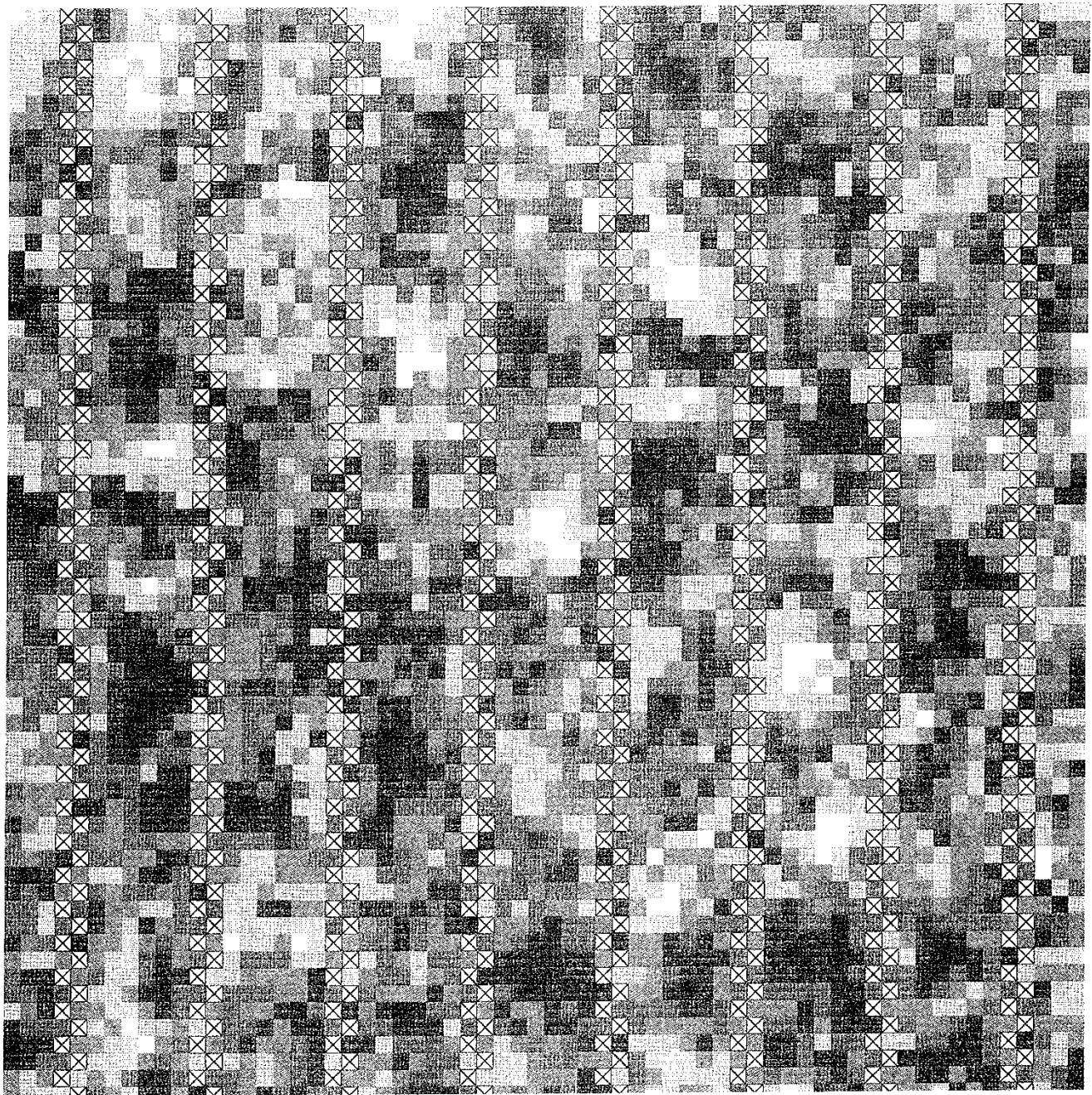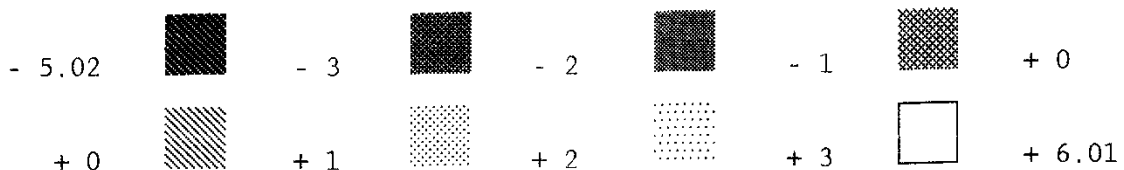
BOREHOLE DATA

Fig. 75 Kriging error for case C .

2-D HYDRAULIC CONDUCTIVITY FIELD

No. of blocks: 8 × 8 $s_{ln(K)}$ = 1.85

RASTER LEGEND (dim[K]=m/s)

0 %	7.8 %	15.6 %	31.3 %
+2.56E-09	+1.49E-08	+5.90E-08	+2.11E-07

21.9 %	14.0 %	7.8 %	1.6 %
+2.11E-07 +7.19E-07	+3.04E-06	+1.89E-05	+2.31E-05
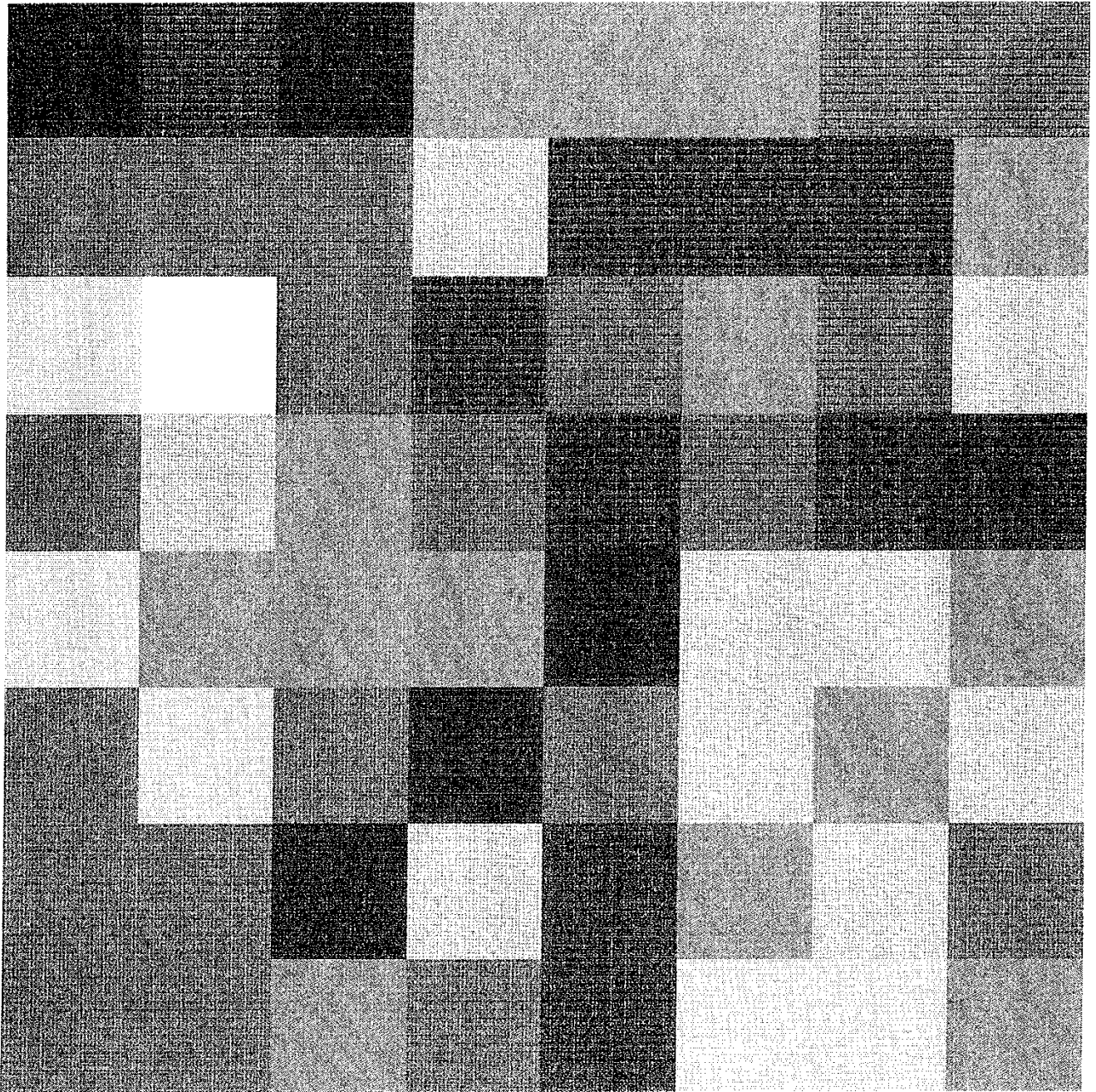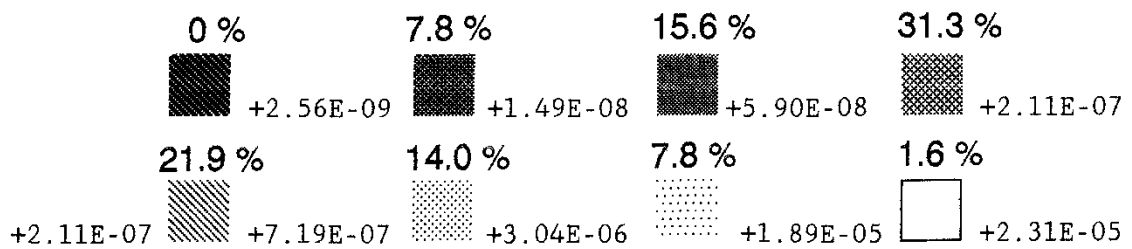
Fig. 76   Case D, geometric mean of all 3m data .
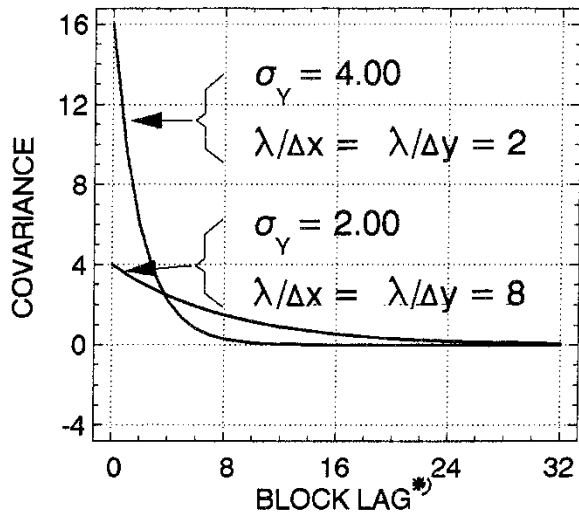
(a) $C_Y(h) = \sigma_Y^2 \exp(-h/\lambda)$
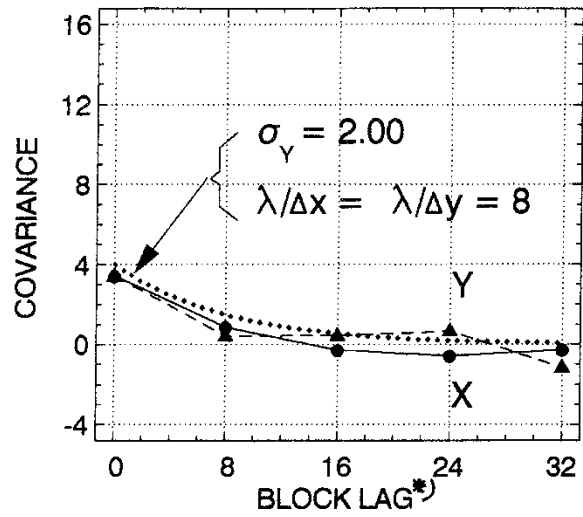
(b) $\exp(m_Y)$: $s_Y = 1.85$
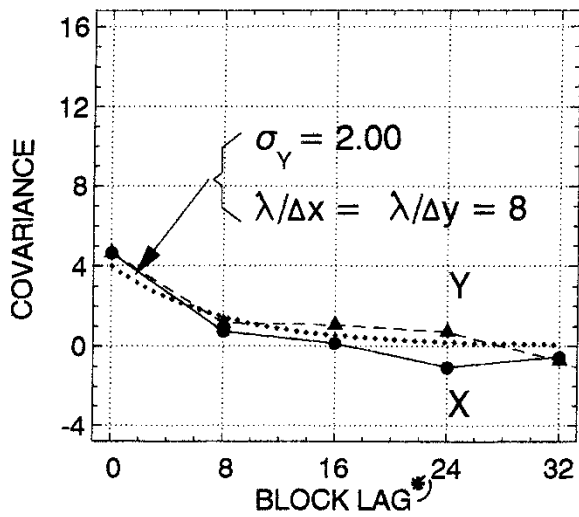
(c) K_{xx} : $s_Y = 2.16$
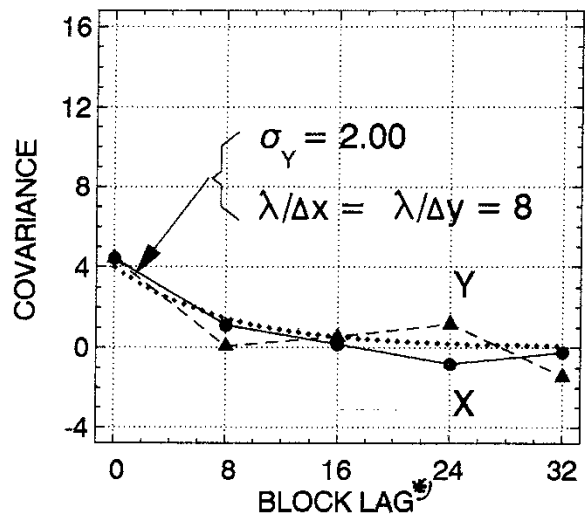
(d) K_{yy} : $s_Y = 2.11$

*) Refers to the original support scale

Fig. 77 Covariances for the hydraulic conductivity of the upscaled blocks
i.e., N = 8 x 8 . In (b) the geometric mean of each block is used
whereas in (c) and (d) the two diagonal components of the hydraulic
conductivity tensor are used, respectively. In (a) two covariance
functions are shown illustrating "conservation of uncertainty" .
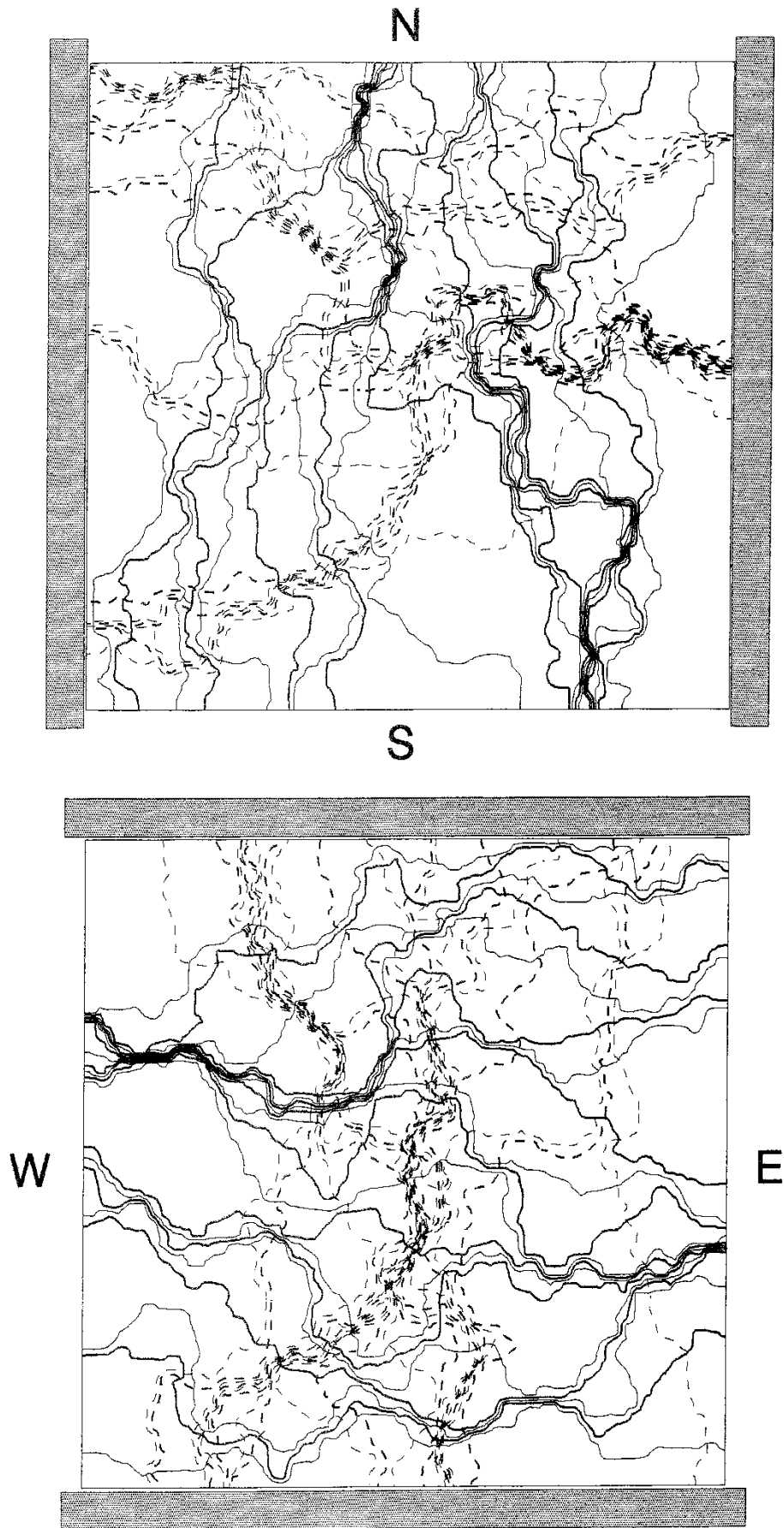
Fig. 78 Flow nets for the a priori case, i.e. case 1-22. N = (64 x 64) blocks,

$\lambda/\Delta x = \lambda/\Delta y = 2$ and $s_{\ln(K)} = 3.89$. Piezometric head (dashed) and

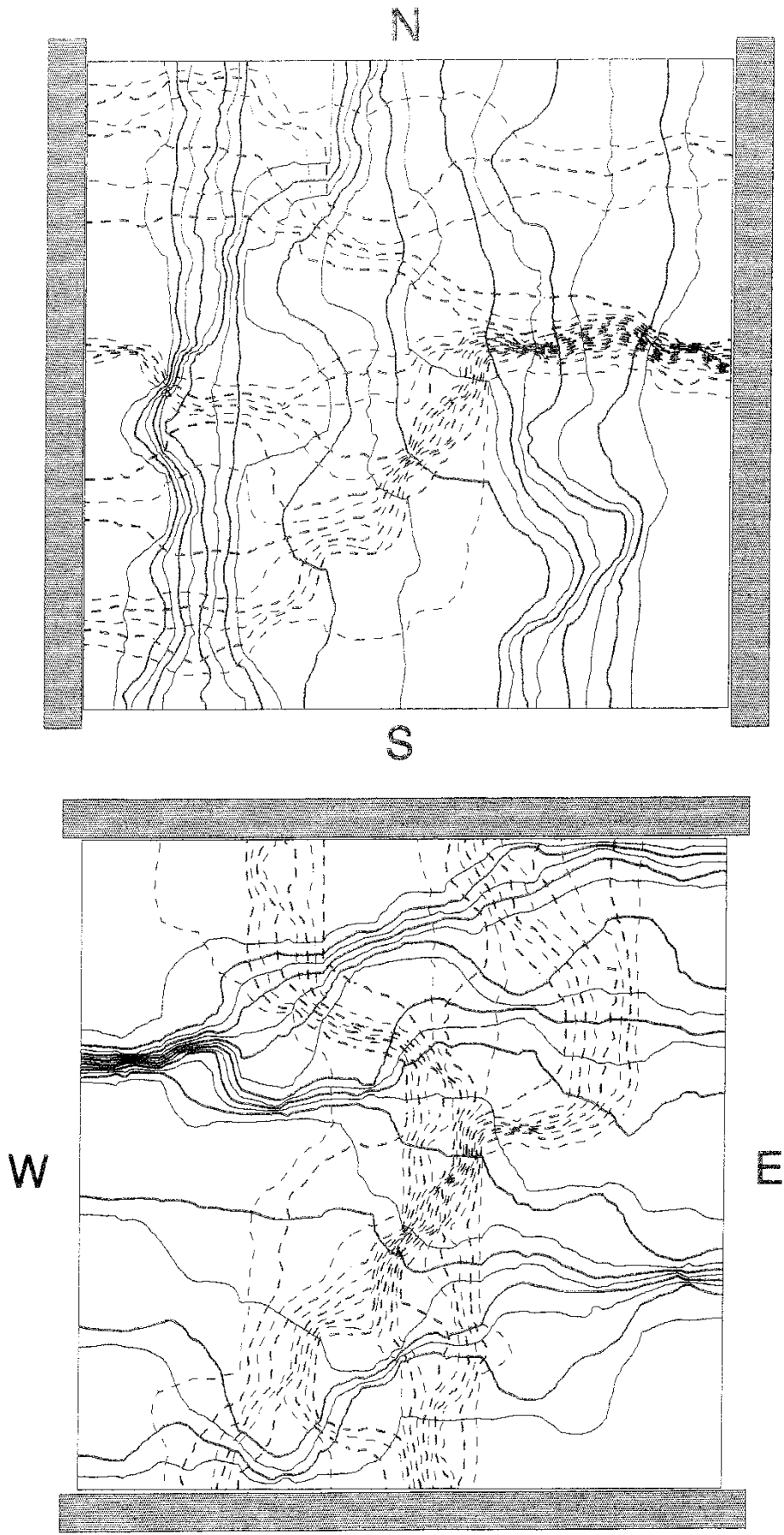stream function levels (solid) are in 5% increments between 0 and 1.

Fig. 79 Flow nets for case A, inverse distance SR ≈ 2λ , N = (64 x 64) .

$S_{In(K)}$ = 2.76 . Piezometric head (dashed) and stream function
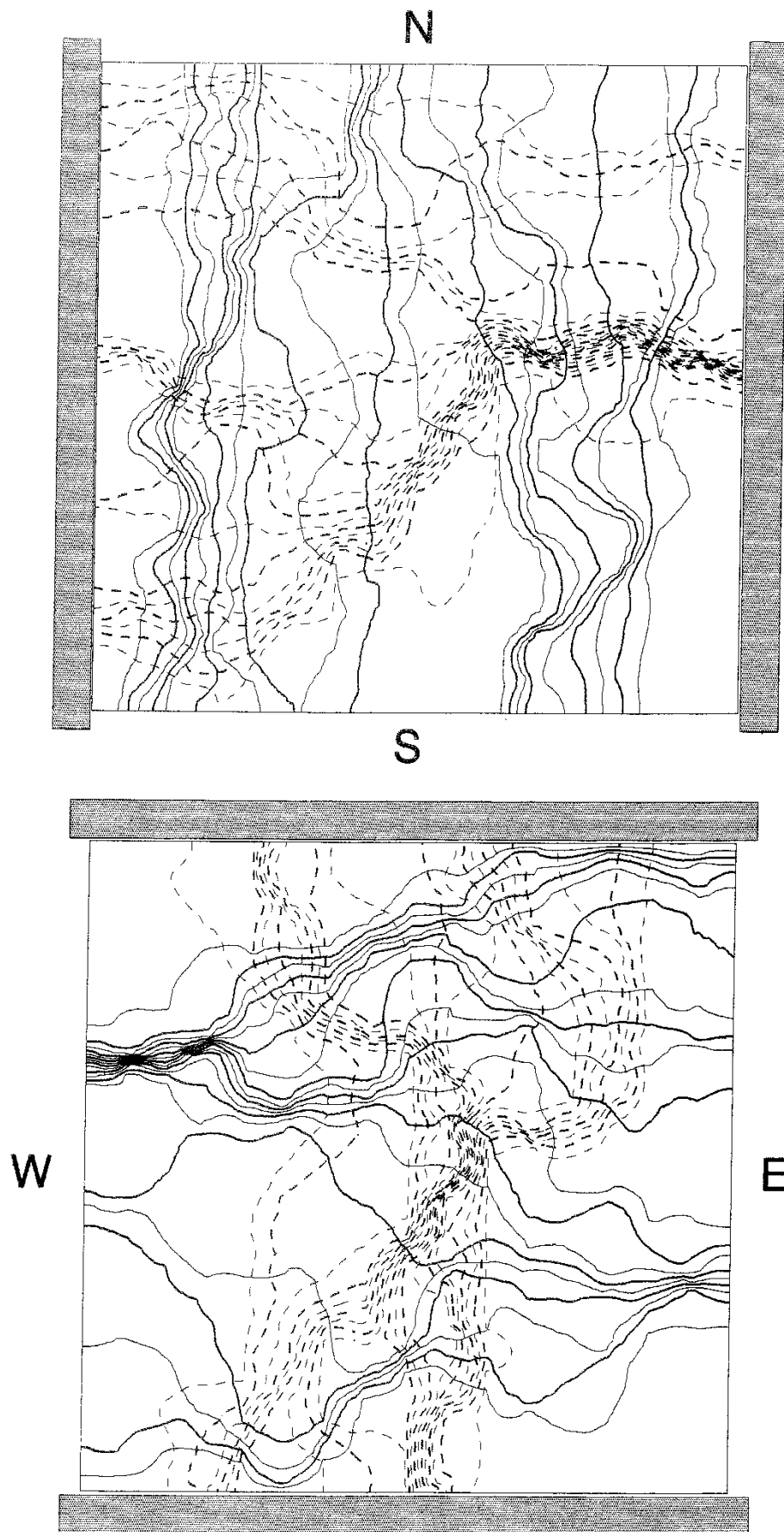
levels (solid) are in 5% increments between 0 and 1.

Fig. 80 Flow nets for case B, ordinary kriging SR ≈ 2 λ, N = (64 x 64) .

$s_{\ln(K)}$ = 2.79 . Piezometric head (dashed) and stream function
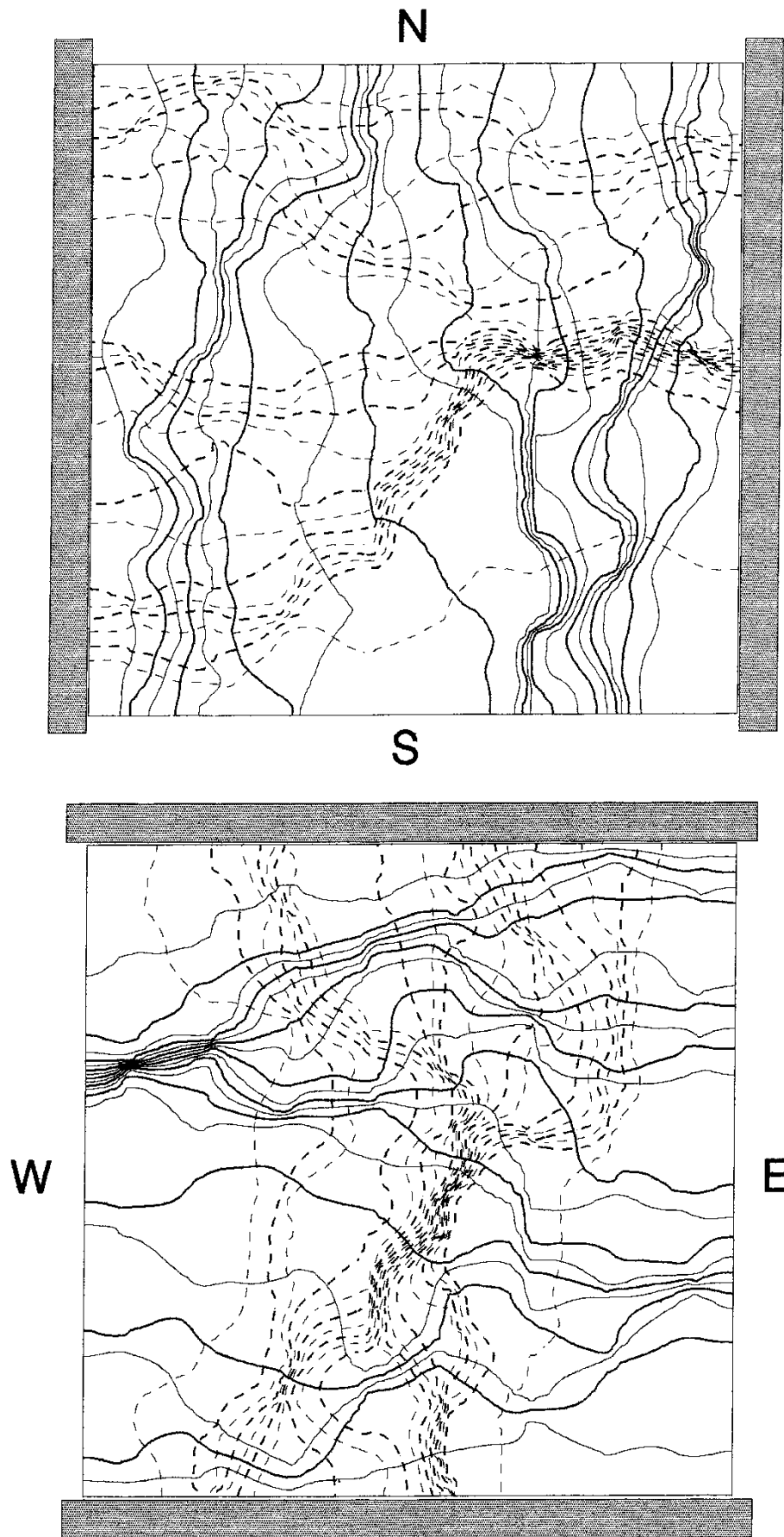
levels (solid) are in 5% increments between 0 and 1.

Fig. 81 Flow nets for case C, ordinary kriging SR $\approx 4\,\lambda$, N = (64 x 64) .

$s_{\ln(K)}$ = 2.33 . Piezometric head (dashed) and stream function
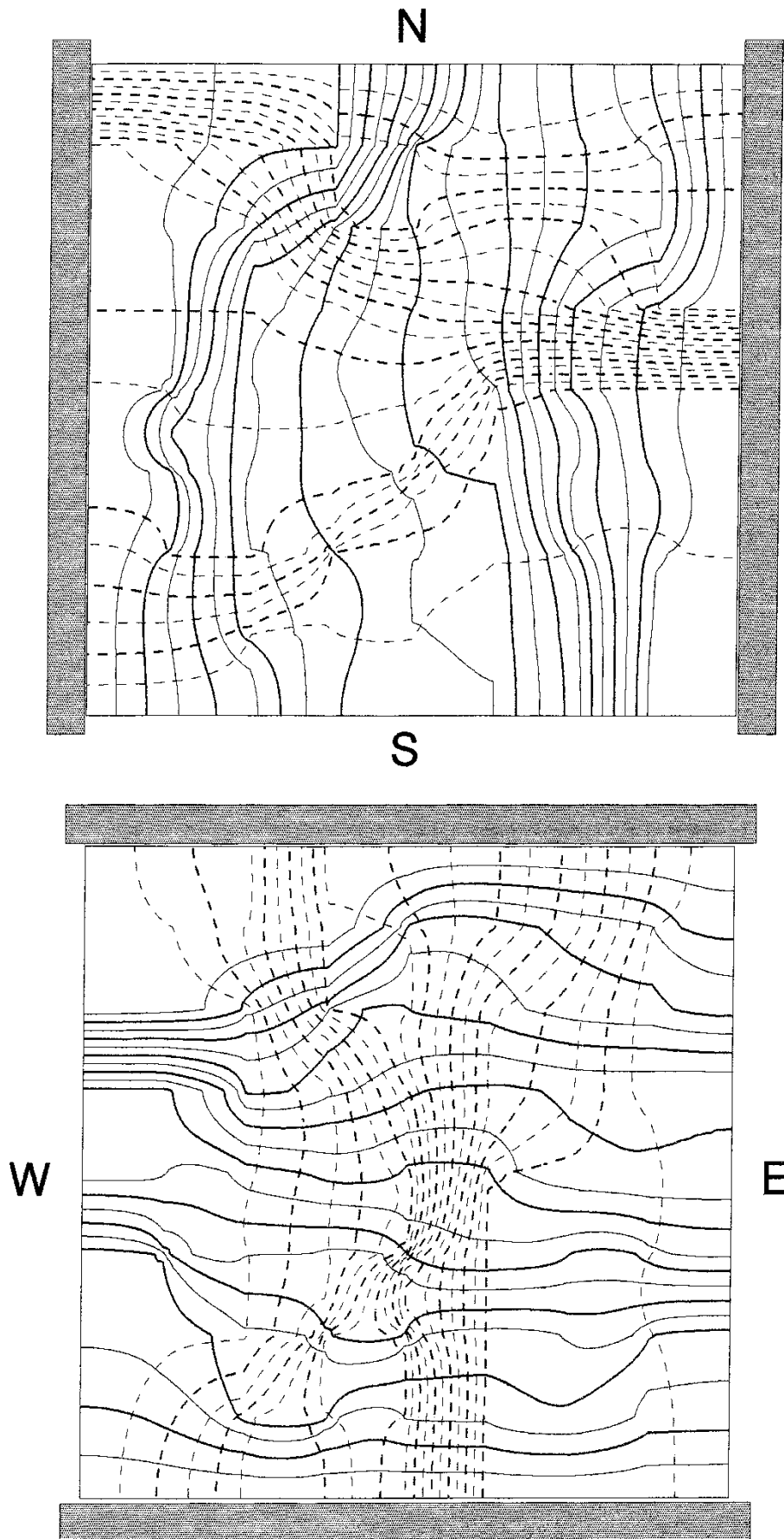
levels (solid) are in 5% increments between 0 and 1.

Fig. 82 Flow nets for case D, geometric mean of all 3m data, N = (8 x 8) .

$s_{\ln(K)}$ = 1.85 . Piezometric head (dashed) and stream function
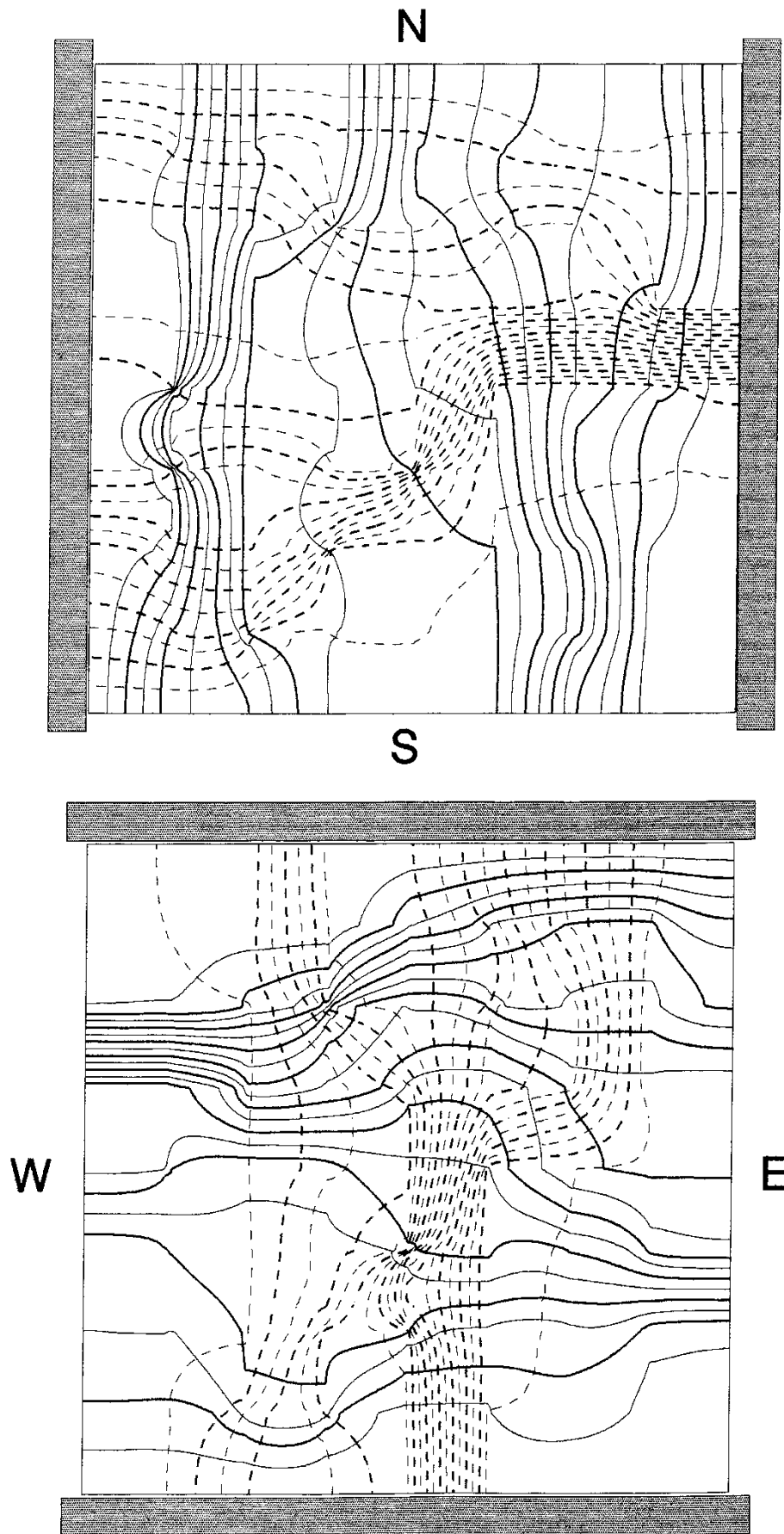
levels (solid) are in 5% increments between 0 and 1.

Fig. 83 Flow nets for case E, ordinary kriging SR ≈ 2 λ, N = (8 x 8) .

$S_{\ln(K)}$ = 2.14 . Piezometric head (dashed) and stream function

levels (solid) are in 5% increments between 0 and 1.

Fig. 84 Flow nets for case F, ordinary kriging SR ≈ 4 λ, N = (8 x 8).

$S_{ln(K)}$ = 1.55 . Piezometric head (dashed) and stream function

levels (solid) are in 5% increments between 0 and 1.

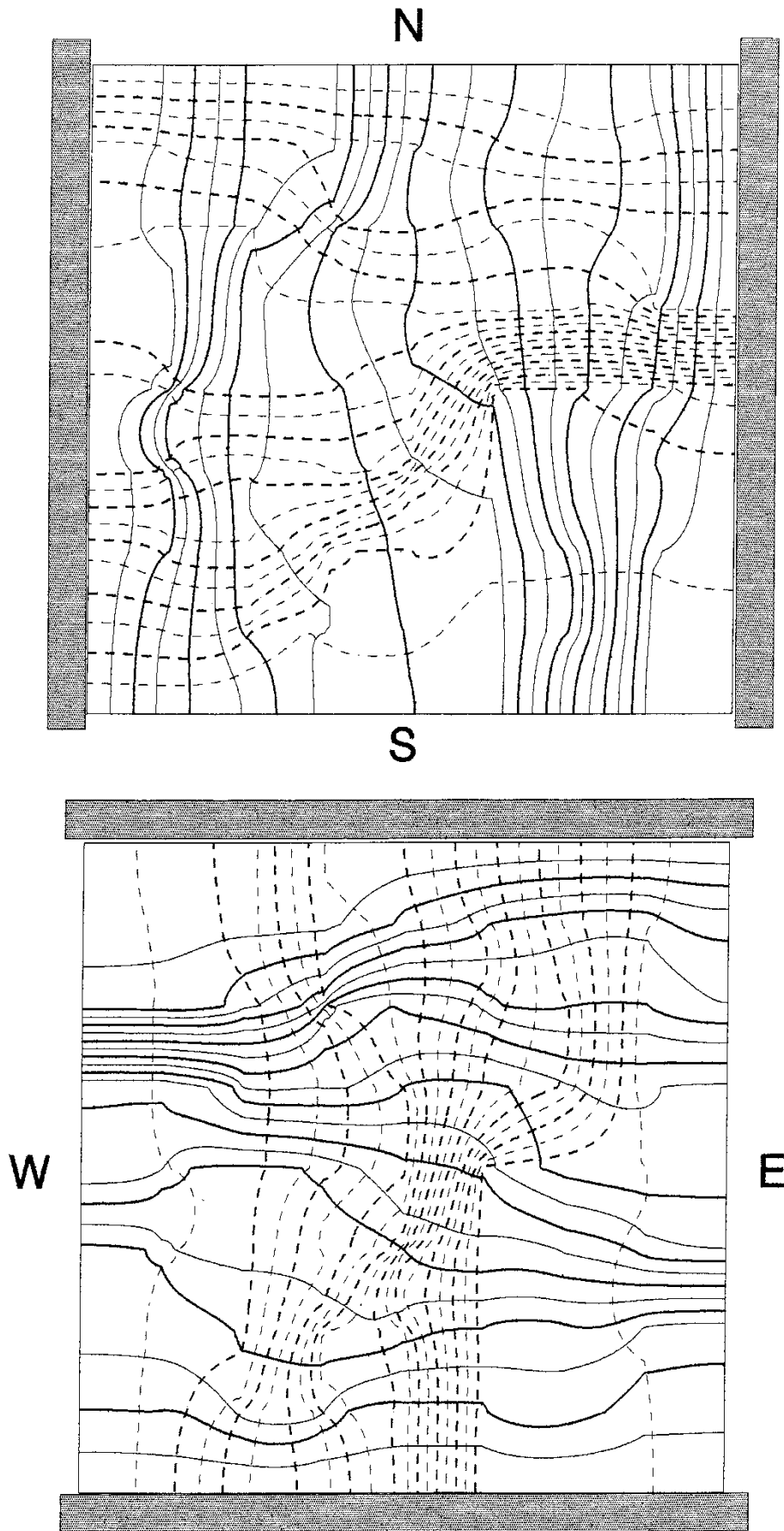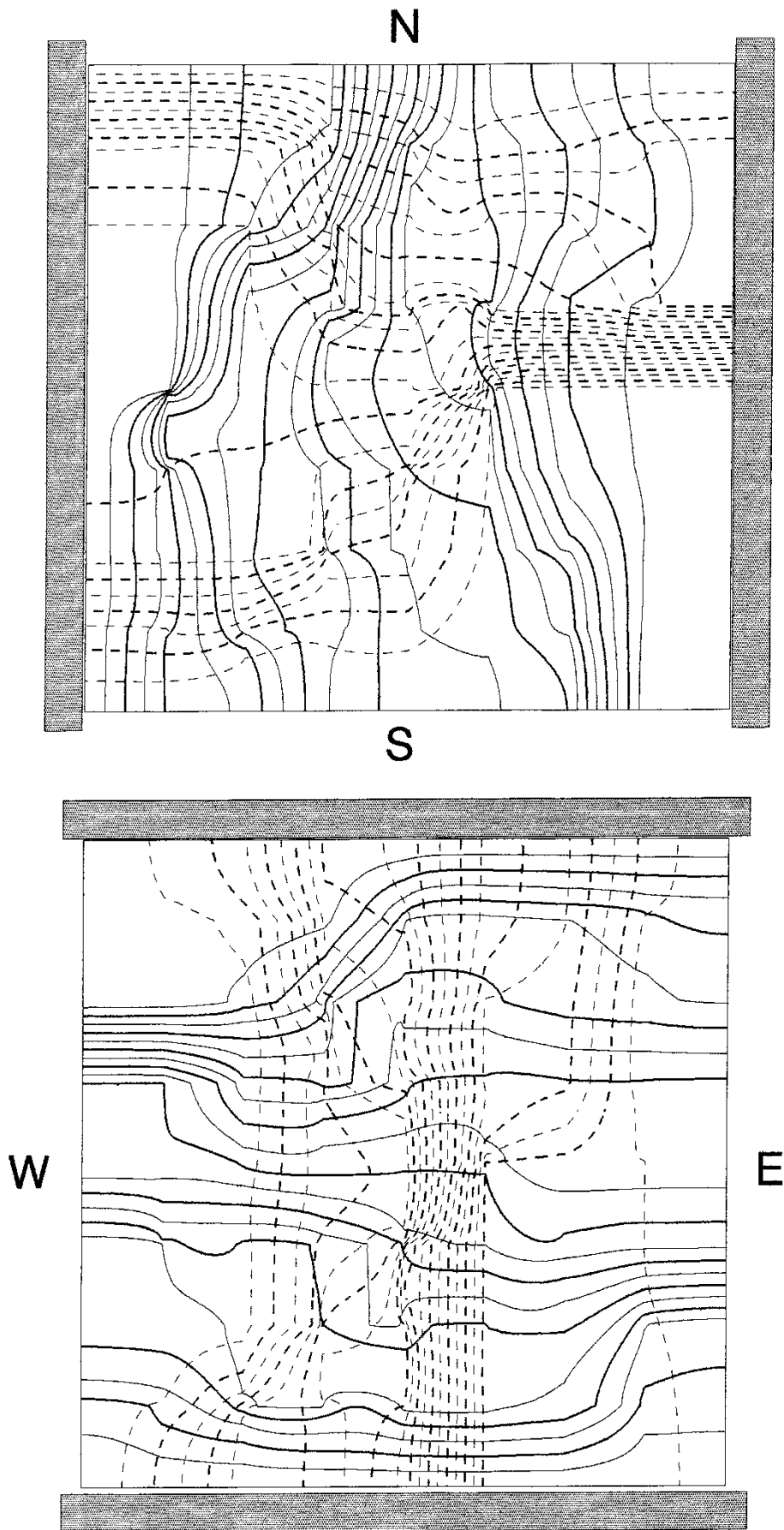Fig. 85 Flow nets for case G, both principal components, N = (8 x 8).

Piezometric head (dashed) and stream function (solid) levels
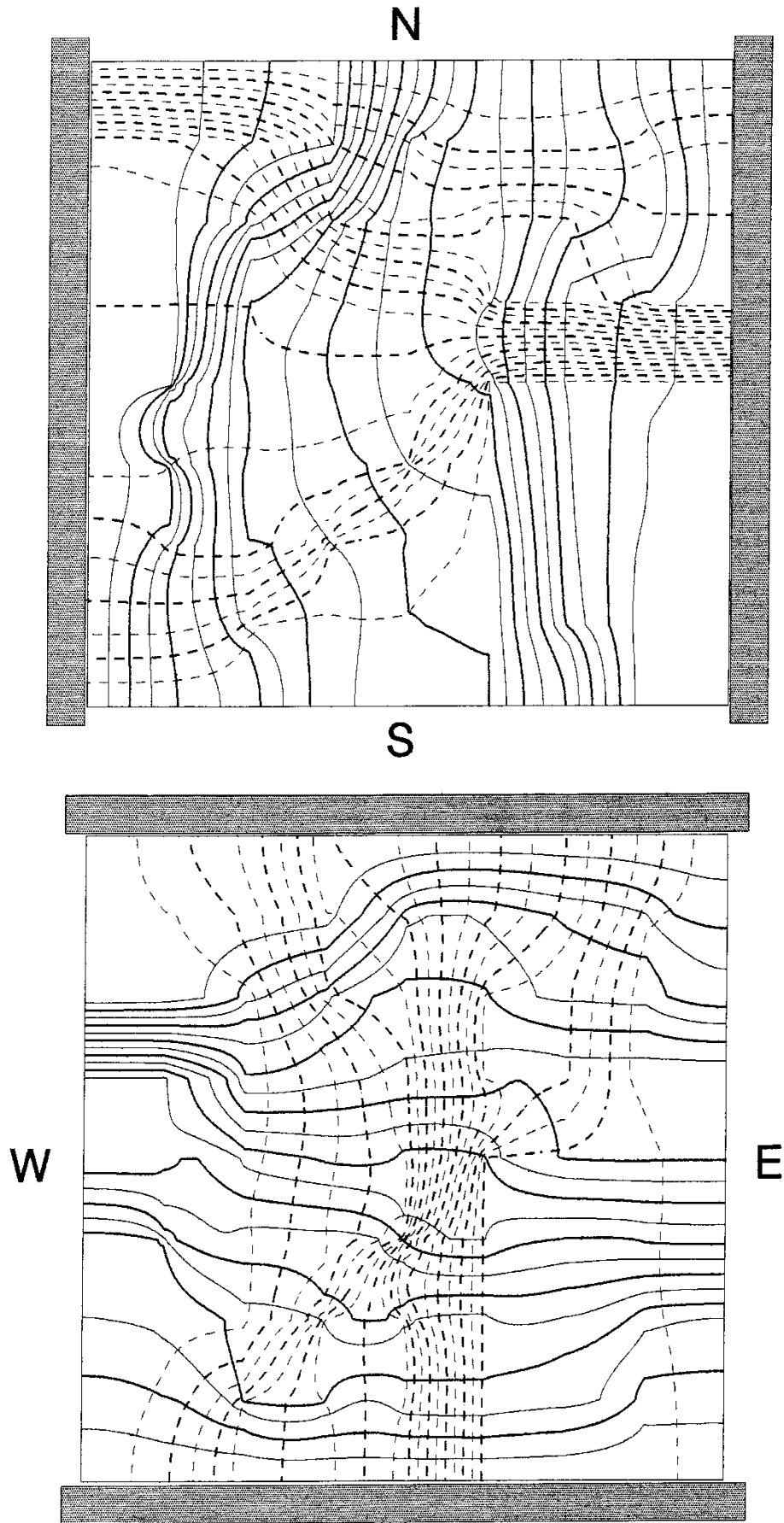
are in 5% increments between 0 and 1.

Fig. 86 Flow nets for case H, geometric mean $\sqrt{(K_{xx} K_{yy})}$, N = (8 x 8).

$S_{\ln(K)}$ = 1.99 . Piezometric head (dashed) and stream function

levels (solid) are in 5% increments between 0 and 1.

Fig. 87 Flow nets for case I, K_{xx} principal component, N = (8 x 8) .

$s_{\ln(K)} = 2.16$. Piezometric head (dashed) and stream function

levels (solid) are in 5% increments between 0 and 1.

Fig. 88 Flow nets for case I, K_{yy} principal component, $N = (8 \times 8)$.

$S_{\ln(K)} = 2.11$. Piezometric head (dashed) and stream function
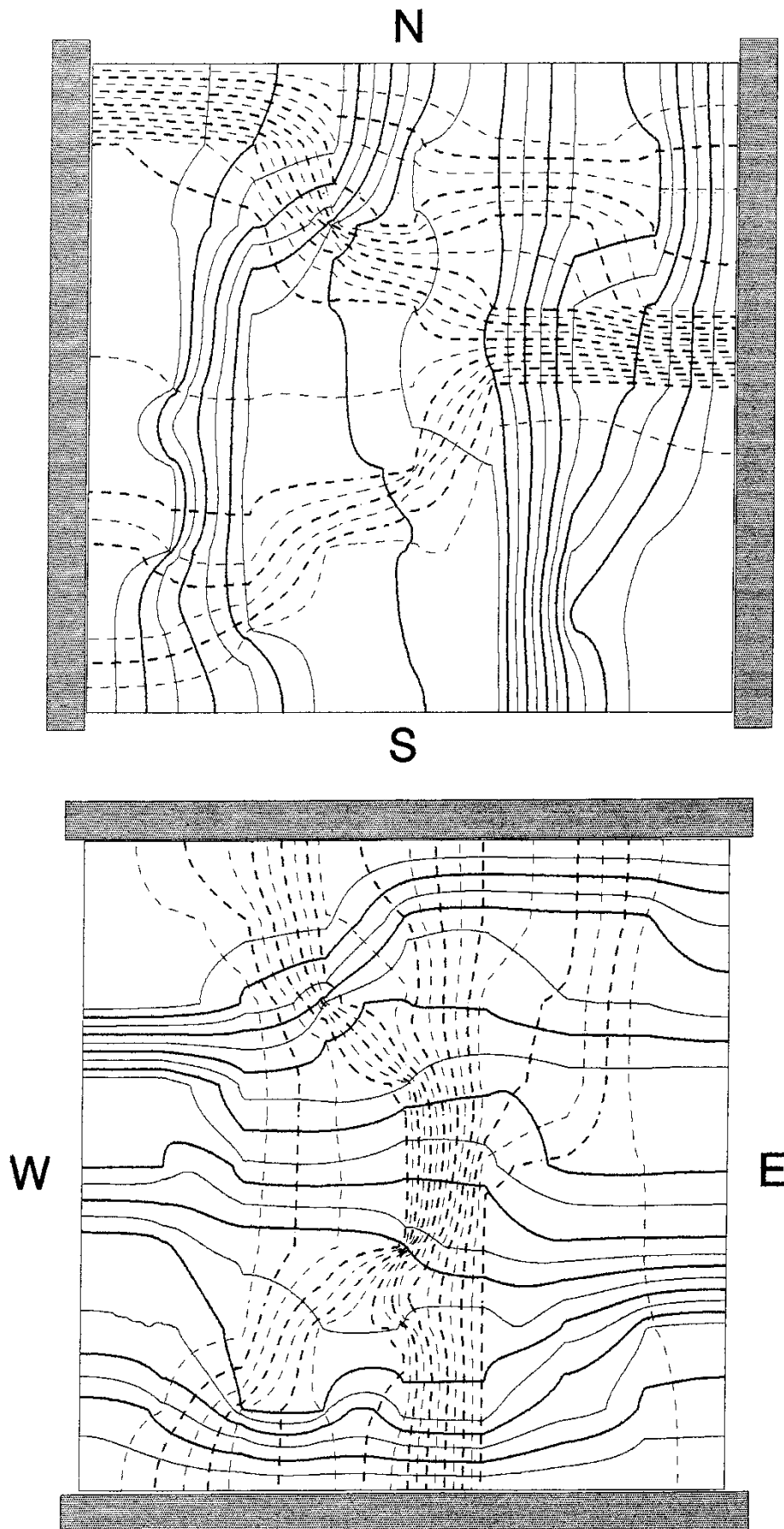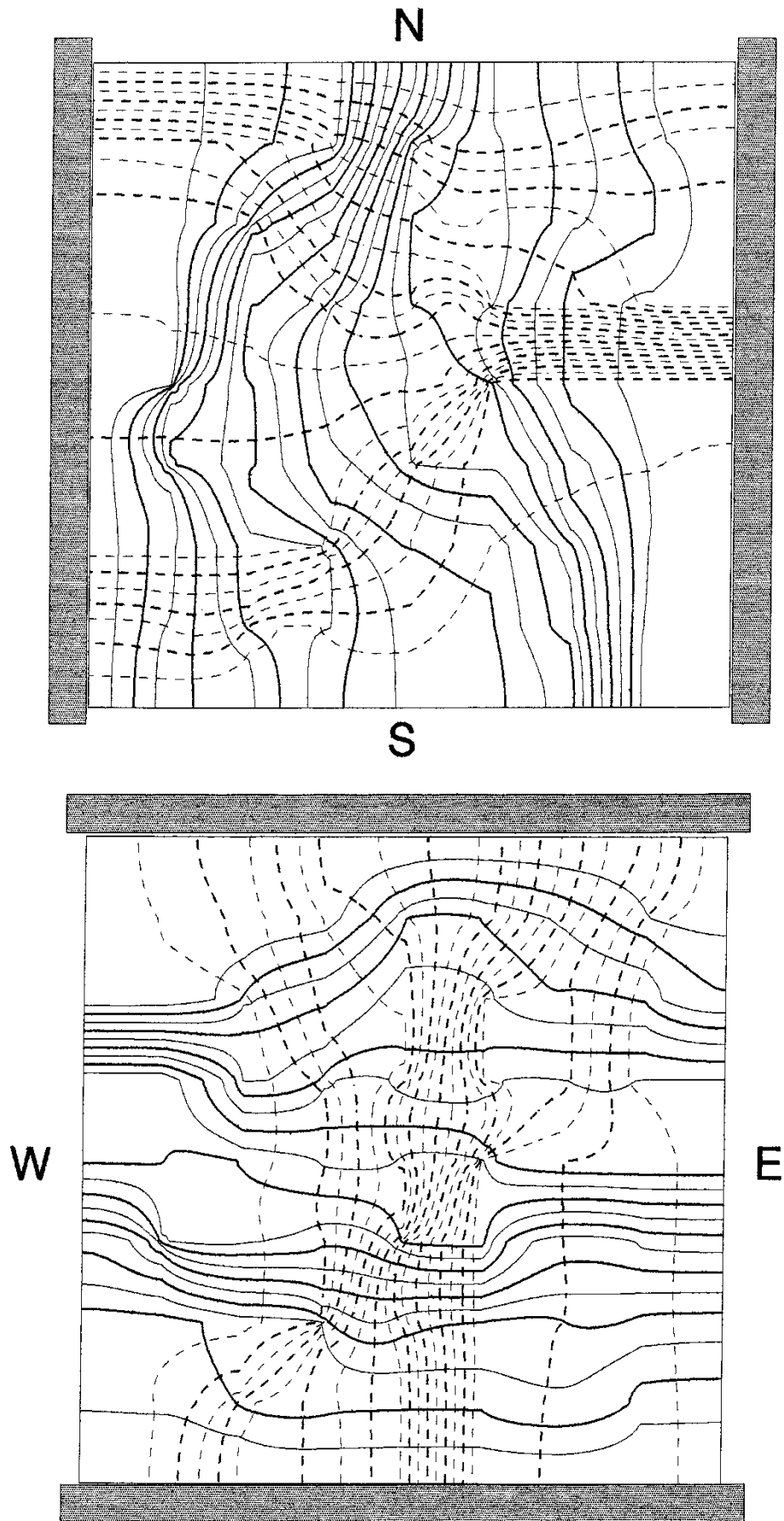
levels (solid) are in 5% increments between 0 and 1.

CASE		N/S flow				W/E flow				
		K_{yy} [n·10⁻⁷ m/s]	E_K^2 [%]	MSE_φ^2 [n·10⁻² m²]	E_φ^2 [%]	K_{xx} [n·10⁻⁷ m/s]	E_K^1 [%]	MSE_φ^1 [n·10⁻² m²]	E_φ^1 [%]	$|OPI|$ [%]
A priori		1.364	0.0	0.0	0.0	1.649	0.0	0.0	0.0	0
Inverse distance, SR ≈ 2λ	A	0.977	-28.3	1.369	12.9	1.318	-20.0	1.232	8.5	70
Ordinary kriging, SR ≈ 2λ	B	1.188	-12.9	1.322	12.5	1.166	-29.3	0.974	6.7	61
Ordinary kriging, SR ≈ 4λ	C	1.535	12.5	0.819	7.7	1.475	-10.5	0.910	6.3	37
Geometric mean, exp(mγ)	D	1.456	6.7	0.477	4.5	1.635	-0.9	0.513	3.5	16
Ordinary kriging, SR ≈ 2λ	E	1.673	22.7	1.513	14.3	1.306	20.8	1.232	8.5	66
Ordinary kriging, SR ≈ 4λ	F	1.663	21.9	1.145	10.8	1.798	9.0	1.000	6.9	49
Both orthogonal components	G	1.388	1.8	0.483	4.6	1.663	-1.0	0.671	4.6	12
Geometric mean, √(Kₓₓ Kyy)	H	1.506	10.4	0.486	4.6	1.727	4.7	0.706	4.9	25
K_{xx} component	–	1.590	16.6	0.692	6.5	1.570	-4.8	0.521	3.6	32
K_{yy} component	–	1.562	14.5	0.469	4.4	2.119	28.5	1.082	7.4	55

Fig. 89 Detailed results for the nine experiments .
(For an explanation of the notation, see (47).)
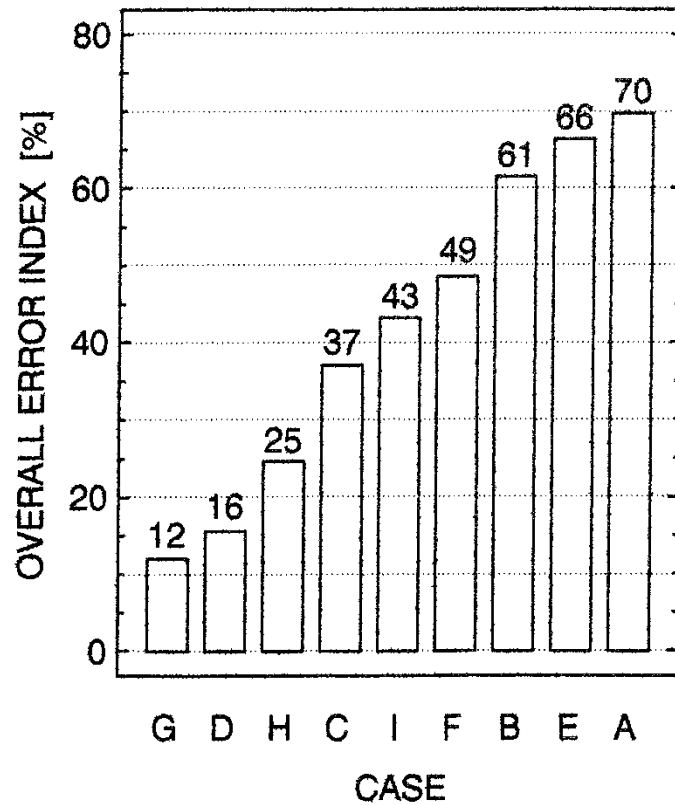
CASE	TYPE [1]	N [2]	SCALE [3]	COMMENT [4]
A	E	64 x 64	3m	Inverse distance, SR $\approx$ 2 λ
B	E	64 x 64	3m	Ordinary kriging, SR $\approx$ 2 λ
C	E	64 x 64	3m	Ordinary kriging, SR $\approx$ 4 λ
D	E	8 x 8	24m	Geometric mean, $\exp(m_y)$
E	E	8 x 8	24m	Ordinary kriging, SR $\approx$ 2 λ
F	E	8 x 8	24m	Ordinary kriging, SR $\approx$ 4 λ
G	H	8 x 8	24m	Both orthogonal components
H	H	8 x 8	24m	Geometric mean, $\sqrt{(K_{xx} K_{yy})}$
I	H	8 x 8	24m	One component

[1] Block conductivities are: E = estimated H = hydraulically determined

[2] Number of support blocks in the flow model

[3] Conceptual side length of each block in the flow model

[4] SR = search range (radius) for estimation

Fig. 90 Overall error indices (OEI) for the nine experiments .

3.5 Simulation of solute transport

Few problems in subsurface hydrology bring more attention than the transport of solutes in heterogeneous geological media. Because of the well-documented scale dependence in a large number of field and laboratory experiments, the relevance of using the traditional advection-dispersion equation is questioned. The field observations imply that the dispersivities are dependent on the elapsed travel time. Hence, a Fickian diffusion process from the onset of a solute injection is not an adequate description of the hydrodynamic dispersion phenomenon on all scales.

In recent years, the stochastic continuum theory has been increasingly used to study the scale dependence of advection-dispersion phenomena, and different approaches are reported in the literature. The developments used here are limited to deal with uniform average flow in two dimensions under a rather moderate heterogeneity of the log-conductivity field, i.e. $\sigma_Y^2 \leq 1$. This limitation stems from a use of "first-order theory", i.e. a first-order approximation of a small perturbation of the log-conductivity field. The non-linear effects that arise when $\sigma_Y^2 > 1$ are considered to be important although few results have been reported so far [see, e.g. Dagan, 1988; Neuman & Zhang, 1990; Rubin, 1990].

The objectives here are to investigate the possibility (*i*) to reproduce numerically the analytical results obtained by first-order theory, and (*ii*) to extend the numerical simulations to allow for high conductivity contrasts. Only single realizations of three different cases of heterogeneity are studied. Thus, the simulations undertaken do not treat questions concerning the ensemble statistics. However, the studied realizations are relatively large with respect to the correlation lengths used, i.e. $L/\lambda_Y = \{16, 32, 64\}$. Because the injected solute, which in this study is represented by particles, is released over the entire upstream boundary, it is assumed that the spatial variability is adequately accounted for in order to justify an analysis of the scale dependence of the macro-

dispersivities in each realization. To simplify the problem, both diffusion and local dispersivity are discarded in the numerical simulations, implying that a purely advective transport process is studied. Furthermore, because the implemented finite element model uses only a first-order continuity in the heads in conjunction with a discrete conductivity field of high contrasts, numerical constraints arise while computing the velocity v(x). That is to say, the velocities do not satisfy continuity at the element boundaries [see, e.g. Kinzelbach, 1987a; Durlofsky, 1991]. To circumvent this problem, an alternative procedure is used here in the numerical simulations of advective transport. The procedure is based on the dual formulation of flow [see, e.g. Frind & Matanga, 1985], which is suited for studying transport problems, because the relative difference in the stream function (Ψ) between any two streamlines is proportional to the total discharge ($\Sigma \Delta Q$) of the flow domain. Furthermore, if the distance between the two streamlines is taken into account, the specific discharge of the streamtube is readily computed. However, because the used finite element model furnishes only stream function values at the nodes, an interpolation algorithm is implemented to compute the velocities over the entire flow domain. Goode [1990] discusses the advantages of using a bi-linear interpolation method in relation to other interpolation methods for a finite difference scheme. The method chosen here considers a more general class of quadrilateral elements and is called *isoparametric interpolation* [cf. Bear & Verruijt, 1987].

As mentioned previously, the size of the flow domain is important in transport studies. In this study, the scale associated with an asymptotic behaviour of the macrodispersivity is presumed to be of interest. Whether or not the tortuosity is a relevant indicator of the required scale may be an open question, but the tortuosity is sometimes referred to in conjunction with permeability and dispersivity definitions [see, e.g. Bear, 1972, 1979; Dullien, 1979; Bear & Verruijt, 1987]. As an assumed indicator of the required size, the tortuosity is here computed for three realizations characterized by

$\lambda_Y/\Delta x = \lambda_Y/\Delta y = \{0, 2, 4\}$, and $\sigma_Y = 4$. Following Dullien [1979], the tortuosity (T) may be defined as

$$T = \left(\frac{L_e}{L}\right)^2 \tag{48}$$

with L_e being the "effective average path length" and L the shortest linear distance along the direction of macroscopic flow. Four block sizes are studied for each realization, namely $N = \{8 \times 8, 16 \times 16, 32 \times 32, 64 \times 64\}$, see Figures 91-93. Figure 94 shows that only the largest block size appears to be suited for numerical simulation of solute transport. For $\lambda_Y/\Delta x = \lambda_Y/\Delta y = 4$, however, the tortuosity shows no tendency to be close to an asymptotic behaviour even for the largest block size.

A particular problem in numerical transport studies concerns the implementation of a flux-weighted boundary condition at the upstream boundary. The conventional approach to accomplish a flux-weighted injection is to select a large number of uniformly distributed injection points, and then to inject a flux-weighted number of particles at the selected points. For instance, it is quite common to take the positions of the grid nodes in a regular mesh of finite elements or finite difference cells as injection points [see, for example, Desbarats & Srivastava, 1991]. There is no ambiguity in this approach from a conceptual point of view, but it is found here that such an approach does not reproduce the results derived by first-order theory, unless the spacing between the injection points is very small, the heterogeneity of the conductivity field is quite moderate, i.e. $\sigma_Y^2 \ll 1$, or local dispersion is included. Figures 95 and 96 show four flow patterns for uniformly distributed injection points for N/S-flow and S/N-flow, respectively. In Figure 95, $\sigma_Y = 1$, whereas $\sigma_Y = 4$ in Figure 96. It is readily seen that the N/S-streamlines are different from the S/N-streamlines regardless of the number of particles injected. The present study suggests an approach which is considered to be more consistent from a physical

point of view. The suggested injection technique uses the equidistant contour level positions of the stream function solution on the upstream boundary, and only one particle per streamline needs to be injected. Figures 97-99 demonstrate the approach taken here. Moreover, these figures clearly demonstrate the previously observed differences in the channelling due the value of the correlation length (λ_Y). That is to say, correlated conductivity fields consist of a few major paths of preferential flow, whereas truly random media consist of many minor paths.

Figure 100 shows the spreading of an instantaneous solute injection in terms of particles in two orthogonal flow directions denoted N/S and W/E, respectively. The suggested flux-weighted injection technique described above is used. The flow domain in Figure 100 is characterized by $\lambda_Y/\Delta x = \lambda_Y/\Delta y = 2$, $\sigma_Y = 1$, and $N = 64\times64$. The instantaneous injection consists of 999 particles (streamlines). Thus, the total discharge $(\Sigma \Delta Q)$ is divided into 1000 equally large increments. The spreading in Figure 100 is shown for two travel times: $t_1 = 0.125 \, t_{ref}$ and $t_2 = 0.5 \, t_{ref}$, where t_{ref} denotes the mean transit time of the *fluid*. The spreading of the particles as a function of time is studied by using the non-Fickian position analysis outlined by Dagan [1982, 1984, 1987, 1988]. The analysis is described briefly in Chapter 2. In short, the key entity of interest is the displacement covariance tensor $(\tilde{X})$. The calculation of the longitudinal displacement covariance (X_{11}) as a function of time is essentially a straightforward matter because the flow problem is one-dimensional. The computation of the transverse displacement covariance (X_{22}), however, is more complicated. The present study suggests the following "mixed" analysis:

The equidistant contour level positions of the stream function solution on the upstream boundary are *conceptually* considered to start at a common point. The idea is *figuratively* visualized for $\sigma_Y = 4$ in Figures 101, 102, and 103. Indeed, these figures are merely modifications of Figures 58, 48, and 63, respectively. In other words, by relating the time-dependent lateral positions of a moving particle,

which follows a flux-weighted streamline, to its equidistant contour level position on the upstream boundary, the computation of the "transverse displacement covariance" as a function of time becomes a straightforward matter from a practical point of view.

Figures 104-106 relate to Figure 100. Figures 104 and 105 show the calculated histograms at three different times, $t_1 = 0.125 \ t_{ref}$ $t_2 = 0.25 \ t_{ref}$, and $t_3 = 0.5 \ t_{ref}$, whereas Figure 106 shows the two displacement covariances, X_{11} and X_{22}, computed according to (39a) and (39b), respectively. The differences between the two flow directions, as shown in Figure 106, are interesting. Apparently, the statistics of the studied conductivity field are not invariant by rotation. Figure 111 shows the two corresponding time-dependent dispersivities, A_{11} and A_{22}, as functions of the travel distance. A_{11} and A_{22} are computed according to (40a) and (40b), respectively.

Figure 100 demonstrates a severe problem caused by the channelling phenomenon, i.e. the fastest particles in each flow direction reach the corresponding downstream boundaries at $t \simeq 0.6 \ t_{ref}$. In other words, the non-Fickian particle position analysis is for the case shown in Figure 100 restricted to treating $t < 0.6 \ t_{ref}$, which means that only 50-60% of the transport problem can be studied by the position analysis (cf. Figure 111). For $\sigma_Y = 4$, the situation is even worse, i.e. the time limit is found to be $t < 0.15 \ t_{ref}$, which in fact makes the position analysis more or less useless to what follows below. The obvious approach to circumvent the encountered problem of the position analysis is to consider the non-Fickian arrival time approach. However, the theoretical developments of this approach are currently also limited to $\sigma_Y^2 \leq 1$ [cf. Shapiro & Cvetkovic, 1988]. Because of the interest of knowing the scale where a non-Fickian and a Fickian analysis meet, the results obtained from the non-Fickian position analysis are here compared with a Fickian analysis, which is based on the first two moments of the particle arrival at a fixed plane perpendicular to the mean direction of flow [cf. Kreft & Zuber, 1978]. It is important to note that the arrival time analysis used here is a strict Fickian interpretation, i.e. it

assumes a diffusion process from the onset of the solute injection, thus devoid of any notion of scale. Figures 107-109 show a few *residence-time* and *residence-path* histograms at a fixed plane coinciding with the downstream boundary for *N/S*-flow in the following nine cases: $\lambda_Y/\Delta x = \lambda_Y/\Delta y = \{0, 2, 4\}$, $\sigma_Y = \{0.25, 1, 4\}$. In Figure 110, the residence-time histograms for a uniform porosity field are shown in relation to the residence-time histograms for a positively correlated porosity field. Figure 111 shows the longitudinal and transverse dispersivities for the Fickian arrival time analysis calculated by using (42a) and (42b), respectively.

The principle of reciprocity is used in the present study to verify both the particle tracking algorithm and the suggested injection technique described previously. Figure 112 shows an application to the case shown in Figure 100. It is important to note that in Figure 112, the flow direction is unimportant. That is to say, upon choosing a *N/S*-flow direction, the statistics for the reverse direction (*S/N*-flow) are readily obtained by setting all arrival times at the downstream boundary (*S*) to zero in a backward calculation. In other words, the final dispersivities are independent of the flow direction, although the evolution is dependent on the flow direction. Figure 113 shows longitudinal Fickian arrival time analyses for three different values of σ_Y, i.e. $\sigma_Y = \{1/\sqrt{2}, 1, 4\}$, in relation to (40a). Figures 114-116 show *longitudinal* Fickian arrival time analyses for the aforementioned cases 4-00, 4-22, and 4-44, in relation to (40a). Figure 117 shows the corresponding *transverse* Fickian arrival time analyses for the three cases in relation to (40b). Figure 118 shows a comparison of the non-Fickian position analysis and the Fickian arrival time analysis at a distance of 32 λ_Y from the onset of the solute injection. The asymptotic value of the longitudinal macrodispersivity given by (41a) is also inserted. The comparison is made for different values of σ_Y^2. It is important to note that the non-Fickian position analysis is limited to $\sigma_Y^2 \leq 1$. The obtained results from all the different experiments discussed above are summarized as follows:

The numerical algorithms used for the particle tracking, i.e. the dual formulation of flow and the isoparametric interpolation, are found to be well suited for studying advective transport in a heterogeneous conductivity field.

The suggested technique to accomplish a consistent flux-weighted injection mode by using the equidistant contour level positions of the stream function on the upstream boundary is proved to be appropriate. The validity is verified in the study by the principle of reciprocity.

The analytical results derived by the position analysis under first-order theory are here numerically reproduced for $\lambda_Y/\Delta x = \lambda_Y/\Delta y = 2$, $\sigma_Y^2 = 1$, and $N = 64\times64$. The longitudinal dispersivities computed by means of the Fickian arrival time analysis reach the asymptotic values predicted by first-order theory, at a rate that is surprisingly concordant with the non-Fickian position analysis.

For $\sigma_Y^2 \leq 4$, it is found that a Fickian arrival time analyis deviates moderately from what is predicted by the equations of the position analysis. For $\sigma_Y^2 > 4$, a Fickian arrival time analysis yields the result that (*i*) the transverse dispersivity increases linearly in proportion to σ_Y and (*ii*) the longitudinal dispersivity approaches the asymptotic value at a faster rate than is predicted by the position analysis. For $\sigma_Y^2 = 16$, numerical difficulties are observed. However, the Fickian arrival time analysis shows a remarkable reciprocity considering the immense conductivity contrasts which in this case comprise about 12 $\log_{10}$ cycles in K.

A uniform porosity field shows a larger spreading in arrival times.

Finally, a figurative visualization of the "transverse dispersion" in relation to the aforementioned statistically anisotropic realization is shown in Figure A8 in the appendix.

2-D HYDRAULIC CONDUCTIVITY FIELD

No. of blocks: 64 × 64

$$\sigma_{\ln(K)} = 4.00 \quad \lambda/\Delta x = 0.0 \quad \lambda/\Delta y = 0.0$$
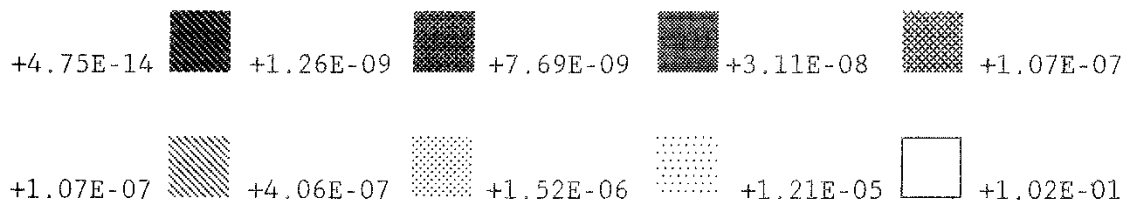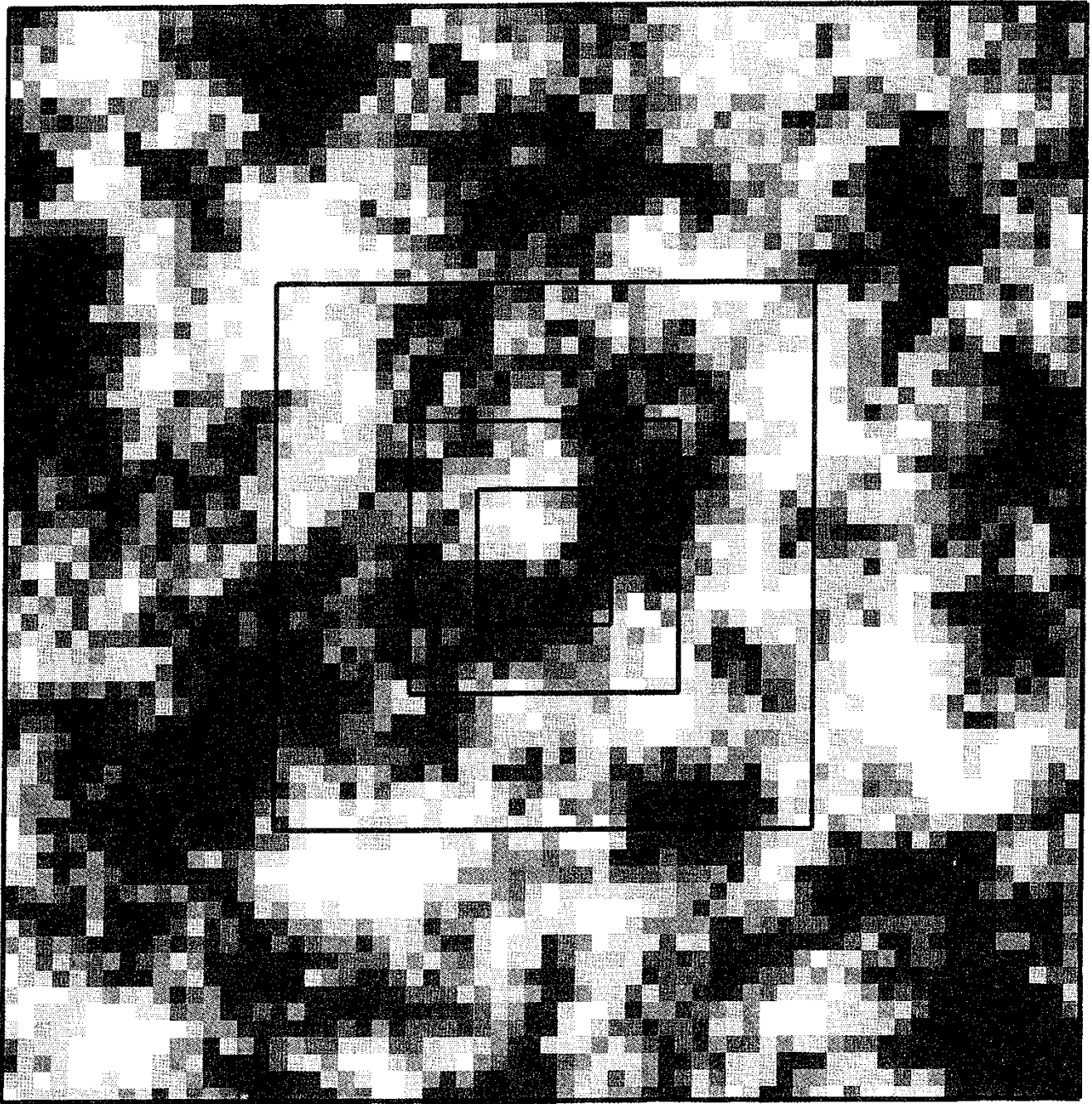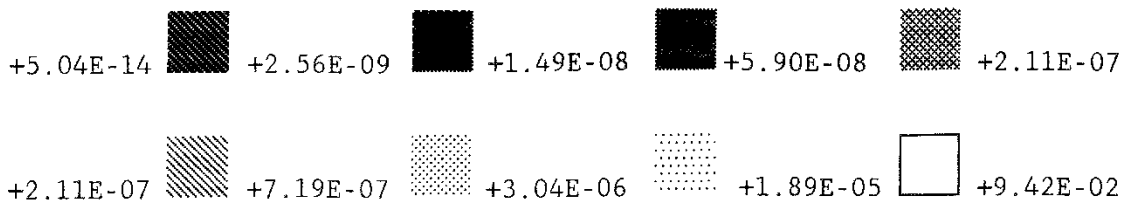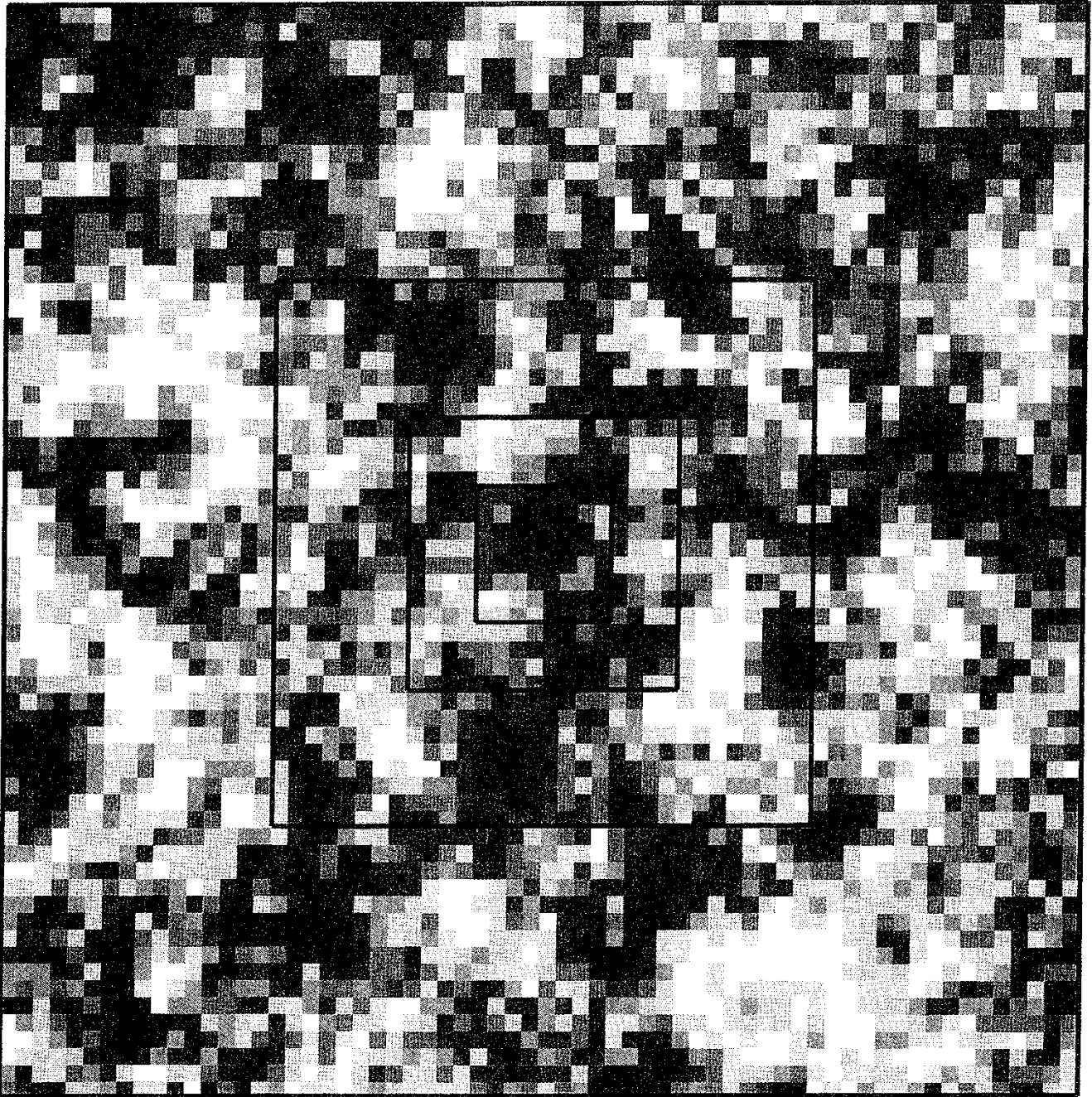

RASTER LEGEND (dim[K]=m/s)

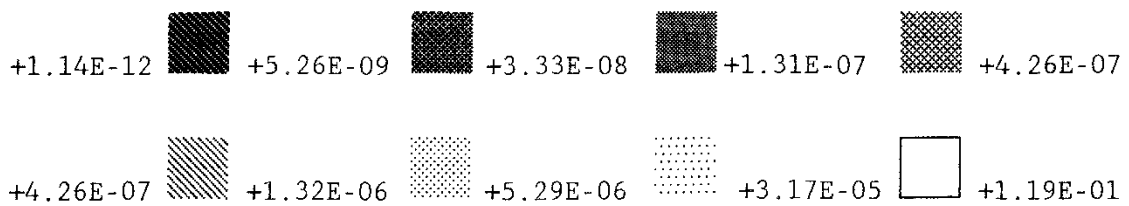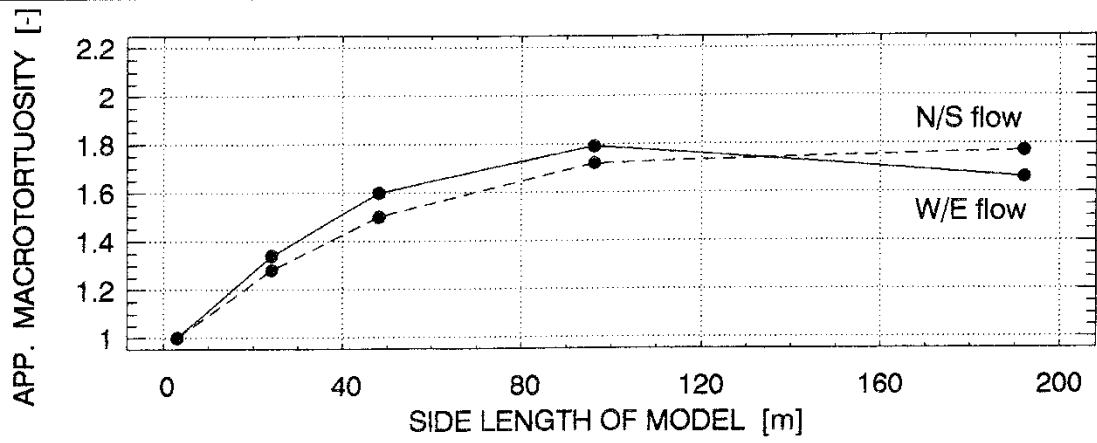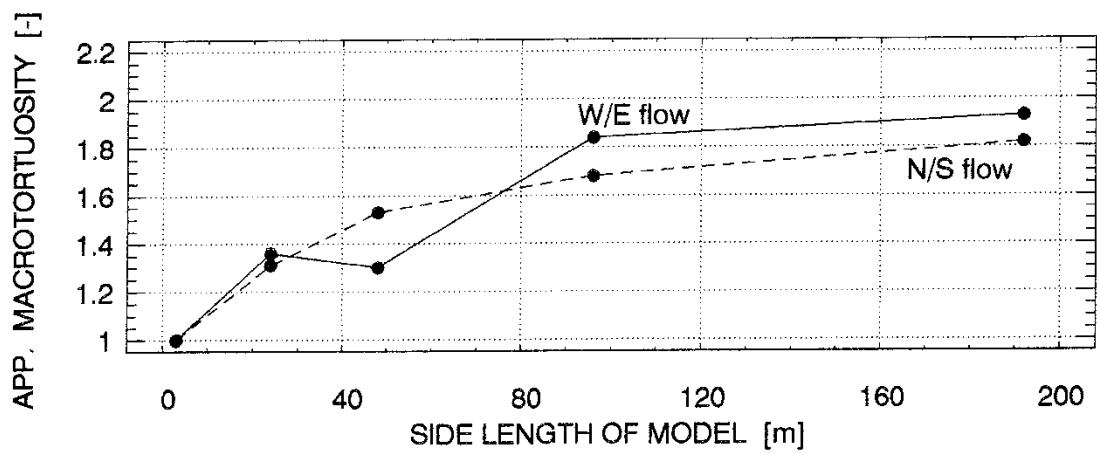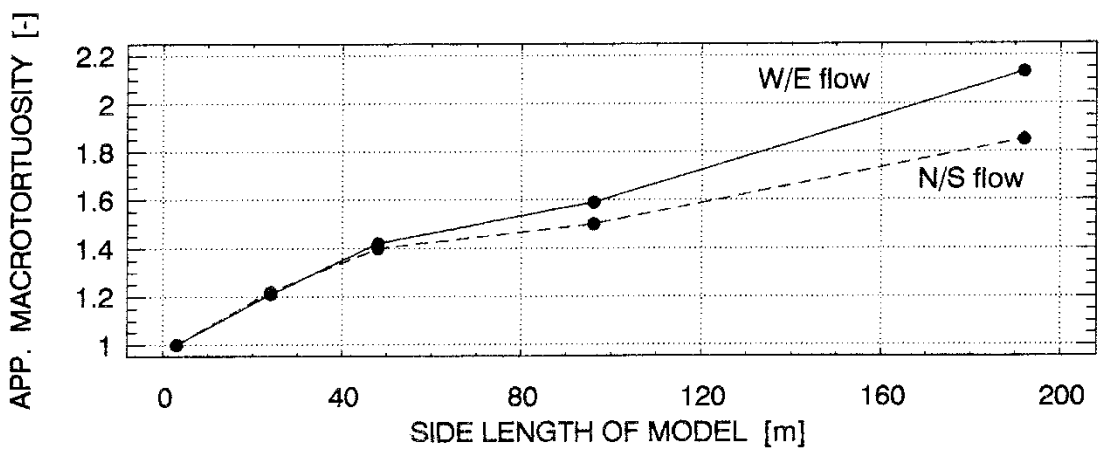|				
+4.75E-14	+1.26E-09	+7.69E-09	+3.11E-08	+1.07E-07
+1.07E-07	+4.06E-07	+1.52E-06	+1.21E-05	+1.02E-01
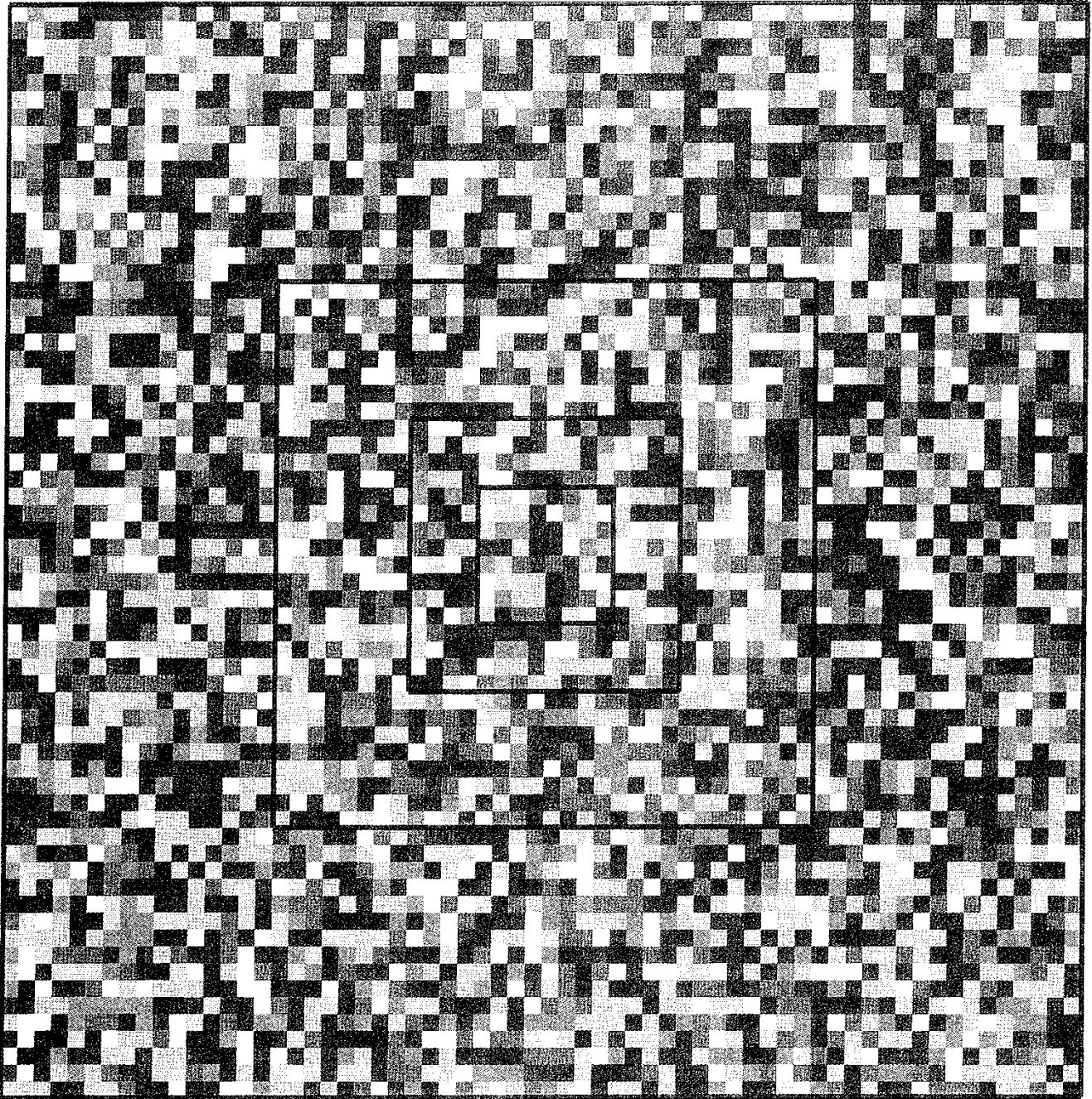
Fig. 91 Case 4-00 , N = (8 x 8 , 16 x 16, 32 x 32, 64 x 64).

2-D HYDRAULIC CONDUCTIVITY FIELD

No. of blocks: 64 × 64

$\sigma_{\ln(K)} = 4.00 \qquad \lambda/\Delta x = 2.0 \qquad \lambda/\Delta y = 2.0$

RASTER LEGEND (dim[K]=m/s)

+5.04E-14	+2.56E-09	+1.49E-08	+5.90E-08	+2.11E-07
+2.11E-07	+7.19E-07	+3.04E-06	+1.89E-05	+9.42E-02

Fig. 92 Case 4-22 , N = (8 x 8 , 16 x 16 , 32 x 32, 64 x 64).

2-D HYDRAULIC CONDUCTIVITY FIELD

No. of blocks: 64 × 64

$\sigma_{\ln(K)} = 4.00 \qquad \lambda/\Delta x = 4.0 \qquad \lambda/\Delta y = 4.0$

RASTER LEGEND (dim[K]=m/s)

+1.14E-12	+5.26E-09	+3.33E-08	+1.31E-07	+4.26E-07
+4.26E-07	+1.32E-06	+5.29E-06	+3.17E-05	+1.19E-01

Fig. 93 Case 4-44 , N = (8 x 8 , 16 x 16, 32 x 32, 64 x 64).

(a) Case 4-00

(b) Case 4-22

(c) Case 4-44

Fig. 94 Apparent macrotortuosity for average uniform flow through a finite heterogeneous medium in 2-D. N = (64 x 64) and $\sigma_{\ln(K)}$ = 4.00 .
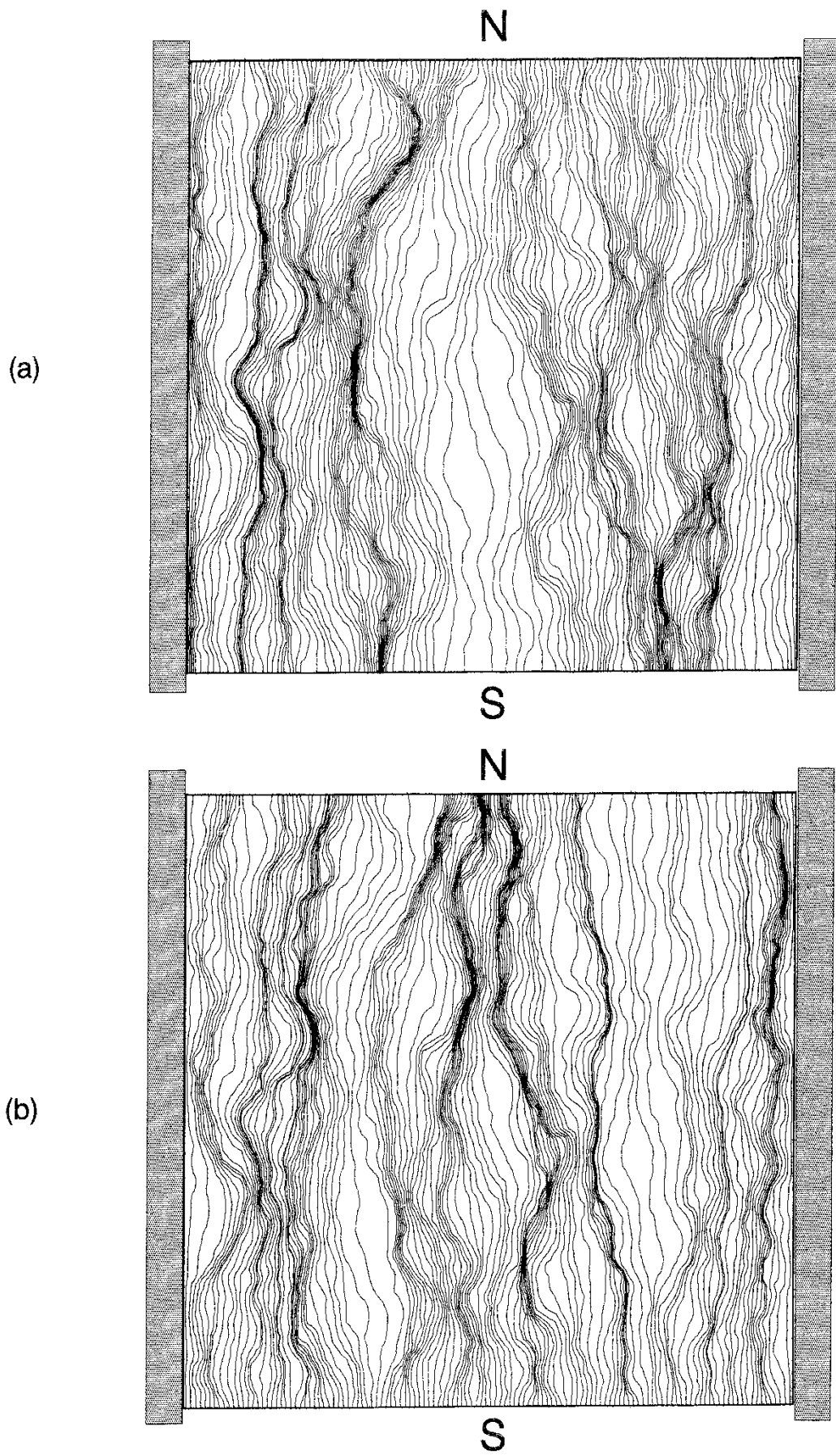
Fig. 95 Uniformly distributed injection points: (a) N/S-flow (b) S/N-flow.

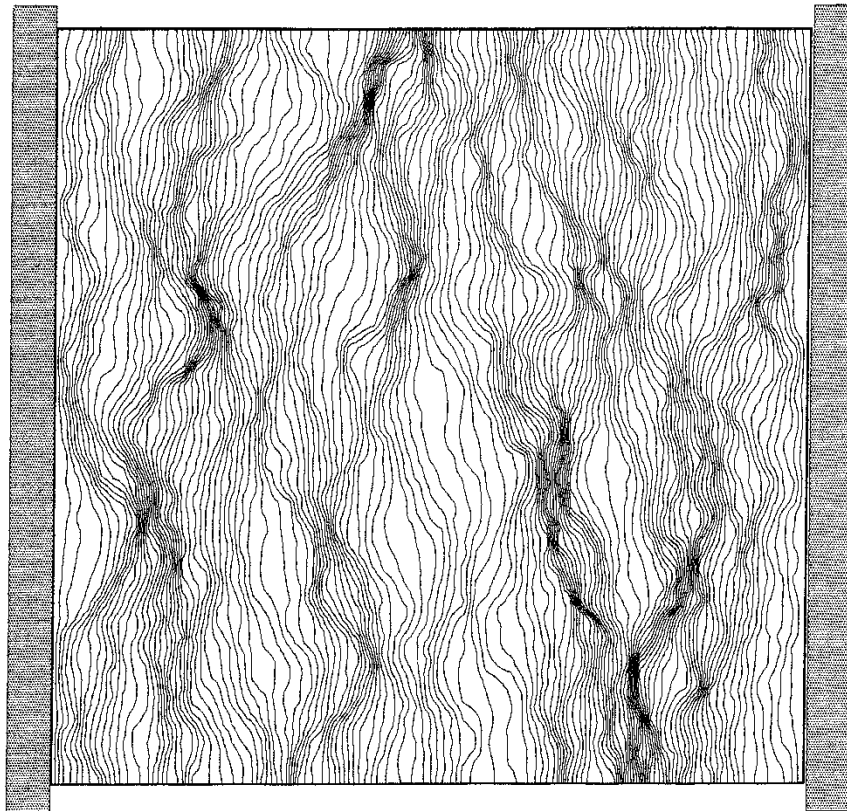$\sigma_Y = 1.00$ and $\lambda/\Delta x = \lambda/\Delta y = 2$. $N = (64 \times 64)$.
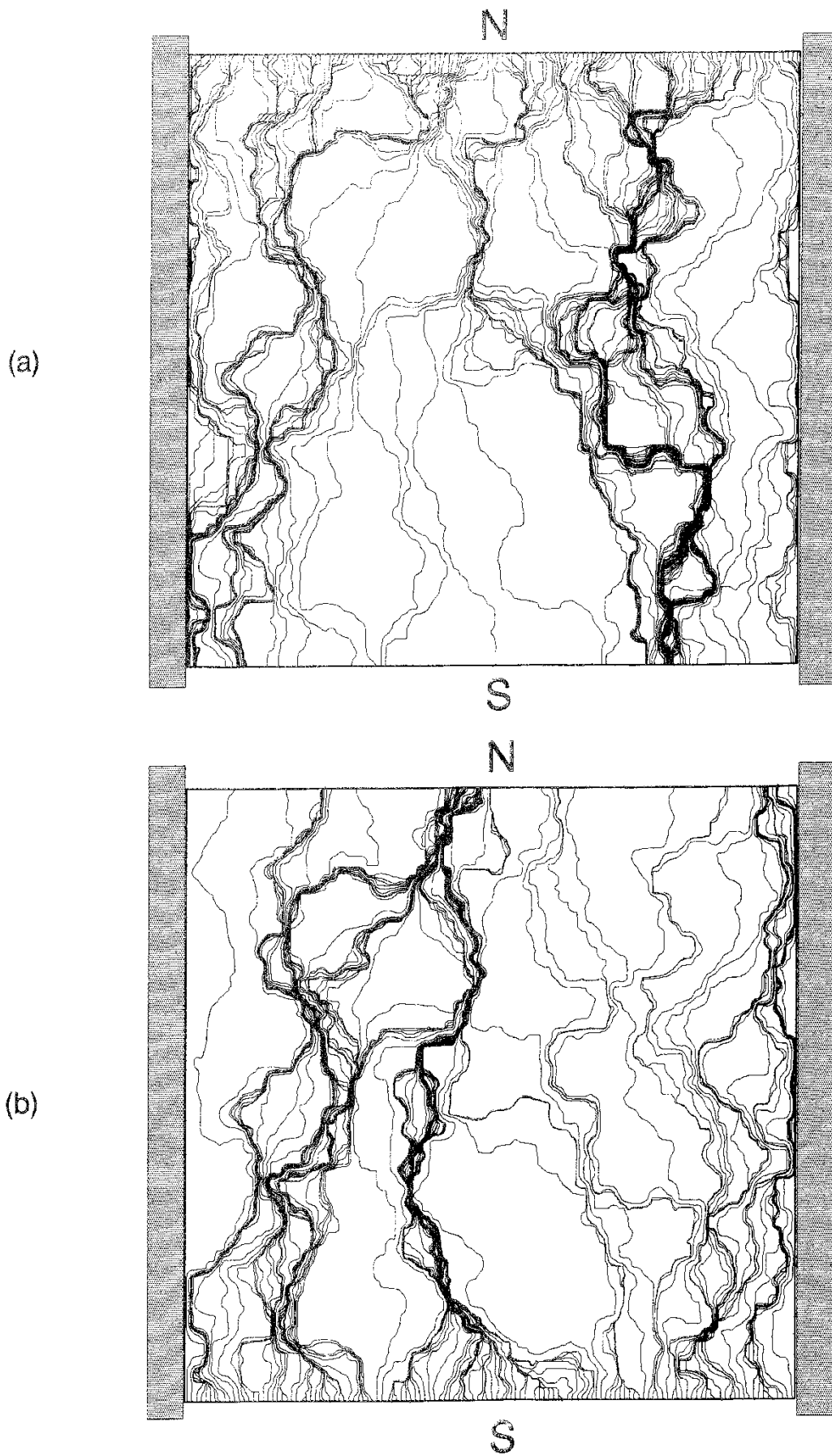
Fig. 96   Uniformly distributed injection points: (a) N/S-flow   (b) S/N-flow .

$$\sigma_Y = 4.00 \text{ and } \lambda/\Delta x = \lambda/\Delta y = 2 . \text{ N} = (64 \times 64) .$$
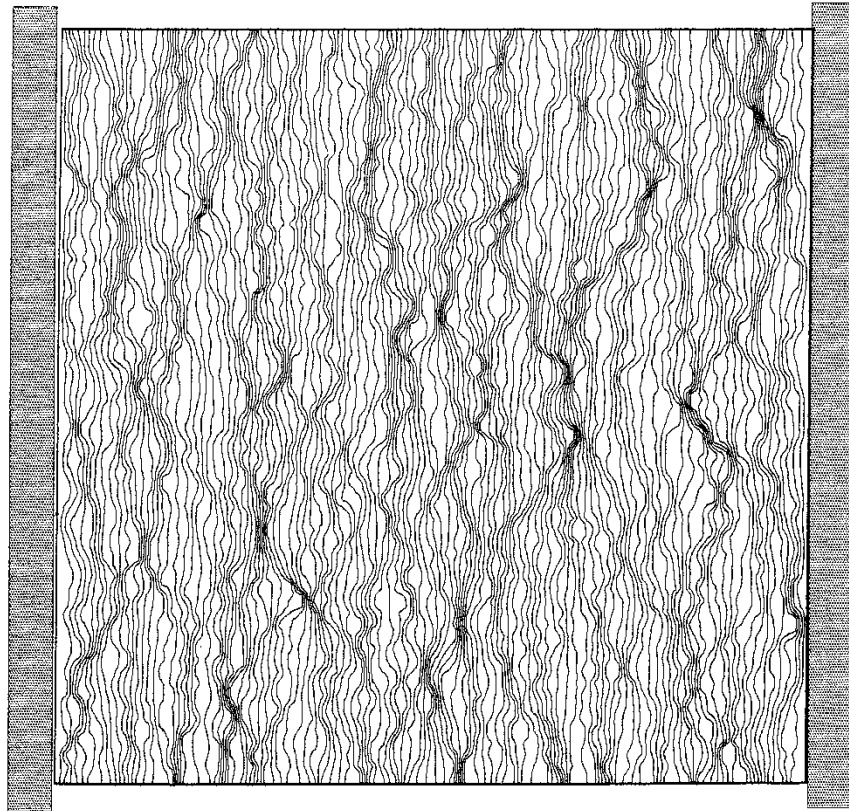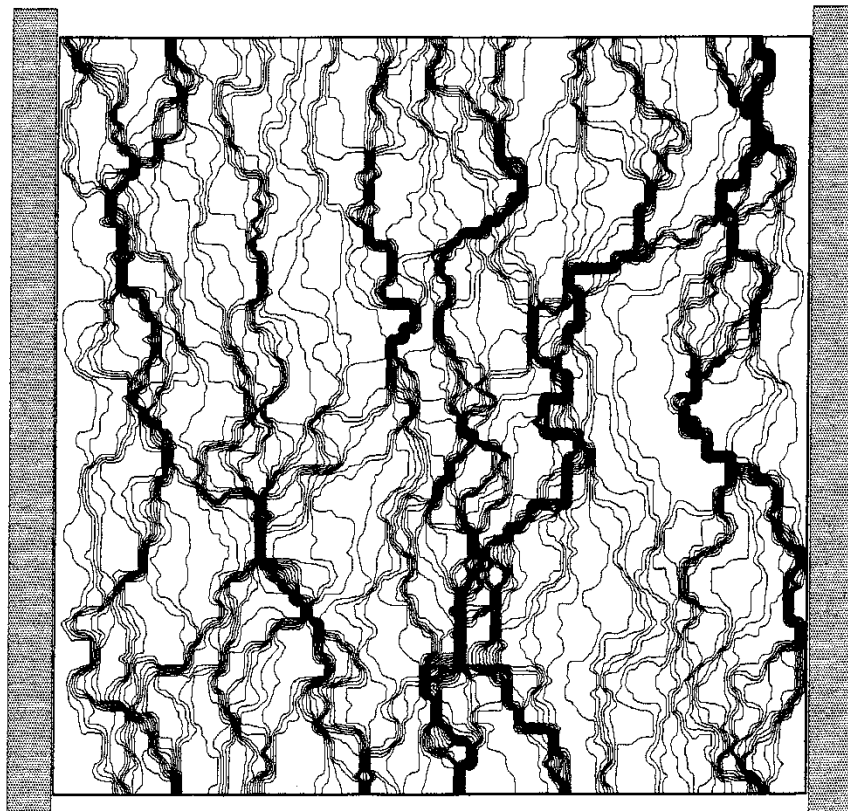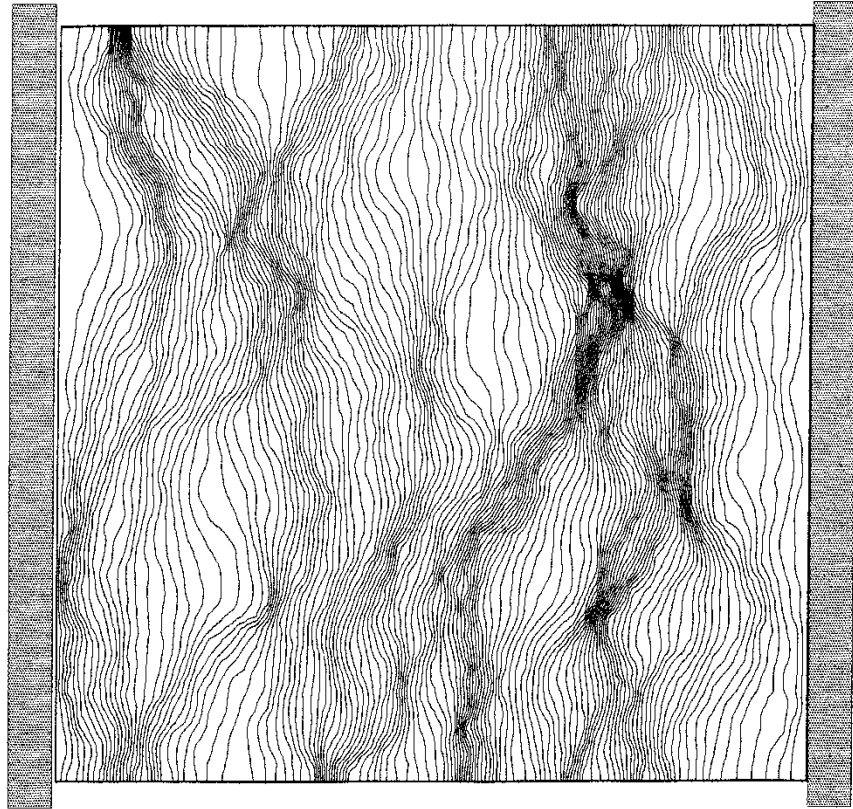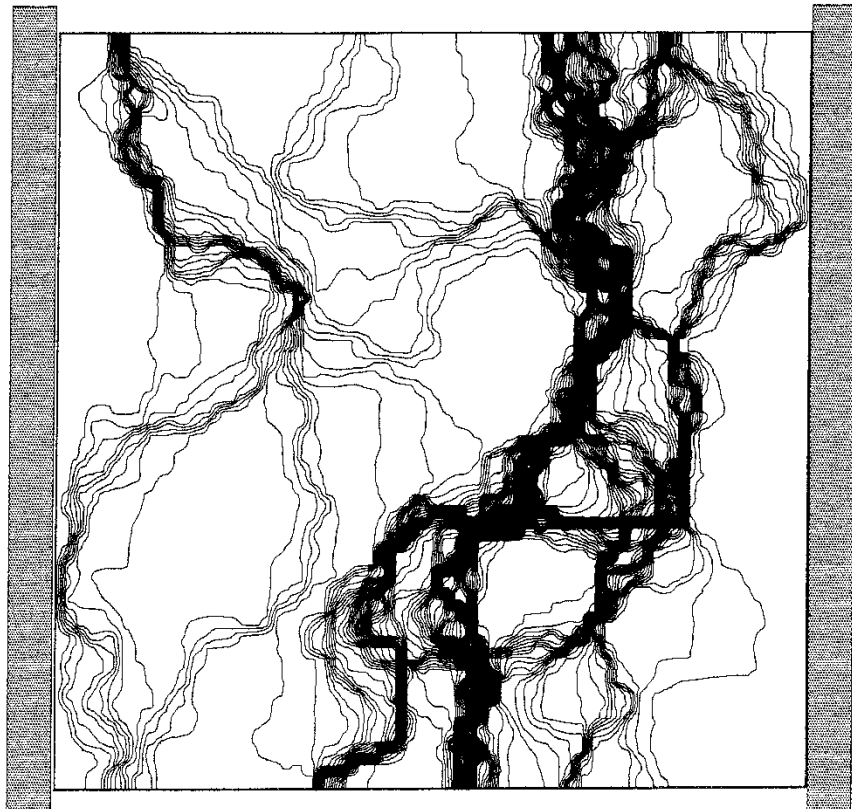
Fig. 97 Flux-weighted distribution of the injection points .

(a) $\sigma_Y = 1.00$ and $\lambda/\Delta x = \lambda/\Delta y = 0$. $N = (64 \times 64)$.

(b) $\sigma_Y = 4.00$ and $\lambda/\Delta x = \lambda/\Delta y = 0$. $N = (64 \times 64)$.
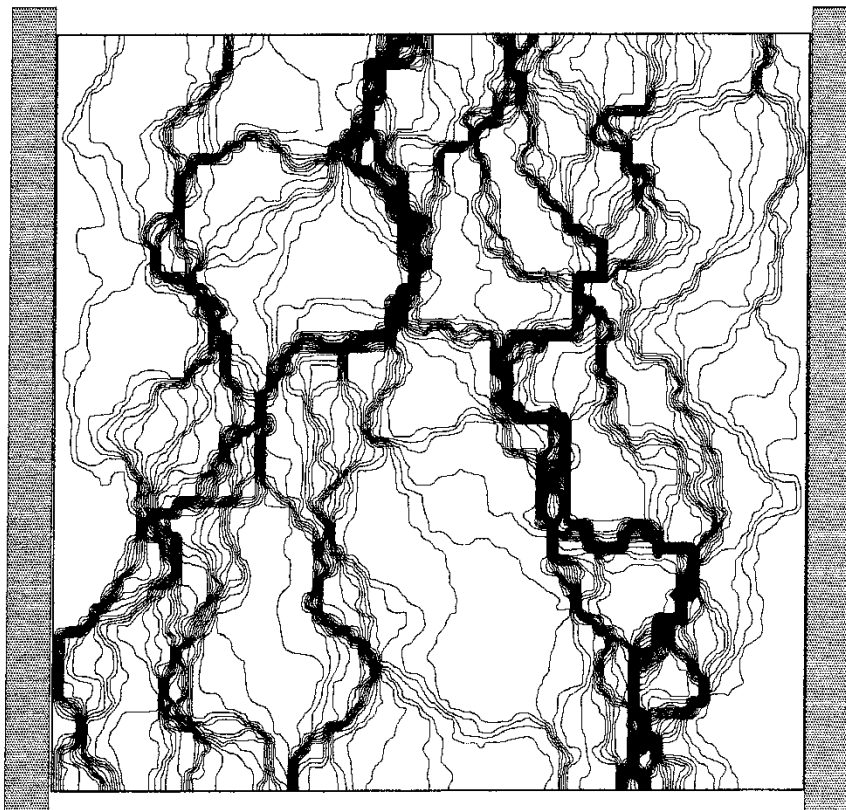
Fig. 98 Flux-weighted distribution of the injection points .

(a) $\sigma_Y = 1.00$ and $\lambda/\Delta x = \lambda/\Delta y = 2$. $N = (64 \times 64)$.

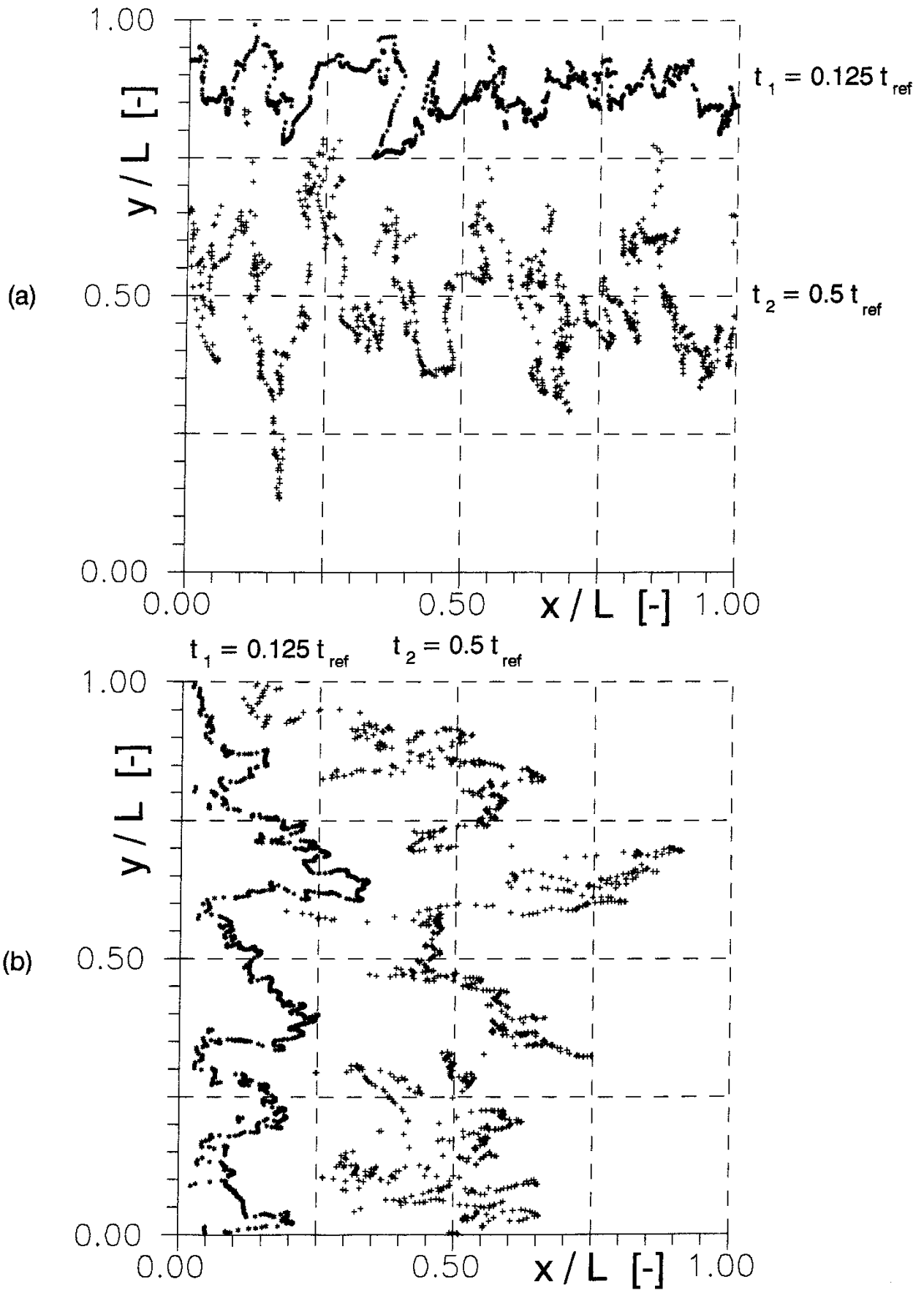(b) $\sigma_Y = 4.00$ and $\lambda/\Delta x = \lambda/\Delta y = 2$. $N = (64 \times 64)$.

Fig. 99 Flux-weighted distribution of the injection points .

(a) $\sigma_Y = 1.00$ and $\lambda/\Delta x = \lambda/\Delta y = 4$. $N = (64 \times 64)$.

(b) $\sigma_Y = 4.00$ and $\lambda/\Delta x = \lambda/\Delta y = 4$. $N = (64 \times 64)$.

Fig. 100 Particle tracking using flux-weighted distribution of the injection points: (a) N/S-flow (b) W/E-flow $t_{ref} = L\,n\,/\,\overline{q_{long}}$. $\sigma_Y = 1.00$ and $\lambda/\Delta x = \lambda/\Delta y = 2$. $N = (64 \times 64)$. $N_p = 999$.
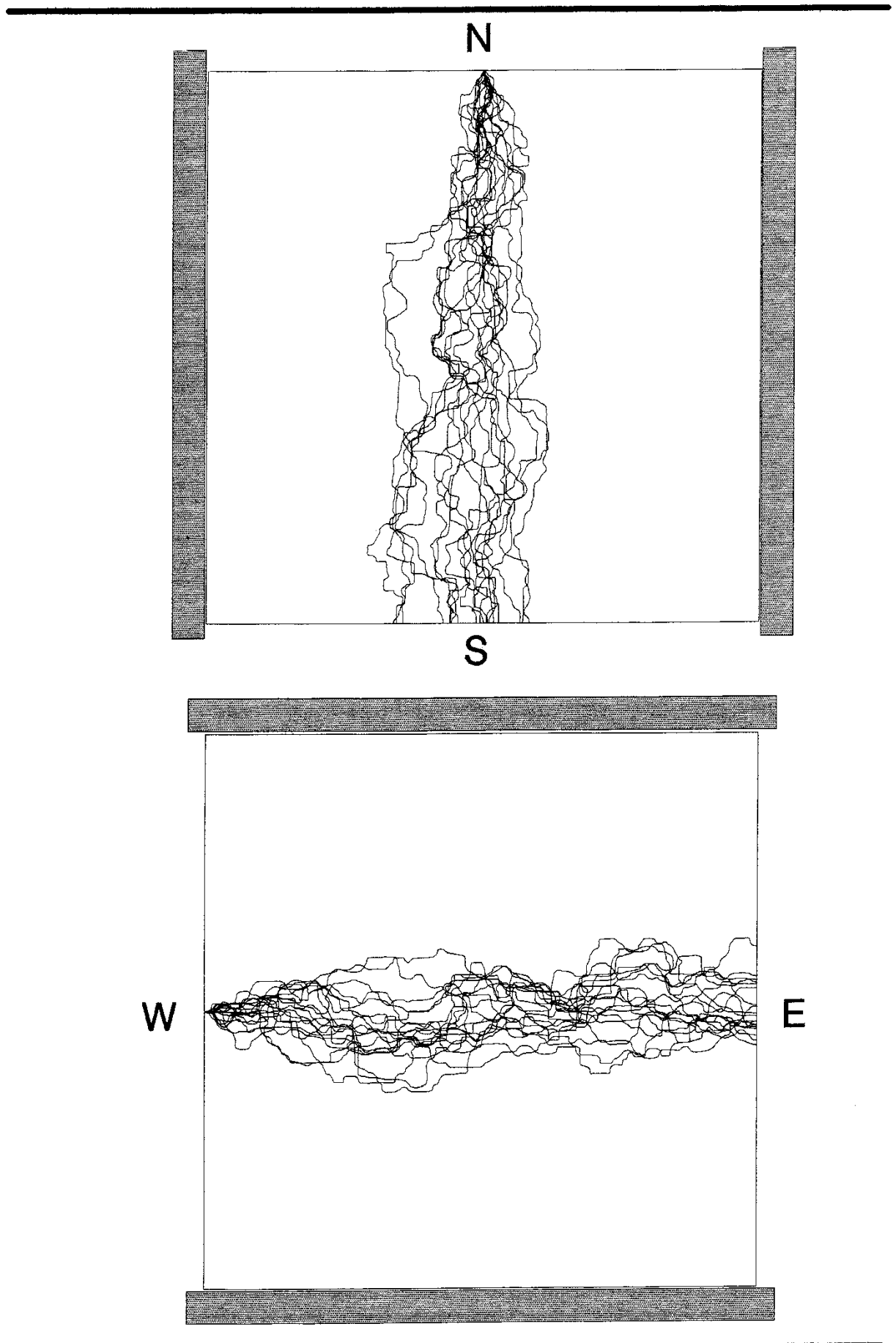
Fig. 101 Figurative plots of apparent transverse macrodispersion, that is,

lateral advective transport is estimated by lumping streamlines.

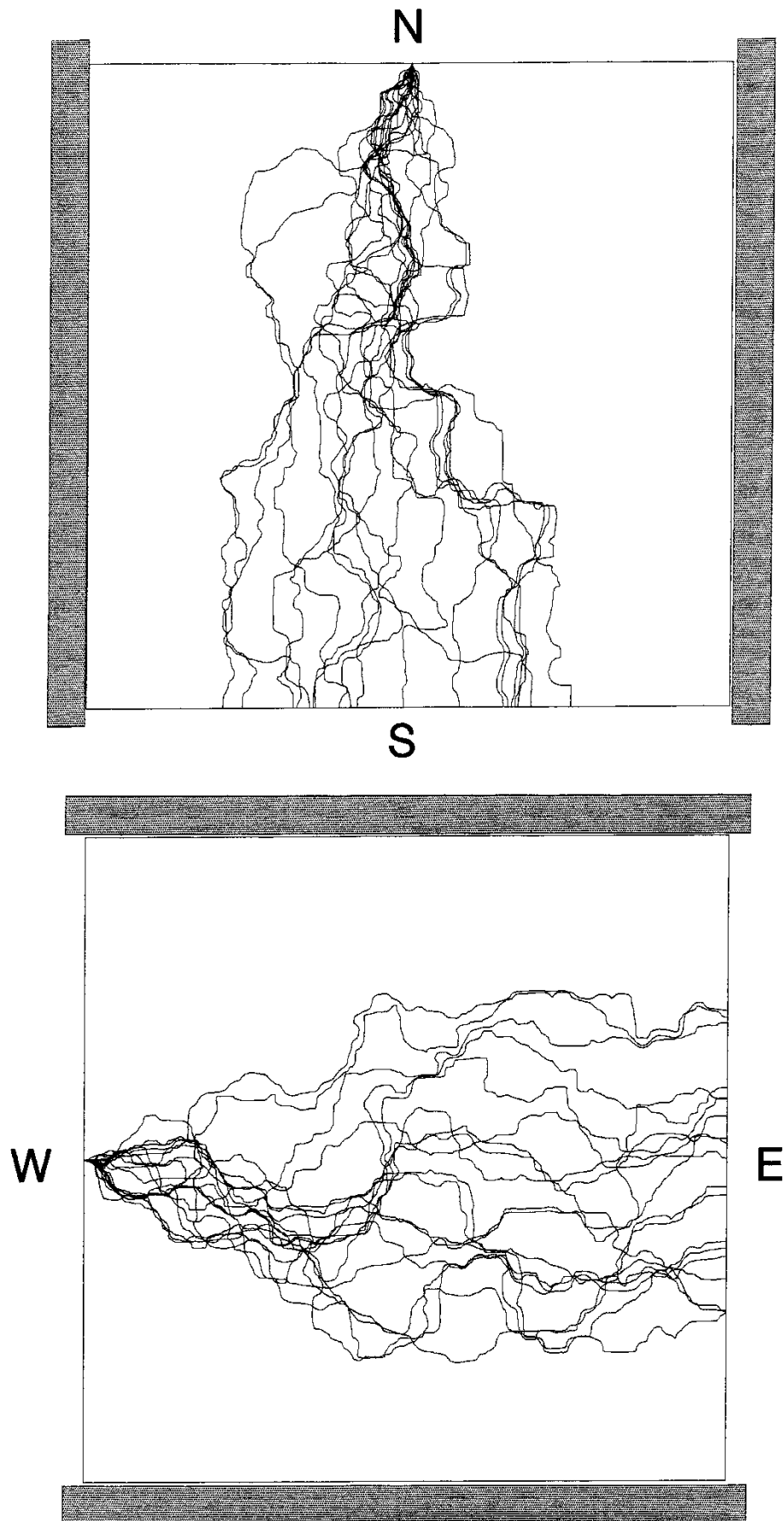$N = (64 \times 64)$, $\lambda/\Delta x = \lambda/\Delta y = 0$ and $\sigma_{\ln(K)} = 4.00$.

Fig. 102 Figurative plots of apparent transverse macrodispersion, that is,

lateral advective transport is estimated by lumping streamlines.

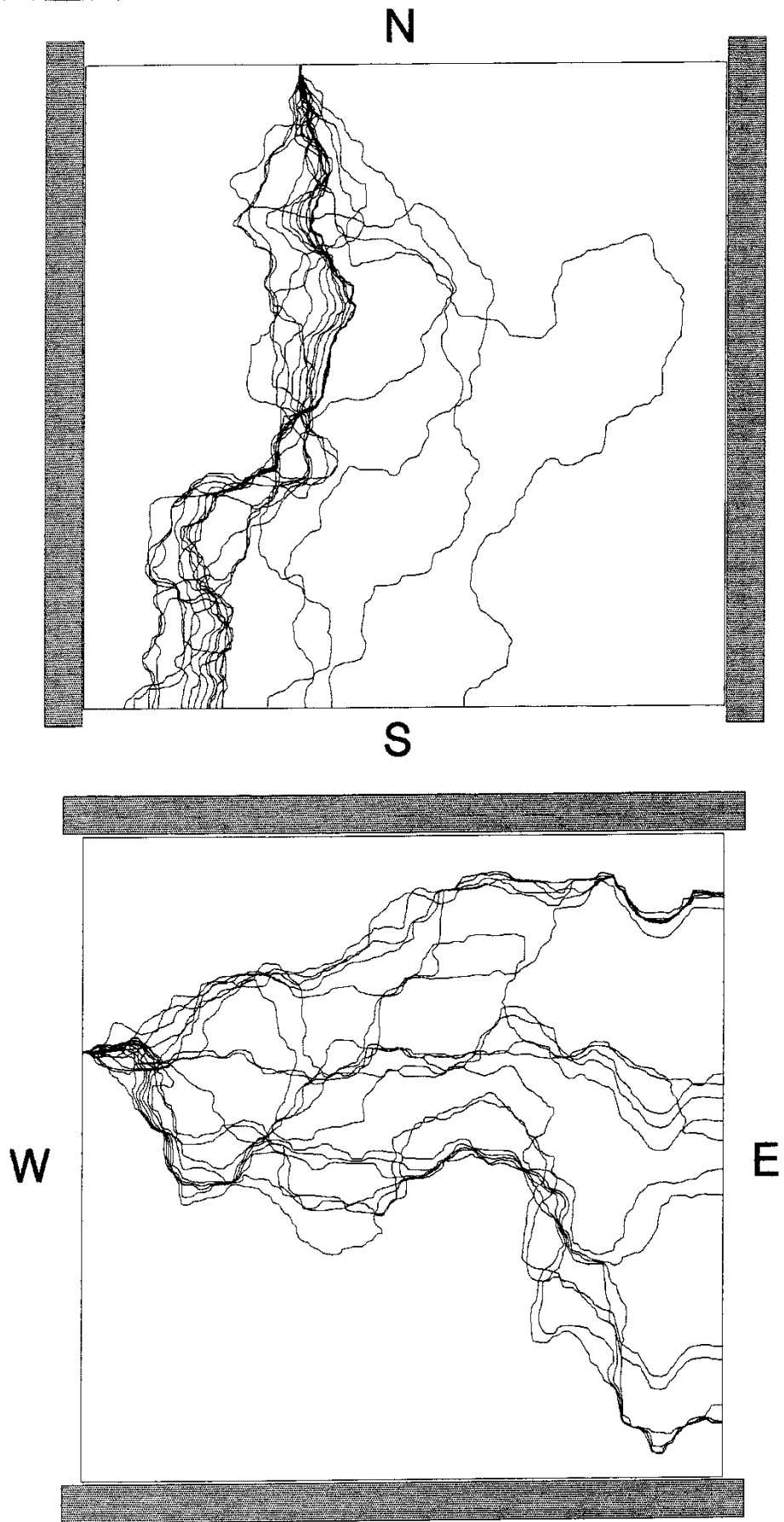$N = (64 \times 64)$, $\lambda/\Delta x = \lambda/\Delta y = 2$ and $\sigma_{\ln(K)} = 4.00$.

Fig. 103 Figurative plots of apparent transverse macrodispersion, that is,

lateral advective transport is estimated by lumping streamlines.

$N = (64 \times 64)$, $\lambda/\Delta x = \lambda/\Delta y = 4$ and $\sigma_{\ln(K)} = 4.00$.

Fig. 104 Histograms showing relative longitudinal and transverse particle displacements. Flow is from N to S. $t_{ref} = L\,n\,/\,\overline{q_{long}}$. $\sigma_Y = 1.00$ and $\lambda/\Delta x = \lambda/\Delta y = 2$. $N = (64 \times 64)$. $N_p = 999$.

W/E FLOW, LONGITUDINAL DIRECTION   W/E FLOW, TRANSVERSE DIRECTION
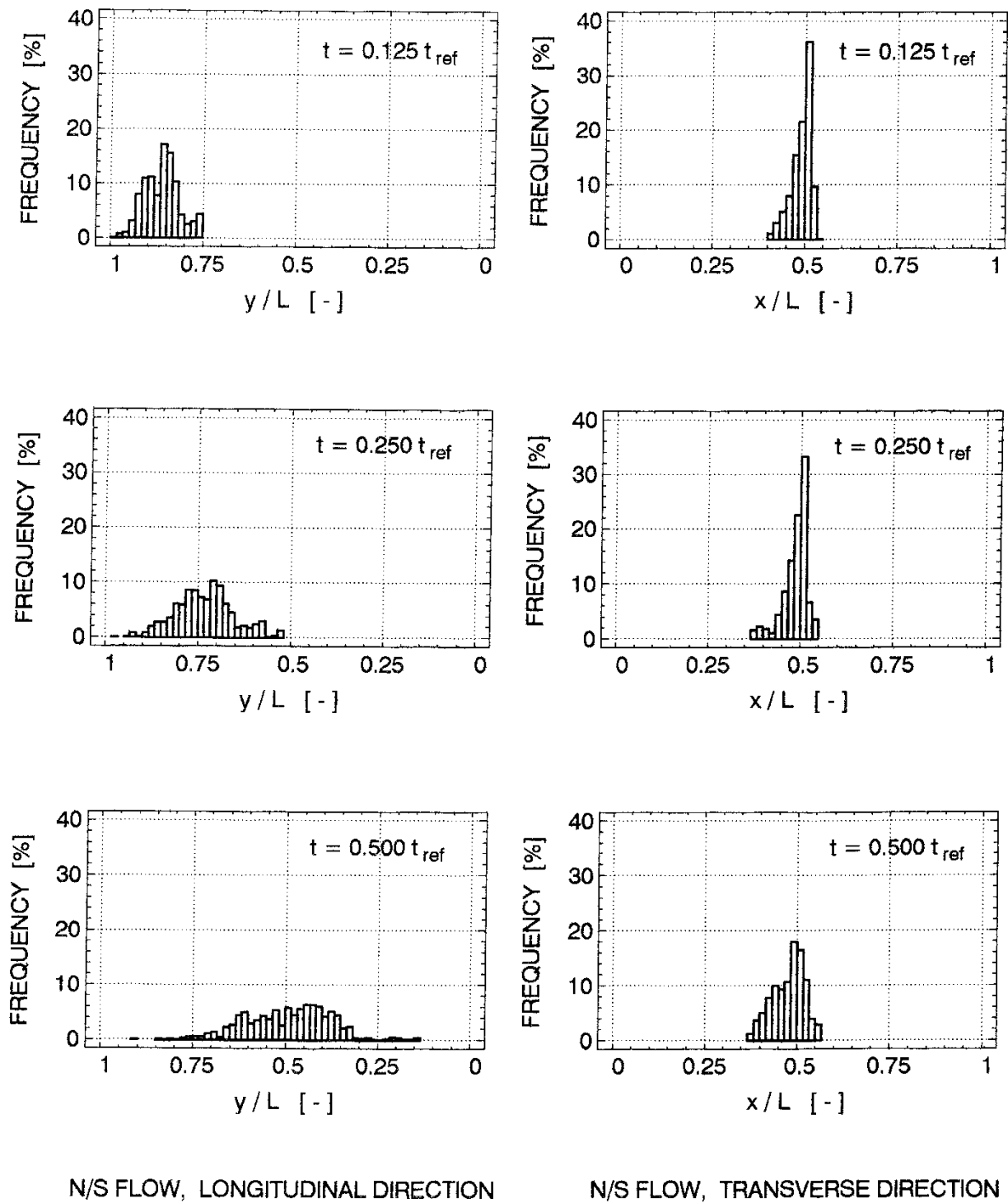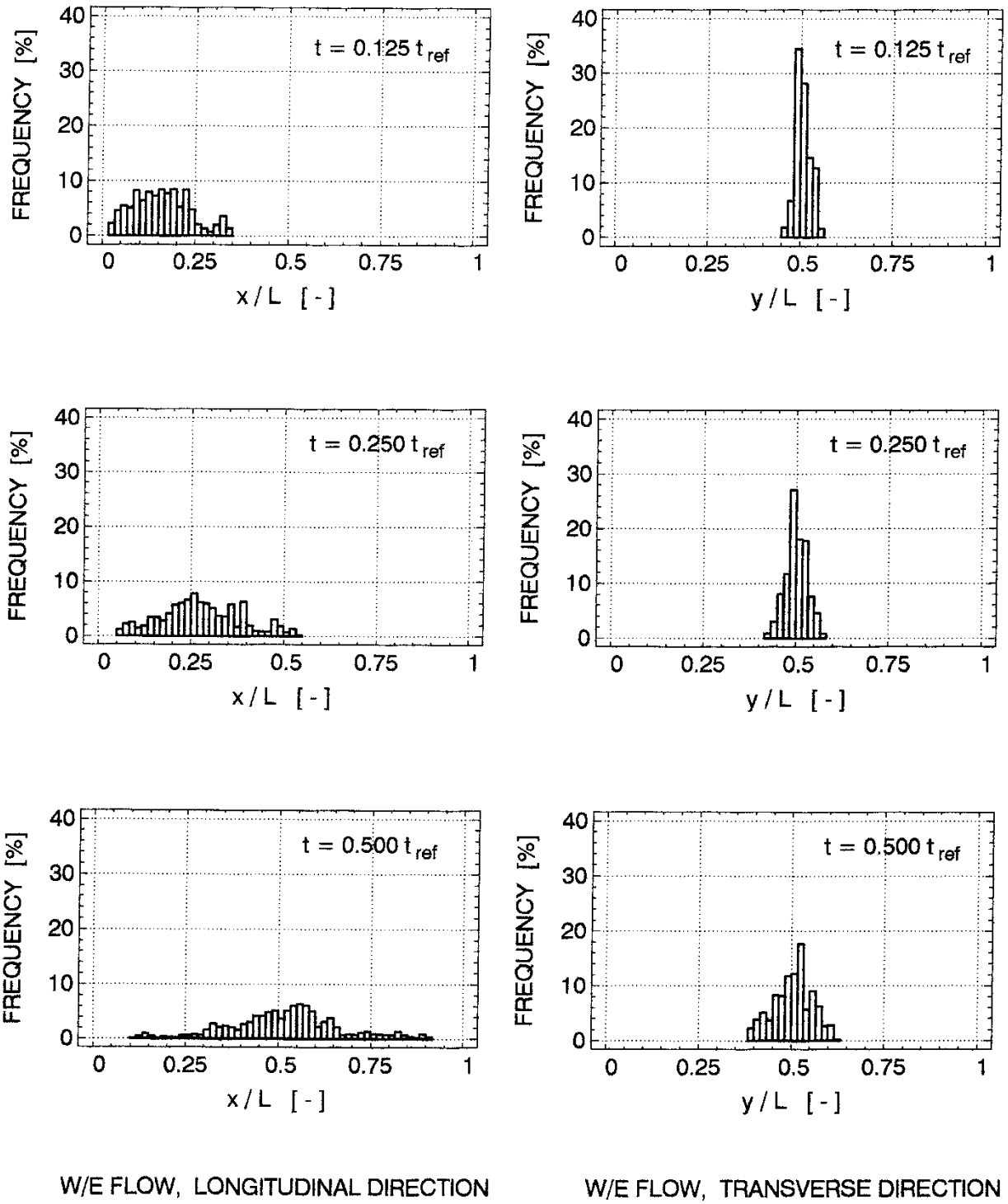
Fig. 105   Histograms showing relative longitudinal and transverse particle displacements. Flow is from W to E. $t_{ref} = L\,n/\overline{q_{long}}$. $\sigma_Y = 1.00$ and $\lambda/\Delta x = \lambda/\Delta y = 2$. $N = (64 \times 64)$. $N_p = 999$.
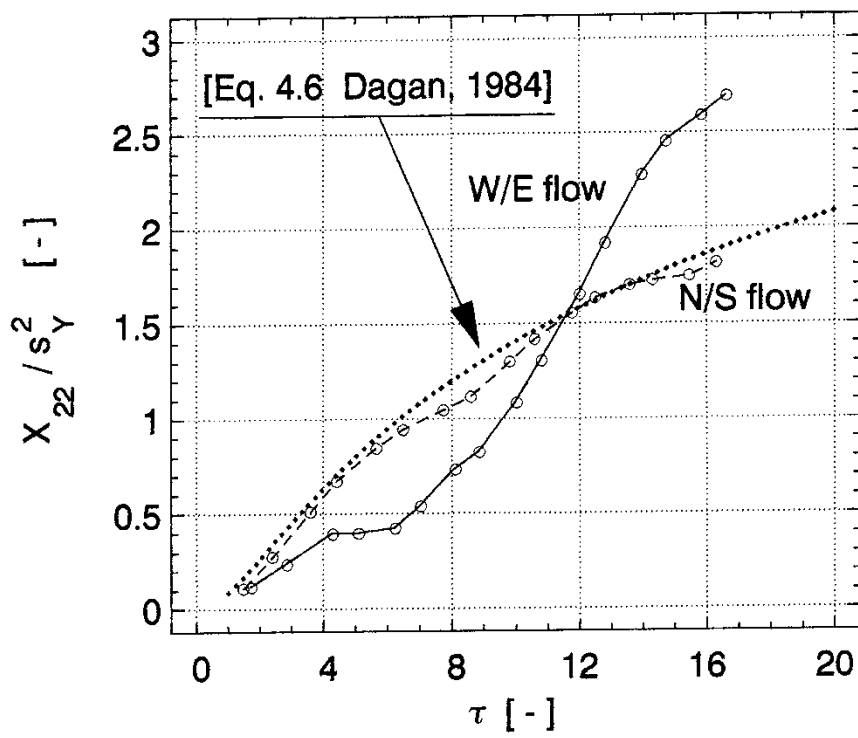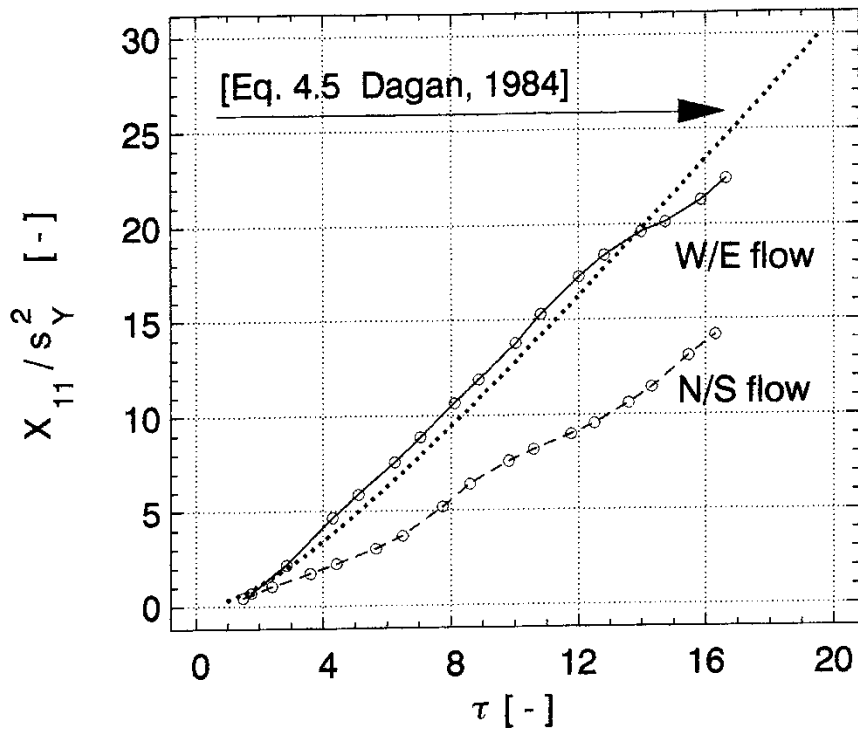
Fig. 106 The displacement covariances as functions of time . X_{11} and X_{22} are made dimensionless with respect to λ^2, and τ with respect to λ / v. $\lambda/\Delta x = \lambda/\Delta y = 2$ and $\sigma_Y = 1.00$.
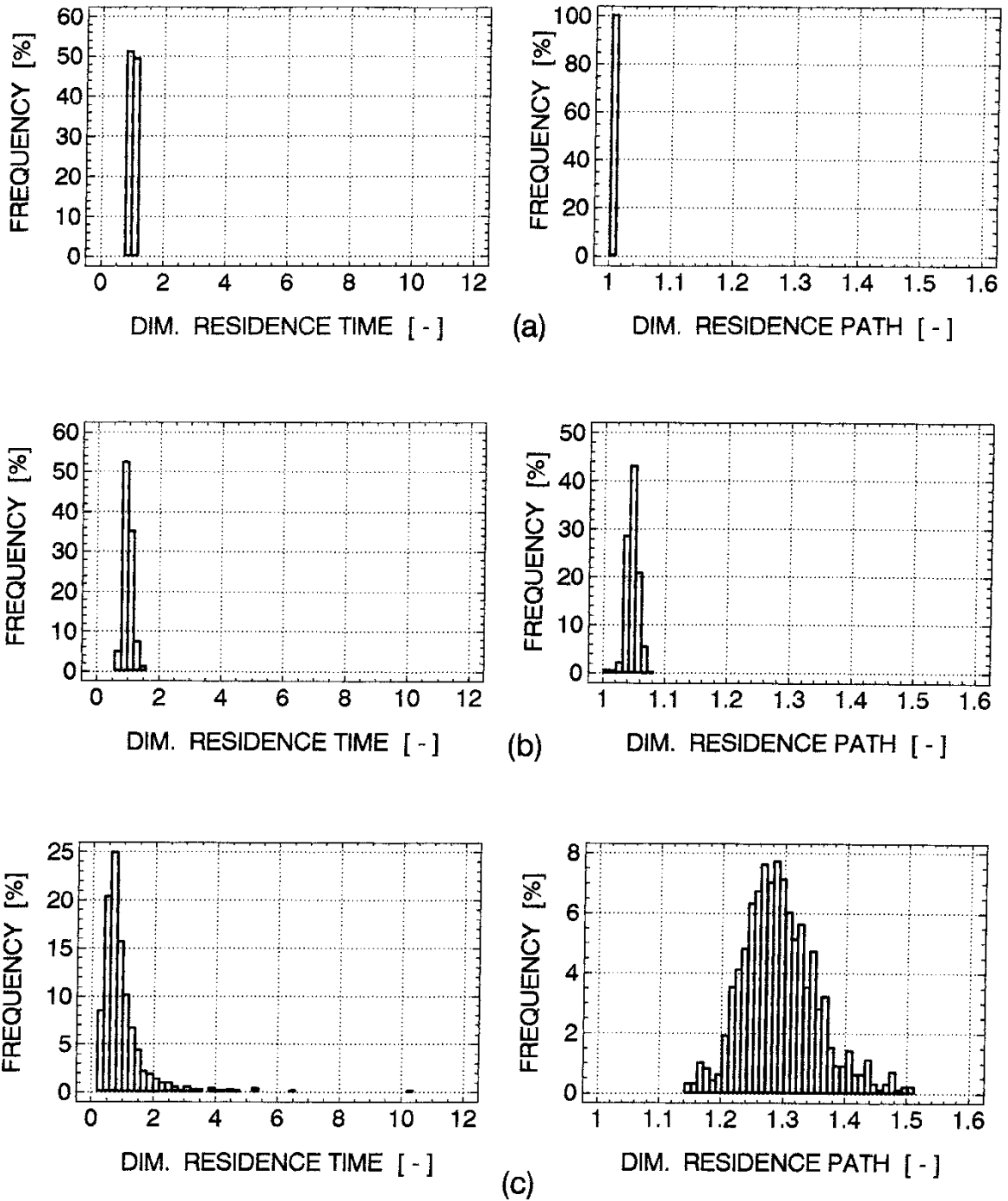
Fig. 107 Residence time and residence path histograms for

$\lambda/\Delta x = \lambda/\Delta y = 0$. N/S flow . N = (64 x 64) .
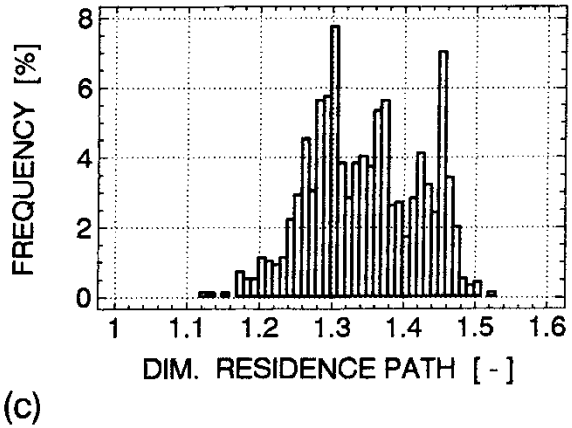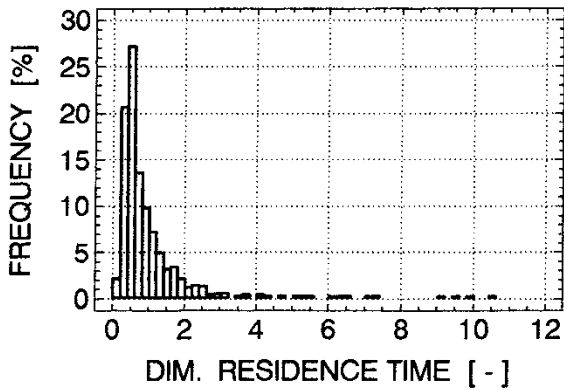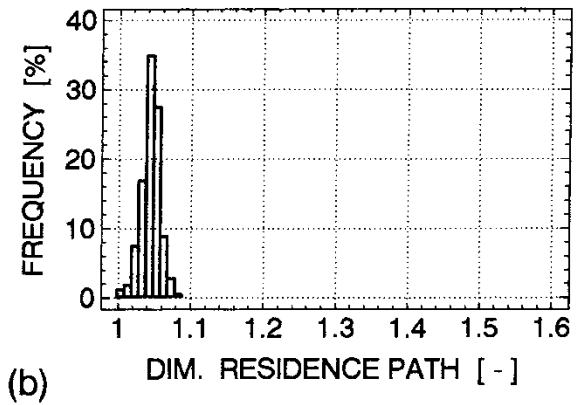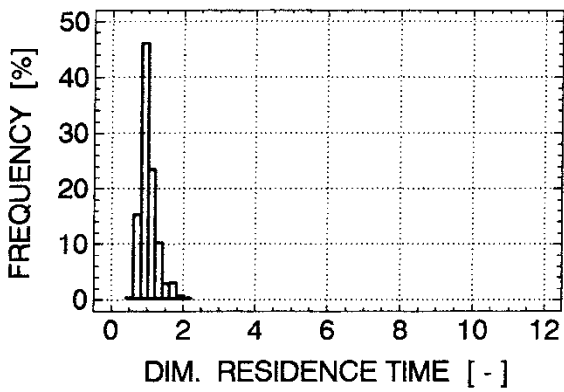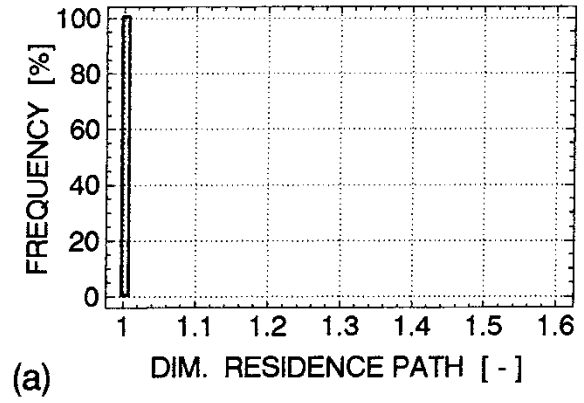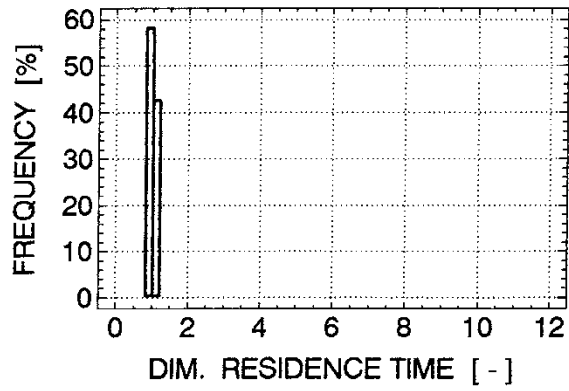
Fig. 108 Residence time and residence path histograms for

$\lambda/\Delta x = \lambda/\Delta y = 2$. N/S flow. N = (64 x 64).
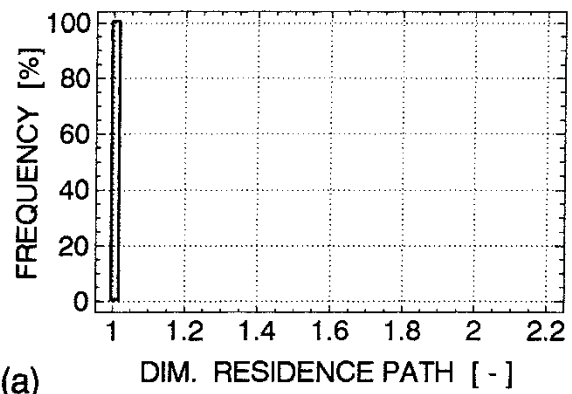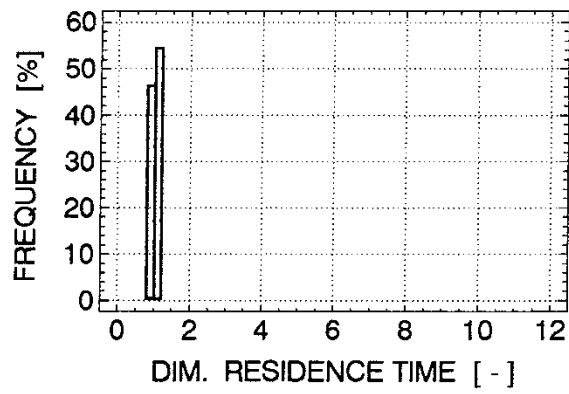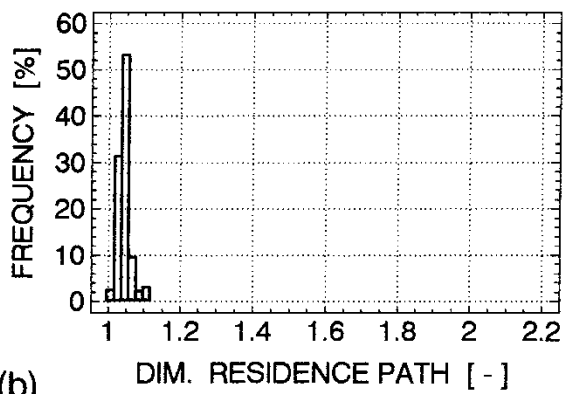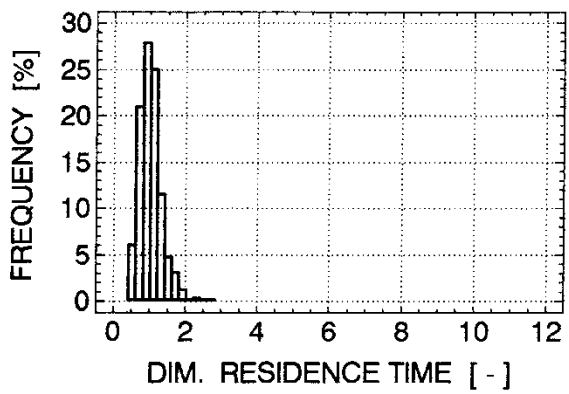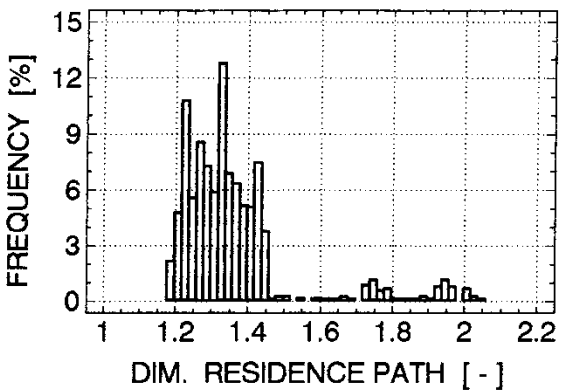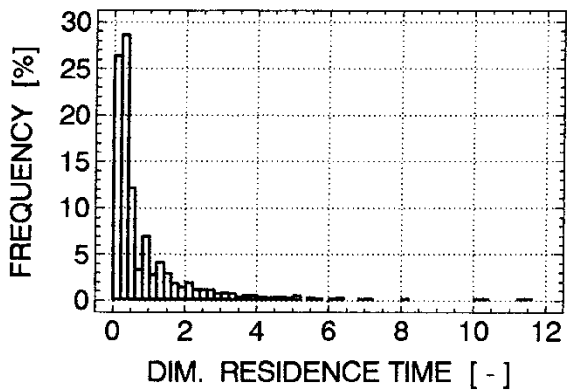
Fig. 109 Residence time and residence path histograms for

$\lambda/\Delta x = \lambda/\Delta y = 4$. N/S flow . N = (64 x 64) .
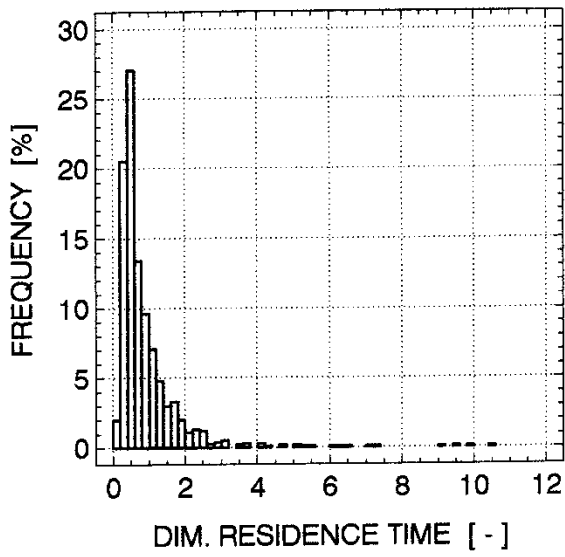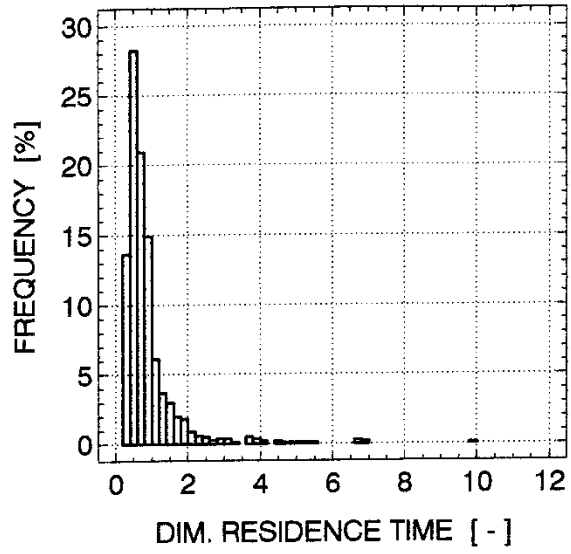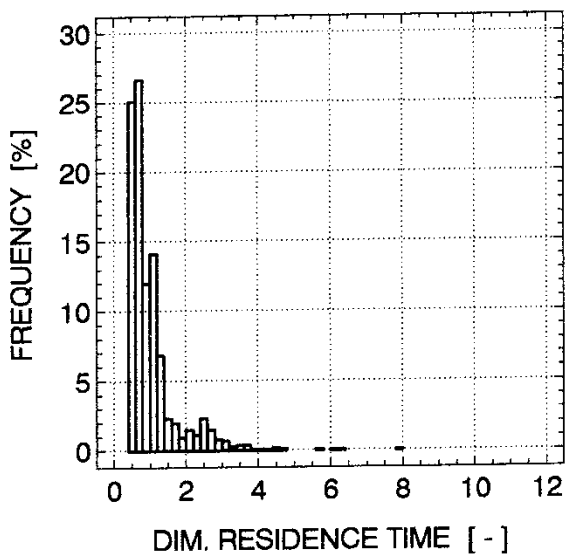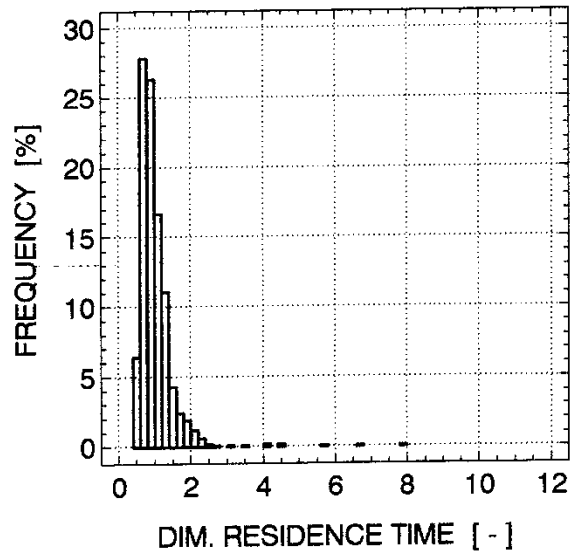
Uniform porosity : (a) N/S flow   (b) W/E flow

Variable porosity : (c) N/S flow   (d) W/E flow

Fig. 110 Residence time histograms for uniform and variable porosity fields.
Case 4-22 .
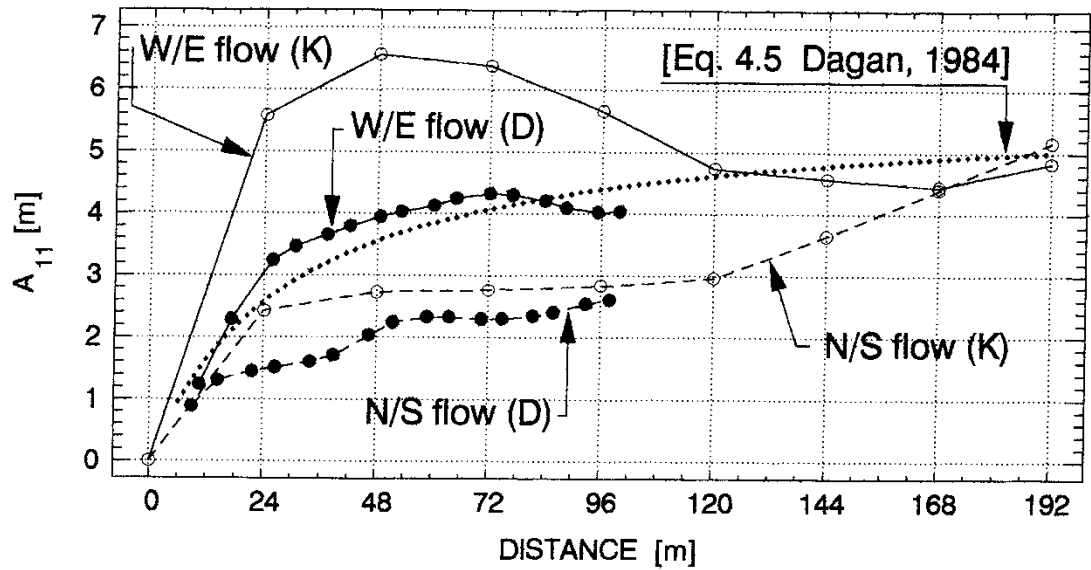
LONGITUDINAL DIRECTION
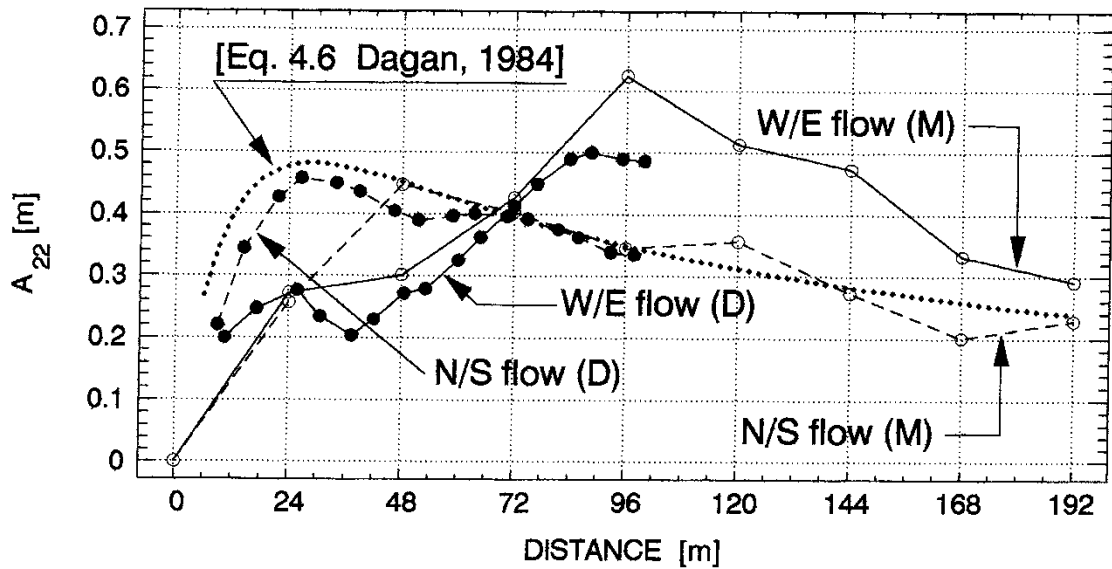
TRANSVERSE DIRECTION

(D): Dagan [1984]   (K): Kreft & Zuber [1978]   (M): Mixed (see (42b))

Fig. 111 Comparison of computed longitudinal and transverse macro-dispersivities. $\lambda/\Delta x = \lambda/\Delta y = 2$ and $\sigma_Y = 1.00$.
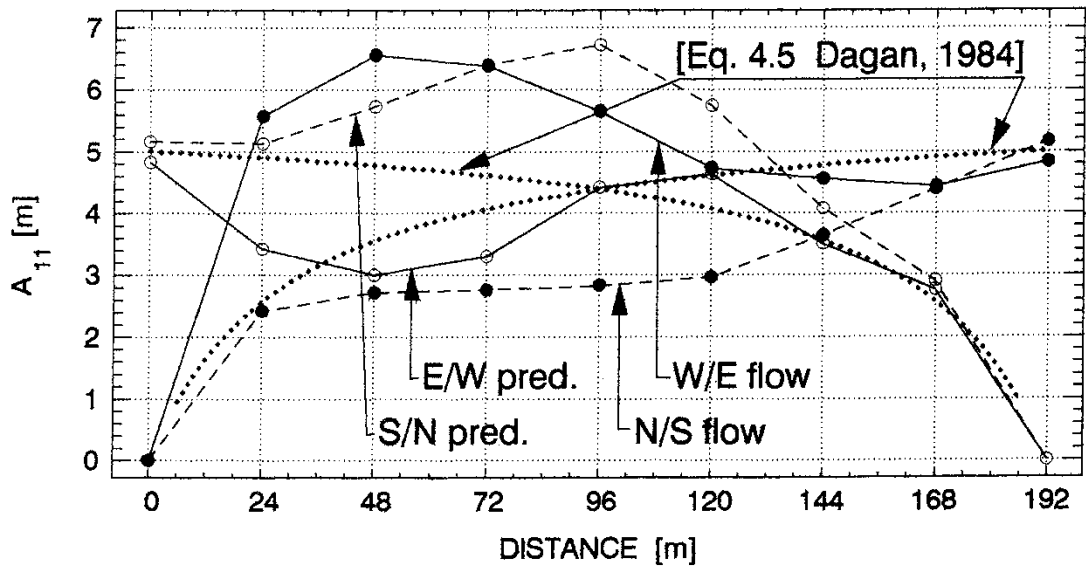
LONGITUDINAL FLOW: W --> E & N --> S

$\lambda/\Delta x = \lambda/\Delta y = 2$ and $\sigma_Y = 1.00$.
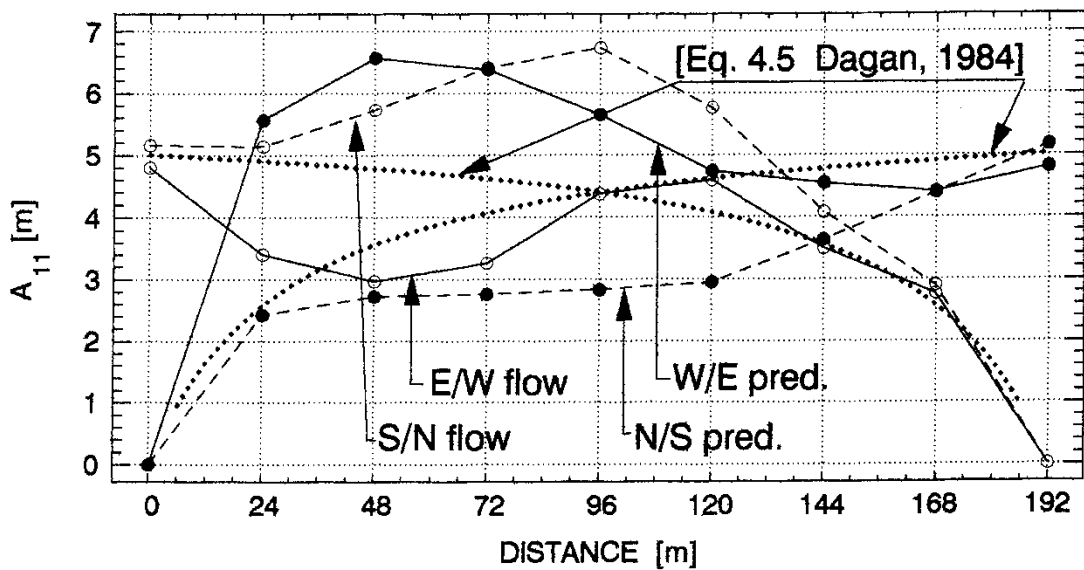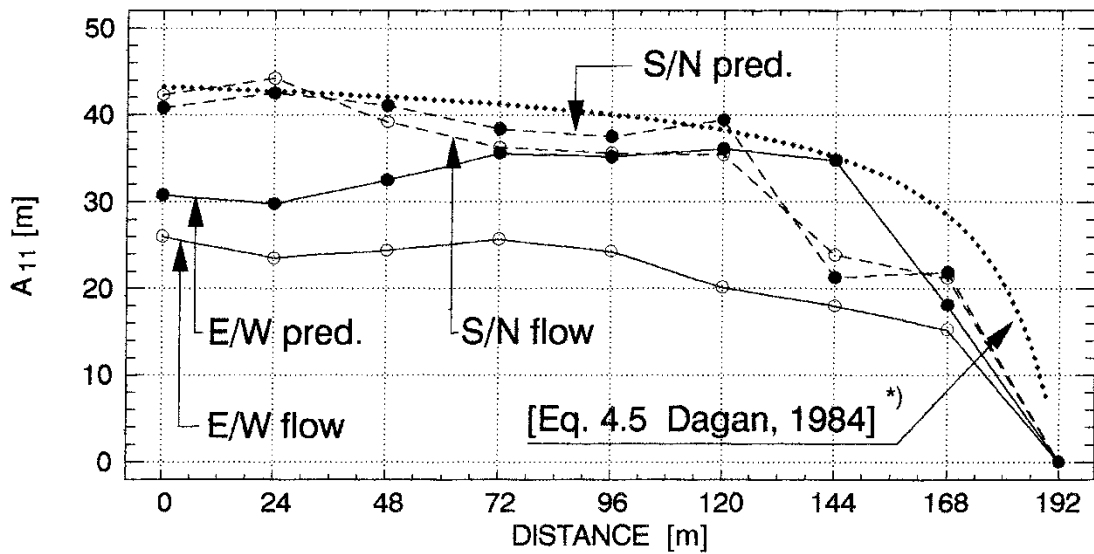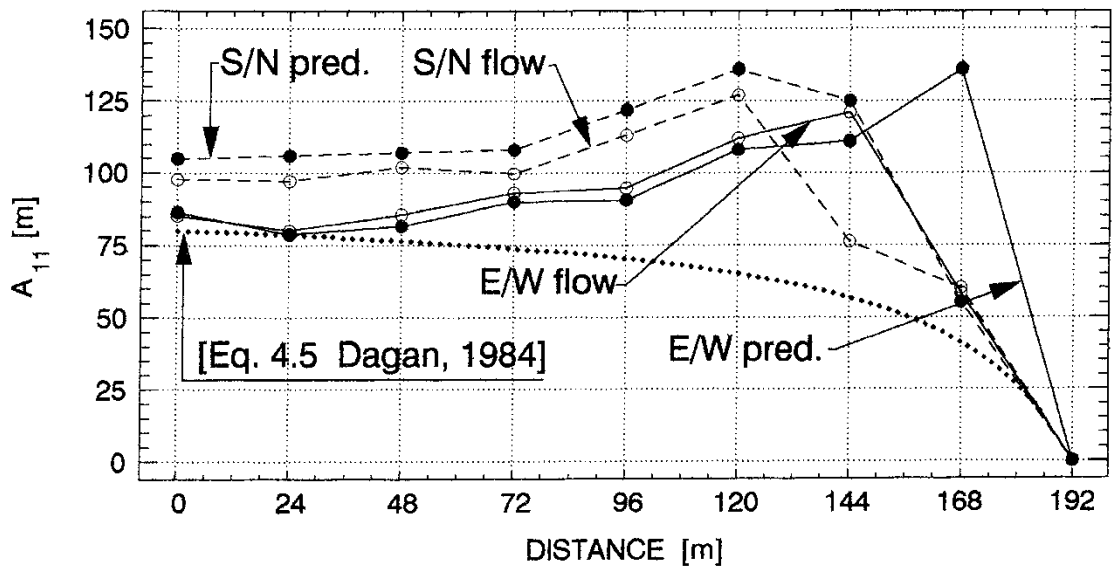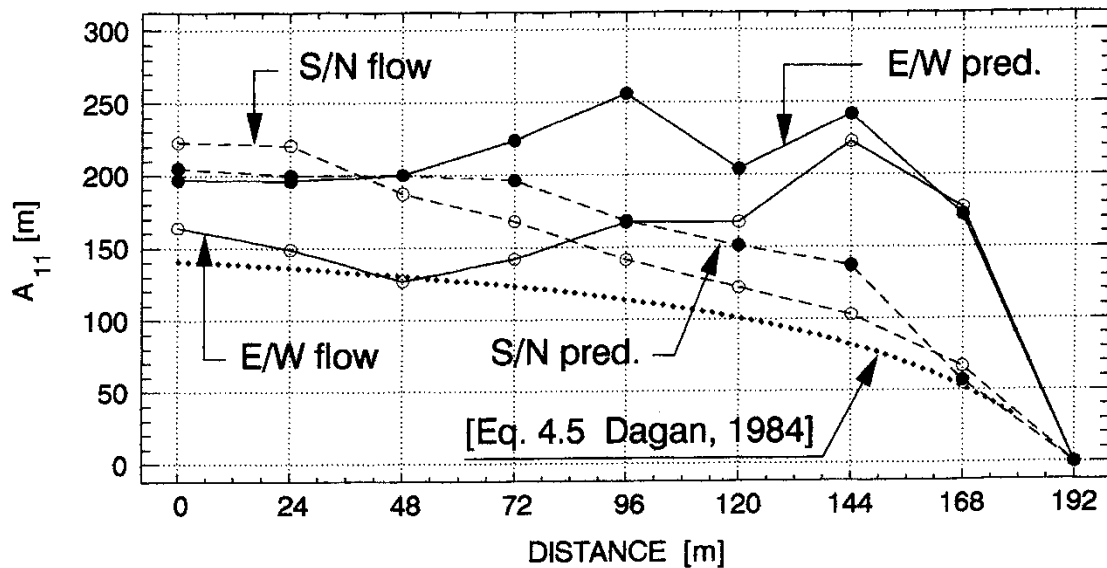
REVERSED LONGITUDINAL FLOW: E --> W & S --> N

$\lambda/\Delta x = \lambda/\Delta y = 2$ and $\sigma_Y = 1.00$.

Fig. 112 Verification of the proposed injection mode by the priciple of

reciprocity. The dispersivities are computed according to

Kreft & Zuber [1978], where 'pred.' stands for predicted values

(assuming reciprocity).

Fig. 113 Longitudinal macrodispersivity vs. distance for three values of σ_Y. The dispersivities are computed according to Kreft & Zuber [1978].

Fig. 114 Deviations from the priciple of reciprocity for case 4-00 . The dispersivities are computed according to Kreft & Zuber [1978], where 'pred.' stands for predicted values (assuming reciprocity).

Fig. 115 Deviations from the priciple of reciprocity for case 4-22 . The
dispersivities are computed according to Kreft & Zuber [1978],
where 'pred.' stands for predicted values (assuming reciprocity).

Fig. 116 Deviations from the priciple of reciprocity for case 4-44 . The dispersivities are computed according to Kreft & Zuber [1978], where 'pred.' stands for predicted values (assuming reciprocity).
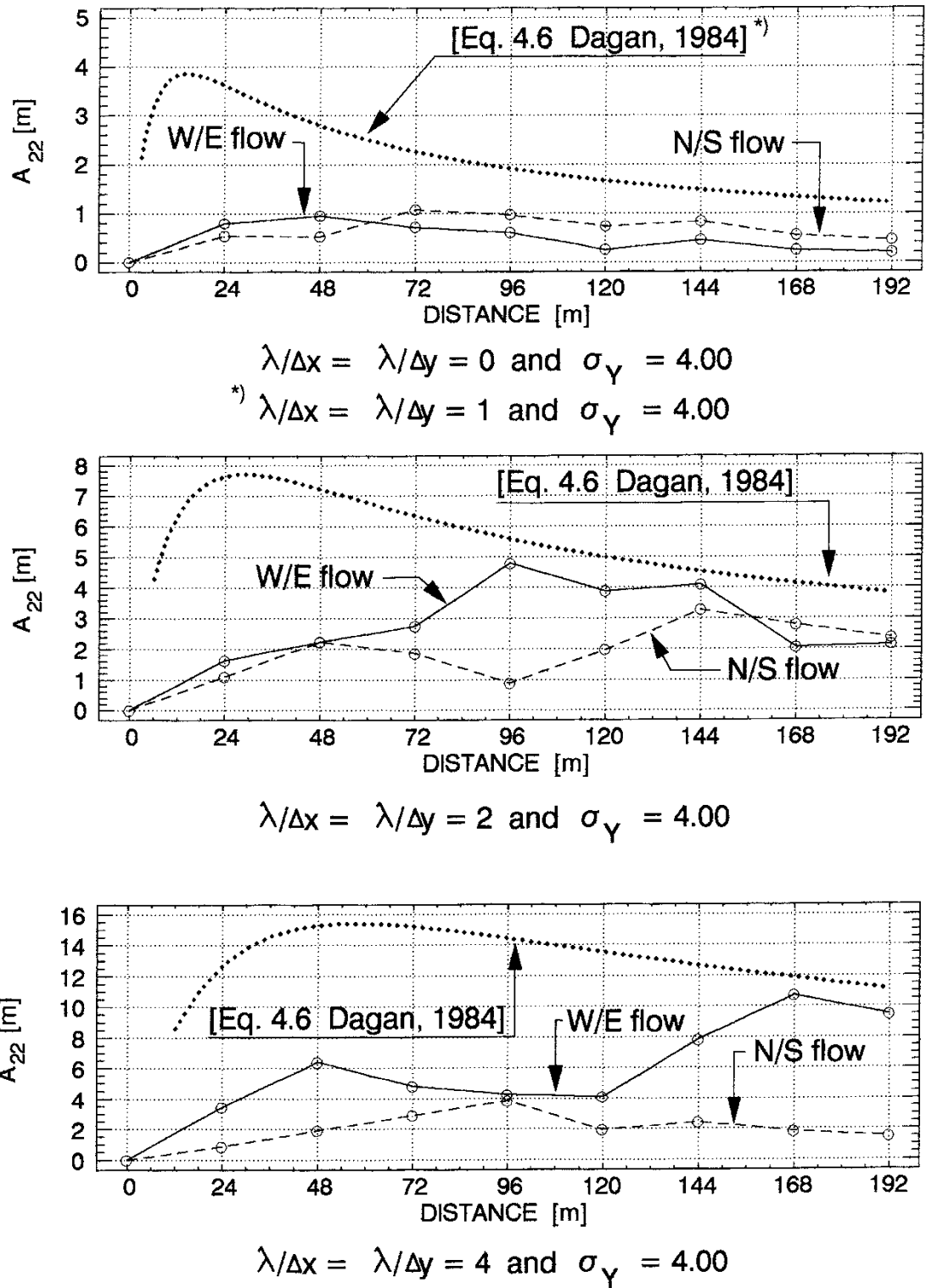
Fig. 117   Transverse macrodispersivity vs. distance for three values of λ .

The dispersivities are computed by a mixed technique, see (42b).
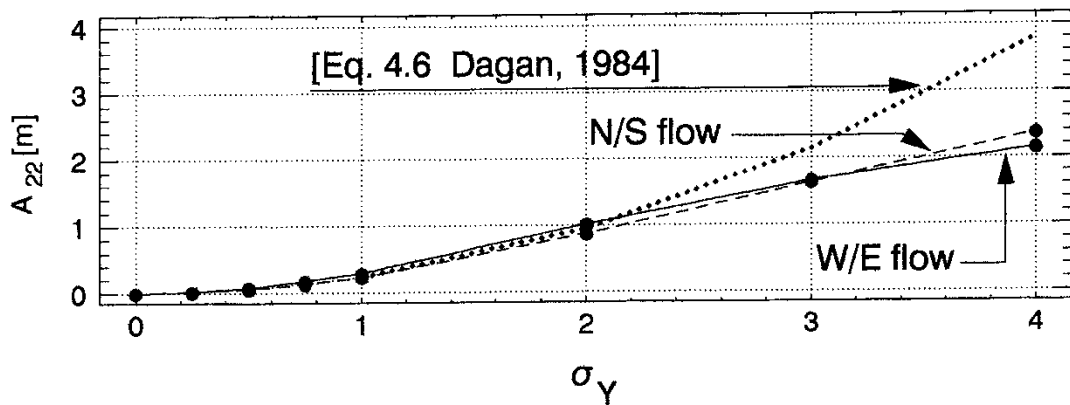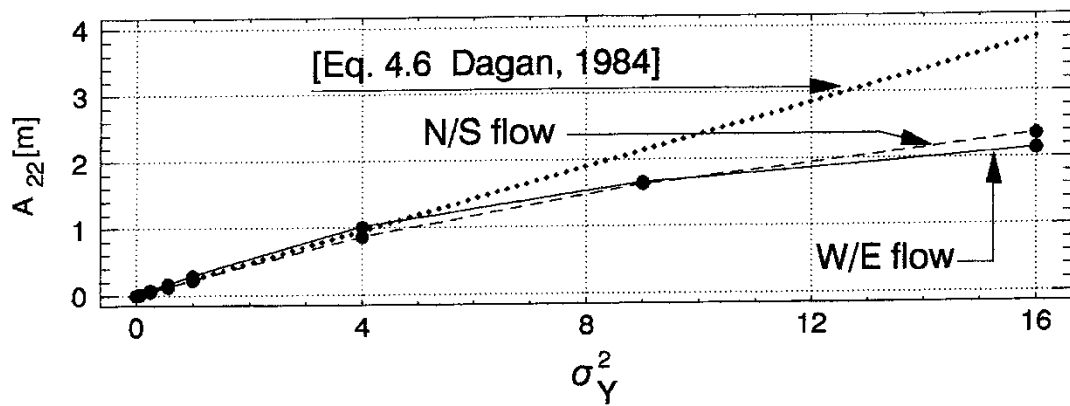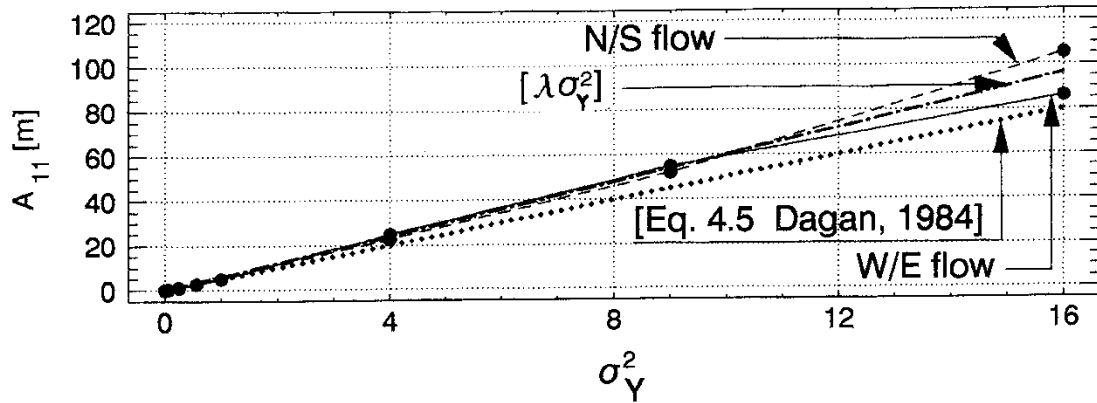
Fig. 118 Longitudinal and transverse macrodispersivities vs. σ_Y^2 (or σ_Y).
The longitudinal dispersivities are computed according to
Kreft & Zuber [1978], whereas the transverse dispersivities are
computed by a mixed technique, see (42b). $L/\lambda = 32$.

3.6 A discontinuum model

The channelling observed in the experiments for $\sigma_Y^2 = 16$ is significant in many ways, see Figures 97-99. It is interesting observation that large portions of the generated flow domain do not contribute to the flow. It is of great interest to find a physical criterion that makes it possible to discard the no-flow portions, because (*i*) the computational constraints will be relaxed, meaning fewer numerical problems and more computer memory at hand, and (*ii*) one will have an opportunity to study the link between continuum models and the more recent discrete fracture network models. An obvious no-flow criterion is the measurement threshold of the double-packer test equipment. For 3m packer tests, the measurement threshold is ap-proximately 10^{-11} m/s [see, e.g. Nilsson, 1989, 1990]. For a typical borehole of 500-600m depth in fractured hard rock, about 20-50% of the measurements are below or at the measurement threshold, so there is a significant loss of information. If the aforementioned measurement threshold of a 3m packer test is translated into a constant-valued aperture of a single fracture by means of the "cubic law" [see, e.g. Witherspoon *et al.*, 1980; Robinson, 1984; Herbert & Splawski, 1990], an aperture of about 3-4 µm is obtained, which in fact is considered to be close to the lower limit of validity of the cubic law [see, e.g. Engelder & Scholz, 1981; Witherspoon, 1986]. Hence, it may be physical features of the rock that cause the loss of information, besides the technical constraints of the double-packer test equipment. The objective here is to examine briefly the differences in flow and transport between continuous and discontinuous conductivity fields. The calculations are limited to two-dimensional flow and the following cases are studied: $\lambda_Y/\Delta x = \lambda_Y/\Delta y = \{0, 2, 4\}$, $\sigma_Y = 4$, denoted 4-00, 4-22, and 4-44, respectively. For each continuous field calculations are made for a corresponding discontinuum field in which that part of the flow domain with a conductivity less than the *conductivity threshold* of 25% is discarded.

A conductivity threshold leads to impermeable boundaries in the interior of the flow domain, see Figure 120. The *stochastic discontinuum* shown in this figure is a replicate of the stochastic continuum shown in Figure 12 subjected to a 25% conductivity threshold. The discontinuities or non-conducting support blocks are indicated by an "X", and are in the following called "X-blocks". In addition to the value of the conductivity threshold, the configurations of the X-blocks are also dependent on the correlation length of the hetero-geneity, see Figures 123, 125, and 127. Therefore, the exact geo-metries of the X-blocks remain unknown until each realization is generated. The analysis required prior to the solution of the flow equations resembles to some extent the problem of determining the connectivity of a discrete fracture network realization [cf., e.g. Robinson, 1984; de Marsily, 1985]. In terms of the dual formulation of flow, the perimeter of any impermeable part of the flow domain constitutes a streamline of unknown stream function value. Thus, while solving the flow equations for the *stream function*, the modeller will face the classical problem of having more unknowns than equations. The simple numerical technique developed in this study to circumvent this problem may be explained as follows:

Consider the discontinuous conductivity field in Figure 120 and, in particular, the two X-blocks placed vertically side-by-side close to the lower-left corner. Upon solution, the perimeter of the two X-blocks constitutes a streamline. Although the stream function value of the perimeter is unknown, it is important to recognize that the perimeter is constant-valued, i.e. all nodes lying on the perimeter have the same Ψ value. In other words, the configuration of the perimeter is unimportant from a node-numbering point of view while seeking the stream function solution (Ψ). The technique suggested here is to renumber the mesh and treat all the nodes on a common perimeter of X-blocks as a *single* node. Thus, the problem of too many unknowns is solved by a strategic node numbering. However, it is important to note that the suggested numbering technique may lead

to problems for the equation solver. For example, neither of the two direct solvers used here, i.e. a frontal method solver [Duff, 1981] and a triangular de-composition solver [Istok, 1989], can treat the resulting problem unless the assembling algorithms are updated.

In Figures 121 and 122, the solutions of the piezometric head (φ) and the Lagrange stream function (Ψ) for two different discretizations of the discontinuous $(48m)^2$ block in Figure 120 are shown. A visual comparison of the two solutions in relation to the corresponding ones shown in Figures 17 and 19, respectively, demonstrates the validity of the suggested technique from a qualitative point of view. A quantitative validation is given in Figure 119, where it is demonstrated that four elements per block in the discontinuous case (Case D-4) give approximately the same results as 64 elements per block in the continuous case (Case C-64). The increased performance is due to less contrasts in the conductivity field.

Case	No. of elements per K-value	W/E-flow K_{xx} $_{-8}$ $[n \cdot 10 \; m/s]$	N/S-flow K_{yy} $_{-8}$ $[n \cdot 10 \; m/s]$
C-1	1	5.0535	6.3140
C-4	4	4.4722	5.8903
D-4	4	4.0998	5.4953
C-16	16	4.1823	5.6853
C-64	64	4.0178	5.5808
D-64	64	3.6240	5.1893

C = Continuous   D = Discontinuous

Fig. 119 Comparison of block conductivities for the continuous conductivity field shown in Figures 12 and the discontinuous conductivity field shown in 120.

Figures 124, 126, and 128 demonstrate the flow patterns for the discontinuous cases shown in Figures 123, 125, and 127, respectively. The flow patterns and the conductivity fields for the corresponding continuous cases are shown in Figures 48/39, 58/55, and 63/60, respectively. (Figure A9, in the appendix, shows a discontinuous realization corresponding to the statistically anisotropic conductivity field shown in Figure A1 for a conductivity threshold of 25%. The corresponding flow pattern is shown in Figure A10.) Figure 129 shows the ratio of the discontinuous block conductivity (K_{th}) to the corresponding continuous block conductivity (K_S) for different values of the conductivity threshold. Figure 130 shows a comparison of the residence-time histograms for case 4-22 and the corresponding discontinuous replicate for a conductivity threshold of 25%. Residence-time histograms are shown in Figure 130 for both directions of flow. Figure 131 shows a comparison of the dispersivities for case 4-22 and the corresponding discontinuous replicate for to a conductivity threshold of 25%. The dispersivities are computed by the Fickian arrival time analysis discussed above. The results for the different flow and transport simulations can be summarized as follows:

Figures 119, 121, and, 122 demonstrate that the suggested extension of the dual formulation of flow to address discontinuous conductivity fields relaxes the numerical constraints associated with high conductivity contrasts.

The solutions for the three discontinuous realizations, see Figures 123-128, reveal that the flow patterns of the corresponding continuous realizations are essentially preserved in spite of discarding all parts with a conductivity below a conductivity threshold of 25%.

The experiments shown in Figure 129 reveal that the main effect of a conductivity threshold is an increasing anisotropy. There is a clear

difference in the anisotropy between the three realizations considered here. The uncorrelated case is observed to be the least sensitive to a conductivity threshold. Moreover, it is observed that for a discontinuous conductivity field, the relation between the spatial geometric mean (K_g) and the corresponding block conductivity (K_{th}) deviates from the analytical relation valid for a continuous conductivity field (see (32)). The differences increase drastically as the conductivity threshold increases.

Figure 130 shows that for the case studied here, i.e. case 4-22 with a conductivity threshold of 25%, the differences in the residence-time histograms between the continuous and discontinuous cases are moderate.

Figure 131 shows that for the case studied here, i.e. case 4-22 with a conductivity threshold of 25%, the "asymptotic values" of the longitudinal dispersivities in two orthogonal directions are somewhat larger compared to the asymptotic values of the longitudinal dispersivities of the corresponding continuous realization. The behaviour of the transverse dispersivities is more complex. In one direction, the transverse dispersivity is somewhat larger, whereas in the other direction, it is much smaller. In both directions, however, they seem to obey the decreasing trend of the corresponding continuous realization.

2-D HYDRAULIC CONDUCTIVITY FIELD

No. of blocks: 16 × 16

$$\sigma_{\ln(K)} = 4.00 \qquad \lambda/\Delta x = 2.0 \qquad \lambda/\Delta y = 2.0$$

RASTER LEGEND (dim[K]=m/s)

+5.04E-14 ■ +7.02E-10 ■ +3.49E-09 ■ +1.73E-08 ▓ +5.86E-08

+5.86E-08 ▨ +2.62E-07 ▒ +9.78E-07 ░ +3.50E-06 □ +2.67E-04
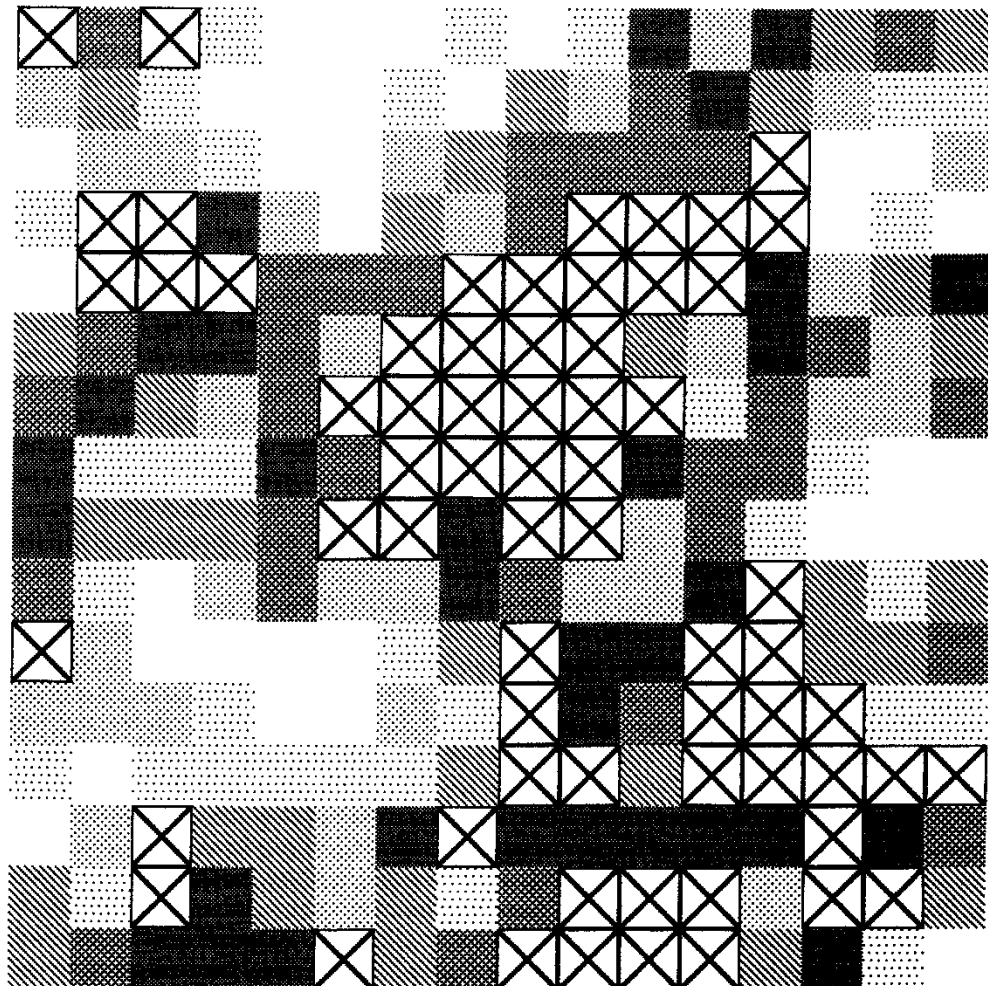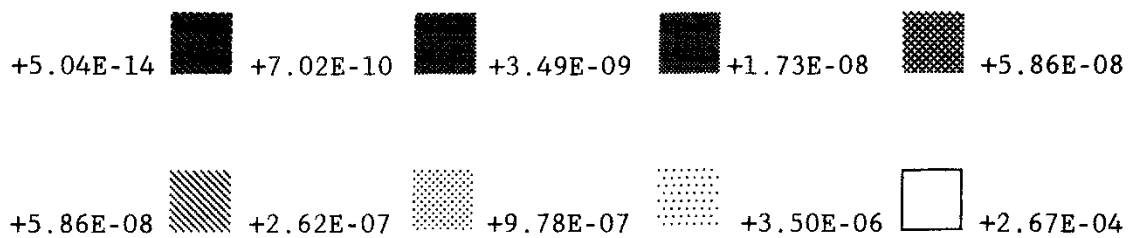
Fig. 120 Illustration of   +5.04E-14 ⊠ +3.49E-09   a 25% conductivity

THRESHOLD
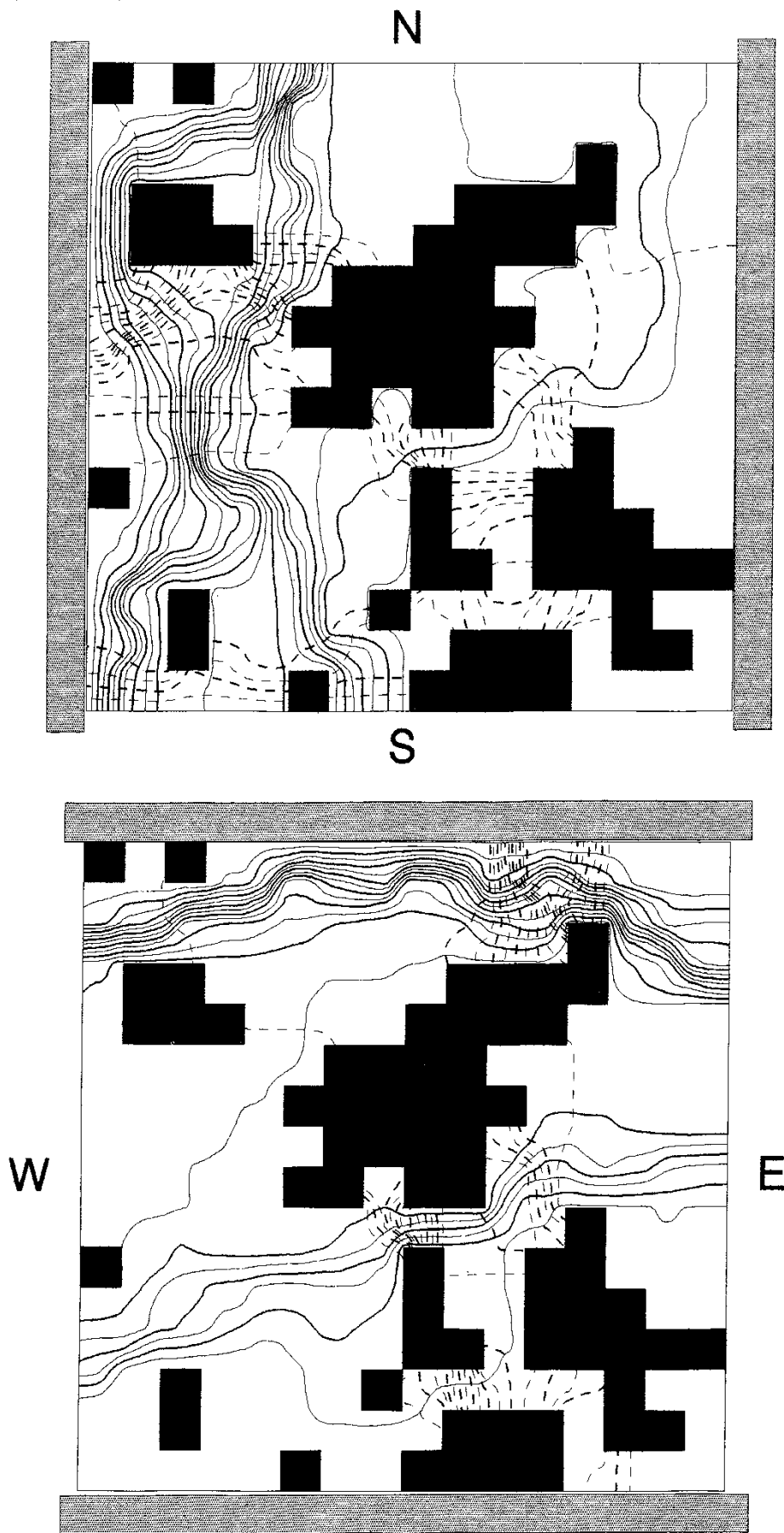
threshold.

Fig. 121 Flow nets for a 25% conductivity threshold, 4 elements/block ,

$\lambda/\Delta x = \lambda/\Delta y = 2$ and $\sigma_{\ln(K)} = 4.00$. Piezometric head (dashed) and

stream function levels (solid) are in 5% increments between 0 and 1.
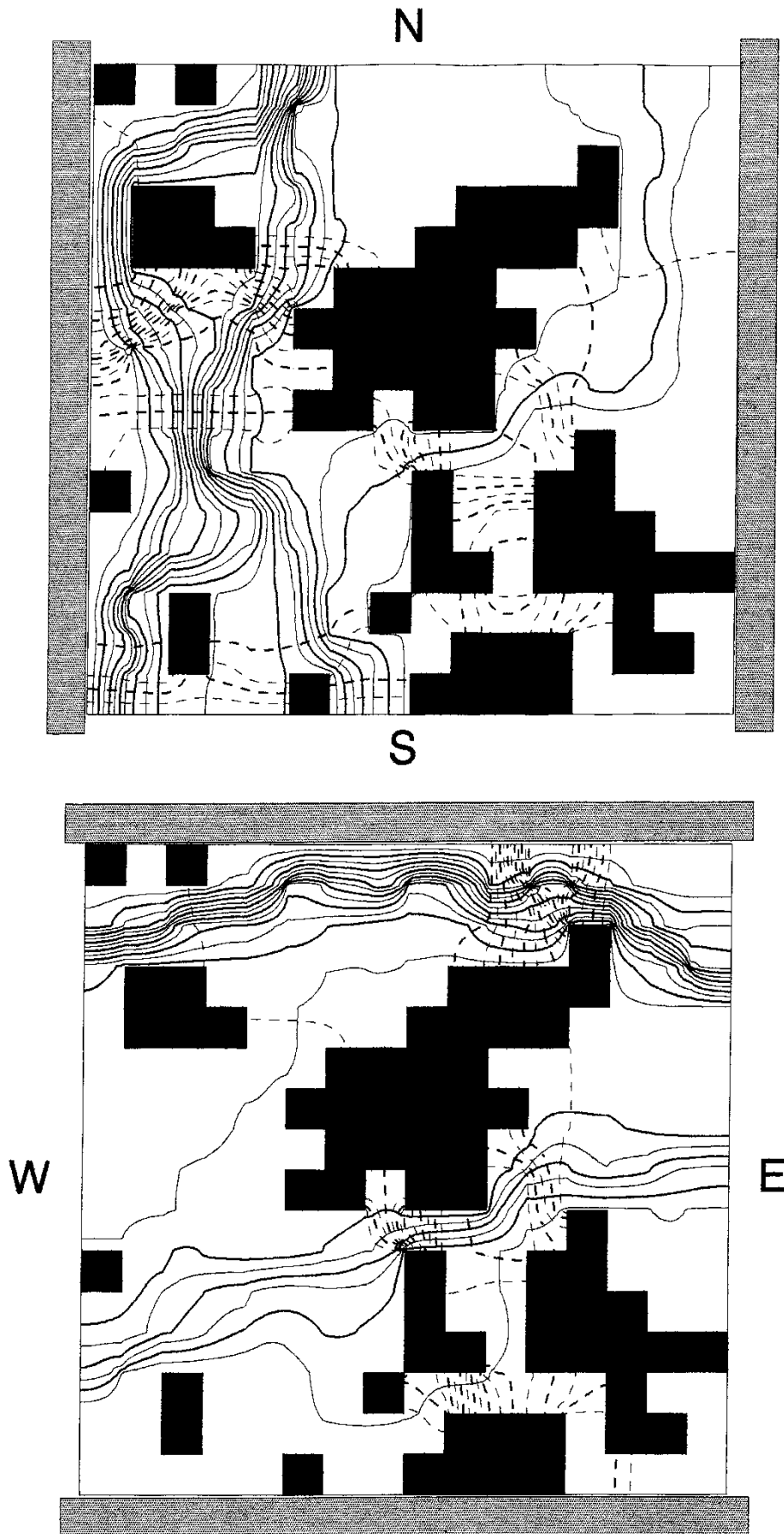
Fig. 122 Flow nets for a 25% conductivity threshold, 64 elements/block,
$\lambda/\Delta x = \lambda/\Delta y = 2$ and $\sigma_{\ln(K)} = 4.00$. Piezometric head (dashed) and
stream function levels (solid) are in 5% increments between 0 and 1.

2-D HYDRAULIC CONDUCTIVITY FIELD

No. of blocks: 64 × 64

$\sigma_{\ln(K)} = 4.00$ $\lambda/\Delta x = 2.0$ $\lambda/\Delta y = 2.0$

RASTER LEGEND (dim[K]=m/s)

+5.04E-14	+2.56E-09	+1.49E-08	+5.90E-08	+2.11E-07
+2.11E-07	+7.19E-07	+3.04E-06	+1.89E-05	+9.42E-02
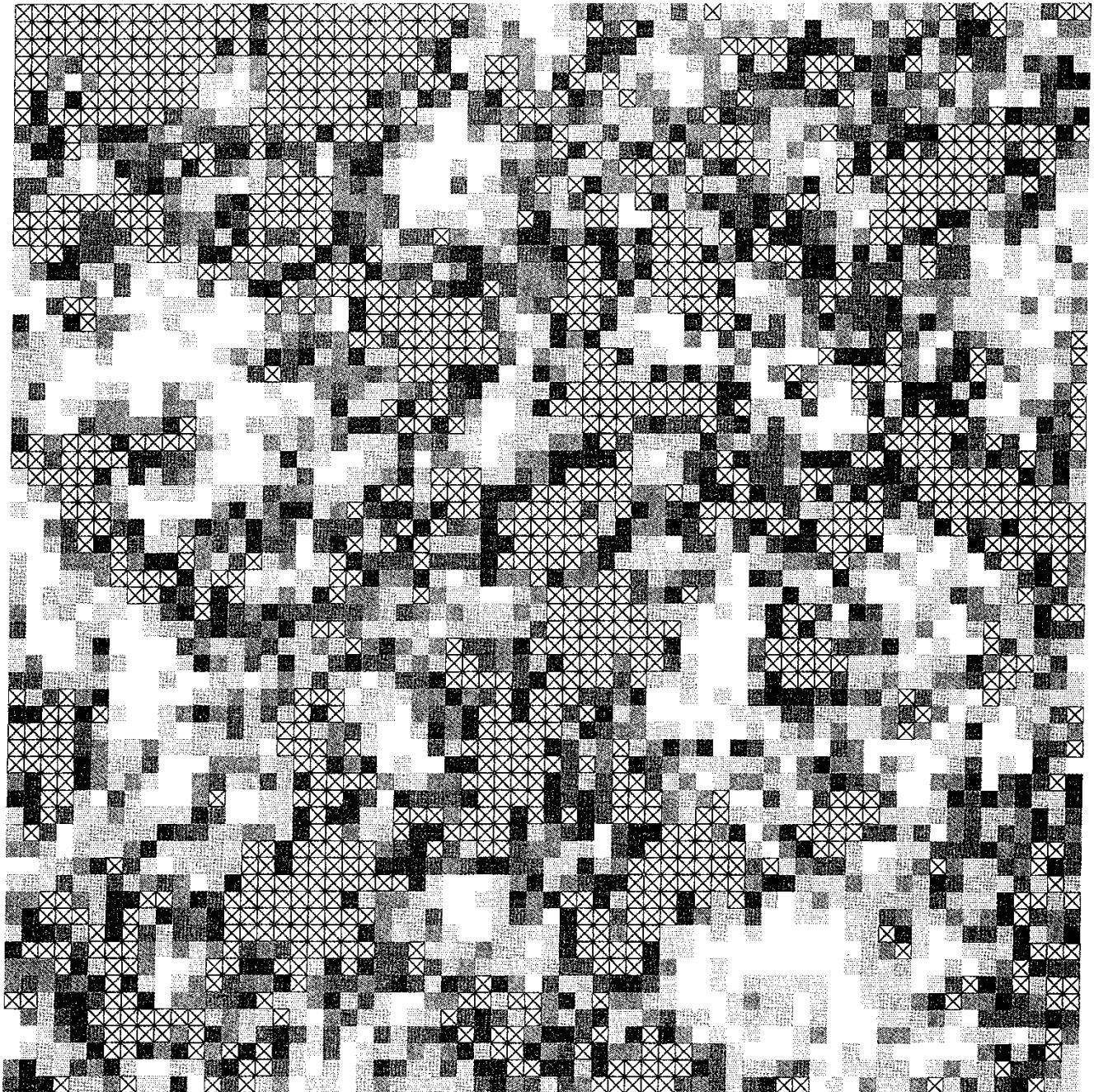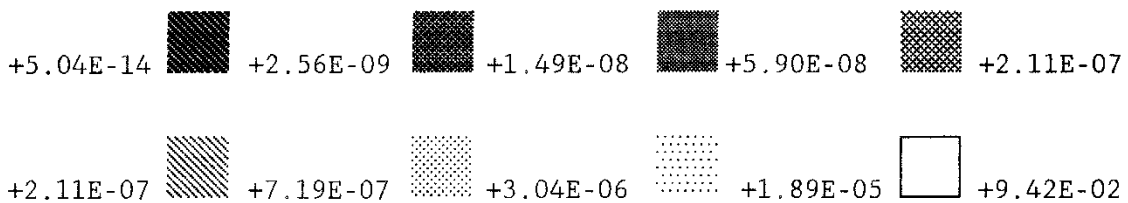
Fig. 123 Case 4-22 with +5.04E-14 ⊠ +1.49E-08 THRESHOLD a 25% conductivity threshold.
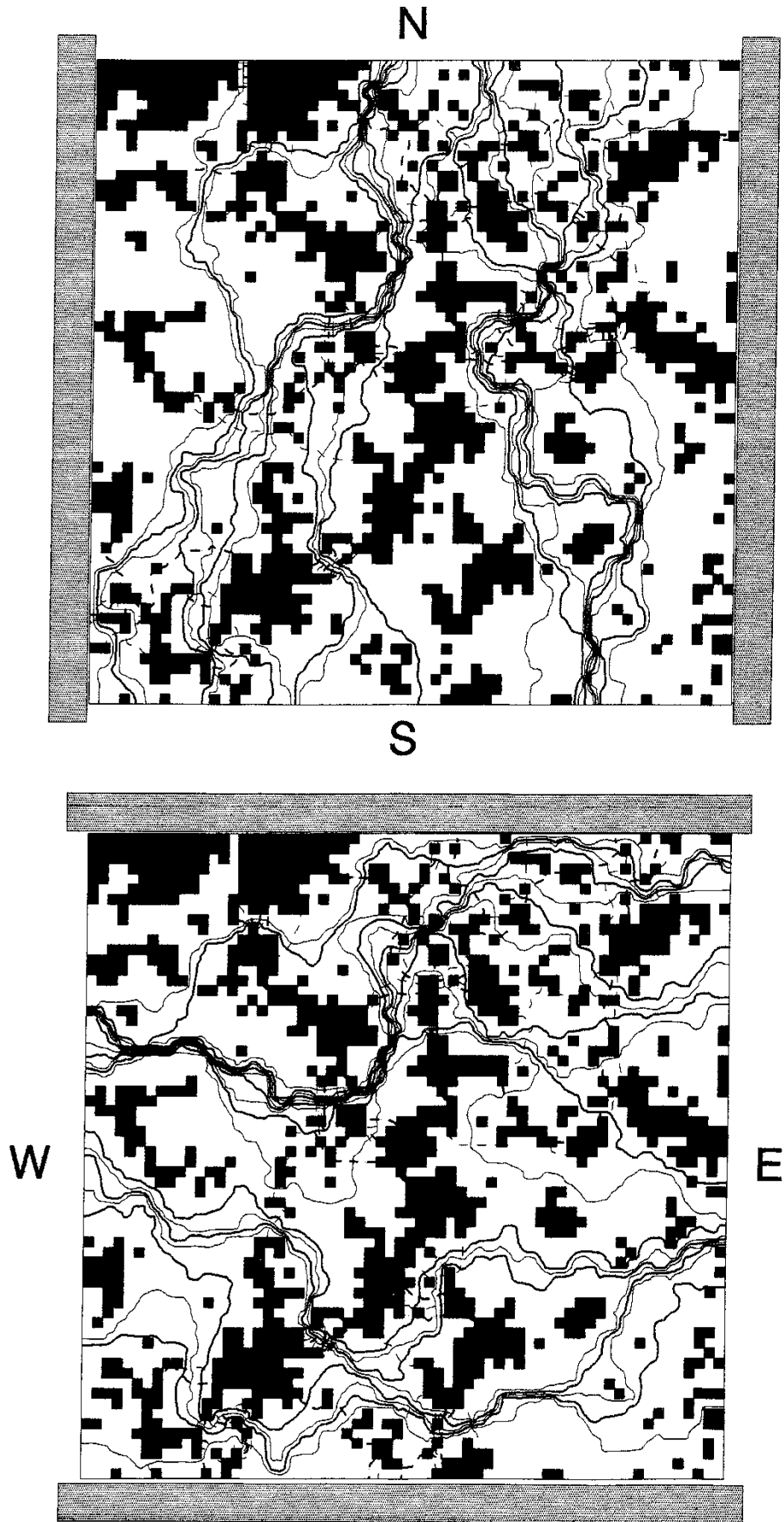
Fig. 124 Flow nets for a 25% conductivity threshold . N = (64 x 64) ,

$\lambda/\Delta x = \lambda/\Delta y = 2$ and $\sigma_{\ln(K)} = 4.00$. Piezometric head (dashed) and

stream function levels (solid) are in 5% increments between 0 and 1.

2-D HYDRAULIC CONDUCTIVITY FIELD

No. of blocks: 64 × 64

$\sigma_{\ln(K)}$ = 4.00 $\lambda/\Delta x$ = 0.0 $\lambda/\Delta y$ = 0.0

RASTER LEGEND (dim[K]=m/s)

+4.75E-14	+1.26E-09	+7.69E-09	+3.11E-08	+1.07E-07
+1.07E-07	+4.06E-07	+1.52E-06	+1.21E-05	+1.02E-01
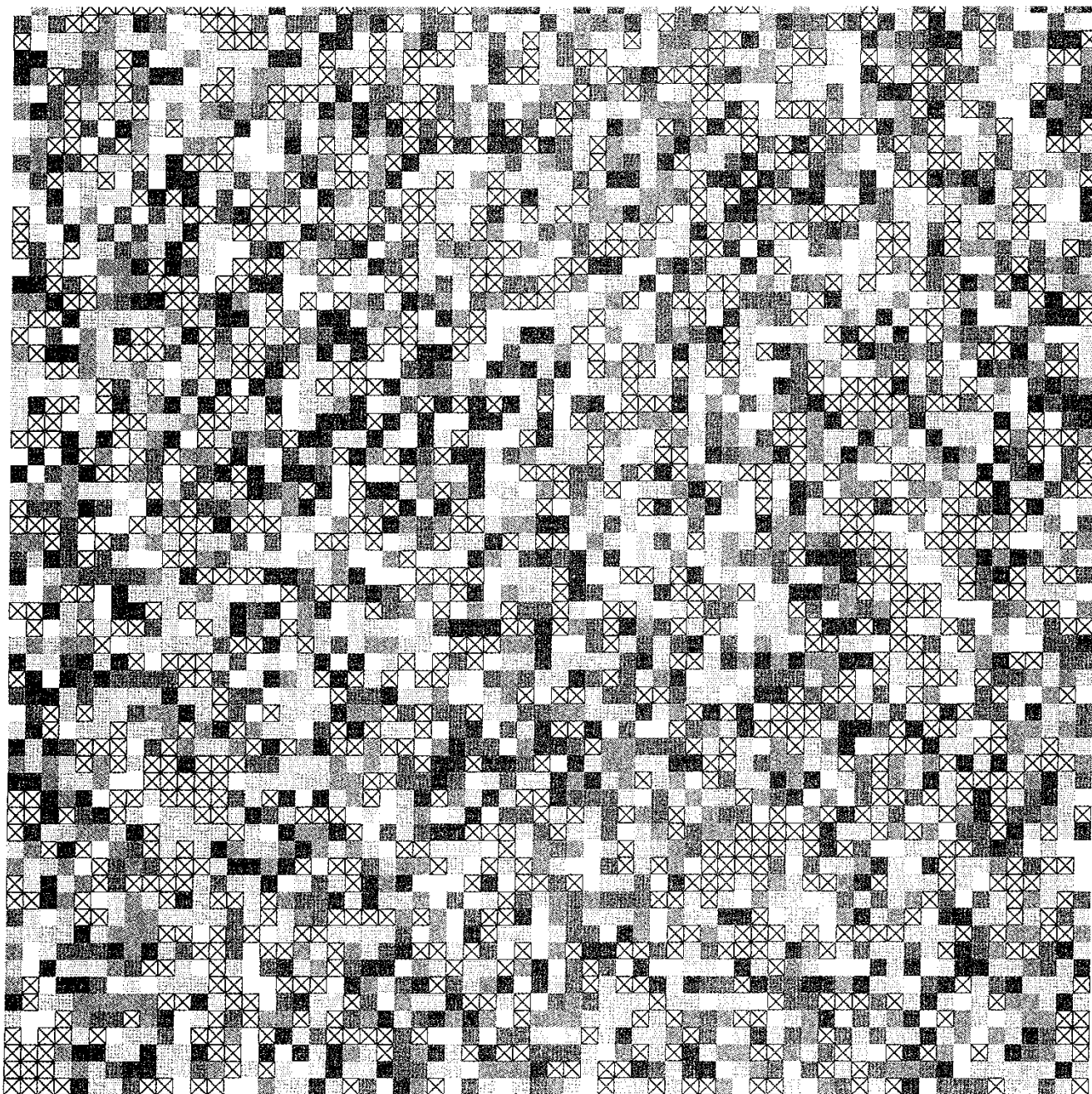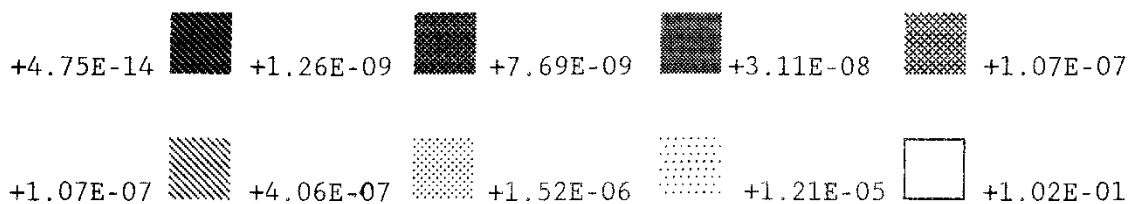
Fig. 125 Case 4-00 with +4.75E-14 ⊠ +7.69E-09 a 25% conductivity

THRESHOLD
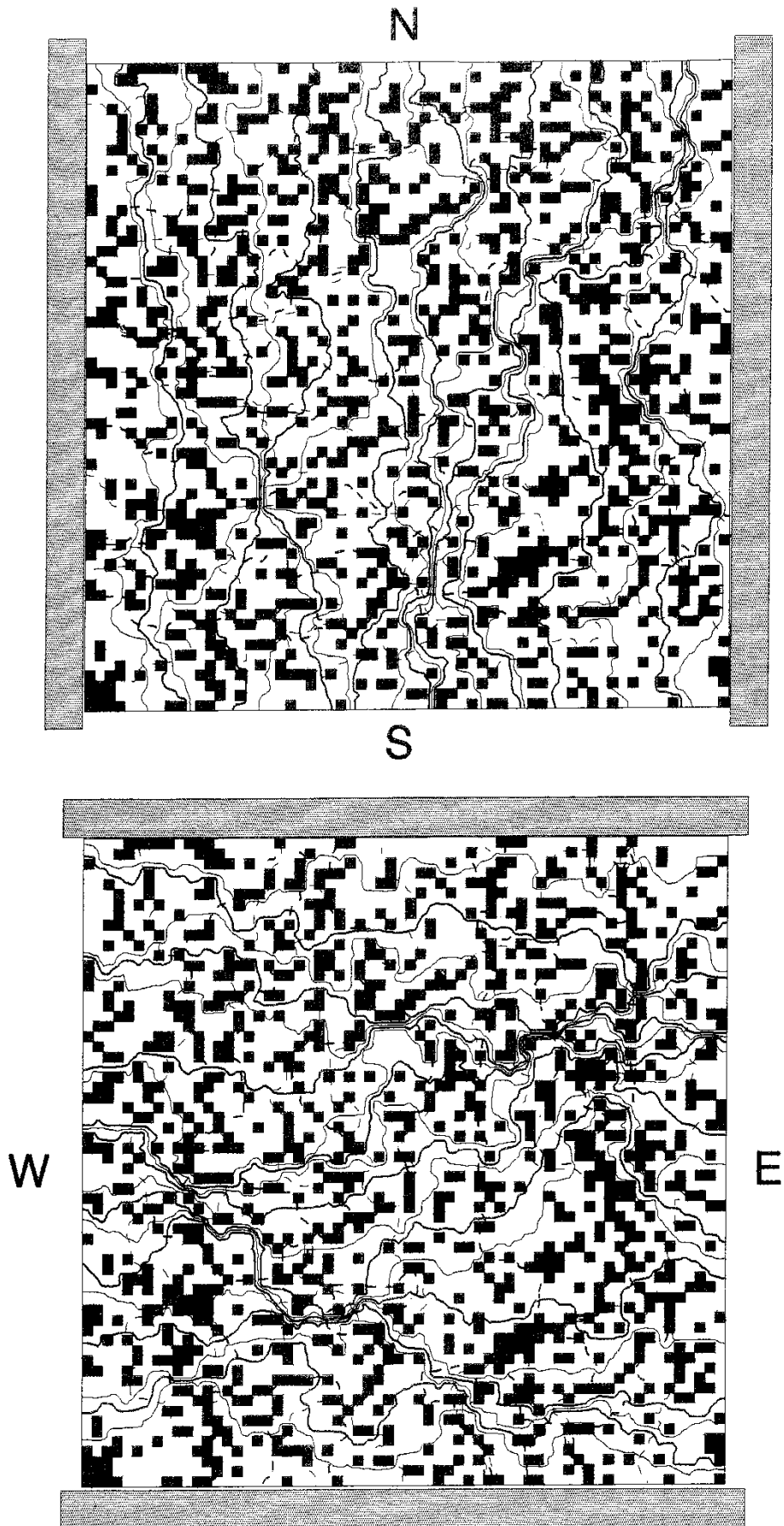
threshold .

Fig. 126 Flow nets for a 25% conductivity threshold . N = (64 x 64) ,

$\lambda/\Delta x = \lambda/\Delta y = 0$ and $\sigma_{\ln(K)} = 4.00$. Piezometric head (dashed) and

stream function levels (solid) are in 5% increments between 0 and 1.

2-D HYDRAULIC CONDUCTIVITY FIELD

No. of blocks: 64 × 64

$\sigma_{\ln(K)} = 4.00$ $\lambda/\Delta x = 4.0$ $\lambda/\Delta y = 4.0$

RASTER LEGEND (dim[K]=m/s)

+1.14E-12 ■ +5.26E-09 ■ +3.33E-08 ■ +1.31E-07 ■ +4.26E-07 ▦

+4.26E-07 ▨ +1.32E-06 +5.29E-06 +3.17E-05 +1.19E-01 □
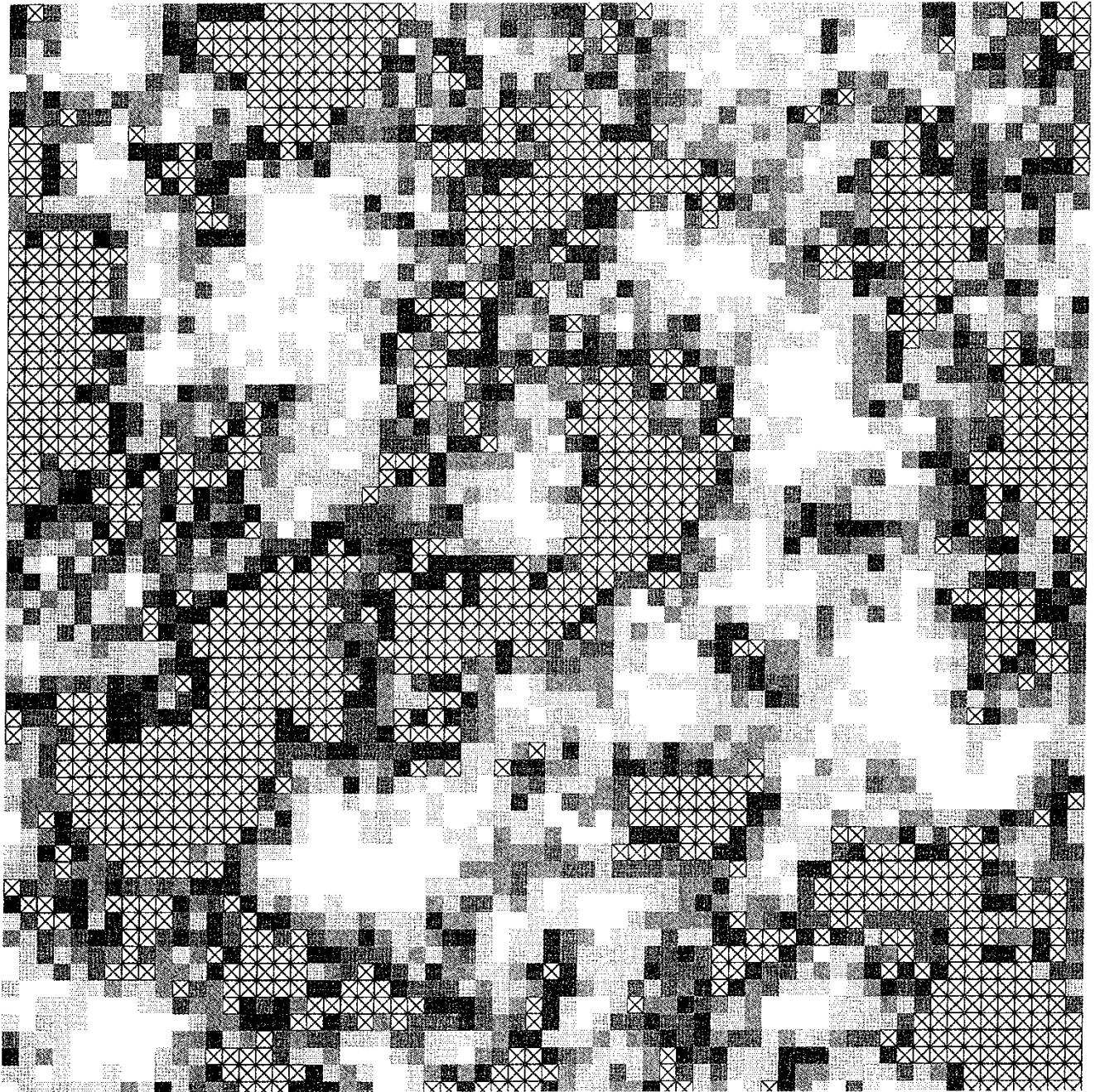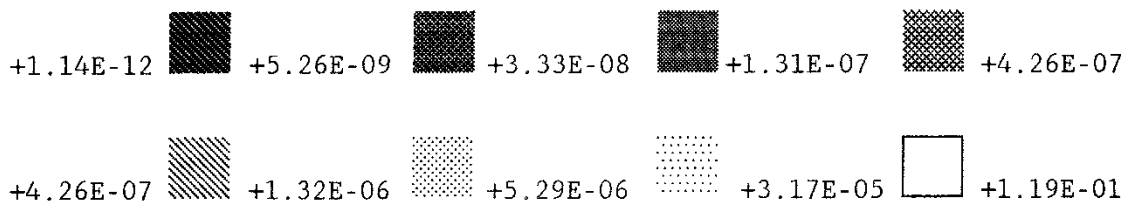
Fig. 127 Case 4-44 with   +1.14E-12 ⊠ +3.33E-08
THRESHOLD   a 25% conductivity threshold .
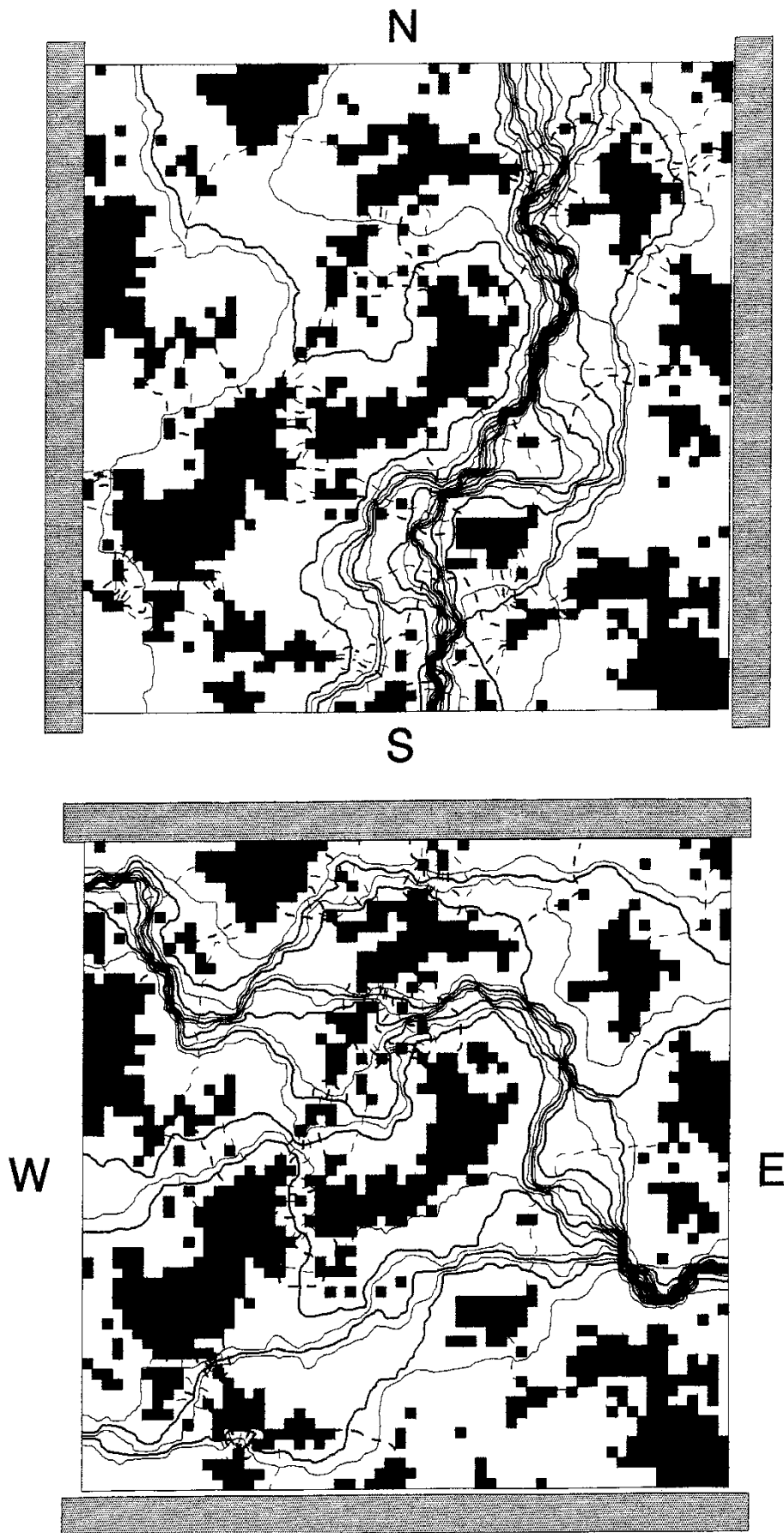
Fig. 128 Flow nets for a 25% conductivity threshold . N = (64 x 64) ,

$\lambda/\Delta x = \lambda/\Delta y = 4$ and $\sigma_{\ln(K)} = 4.00$. Piezometric head (dashed) and

stream function levels (solid) are in 5% increments between 0 and 1.
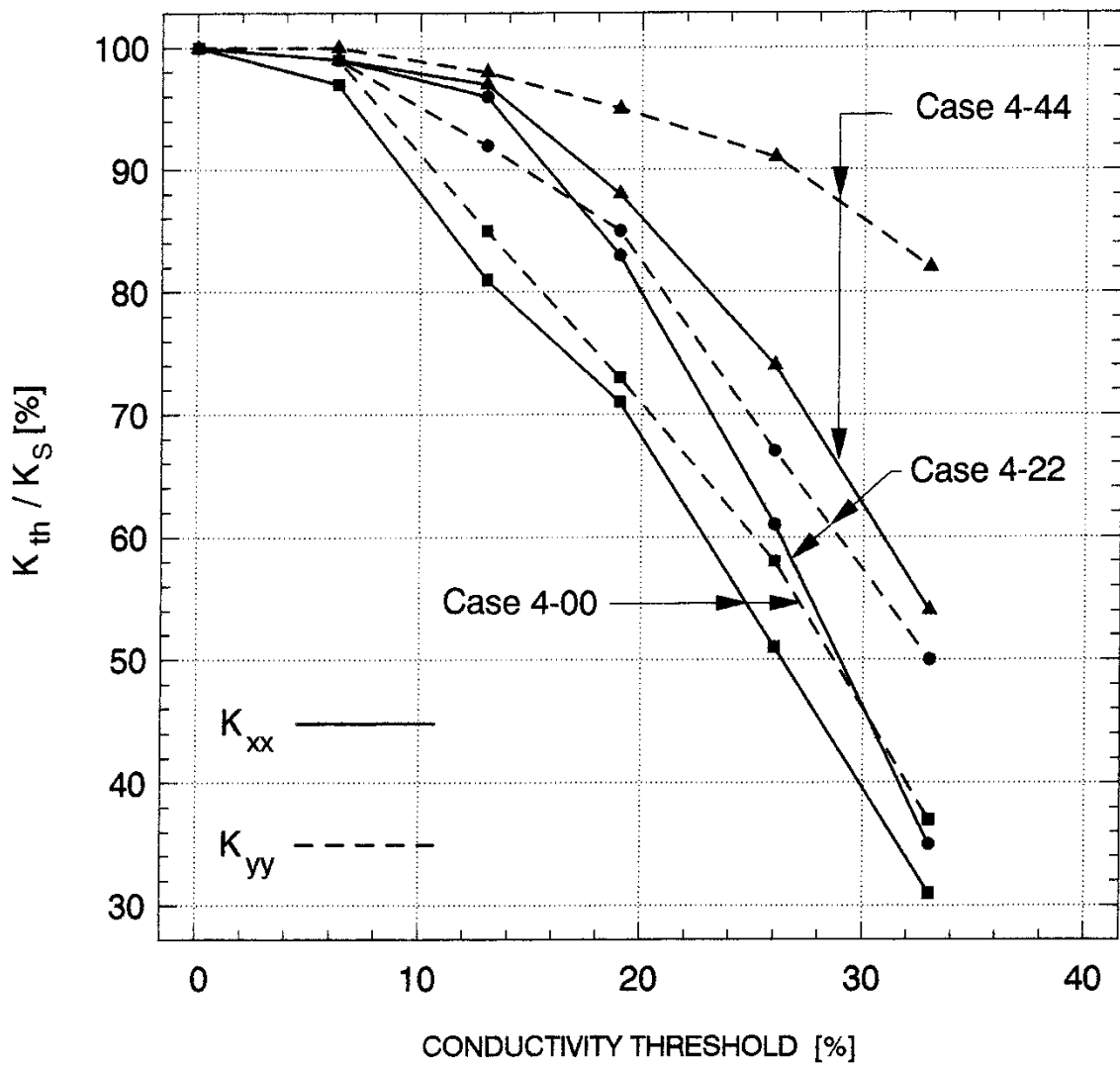
Fig. 129 Threshold conductivity ratio versus conductivity threshold for the studied cases .
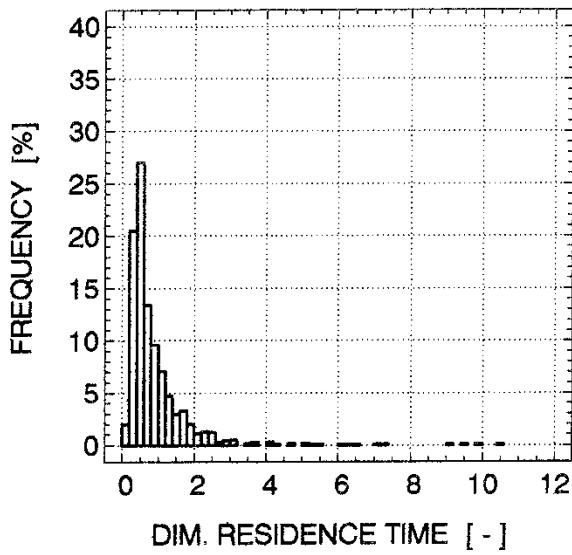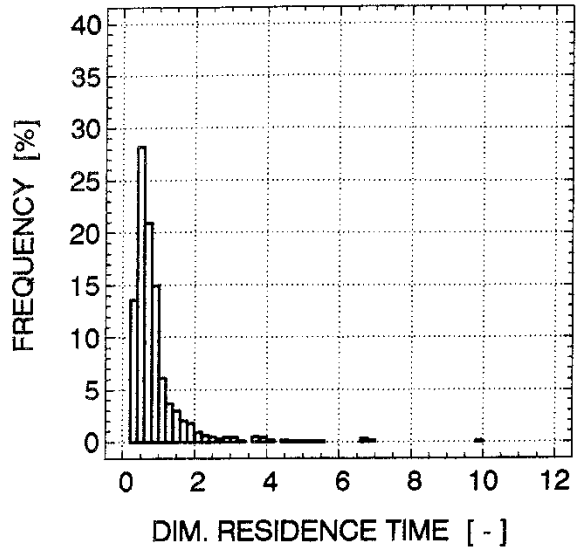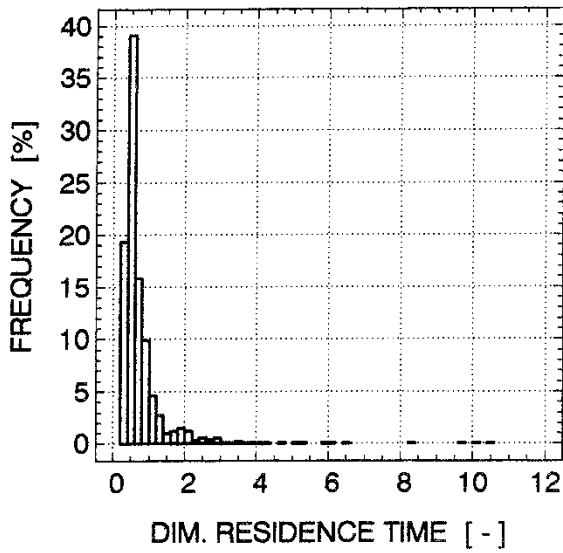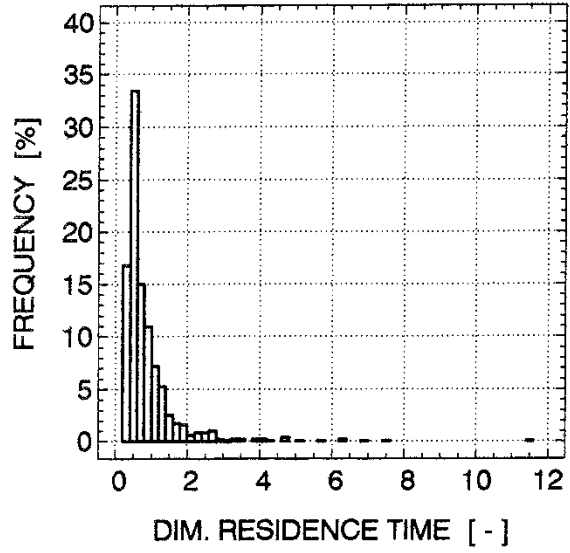
Fig. 130 Residence time histograms for continuous and discontinuous
conductivity fields .   Case 4-22 .
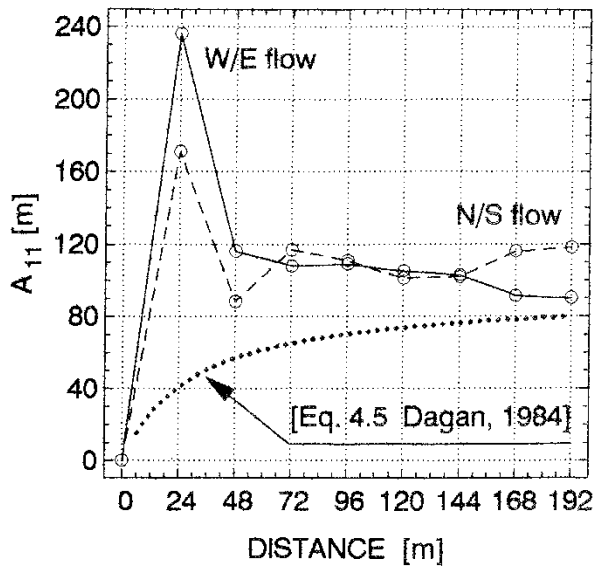
(a)
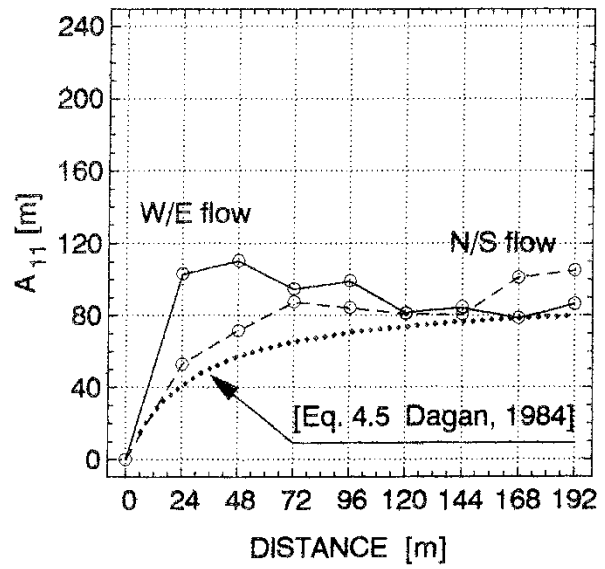
(b)

LONGITUDINAL DIRECTION

$\lambda/\Delta x = \lambda/\Delta y = 2$ and $\sigma_Y = 4.00$

(A_{11} is computed according to (42a))
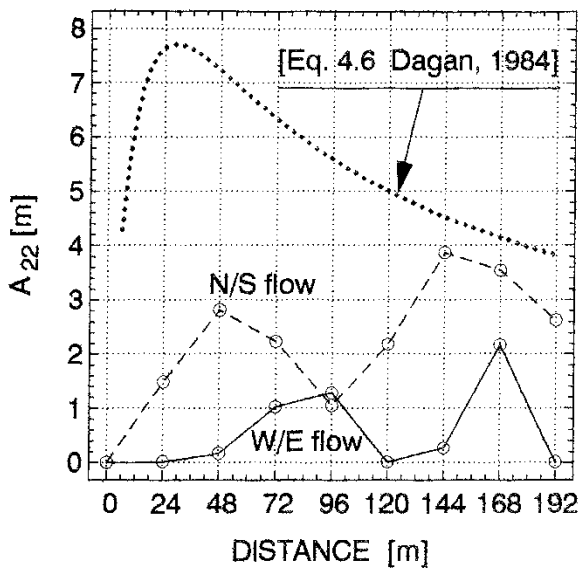
(c)
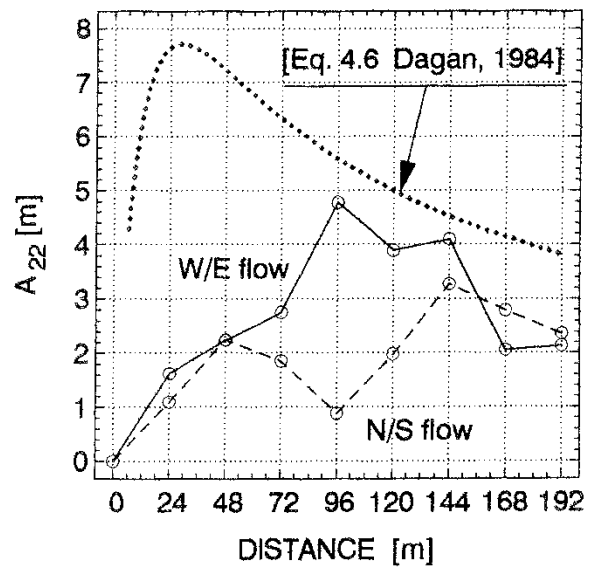
(d)

TRANSVERSE DIRECTION

$\lambda/\Delta x = \lambda/\Delta y = 2$ and $\sigma_Y = 4.00$

(A_{22} is computed according to (42b))

Fig. 131 Comparison of computed macrodispersivities for case 4-22 :

(a) (c)   with a 25% conductivity threshold,   (b) (d)   no threshold.

4 SUMMARY AND CONCLUSIONS

The upscaling of model parameters, i.e. scale-dependent parameters, is a key issue in many research fields concerned with parameter heterogeneity. The present study deals with groundwater flow and solute transport in fractured hard rock treated as a stochastic continuum on a 3m scale, i.e. the real world problem of *three-dimensional* flow and transport in a *fractured* hard rock is here simplified to a *two-dimensional* numerical flow model of a *continuum*.

4.1 General background

Geological properties vary naturally over space as a consequence of the complex processes through which the media evolve. Evidence that geological media are heterogeneous even within well defined geological units, is provided by laboratory analyses of soil and rock samples, lithological and geophysical logs of boreholes, well tests, surface geophysical surveys, and direct geological observations. This evidence is in clear contradiction to the classical approach of regarding all subsurface materials as continua in which material characteristics are represented by constant parameters. Substantial research activity is taking place not only to understand the effect of this heterogeneity on flow and transport in geological media but also to characterize media properties on scales appropriate to the development of subsurface flow and transport models. Much of the work reported in the literature depends on the development of models that statistically describe the spatial distribution of media properties and permit their numerical simulation. Therefore, research in physically based distributed modelling is becoming increasingly concerned with the incorporation of stochastic elements into such models, particularly dealing with spatial variability and sub-grid scale effects. Although a number of operational models have been

developed, fundamental difficulties still exist both on the conceptual level and in the numerical simulation. For instance, material properties represented by parameters cannot be regarded as representatives of the true material characteristics but only, at best, as some scale-dependent average quantities of the latter. The objectives of the present study can be summarized as follows:

Unconditional simulation of flow: The objective is to investigate the relationship between the statistical (spatial) geometric mean of local conductivities and the numerically computed equivalent block conductivity as a function of scale, i.e. block size. The underlying hypothesis is that present statistical upscaling techniques underestimate the conductivity of finite blocks, due to their inability to take the effects of hydraulic anisotropy into account.

Flow field analysis: The objectives are (*i*) to validate the implementation of the flow model and its capability to deal with high conductivity contrasts, and (*ii*) to improve the understanding of the parameters used to characterize random heterogeneity and the impact of these parameters on the flux.

Simulation of flow on different scales: The objectives are to investigate (*i*) the validity of applying the results obtained from the unconditional simulations, and (*ii*) the differences between two scales of support.

Simulation of solute transport: The objectives are to investigate the possibility (*i*) to reproduce numerically the analytical results obtained by first-order theory, and (*ii*) to extend the numerical simulations to deal with high conductivity contrasts.

A discontinuum model: The objective is to examine briefly the differences in flow and transport between continuous and discontinuous conductivity fields.

4.2 Unconditional simulation of block conductivity

Values of unconditional block conductivity are computed under the assumption of uniform average flow in a finite two-dimensional domain. The computations are made with a numerical flow model and the heterogeneities are generarted synthetically. Three kinds of heterogeneity is studied, namely $\lambda_Y/\Delta x = \lambda_Y/\Delta y = \{0, 2, 4\}$. The mean and standard deviation of the underlying, infinite log-conductivity field are set to $\mu_Y = -16$ and $\sigma_Y = 4$, respectively. The chosen parameter values are characteristic of the statistics of 3m packer tests down to depths of about 500m in Swedish fractured hard rock.

For each realization, both the spatial geometric mean of the local conductivity values and the conductivity in two orthogonal directions are computed.The computations are made for six different block sizes. Because all blocks are of finite dimensions, the term (equivalent) *block conductivity* is used. In the present study, the term *effective conductivity* represents the equivalent conductivity for uniform average flow in an unbounded (infinite) heterogeneous medium.

The results from the unconditional simulations can be summarized as follows:

1. The spatial geometric mean of the local conductivities within a block is a random variable, where the expected value is found to decrease with an increasing block size. The upper and lower limits correspond to the arithmetic and geometric means, respectively, of the underlying *PDF* of the local conductivities. A Monte Carlo experiment reveals that the *PDF* of the spatial geometric mean for a given block size is log-normal for small and moderate block sizes and approximately symmetric for very large block sizes. The infinite "block" has by definition no variance.

2. The expected value of the ratio between the block conductivity in either of the two orthogonal directions and the spatial geometric

mean is greater than or equal to unity. The maximum value is obtained for a block size equal to the scale of the heterogeneity, i.e. the range of the correlation.

This result suggests that the spatial geometric mean tends to underestimate the block conductivity of finite blocks. However, the study of flow through single blocks prohibits any inference about the effect of block interaction. Thus, it is not possible to extend the result to include the case of flow in an aggregate of blocks. This is discussed below.

3. The expected value of the ratio between the block conductivities in the two orthogonal directions is greater than or equal to unity. The ratio reaches its maximum value for a block size approximately equal to the scale of heterogeneity, i.e. the range of the correlation.

This result suggests that the block conductivity of a heterogeneous block of finite extent must be treated as an anisotropic entity. Hence, for small and moderate block sizes the block conductivity is a tensor quantity and not a scalar as usually assumed by statistical upscaling techniques. However, the present boundary conditions of the numerical experiments provide no information about the components of the full tensor in terms of rotation. Furthermore, the study of flow through single blocks prohibits any inference about the effect of block interaction. Thus, it is not possible to extend the result about anisotropy to include the case of flow in an aggregate of blocks. This is discussed below.

The question of anisotropy deserves more appraisal for the modelling of flow and transport in the far field. Current single-hole packer test procedures provide no information about the anisotropy. Given the statistics of 3m packer tests discussed

above, the two-dimensional numerical flow test experiments yield the result that the scale of maximum anisotropy is of the same order of magnitude as:

(i) *the most common single-hole packer test straddle interval used for study site investigations in Swedish fractured hard rock, i.e. 20-30m*

(ii) *the smallest block scales that are used for the modelling of groundwater flow and solute transport in the far field with continuum models within the Äspö Hard Rock Laboratory and the SKB-91 project, i.e. $(50m)^3$ and $(36m)^3$, respectively.*

It is suggested that the conventional interpretation techniques for single-hole double-packer tests should be reviewed and, if possible, updated. Recent developments concerning fractals and fractional dimensions may be of interest, for example. Furthermore, it is considered that it would be of great interest to develop a pumping test configuration that takes anisotropy into account. However, this may be a cumbersome avenue of progress. Meanwhile, it is suggested that both vertical and horizontal boreholes are used whenever possible in order to gain more experience about the directional dependence of the conductivity.

4. The expected value of the log-conductivity standard deviation is found to decrease with the block size in a manner that mimics the reported field findings concerning the relationship between packer tests on the 3m and 30m straddle interval scales.

This result suggests that extreme contrasts in spatial variability of the conductivity (like those observed by means of 3m packer tests in fractured hard rock) can be studied by numerical experiments.

The dual formulation for steady flow in two dimensions is used to compute flow patterns for a nine different cases of heterogeneity. Because the conductivity is a random function, the specific discharge is a random vector function. Therefore, each computed flow pattern is accompanied by a brief statistical analysis of the correlation structure of the flux field. These analyses are neither intended nor valid for any inference about the statistics of the ensemble.

One subset of the nine realizations differs in the correlation length, $\lambda_Y/\Delta x = \lambda_Y/\Delta y = \{0, 2, 4\}$, whereas a second subset differs in the standard deviation, $\sigma_Y = \{0.25, 1.00, 4.00\}$. The three values of σ_Y correspond to (*i*) an approximately homogeneous medium, (*ii*) the upper limit of first-order theory, and (*iii*) the observed spatial variability for 3m packer tests, respectively.

In addition to the common assumption of a homogeneous effective porosity n for the computation of the (transport) velocity, the case of a heterogeneous porosity is also studied, although under the limiting assumption of a positive linear correlation.

The following results are obtained in the qualitative analyses of the different flow patterns and the statistical analyses of the flux fields:

1. The representation of equidistant contour levels of the stream function is found to be superior for the visualization of the interaction between σ_Y and λ_Y and their impact on the spatial variability of the flux field, especially in conjunction with a raster graphics map of the percentiles of the flux.

2. Patches of low conductivity generally correspond to patches of no flow, whereas patches of high conductivity do not necessarily correspond to patches of high flow. Accordingly, the occurrence of preferential flow paths (channelling) appears to be related to

the correlation structure of the low conductivity patches. Furthermore, the number of channels and their relative strength, i.e. streamline density, differ clearly between uncorrelated and correlated conductivity fields. It is observed that an uncorrelated field contains several minor channels of weak intensity, whereas a correlated field contains one or a few major channels of great intensity depending on the correlation length. For instance, it is demonstrated in some of the studied correlated realizations that about 50% of the flux flows through less than 2% of the total width of the available flow domain. An interesting effect is the back flow phenomenon, i.e. streamlines such that the local flow is oppositely directed to the mean flow. A pronounced back flow behaviour is believed to be an artifact of the two-dimensional flow domain.

The drastic differences in the channelling between uncorrelated and correlated conductivity fields, as inferred from the numerical experiments, are considered to be of importance for the far field modelling of groundwater flow and solute transport in fractured hard rock by means of continuum approximations. It is suggested that the current field procedures for packer tests should be improved in order to make full use of a geostatistical analysis so that the correlation, if it exists, can be inferred.

3. For $\sigma_Y^2 = 16$, it is observed that the probability density function (*PDF*) of the transverse component of the flux is normal, whereas the *PDF* of the longitudinal distribution is approximately log-normal provided that the back flow is discarded. The variograms of the transverse component reveal that this component is poorly auto-correlated. The correlation is, however, somewhat better perpendicular to the mean direction of flow. The variograms of the longitudinal component show the opposite situation. This component is considerably well correlated, especially parallel to the mean direction of flow. Accordingly, the *PDF* and the

variograms of the resultant flux vector are dominated by the statistics of the longitudinal component of the flux. It is found, however, that the sills of the variograms of the resultant flux vector equal the sums of the corresponding sills of the variograms of its longitudinal and transverse components. This additive variance relationship suggests a poor cross correlation between the two orthogonal components of the flux. The observation is confirmed by examining their cross variogram. The absence of correlation shows up as pure nugget effect, i.e. a constant-valued variogram at all lags (separation distances).

The fact that the two orthogonal components of the flux vector are uncorrelated does not necessarily mean that they are independent. However, the observations that (*i*) the variances of the orthogonal components of the flux are additive, and (*ii*) the probability density functions are different in nature, suggest that the resultant flux field can be obtained as the sum of two independent realizations. From an experimental point of view this observation might be of interest. For instance, it suggests an approach to generate a large number of realizations of the flux field for numerical transport experiments as an alternative to going through an often tedious stage of solving the flow equations. This approach, of course, is not validated by the observations in this study, because we rely upon too few realizations. It is definitely not valid in cases where the flux may be non-stationary. Therefore, it is suggested that more experiments should be made to investigate the statistical and hydraulic nature of the flux field under a variety of circumstances. It is important to bear in mind that the results obtained are also subjected to a number of physical simplifications. For example, the flow and transport equations are assumed to be uncoupled, which implies a constant water density.

4. The close relationship between $K(\mathbf{x})$ and $\mathbf{q}(\mathbf{x})$, as suggested by Darcy's law, is clarified by an analysis in the log-space. With respect to the observed differences in the shape of the *PDF*'s and the variograms, it is concluded that the statistics of the flux field are highly influenced by the correlation of the random heterogeneity of the conductivity field.

5. A positive linear correlation between the porosity and the conductivity in the log-space is observed to counteract the effects discussed above of a spatial varying conductivity field. That is to say, the *PDF* of the log-velocity is more symmetric and of less variance, and the variograms are more statistically isotropic than the corresponding statistics of the log-flux.

This result suggests that advective travel times will show less variance in the case of a positive linear correlation between the porosity and the conductivity in the log-space.

4.4 Simulation of flow on different scales

In the experimental study concerning simulation of flow on different scales, two main cases are studied: (*i*) the conductivity field is totally determined (deterministic case), and (*ii*) the conductivity field is only sparsely determined (stochastic case). In the latter case the remaining (unknown) values are estimated. There are several methods in common practice. The ones compared here are the inverse distance method and ordinary kriging. The latter takes the correlation into account, whereas the former does not.

The differences in the hydraulic behaviour between the deterministic and the stochastic simulations are studied with respect to the hydraulic behaviour of an a priori case representing an assumed known realization of the flow domain. The hydraulic behaviour of the a priori case is of course completely known. The interest here is

- 211 -

focused on investigating the relevance of simulating the a priori behaviour on a different scale, or even on the same scale as the a priori case but with less conditional data.

The two scales chosen here are the "24m scale" and the "3m scale". On the 24m scale, the a priori case is substituted by 64 $(24m)^2$ blocks, whereas on the 3m scale it is "substituted" by 4,096 $(3m)^2$ blocks. The degree of disagreement between the simulation experiments (being deterministic or stochastic; on the 3m scale or on the 24m scale) and the a priori case is studied. The hydraulic behaviour is studied in two orthogonal directions, which provides an opportunity to estimate the role of anisotropy. The objectives of the simulations are to investigate (*i*) the validity of applying the results obtained from the unconditional simulations of flow in single blocks to flow in an aggregate of blocks, and (*ii*) the differences between the two scales of support. The hypothesis is that anisotropy is important for the upscaling process.

Three cases of conditioning and interpolation are studied on the 3m scale: (*i*) the inverse distance method with a search radius of $r = 2 \lambda_Y$, (*ii*) ordinary kriging with $r = 2 \lambda_Y$, and (*iii*) ordinary kriging with $r = 4 \lambda_Y$. On the larger block scale, i.e. the 24m scale, the block conductivities are obtained in two different ways, one deterministic and one stochastic. In the deterministic case, the block conductivities are represented by 24m packer tests using the eight boreholes mentioned previously. In the stochastic case, the block conductivities are estimated by means of ordinary kriging. Two search radii are used in the stochastic case $r = \{2 \lambda_Y, 4 \lambda_Y\}$. In all, nine different experiments are studied, three on the 3m scale and six on the 24m scale.

The present study is dependent on two assumptions, namely that (*i*) the conductivity tensor on the 24m scale is in a diagonal form, and (*ii*) the principal components of this tensor are equal to the conductivities in two fixed orthogonal directions. Strictly speaking, both these assumptions are physically incorrect, at least for small

and moderate block sizes. On the other hand, it is demonstrated in the present study that these assumptions are more appropriate than the statistical assumptions generally discussed in the literature. Hence, in spite of the tremendous progress in subsurface hydrology owing to the developments in stochastic continuum theory, it must not be forgotten that physics is an experimental science. In other words, anisotropy deserves much more attention in the upscaling process. Consequently, there is a need for a pumping test configuration that takes anisotropy into account.

4.5 Simulation of solute transport

In recent years, the stochastic continuum theory has been increasingly used to study the scale dependence of advection-dispersion phenomena, and different approaches are reported in the literature. The developments used here are limited to deal with uniform average flow in two dimensions under a rather moderate heterogeneity of the log-conductivity field, i.e. $\sigma_Y^2 \leq 1$. This limitation stems from a use of "first-order theory", i.e. a first-order approximation of a small perturbation of the log-conductivity field. The non-linear effects that arise when $\sigma_Y^2 > 1$ are considered to be important although few results have been reported so far.

The objectives in this study are to investigate the possibility (*i*) to reproduce numerically the analytical results obtained by first-order theory, and (*ii*) to extend the numerical simulations to allow for high conductivity contrasts. Only single realizations of three different cases of heterogeneity are studied. Thus, the simulations undertaken do not treat questions concerning the ensemble statistics. However, the studied realizations are relatively large with respect to the correlation lengths used, i.e. $L/\lambda_Y = \{16, 32, 64\}$. Because the injected solute, which in this study is represented by particles, is released over the entire upstream boundary, it is assumed that the spatial variability is adequately accounted for in

order to justify an analysis of the scale dependence of the macro-dispersivities in each realization.

The obtained results from the experiments may be summarized as follows:

1. The numerical algorithms used for the particle tracking, i.e. the dual formulation of flow and the isoparametric interpolation, are found to be well suited for studying advective transport in a heterogeneous conductivity field.

2. The suggested technique of mine, the equidistant contour level positions of the stream function solution on the upstream boundary, to establish a consistent flux-weighted injection mode is proved to be appropriate. Its validity is verified in the study by the principle of reciprocity.

3. The analytical results derived by the position analysis under first-order theory are here numerically reproduced for $\lambda_Y/\Delta x = \lambda_Y/\Delta y = 2$, $\sigma_Y^2 = 1$, and $N = 64{\times}64$. The longitudinal dispersivities computed by means of the Fickian arrival time analysis reach the asymptotic values predicted by first-order theory, at a rate that is surprisingly concordant with the non-Fickian position analysis.

A general observation in the numerical simulations is that it is not possible to apply the non-Fickan position analysis over the total range of heterogeneity. This limitation is caused by the channelling phenomenon, which leads to a loss of particles before the position analysis is satisfactory completed. Analytical solutions are presently limited to $\sigma_Y^2 \leq 1$, whereas the Fickian arrival time analysis, which assumes a diffusion process, is devoid of any notion of uncertainty in $ln(K)$.

4. For $\sigma_Y^2 \leq 4$, it is found that a Fickian arrival time analysis deviates moderately from what is predicted by the equations of the position analysis. For $\sigma_Y^2 > 4$, a Fickian arrival time analysis yields the result that (*i*) the transverse dispersivity increases linearly in proportion to σ_Y and (*ii*) the longitudinal dispersivity approaches the asymptotic value at a faster rate than is predicted by the position analysis. For $\sigma_Y^2 = 16$, numerical difficulties are observed. However, the dispersivities in two opposite directions, as computed with the Fickian arrival time analysis, show a remarkable reciprocity considering the immense conductivity contrasts, which comprise about 12 $\log_{10}$ cycles in K.

Non-Fickian behaviour of transport for short travel times is well documented in the literature. In spite of this fact, a diffusion process from the onset of a solute injection is often assumed in practical applications dealing with, for example, groundwater pollution. Although more research is required in order to determine the limitations of using the advection-dispersion equation, the results obtained here are important and are therefore worth a few comments. It should be noted that even though the dispersivities computed by the Fickian arrival-time analysis are surprisingly concordant with the predictions of the non-Fickian position analysis, there is a severe objection to using either constant-valued or scale-dependent dispersivities in numerical models to simulate far field solute transport in fractured hard rock. In other words, contrasts in the conductivity field constrict the flow into preferential flow paths. For $\lambda_Y/\Delta x = \lambda_Y/\Delta y = \{2, 4\}$ and $\sigma_Y^2 = 16$, a persistent channelling is observed throughout the studied flow domains $((192m)^2)$. The conclusion reached here is that the coefficients in the classical advection-dispersion equation can never reproduce such a channelling within a large model block. In other words, the choice of support scale for the conductivity field is crucial for the modelling of solute transport.

4.6 A discontinuum model

The channelling observed in the experiments for $\sigma_Y^2 = 16$ is significant in many ways. It is an interesting observation that large portions of the generated flow domain do not contribute to the flow. It is of great interest to find a physical criterion that makes it possible to discard the no-flow portions, because (*i*) the computational constraints will be relaxed, meaning fewer numerical problems and more computer memory at hand, and (*ii*) one will have an opportunity to study the link between continuum models and the more recent discrete fracture network models.

For 3m packer tests, the measurement threshold is approximately 10^{-11} m/s. For a typical borehole of 500-600m depth in fractured hard rock, about 20-50% of the measurements are below or at the measurement threshold, which is a significant loss of information. The objective here is to examine briefly the differences in flow and transport between continuous and discontinuous conductivity fields. The continuous case solutions are here compared to the solutions corresponding to a conductivity threshold of 25%. A conductivity threshold causes impermeable boundaries in the interior of the flow domain. The numerical solution of the problem presented here constitutes a powerful extension of the dual formulation of flow.

1. The suggested extension of the dual formulation of flow, comprising discontinuous conductivity fields, relaxes the numerical constraints associated with high conductivity contrasts.

2. The solutions of the three discontinuous realizations reveal that the flow patterns of the corresponding continuous realizations are essentially preserved in spite of an imposed conductivity threshold of 25%.

This is an interesting result, because it supports the working hypothesis that flow in a continuous medium, which is subjected

to high contrasts in conductivity, can be replaced by a model of a discontinuous medium. Although the real world complex problem is not investigated here, it is argued that fractured hard rock can be regarded as a heterogeneous discontinuum. By way of conclusion, the modelling of flow in fractured hard rock by means of porous media models based on dis-/continuum approximations remains of interest.

3. The experiments undertaken here reveal that the main effect of a conductivity threshold is an increasing anisotropy. There is a clear difference in the anisotropy between the three realizations considered here; the uncorrelated case is observed to be the least sensitive to a conductivity threshold. Moreover, it is observed that for a discontinuous conductivity field, the relation between the statistical (spatial) geometric mean and the corresponding block conductivity deviates from the analytical relation valid for a continuous conductivity field in two dimensions. The differences increase drastically as the conductivity threshold increases.

This result suggests that the asymptotic block conductivity of a discontinuous conductivity field, if it exists, is a different physical entity from the effective conductivity of an infinite continuous conductivity field. However, a large number of experiments are required in order to investigate whether the conductivity for a given threshold value approaches an asymptotic value at any order of scale.

4. For a conductivity threshold of 25%, the differences in the residence time histograms between the continuous and discontinuous cases are moderate.

5. For a conductivity threshold of 25%, the "asymptotic values" of the longitudinal dispersivities in two orthogonal directions are

somewhat almost the same as those of the longitudinal dispersivities of the corresponding continuous case. The behaviour of the transverse dispersivities is more complex. In one direction, the transverse dispersivity is somewhat larger, whereas in the other direction, it is much smaller. In both directions, however, they seem to obey the decreasing trend of the corresponding continuous case.

Of course. it is not possible to make final conclusions on the basis of the brief experiments discussed above. The purpose here is to investigate whether there are any *significant* differences between a discontinuous case in relation to a continuous case. It is interesting to note that the observed differences are quite moderate in spite of a conductivity threshold of 25%. However, based on the different flow and transport experiments undertaken throughout the present study, the general conclusion is that macroscopic (asymptotic) properties in fractured hard rock, if they exist, require such large averaging volumes that the relation to the real world problem is lost.

4.7 Concluding remarks

A number of important assumptions are made throughout the study. The assumptions are generally working hypotheses and it is important to keep them in mind, because they affect the validity of the results and the conclusions. In the following, some of the assumptions concerning the local conductivity fields are discussed.

1. The local conductivity field is a random scalar function.

This assumption is indeed a working hypothesis. There are good reasons to accept it from a theoretical point of view, whereas there are few, if any, reasons to accept it from a physical point

of view. In the study, the assumption is motivated by two facts: (i) there is no information about the anisotropy on the 3m scale, and (ii) the stochastic continuum theory, which is used here to verify the numerical experiments, assumes a random scalar function in the local scale. It is important to note, however, that the dual formulation of flow is not limited to a scalar conductivity field. On the contrary, the dual formulation of flow readily comprises anisotropy in the local scale. One way to investigate the assumption of isotropy in the field is to use cross-hole tests over short distances.

2. The local conductivity field has a point-consistent scale of support.

This assumption is also a working hypothesis. It implies that the volume associated with the determination of the conductivity in the field is neither a function of the conductivity value as such nor any other variable of interest, e.g. position. Thus, all measurements on a given scale are assumed to be of constant volume. This assumption is physically unreal, because the radius of influence in a well test is a function of the hydraulic properties. For instance, if all parameters are constant except the conductivity, the radius of influence is greater for a high conductivity value than for a low conductivity value. In the study, the assumption is motivated by the facts that (i) 3m packer tests are devoid of any notion about volume, and (ii) the use of ordinary kriging assumes a point-consistent scale of support. One possible solution to the case of varying volumes is to use co-kriging in the conditional simulations.

3. The realizations are statistically stationary and isotropic.

In general, it is observed that the conductivity of fractured hard rock is a function of depth, at least down to a depth of

about 500m, although there are also many examples of observations without depth dependence. Accordingly, statistical stationarity is an open question. Statistical stationarity is one of the pre-requisites of the results derived by stochastic continuum theory that are used here for verification. Concerning statistical iso-tropy, there are no reasons to expect that the conductivity field of fractured hard rock is statistically isotropic. In this study, the reasons for assuming statistical isotropy are (*i*) there is no information about statistical anisotropy on the 3m scale, and (*ii*) it is one of the prerequisites of the results derived by stochastic continuum theory that are used here for verification. One way to investigate the assumption of statistical isotropy in the field is to use both vertical and horizontal boreholes in a given rock block.

4. The local conductivity values are synthetically generated.

All data that are used in the computations are synthetically generated, which means that no data used here are measured in situ. The study is of generic interest. Hence, conceptual ques-tions are addressed and the use of site-specific data would therefore counteract this objective. Furthermore, the studied cases of spatial variability, as expressed by the standard deviation and the correlation length of the log-conductivity, are consistent with the field observations at the Swedish study sites. This condition is considered to be more important for the main objectives of the study than the use of site-specific data.

5. All experiments are in two dimensions.

There are computational reasons for the use of two-dimensional models, whereas there are few, if any, physical reasons for two-dimensional flow. For instance, the back flow phenomenon is expected to be attenuated and replaced by a "side flow" effect in

three-dimensional flow. Hence, the probability of an early arrival of dissolved constituents is perhaps underestimated in a two-dimensional model. It is an open question to what extent a two-dimensional analysis is valid. Nevertheless, it is argued that the scope of the study is unaffected. The main reasons for the choice of two-dimensional flow are as follows:

a. The theoretical derivation of the effective conductivity in
two dimensions is not limited to small values of σ_Y, whereas the theoretical derivation of the effective conductivity in three dimensions is at present limited to $\sigma_Y^2 \leq 1$.

b. Theoretical results for solute transport, which are based on
the first-order approximation of a small perturbation of the log-conductivity, suggest that the longitudinal dispersivities in two and three dimensions are not too different.

c. The classical continuum approximations that are commonly used
to interpret double-packer tests are often based on the assumption of a predominantly radial flow regime, i.e. a horizontal and axi-symmetric flow.

d. The dual formulation of flow adopted is more readily applied
to flow in two dimensions than in three dimensions, the computational constraints are relaxed, and the impact of the parameters used to characterize random heterogeneity, namely σ_Y and λ_Y, is more easily visualized.

REFERENCES

Ababou, R. & E.F.Wood [1990] Comment on "Effective groundwater
model parameter values: Influence of spatial variability of
hydraulic conductivity, leakance, and recharge" by J.J.Gómez-
Hernández and S.M.Gorelick, *Water Resour. Res.*, 26(8), 1843-
1846.

Abelin, H. [1986] Migration in a single fracture. An in situ
experiment in a natural fracture, *Dept. of Chemical
Engineering, Royal Inst. of Technology*, Stockholm.

Almén, K.E., J.E.Andersson, L.Carlsson, K.Hansson & N.Å.Larsson
[1986] Hydraulic testing in crystalline rock. A comparative
study of single hole test methods, *SKB Technical Report 86-27*,
Stockholm.

Andersson, J., C.Braester, A.Shapiro & R.Thunvik [1983] Transport
Phenomena in Fractured Rock, *Dept. of Land Improvement and
Drainage, Trita-Kut 1031, Royal Inst. of Technology*, Stockholm.

Andersson, J.E., L.Ekman & A.Winberg [1988] Detailed hydraulic
characterization of a fracture zone in the Brändan area,
Finnsjön, Sweden, In: Hitchon, B. *et al.* (eds.) *Proc. 4th
Canadian/American Conf. on Hydrogeology, Alberta*, 32-39,
National Water Well Association, Dublin, Ohio.

Andersson, J.E., L.Ekman, R.Nordqvist & A.Winberg [1991] Hydraulic
testing and modelling of a low-angle fracture zone at Finnsjön,
Sweden, *J. Hydrol.*, 126, 45-77.

Barenblatt, G.E., I.P.Zheltov & I.N.Kochina [1960] Basic concepts in
the theory of seepage of homogeneous liquids in fissured rocks,
J. Appl. Math. Mech., 24(5) 1286-1303. (English translation.)

Barker, J.A. [1988] A generalized radial flow model for hydraulic
tests in fractured rock, *Water Resour. Res.*, 24(10), 1796-1804.

Bear, J. [1972] *Dynamics of fluids in porous media*, American
Elsevier, New York.

Bear, J. [1979] *Hydraulics of Groundwater*, McGraw-Hill, New York.

Bear, J. & A.Verruijt [1987] *Modeling Groundwater Flow and
Pollution*, D. Reidel, Dordrecht.

Beims, U. [1983] Planung, Durchfürung und Auswertung von
Gütepumpversuchen, *Zeitschrift für angewandte Geologie*, 29(10),
482-490.

Beran, M.J. [1968] *Statistical Continuum Theories*, Interscience, New York.

Boulton, N.S. & T.D.Streltsova [1977] Unsteady flow to a pump well in a fissured water-bearing formation, *J. Hydrol.*, 35, 257-269.

Braester, C. & R.Thunvik [1982] Numerical simulation of double-packer tests. Calculations of rock permeability, *SKBF/KBS Teknisk Rapport 82-06*, Stockholm.

Braester, C. & R.Thunvik [1984] Determination of formation permeability by double-packer tests, *J. Hydrol.*, 72, 375-389.

Cacas, M.C., E.Ledoux, G.de Marsily, B.Tillie, A.Barbreau, E.Durand, B.Fuega & P.Peaudecerf [1990] Modelling fracture flow with a discrete fracture network: Calibration and validation, 1. The flow model, *Water Resour. Res.*, 26(3), 479-489.

Cacas, M.C., P.Lachassagne, E.Ledoux & G.de Marsily [1991] Stochastic description of heterogeneities of permeability within groundwater flow models, In: *Proc. OECD/NEA Workshop on Heterogeneity of Groundwater Flow and Site Evaluation*, 36-46, Paris.

Carlsson, A. & T.Olsson [1981] Hydraulic properties of a fractured granitic rock mass at Forsmark, Sweden, *Swedish Geological Survey, Series C783*, Uppsala.

Carlsson, L., B.Gentzschein, G.Gidlund, K.Hansson, T.Svenson & U.Thoregren [1980] Kompletterande permeabilitetsmätningar i finnsjöområdet, *SKBF/KBS Teknisk Rapport 80-10*, Stockholm. (In Swedish.)

Clark, I. [1979] *Practical geostatistics*, Elsevier, London.

Cushman, J.H. [1983] Volume averaging, probabilistic averaging, and ergodicity, *Adv. Water Resour.*, 6(3), 182-184.

Cushman, J.H. [1986] On measurement scale and scaling, *Water Resour. Res.*, 22(2), 129-134.

Cvetkovic, V. & C.S.Kung [1989] Variogram analysis of single-hole packer test data from the Finnsjön site, *SKB AR 89-17*, Stockholm.

Cvetkovic, V. & A.Shapiro [1989] Solute advection in stratified formations, *Water Resour. Res.*, 25(6), 1283-1290.

Dagan, G. [1978] A note on packer, slug and recovery tests in unconfined aquifers, *Water Resour. Res.*, 14(5), 929-934.

Dagan, G. [1979] Models of groundwater flow in statistically homogeneous porous formations, *Water Resour. Res.*, 15(1), 47-63.

Dagan, G. [1982] Stochastic modeling of groundwater flow by unconditional and conditional probabilities, 2. The solute transport, *Water Resour. Res.*, 18(4), 835-848.

Dagan, G. [1984] Solute transport in heterogeneous porous formations, *J. Fluid Mech.*, 145, 151-177.

Dagan, G. [1986] Statistical theory of groundwater flow and transport: Pore to laboratory, laboratory to formation, and formation to regional scale, *Water Resour. Res.*, 22(9), 120S-134S.

Dagan, G. [1987] Theory of solute transport by groundwater, *Annual Reviews of Fluid Mechanics*, 19, 183-215.

Dagan, G. [1988] Time dependent macrodispersion for solute transport in anisotropic heterogeneous aquifers, *Water Resour. Res.*, 24(9), 1491-1500.

Dagan, G. [1989] *Flow and Transport in Porous Formations*, Springer-Verlag, Berlin.

Dagan, G. [1990] Transport in heterogeneous porous formations: Spatial moments, ergodicity, and effective dispersion, *Water Resour. Res.*, 26(6), 1281-1290.

Davis, A.D. [1986] Deterministic modeling of dispersion in heterogeneous permeable media, *Ground Water*, 24(5), 609-615.

Delhomme, J.P. [1978] Kriging in the hydrosciences, *Adv. Water Resour.*, 1(5), 251-266.

Delhomme, J.P. [1979] Spatial variability and uncertainty in groundwater flow parameters: a geostatistical approach, *Water Resour. Res.*, 15(2), 269-280.

Desbarats, A.J. [1990] Macrodispersion in sand-shale sequences, *Water Resour. Res.*, 26(1), 153-163.

Desbarats, A.J. [1991a] Numerical tracer test in a simulated heterogeneous aquifer, In: Moltyaner, G.L. *et al.* (eds.) *Proc. Conf. Transport and Mass Exchange Processes in Sand and Gravel Aquifers: Field and Modeling Studies*, Ottawa, Ontario. (In press.)

Desbarats, A.J. [1991b] Spatial averaging of transmissivity, In: Bachu, S. (ed.) *Proc. 5th Canadian/American Conf. on Hydrogeology*, National Well Water Ass., Dublin, Ohio. (In press.)

Desbarats, A.J. & R.M.Srivastava [1991] Geostatistical analysis of groundwater flow parameters in a simulated aquifer, *Water Resour. Res.*, 27(5), 687-698.

Doe, T.W. & J.Remer [1982] Analysis of constant-head well tests in nonporous fractured rock, In: Doe, T.W. & W.J.Schwartz (eds.) *roc. 3rd Int. Well-testing Symp.*, LBL-12076, *Earth Sciences Division*, Berkeley.

Doe, T.W. & J.E.Geier [1990] Interpretation of fracture system geometry using well test data, *OECD/NEA Internal report of the Stripa Project, 91-03*, SKB, Stockholm.

Duff, I.S. [1981] MA32 - A package for solving sparse unsymmetric systems using the frontal method, *UKAEA Report AERE - R10079*, Oxfordshire.

Duguid, J.O. & P.C.Y.Lee [1977] Flow in fractured porous media, *Water Resour. Res.*, 13(3), 558-566.

Dullien, F.A.L. [1979] *Porous Media: Fluid Transport and Pore Structure*, Academic Press, New York.

Durlofsky, L.J. [1991] Numerical calculation of equivalent grid block permeability tensors for heterogeneous porous media, *Water Resour. Res.*, 27(5), 699-708.

Engelder, T. & C.H.Scholz [1981] Fluid flow along very smooth joints at effective pressures up to 200 Megapascals, In: Carter, N.L. *et al.* (eds.) *Mechanical Behaviour of Crustal Rocks, AGU Geophysical Monograph 24*, 147-152, Washington D.C.

Follin, S. [1989] Statistical analysis of representative sample sizes in heterogeneous formations, *SKB AR 89-35*, Stockholm.

Follin, S. [1990] Effective hydraulic conductivity for fractured media, In: Kovar, K. (ed.) *Proc. IAHS Conf. ModelCARE90 on Calibration and Reliability in Groundwater Modelling*, 251-260, IAHS Publication 195, IAHS Press, Oxfordshire.

Freeze, R.A. [1975] A stochastic-conceptual analysis of one-dimensional ground water flow in nonuniform homogeneous media, *Water Resour. Res.*, 11(5), 725-741.

Freeze, R.A., J.Massmann, L.Smith, T.Sperling & B.James [1990] Hydrogeological decision analysis: 1. A framework, *Ground Water*, 28(5), 738-766.

Frind, E.O. & G.B.Matanga [1985] The dual formulation of flow for contaminant transport modeling, 1. Review of theory and accuracy aspects, *Water Resour. Res.*, 21(2), 159-169.

Frind, E.O., E.A.Sudicky & S.L.Schellenberg [1987] Micro-scale modelling in the study of plume evolution in heterogeneous media, *Stochastic Hydrology and Hydraulics*, 1, 241-262.

Geier, J.E. & C.L.Axelsson [1991] Discrete fracture modelling of the Finnsjön rock mass, Phase 1: Feasibility study, *SKB Technical Report 91-13*, Stockholm.

Gelhar, L.W., A.L.Gutjahr & R.L.Naff [1979] Stochastic analysis of macrodispersion in a stratified aquifer, *Water Resour. Res.*, 15(6), 1387-1397.

Gelhar, L.W. & C.L.Axness [1983] Three-dimensional stochastic analysis of macrodispersion in aquifers, *Water Resour. Res.*, 19(1), 161-180.

Gelhar, L.W. [1986] Stochastic subsurface hydrology from theory to application, *Water Resour. Res.*, 22(9), 135S-145S.

Gómez-Hernández, J.J. & S.M.Gorelick [1988] Influence of spatial variability of aquifer and recharge properties in determining effective parameter values, In: Peck, A. *et al.* (eds.) *Consequences of Spatial Variability in Aquifer Properties and Data Limitations for Groundwater Modelling Practice, IAHS Publication 175*, 217-272, IAHS Press, Oxfordshire.

Gómez-Hernández, J.J. [1991] Generation of hydraulic conductivity fields with significant connectivity of extreme values, In: *Proc. OECD/NEA Workshop on Heterogeneity of Groundwater Flow and Site Evaluation*, 59-65, Paris.

Goode, D.J. [1990] Particle velocity interpolation in block-centered finite difference groundwater flow models, *Water Resour. Res.*, 26(5), 925-940.

Goode, D.J. & A.M.Shapiro [1991a] Comment on "Flow and tracer transport in a single fracture: A stochastic model and its relation to some field observations" by L. Moreno *et al.*, *Water Resour. Res.*, 27(1), 129-131.

Goode, D.J. & A.M.Shapiro [1991b] Comment on "Macrodispersion in sand-shale sequences" by A.J. Desbarats, *Water Resour. Res.*, 27(1), 135-139.

Graham, W. & D.McLaughlin [1989] Stochastic analysis of non-stationary subsurface solute transport, 1. Unconditional moments, *Water Resour. Res.*, 25(2), 215-232.

Gutjahr, A.L., L.W.Gelhar, A.A.Bakr & J.R.McMillan [1978] Stochastic analysis of spatial variability in subsurface flow, 2. Evaluation and application, *Water Resour. Res.*, 14(5), 953-959.

Heijde, P. van der, Y.Bachmat, J.Bredehoeft, B.Andrews, D.Holz & S.Sebastian [1985] *Groundwater Management: the use of numerical models*, *AGU Water Resour. Monograph 5*, Washington D.C.

Herbert, A. & B.Splawski [1990] Prediction of inflow into the D-holes at the Stripa Mine, *OECD/NEA Internal report of the Stripa Project, 90-14*, SKB, Stockholm.

Holmes, D.C. [1989] Site characterization and validation - Single borehole hydraulic testing, Stage 1. *OECD/NEA Internal report of the Stripa Project, 89-04*, SKB, Stockholm.

Hsieh, P.A. & S.P.Neuman [1985] Field determination of the three-dimensional hydraulic conductivity tensor of anisotropic media, 1. Theory, *Water Resour. Res.*, 21(11), 1655-1665.

Hsieh, P.A., S.P.Neuman, G.K.Stiles & E.S.Simpson [1985] Field determination of the three-dimensional hydraulic conductivity tensor of anisotropic media, 2. Methodology and application to fractured rocks, *Water Resour. Res.*, 21(11), 1667-1676.

Hubbert, M.K. [1956] Darcy law and the field equations of flow of the underground fluids, *Trans. Am. Inst. Min. Metall. Pet. Eng.*, 207, 222-239.

Istok, J.D. [1989] *Groundwater Modeling by the Finite Element Method*, *AGU Water Resour. Monograph 13*, Washington D.C.

Istok, J.D. & A.L.Flint [1991] Geostatistical methods for site characterization at Yucca Mountain, In: *Proc. OECD/NEA Workshop on Heterogeneity of Groundwater Flow and Site Evaluation*, 47-58, Paris.

Jacob, C.E. & S.Lohman [1952] Nonsteady flow to a well of constant drawdown in an extensive aquifer, *Trans. Am. Geophys. Union*, 33(4), 559-569.

Javandel, I., C.Doughty & C.F.Tsang [1984] *Groundwater Transport: Handbook of Mathematical Models*, *AGU Water Resour. Monograph 10*, Washington D.C.

Journel, A.G. & C.Huijbregts [1978] *Mining Geostatistics*, Academic Press, San Diego.

Journel, A.G., C.Deutsch & A.J.Desbarats [1986] Power averaging for block permeability, *Soc. Petr. Eng.*, *SPE 15128*, 329-333.

KBS-3 [1983] Final storage of spent nuclear fuel, KBS-3, Parts 1-4, *SKBF/KBS*, Stockholm.

Kinzelbach, W. [1987a] *Groundwater Modelling - An Introduction with Sample Programs in BASIC, Developments in Water Science 25*, Elsevier, Amsterdam.

Kinzelbach, W. [1987b] The random-walk method in pollutant transport simulation, In: Custodio, E. *et al.* (eds.) *Groundwater Flow and Quality Modelling, NATO ASI Series, Series C: No.224,* 227-246.

Kreft, A. & A.Zuber [1978] On the physical meaning of the dispersion equation and its solution for different initial and boundary conditions, *Chem. Eng. Sci.,* 33, 1471-1480.

Liedholm, M. [1991a] Technical note no. 8, In: Liedholm, M. (ed.) *Conceptual Modeling of Aspö Technical Notes 1-17, SKB Progress Report 25-90-16a,* Stockholm.

Liedholm, M. [1991b] Technical note no. 9, In: Liedholm, M. (ed.) *Conceptual Modeling of Aspö Technical Notes 1-17, SKB Progress Report 25-90-16a,* Stockholm.

Liedholm, M. [1991c] Technical note no. 19, In: Liedholm, M. (ed.) *Conceptual Modeling of Aspö Technical Notes 19-32, SKB Progress Report 25-90-16b,* Stockholm.

Loague, K. & R.E.Green [1990] Criteria for evaluating pesticide leaching models, In: Roth, K. *et al.* (eds.) *Field-Scale Water and Solute Flux in Soils,* 175-208, Birkhäuser Verlag, Basel.

Long, J.C.S., J.S.Remer, C.R.Wilson & P.A.Witherspoon [1982] Porous media equivalents for networks of discontinuous fractures, *Water Resour. Res.,* 18(3), 645-658.

Mangold, D.C. & C.F.Tsang [1991] A summary of subsurface hydrological and hydrochemical models, *Reviews of Geophysics,* 29(1), 51-79.

Mantoglou, A. & J.L.Wilson [1982] The Turning Bands method for simulation of random fields using line generation by a spectral method, *Water Resour. Res.,* 18(5), 1379-1394.

Marsily, G. de [1985] Flow and transport in fractured rocks: Connectivity and scale effect, In: *Hydrogeology of Rocks of Low Permeability, Committee of U.S.A.Members of JAM,* 17, 267-277.

Marsily, G. de [1986] *Quantitative Hydrogeology,* Academic Press, Orlando.

Matheron, G. [1967] *Eléments Pour une Théorie des Milieux Poreux,* Masson, Paris.

Matheron, G. & G.de Marsily [1980] Is transport in porous media always diffusive? A counterexample, *Water Resour. Res.*, 16(5), 901-917.

Moreno, L., Y.W.Tsang, C.F.Tsang, F.V.Hale & I.Neretniks [1988] Flow and tracer transport in a single fracture: A stochastic model and its relation to some field observations, *Water Resour. Res.*, 24(12), 2033-2048.

Moye, D.G. [1967] Diamond drilling for foundation exploration, *Civ. Eng. Trans. 7th, Inst. Eng. Australia*, 95-100.

Naff, R.L [1990] On the nature of the dispersive flux in saturated heterogeneous porous media, *Water Resour. Res.*, 26(5), 1013-1026.

Nelson, R.A. [1987] Fractured reservoirs: Turning knowledge into practice, *SPE 16470, J. Petr. Tech.*, 407-414.

Neuman, S.P [1982] Statistical characterization of aquifer hetero-geneities: An overview, In: Narasimhan, T.N. (ed.) *Recent Trends in Hydrogeology, Geol. Soc. Am. Spec. Pap. 189*, 81-102.

Neuman, S.P. [1987] Stochastic continuum representation of fractured rock permeability as an alternative to the REV and fracture network concepts, In: Farmer, I.W. *et al.* (eds.) *Proc. 28th U.S. Symp. Rock. Mech.*, 533-561, Balkema, Rotterdam.

Neuman, S.P., C.L.Winter & C.M.Newman [1987] Stochastic theory of field-scale Fickian dispersion in anisotropic porous media, *Water Resour. Res.*, 23(3), 453-466.

Neuman, S.P. [1988] A proposed conceptual framework and methodology for investigating flow and transport in Swedish crystalline rocks, *SKB AR 88-37*, Stockholm.

Neuman, S.P. & Y.K.Zhang [1990] A quasi-linear theory of non-Fickian and Fickian subsurface dispersion, 1. Theoretical analysis with application to isotropic media, *Water Resour. Res.*, 26(5), 887-902.

Neuman, S.P. [1990] Universal scaling of hydraulic conductivities and dispersivities in geologic media, *Water Resour. Res.*, 26(8), 1749-1758.

Nilsson, L. [1989] Hydraulic tests at Äspö and Laxemar, Evaluation, *SKB Progress Report 25-88-14*, Stockholm.

Nilsson, L. [1990] Hydraulic tests at Äspö, KAS05-KAS08, HAS13-HAS17, Evaluation, *SKB Progress Report 25-89-20*, Stockholm.

Parker, J.C. & M.T.van Genuchten [1984] Flux-averaged and volume averaged concentrations in continuum approaches to solute transport, *Water Resour. Res.*, 20(7), 866-872.

Peck, A., S.Gorelick, G.de Marsily, S.Foster & V.Kovalevsky [1988] *Consequences of Spatial Variability in Aquifer Properties and Data Limitations for Groundwater Modelling Practice, IAHS Publication 175*, IAHS Press, Oxfordshire.

Pickens, J.F. & G.E.Grisak [1981] Scale-dependent dispersion in a stratified granular aquifer, *Water Resour. Res.*, 17(4), 1191-1211.

Pickens, J.F., G.E.Grisak, J.D.Avis, D.W.Belanger & M.Thury [1987] Analysis and interpretation of borehole hydraulic tests in deep boreholes: Principles, model development, and applications, *Water Resour. Res.*, 23(7), 1341-1375.

Price, N.J. [1975] *Fault and Joint Development in Brittle and Semi-Brittle Rock*, Pergamon Press, New York.

Robinson, P.C. [1984] Connectivity, flow and transport in network models of fractured media, Ph.D. thesis, Oxford University, *TP.1072, Theoretical Physics Div., AERE Harwell*, Oxfordshire.

Rubin, Y. [1990] Stochastic modeling of macrodispersion in heterogeneous porus media, *Water Resour. Res.*, 26(1), 133-141.

Rubin, Y. & J.J.Gómez-Hernández [1990] A stochastic approach to the problem of upscaling of conductivity in disordered media: Theory and unconditional numerical simulations, *Water Resour. Res.*, 26(4), 691-701.

Sagar, B. [1978] Galerkin finite element procedure for analyzing flow through random media, *Water Resour. Res.*, 14(6), 1035-1044.

Sagar, B. & A.Runchal [1982] Permeability in fractured rock: Effect of fracture size and data uncertainties, *Water Resour. Res.*, 18(2), 266-274.

Sauveplane, C. [1984] Pumping test analysis in fractured aquifer formations: State of the art and some perspectives, In: Rosenhein, J. & G.D.Bennett (eds.) *Groundwater Hydraulics, AGU Water Resour. Monograph 9*, 171-206, Washington D.C.

Scheidegger, A.E. [1961] General theory of dispersion in porous media, *J. Geophys. Res.*, 66, 3273-3278.

Schrage, L. [1969] A more portable FORTRAN random number generator, *ACM Trans. on Mathematical Software*, 5(2), 132-138.

Schwartz, F.W. [1977] Macroscopic dispersion in porous media: The controlling factors, *Water Resour. Res.*, 13(4), 743-752.

Shapiro, A.M. [1987] Transport equations for fractured porous media, In: Bear, J. & M.Y.Corapcioglu (eds.) *Advances in Transport Phenomena, NATO ASI Series, Series E: No.128*, 405-471.

Shapiro, A.M. & V.Cvetkovic [1988] Stochastic analysis of solute arrival time in heterogeneous porous media, *Water Resour. Res.*, 24(10), 1711-1718.

Silliman, S.E. & A.L.Wright [1988] Stochastic analysis of paths of high hydraulic conductivity in porous media, *Water Resour. Res.*, 24(11), 1901-1910.

Smith, L. & R.A.Freeze [1979] Stochastic analysis of steady state groundwater flow in bounded domain, 2. Two-dimensional simulations, *Water Resour. Res.*, 15(6), 1543-1559.

Smith, L. & F.W.Schwartz [1980] Mass transport, 1. A stochastic analysis of macroscopic dispersion, *Water Resour. Res.*, 16(2), 303-313.

Smith, L. & F.W.Schwartz [1981] Mass transport, 2. Analysis of uncertainty in prediction, *Water Resour. Res.*, 17(2), 351-369.

Stokes, J. [1980] On the description of the properties of fractured rock using the concept of a porous medium, *SKBF/KBS Teknisk Rapport 80-05*, Stockholm.

Taylor, G.I. [1921] Diffusion by continuous movements, *Proc. Lond. Math. Soc.*, 20(2), 196-212.

Tsang, Y.W. & C.F.Tsang [1989] Flow channeling in a single fracture as a two-dimensional strongly heterogeneous permeable medium, *Water Resour, Res.*, 25(9), 1076-2080.

Vanmarke, E. [1983] *Random Fields: Analysis and Synthesis*, MIT Press, Cambridge, Massachusetts.

Warren, J.E. & H.S.Price [1961] Flow in heterogeneous porous media, *Soc. Pet. Eng. J.*, 1, 153-169.

Warren, J.E. & P.J.Root [1963] The behaviour of naturally fractured reservoirs, *Soc. Petr. Eng. J.*, 9, 245-255.

Warren, J.E. & F.F.Skiba [1964] Macroscopic dispersion, *Trans. Am. Inst. Min. Metall. Pet. Eng.*, 231, 215-230.

Warrick, A.W., R.Zhang, M.M.Moody & D.E.Myers [1990] Kriging versus alternative interpolators: Errors and sensitivity to model inputs, In: Roth, K. *et al.* (eds.) *Field-Scale Water and Solute Flux in Soils*, 157-164, Birkhäuser Verlag, Basel.

White, C.D. & R.N.Horne [1987] Computing absolute transmissibility in the presence of fine-scale heterogeneity, *SPE 16011*, *Presented at the 9th SPE Symp. on Reservoir Simulation*, San Antonio, Texas.

Winberg, A., C.S.Kung, X.W.Huan & V.Cvetkovic [1990] SKB91 Stochastic continuum modelling of mass arrival at Finnsjön: Parametric and nonparametric approaches, *SKB AR 90-40*, Stockholm.

Witherspoon, P.A., J.S.Y.Wang, K.Iwai & J.E.Gale [1980] Validity of cubic law for fluid flow in a deformable rock fracture, *Water Resour. Res.*, 16(6), 1016-1024.

Witherspoon, P.A. [1986] Flow of groundwater in fractured rocks, *Bull. Int. Ass. Eng. Geol.*, *34*, 103-115, Paris.

A P P E N D I X

Figures A1-A10 demonstrate uniform average flow in a *statistically anisotropic* stochastic continuum. The following values of λ_Y and σ_Y are studied: $\lambda_Y/\Delta x = 4$, $\lambda_Y/\Delta y = 1$, and $\sigma_Y = \{0.25, 1, 4\}$ ($\sigma_Y = 4$ is denoted 4-41). The size of the flow domain is $N = 64\times64$. The information given in Figures A1-A10 is discussed in detail in Chapter 3.

2-D HYDRAULIC CONDUCTIVITY FIELD
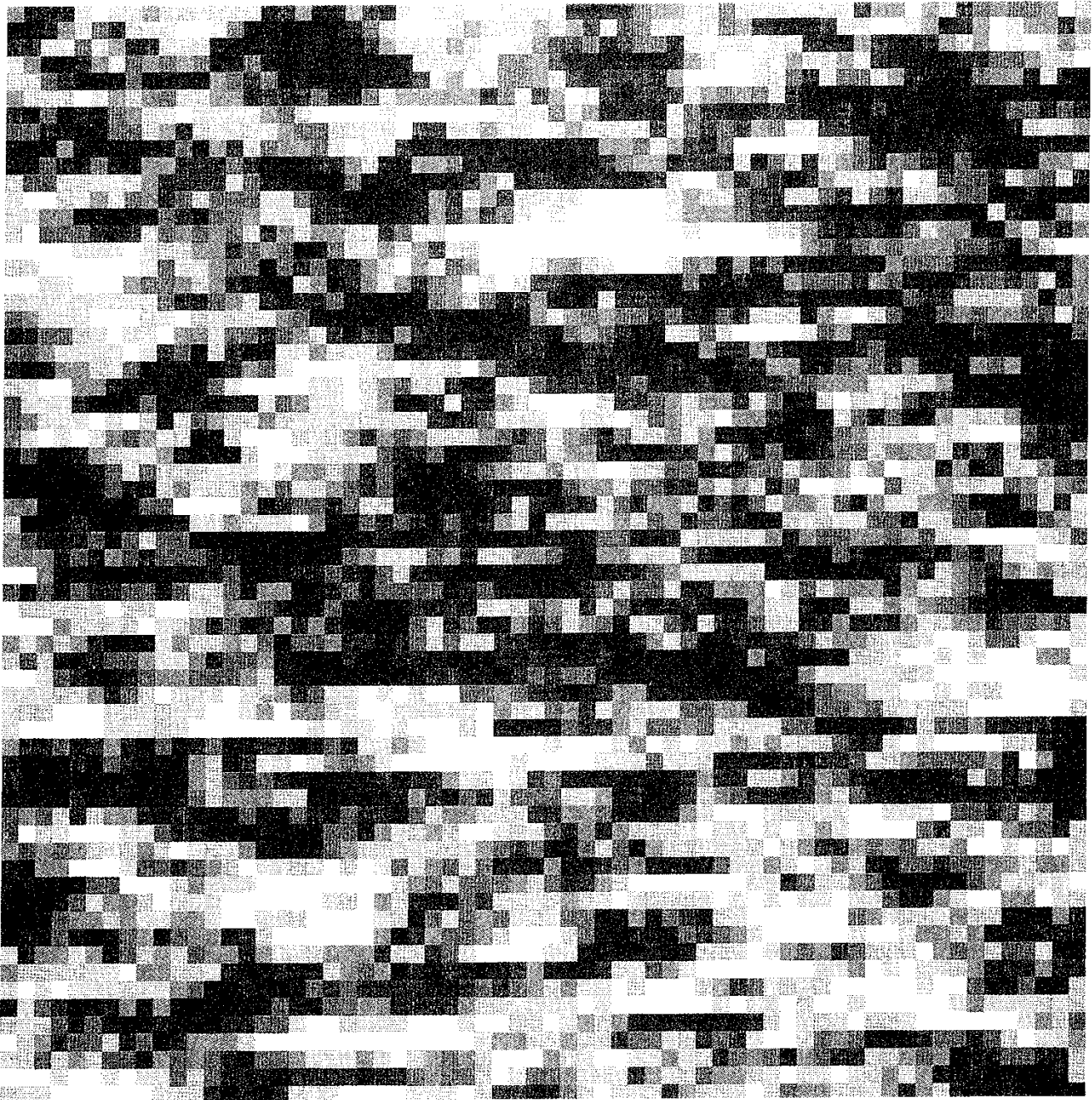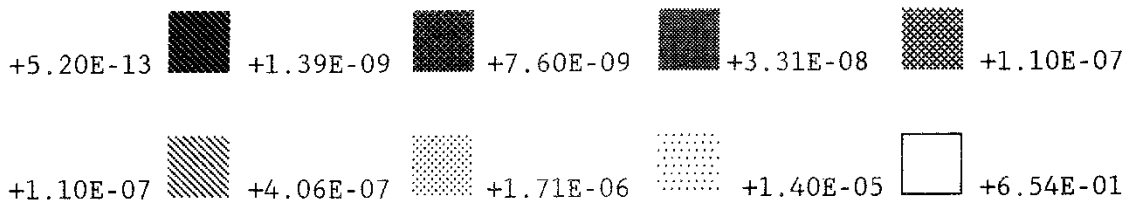
No. of blocks: 64 × 64

$\sigma_{\ln(K)} = 4.00 \qquad \lambda/\Delta x = 4.0 \qquad \lambda/\Delta y = 1.0$

RASTER LEGEND (dim[K]=m/s)

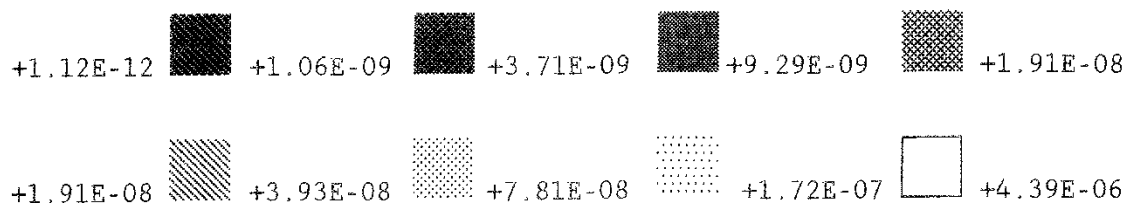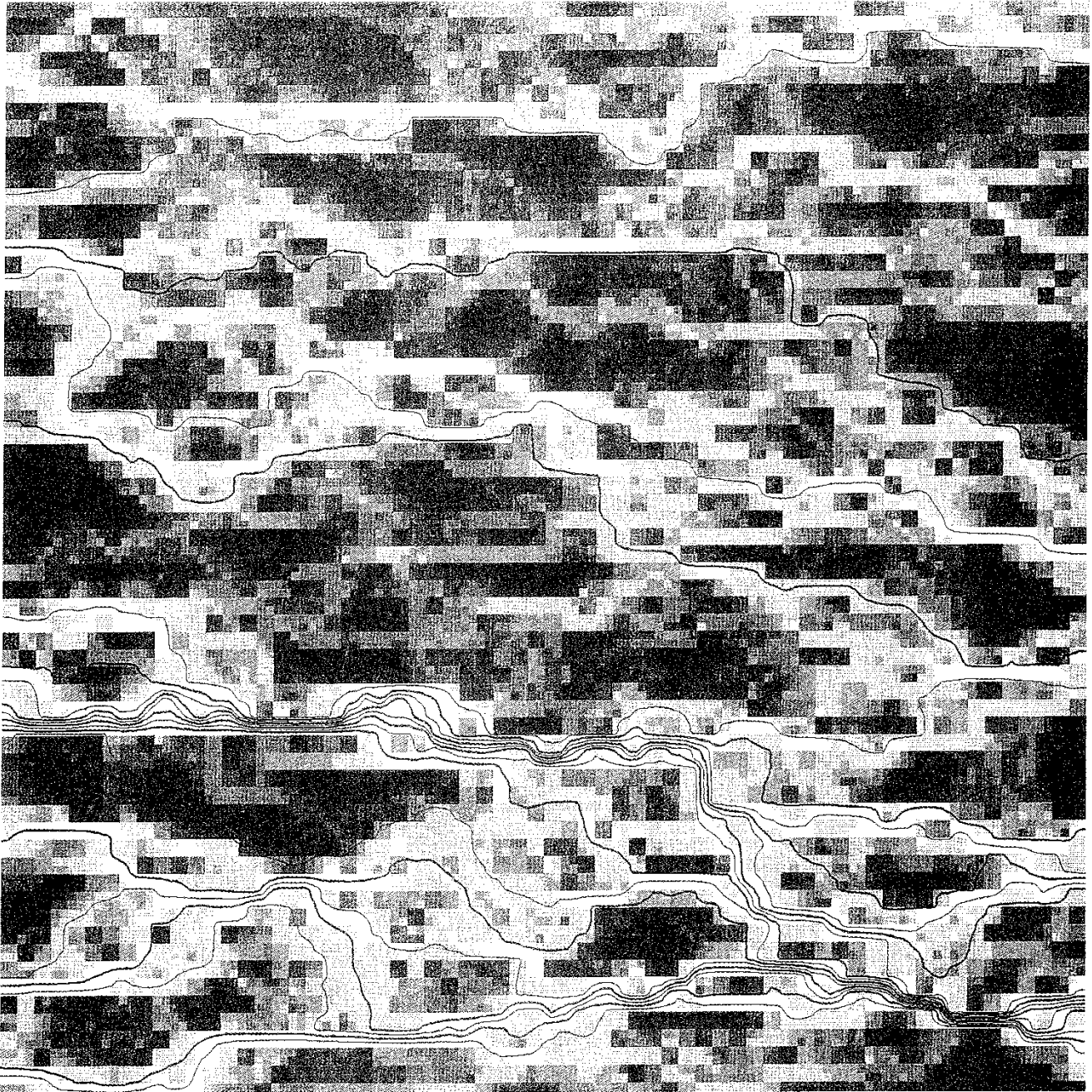|				
+5.20E-13	+1.39E-09	+7.60E-09	+3.31E-08	+1.10E-07
+1.10E-07	+4.06E-07	+1.71E-06	+1.40E-05	+6.54E-01

Fig. A1 Case 4-41: $\sigma_Y = 4$ and $\lambda/\Delta x = 4$ $\lambda/\Delta y = 1$.

2-D SPECIFIC DISCHARGE FIELD

No. of blocks: 64 × 64

$\sigma_{\ln(K)} = 4.00 \quad \lambda/\Delta x = 4.0 \quad \lambda/\Delta y = 1.0$
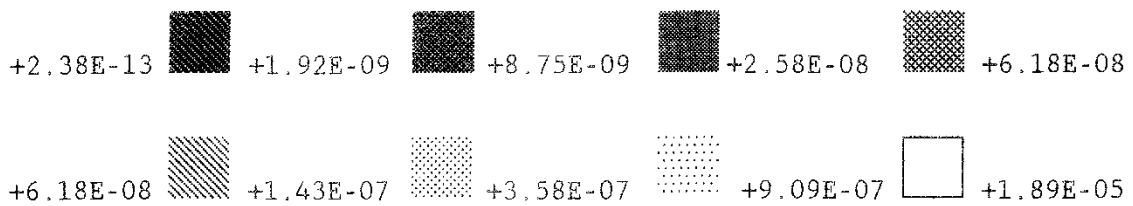
RASTER LEGEND (dim[q]=m/s)

+1.12E-12 +1.06E-09 +3.71E-09 +9.29E-09 +1.91E-08

+1.91E-08 +3.93E-08 +7.81E-08 +1.72E-07 +4.39E-06

Fig. A2 N/S-flow: $\sigma_\gamma = 4$ and $\lambda/\Delta x = 4$ $\lambda/\Delta y = 1$.

2-D SPECIFIC DISCHARGE FIELD

No. of blocks: 64 x 64

$\sigma_{\ln(K)} = 4.00 \qquad \lambda/\Delta x = 4.0 \qquad \lambda/\Delta y = 1.0$

RASTER LEGEND (dim[q]=m/s)

+2.38E-13	▨	+1.92E-09	▨	+8.75E-09	▨	+2.58E-08	▨	+6.18E-08
+6.18E-08	▨	+1.43E-07	▨	+3.58E-07	▨	+9.09E-07	☐	+1.89E-05
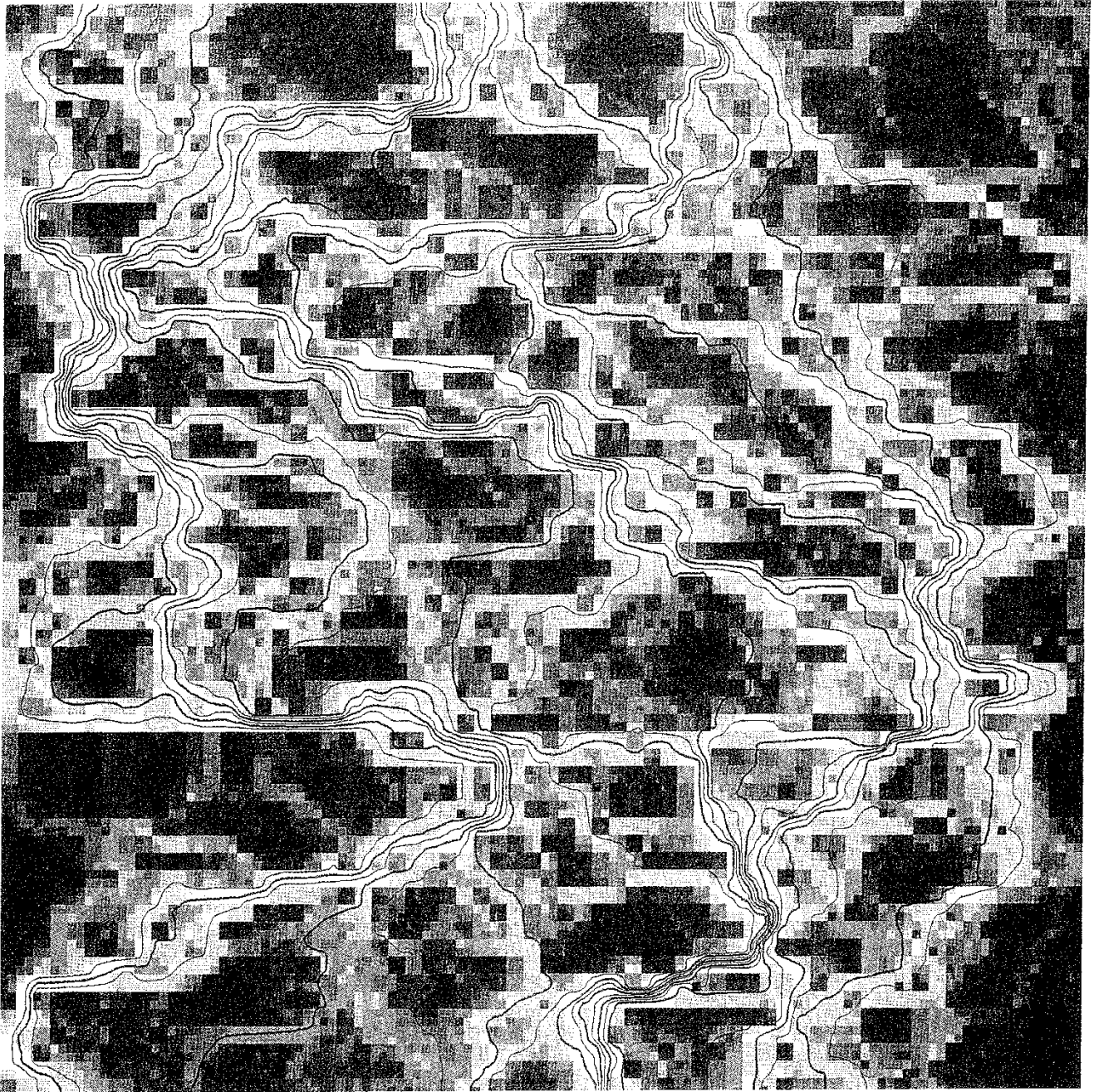
Fig. A3 W/E-flow: $\sigma_Y = 4$ and $\lambda/\Delta x = 4 \quad \lambda/\Delta y = 1$.

Fig. A4 Flow nets for N/S and W/E flow respectively. N = (64 x 64),

$\lambda/\Delta x = 4$, $\lambda/\Delta y = 1$ and $\sigma_{\ln(K)} = 0.25$. Piezometric head (dashed) and

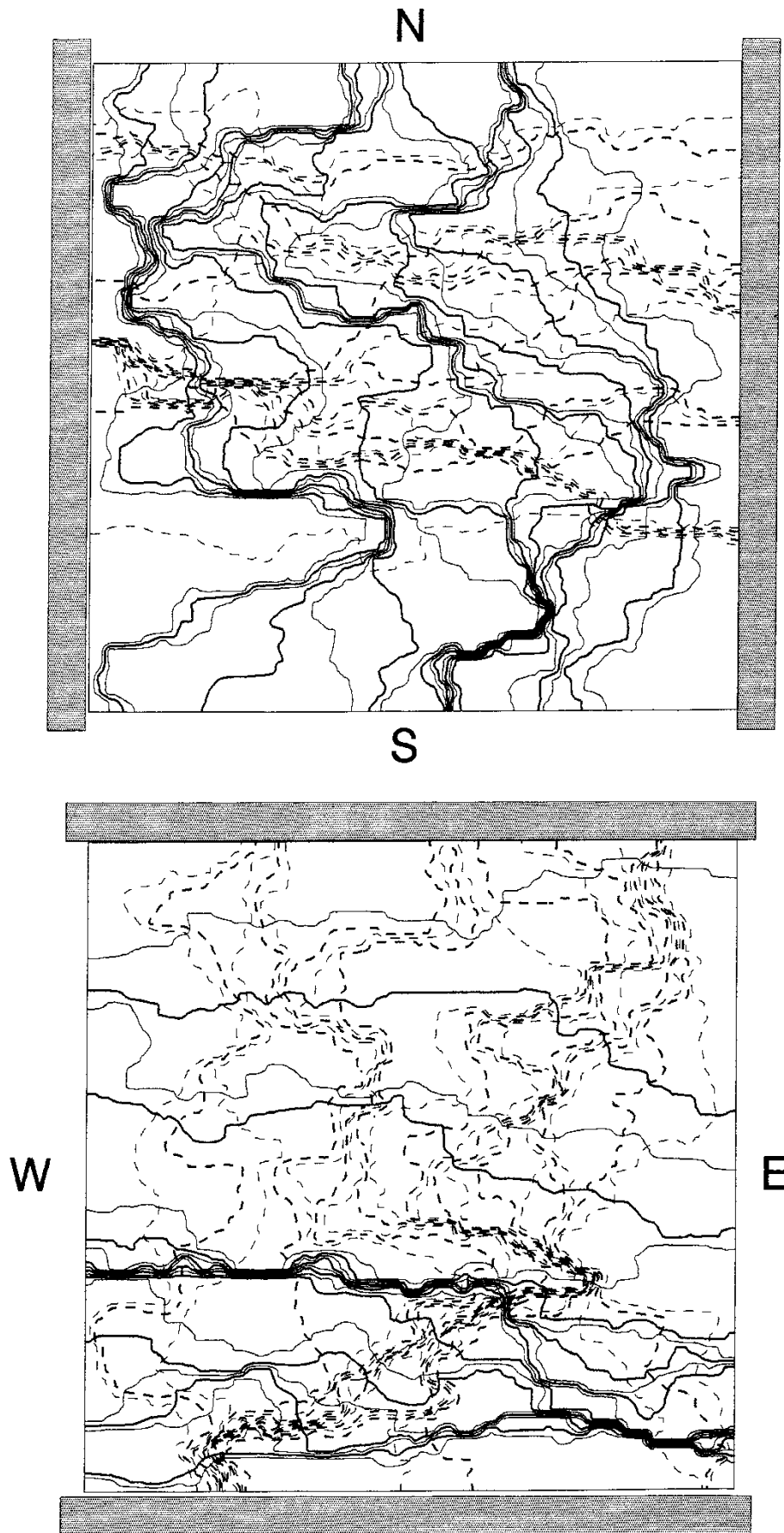stream function levels (solid) are in 5% increments between 0 and 1.
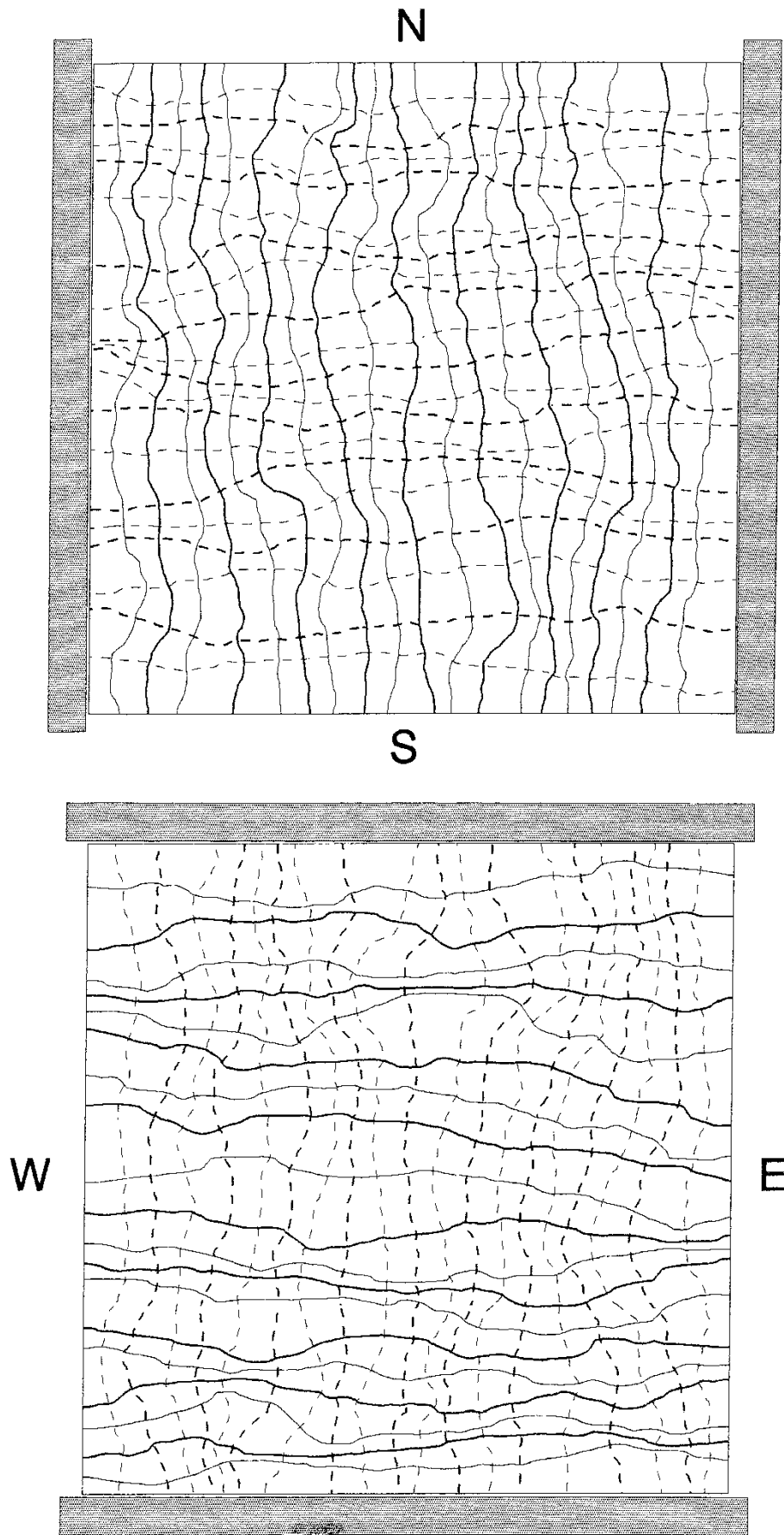
Fig. A5 Flow nets for N/S and W/E flow respectively. N = (64 x 64),

$\lambda/\Delta x = 4$, $\lambda/\Delta y = 1$ and $\sigma_{\ln(K)} = 1.00$. Piezometric head (dashed) and

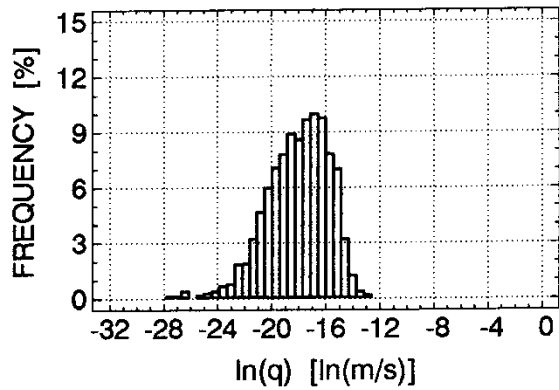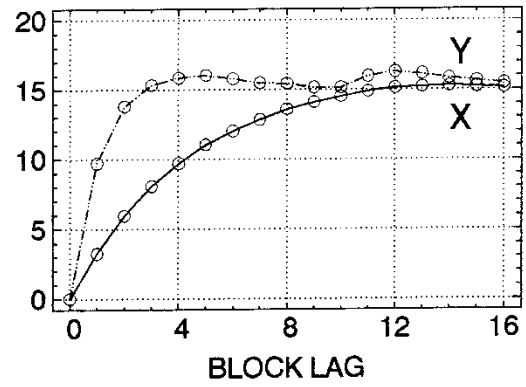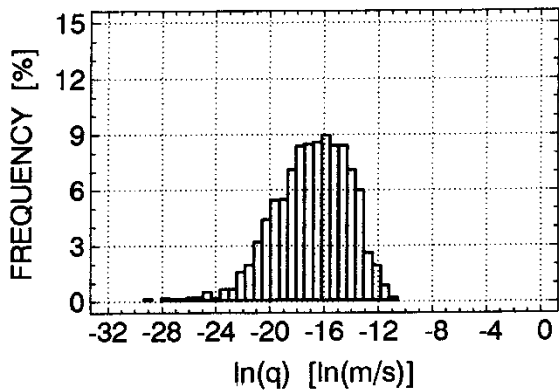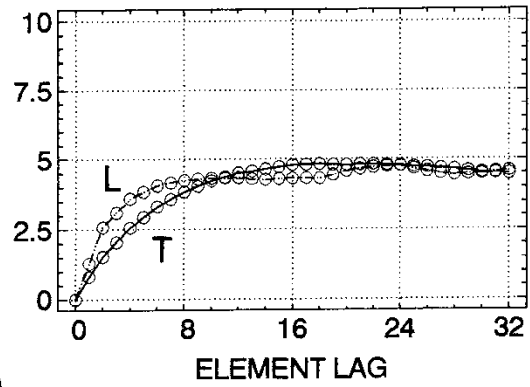stream function levels (solid) are in 5% increments between 0 and 1.

Fig. A6 Flow nets for N/S and W/E flow respectively. $N = (64 \times 64)$,

$\lambda/\Delta x = 4$, $\lambda/\Delta y = 1$ and $\sigma_{\ln(K)} = 4.00$. Piezometric head (dashed) and

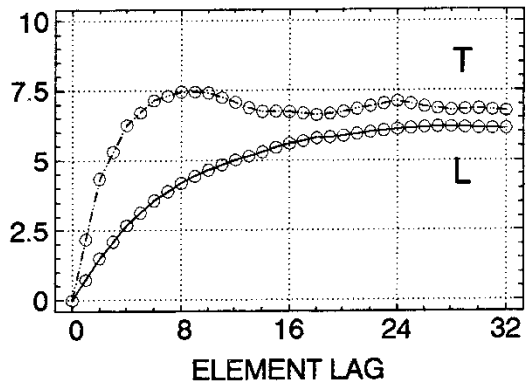stream function levels (solid) are in 5% increments between 0 and 1.
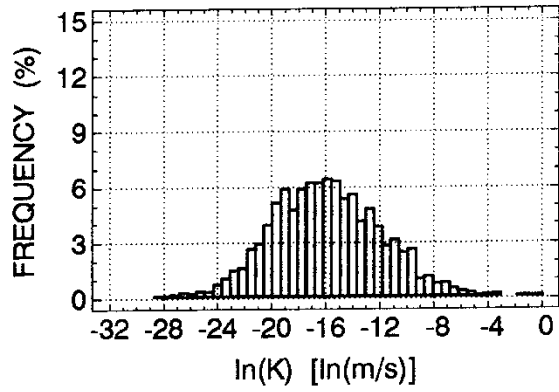
T = transverse   L = longitudinal

(a) ln(K)   (b) ln(q) N/S flow   (c) ln(q) W/E flow

Fig. A7 Histograms and variograms of ln(K) and ln(q) for case 4-41 .

$\lambda/\Delta x = 4$, $\lambda/\Delta y = 1$ and $\sigma_{\ln(K)} = 4.00$.
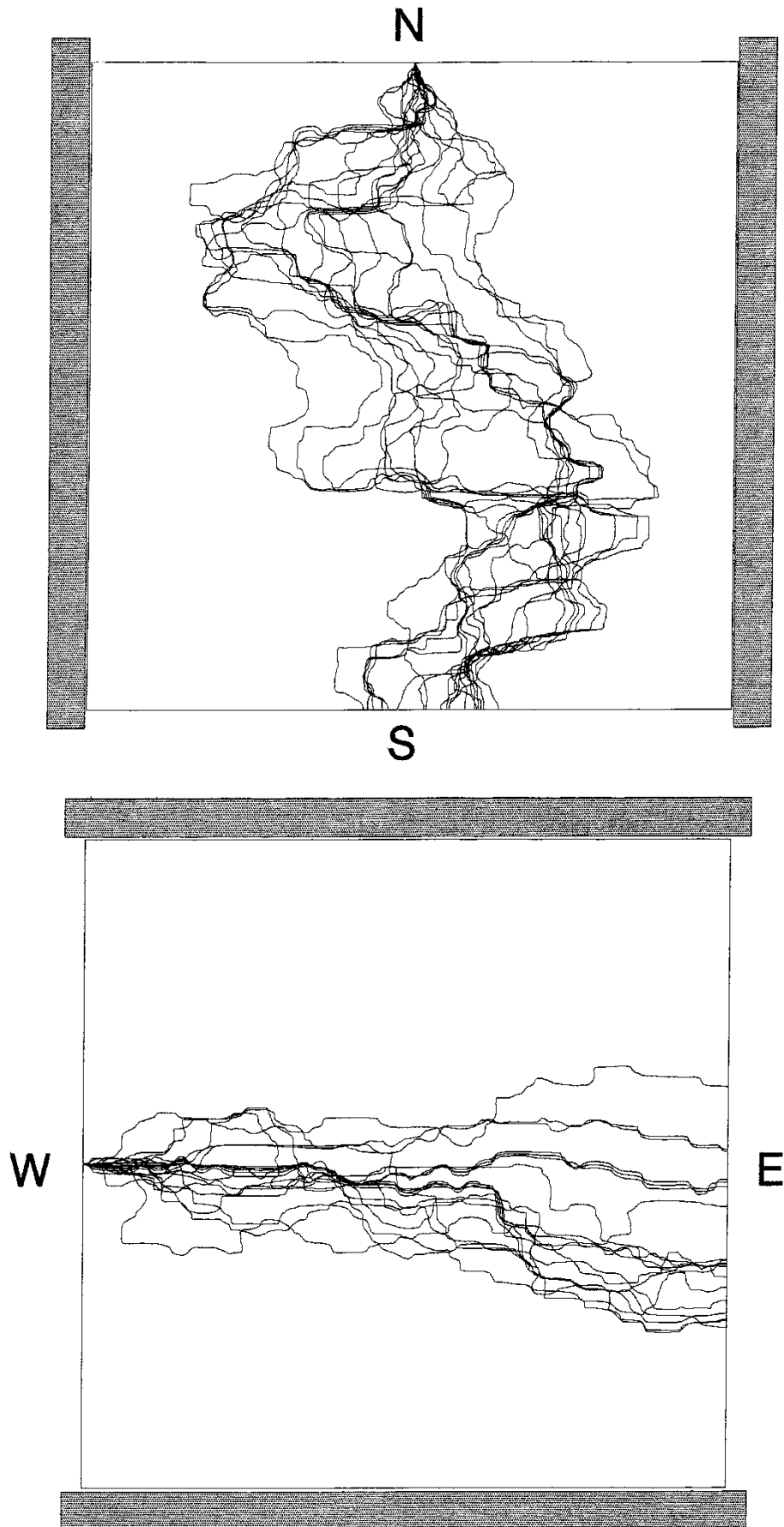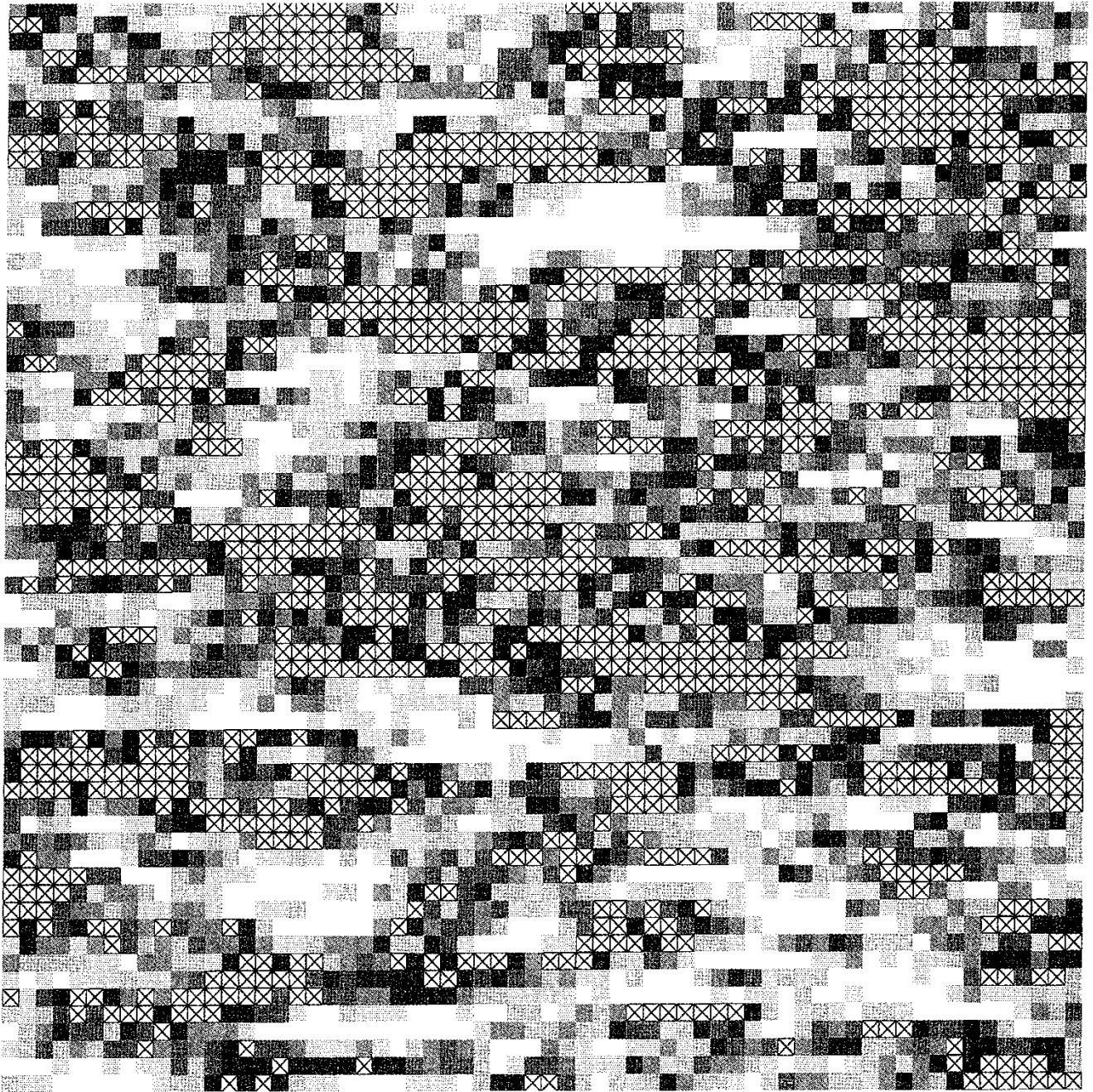
Fig. A8 Figurative plots of apparent transverse macrodispersion, that is,

lateral advective transport is estimated by lumping streamlines.

$N = (64 \times 64)$, $\lambda/\Delta x = 4$, $\lambda/\Delta y = 1$ and $\sigma_{\ln(K)} = 4.00$.

2-D HYDRAULIC CONDUCTIVITY FIELD

No. of blocks: 64 × 64

$\sigma_{\ln(K)} = 4.00 \qquad \lambda/\Delta x = 4.0 \qquad \lambda/\Delta y = 1.0$

RASTER LEGEND (dim[K]=m/s)

+5.20E-13 ▧ +1.39E-09 ▧ +7.60E-09 ▧ +3.31E-08 ▧ +1.10E-07

+1.10E-07 ▨ +4.05E-07 ▦ +1.71E-06 ▦ +1.40E-05 ▢ +6.54E-01
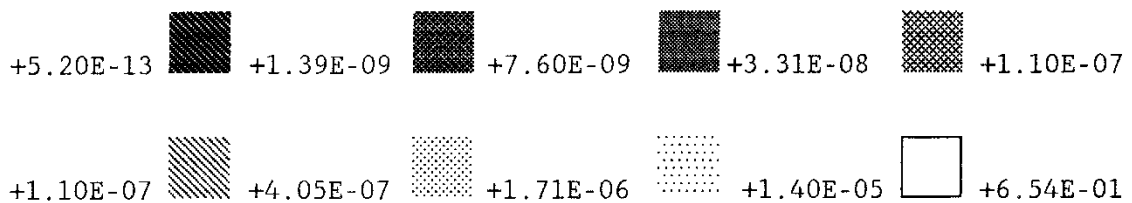
Fig. A9 Case 4-41 with +5.20E-13 ⊠ +7.60E-09 THRESHOLD a 25% conductivity threshold .
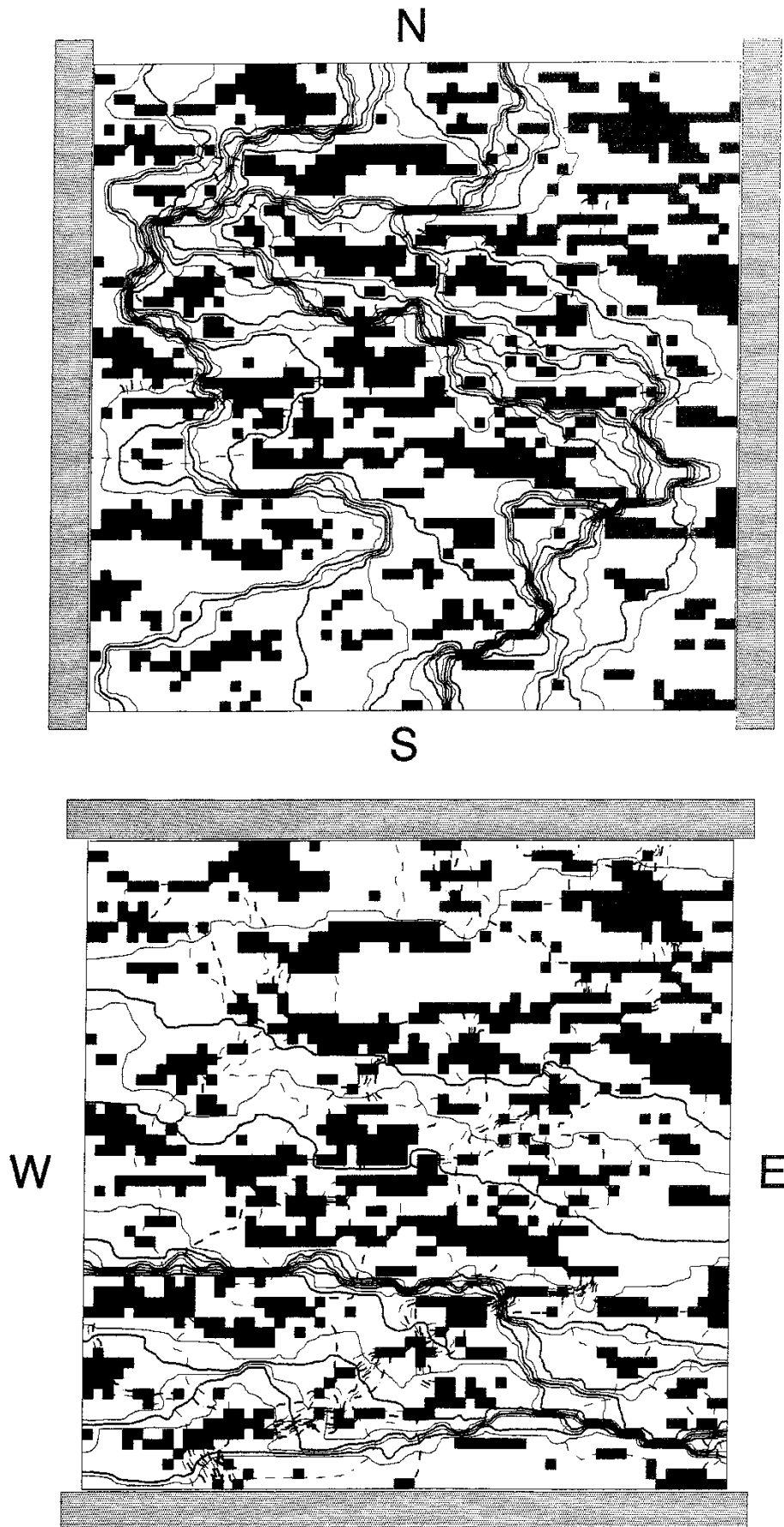
Fig. A10 Flow nets for a 25% conductivity threshold . N = (64 x 64) ,

$\lambda/\Delta x = 4$, $\lambda/\Delta y = 1$ and $\sigma_{\ln(K)} = 4.00$. Piezometric head (dashed) and

stream function levels (solid) are in 5% increments between 0 and 1.

List of SKB reports

Annual Reports

1977-78
TR 121
KBS Technical Reports 1 – 120
Summaries
Stockholm, May 1979

1979
TR 79-28
The KBS Annual Report 1979
KBS Technical Reports 79-01 – 79-27
Summaries
Stockholm, March 1980

1980
TR 80-26
The KBS Annual Report 1980
KBS Technical Reports 80-01 – 80-25
Summaries
Stockholm, March 1981

1981
TR 81-17
The KBS Annual Report 1981
KBS Technical Reports 81-01 – 81-16
Summaries
Stockholm, April 1982

1982
TR 82-28
The KBS Annual Report 1982
KBS Technical Reports 82-01 – 82-27
Summaries
Stockholm, July 1983

1983
TR 83-77
The KBS Annual Report 1983
KBS Technical Reports 83-01 – 83-76
Summaries
Stockholm, June 1984

1984
TR 85-01
Annual Research and Development Report 1984
Including Summaries of Technical Reports Issued during 1984. (Technical Reports 84-01 – 84-19)
Stockholm, June 1985

1985
TR 85-20
Annual Research and Development Report 1985
Including Summaries of Technical Reports Issued during 1985. (Technical Reports 85-01 – 85-19)
Stockholm, May 1986

1986
TR 86-31
SKB Annual Report 1986
Including Summaries of Technical Reports Issued during 1986
Stockholm, May 1987

1987
TR 87-33
SKB Annual Report 1987
Including Summaries of Technical Reports Issued during 1987
Stockholm, May 1988

1988
TR 88-32
SKB Annual Report 1988
Including Summaries of Technical Reports Issued during 1988
Stockholm, May 1989

1989
TR 89-40
SKB Annual Report 1989
Including Summaries of Technical Reports Issued during 1989
Stockholm, May 1990

1990
TR 90-46
SKB Annual Report 1990
Including Summaries of Technical Reports Issued during 1990
Stockholm, May 1991

1991
TR 91-64
SKB Annual Report 1991
Including Summaries of Technical Reports Issued during 1991
Stockholm, April 1992

Technical Reports
List of SKB Technical Reports 1992

TR 92-01
GEOTAB. Overview
Ebbe Eriksson[1], Bertil Johansson[2], Margareta Gerlach[3], Stefan Magnusson[2], Ann-Chatrin Nilsson[4], Stefan Sehlstedt[3], Tomas Stark[1]
[1]SGAB, [2]ERGODATA AB, [3]MRM Konsult AB
[4]KTH
January 1992

TR 92-02
Sternö study site. Scope of activities and main results
Kaj Ahlbom[1], Jan-Erik Andersson[2], Rune Nordqvist[2], Christer Ljunggren[3], Sven Tirén[2], Clifford Voss[4]
[1]Conterra AB, [2]Geosigma AB, [3]Renco AB, [4]U.S. Geological Survey
January 1992

TR 92-03
Numerical groundwater flow calculations at the Finnsjön study site – extended regional area
Björn Lindbom, Anders Boghammar
Kemakta Consultants Co, Stockholm
March 1992

TR 92-04
Low temperature creep of copper intended for nuclear waste containers
P J Henderson, J-O Österberg, B Ivarsson
Swedish Institute for Metals Research, Stockholm
March 1992

TR 92-05
Boyancy flow in fractured rock with a salt gradient in the groundwater – An initital study
Johan Claesson
Department of Building Physics, Lund University, Sweden
February 1992

TR 92-06
Characterization of nearfield rock – A basis for comparison of repository concepts
Roland Pusch, Harald Hökmark
Clay Technology AB and Lund University of Technology
December 1991

TR 92-07
Discrete fracture modelling of the Finnsjön rock mass: Phase 2
J E Geier, C-L Axelsson, L Hässler, A Benabderrahmane
Golden Geosystem AB, Uppsala, Sweden
April 1992

TR 92-08
Statistical inference and comparison of stochastic models for the hydraulic conductivity at the Finnsjön site
Sven Norman
Starprog AB
April 1992

TR 92-09
Description of the transport mechanisms and pathways in the far field of a KBS-3 type repository
Mark Elert[1], Ivars Neretnieks[2], Nils Kjellbert[3], Anders Ström[3]
[1]Kemakta Konsult AB
[2]Royal Institute of Technology
[3]Swedish Nuclear Fuel and Waste Management Co
April 1992

TR 92-10
Description of groundwater chemical data in the SKB database GEOTAB prior to 1990
'Sif Laurent[1], Stefan Magnusson[2], Ann-Chatrin Nilsson[3]
[1]IVL, Stockholm
[2]Ergodata AB, Göteborg
[3]Dept. of Inorg. Chemistry, KTH, Stockholm
April 1992

TR 92-11
Numerical groundwter flow calculations at the Finnsjön study site – the influence of the regional gradient
Björn Lindbom, Anders Boghammar
Kemakta Consultants Co., Stockholm, Sweden
April 1992

TR 92-12
HYDRASTAR – a code for stochastic simulation of groundwater flow
Sven Norman
Abraxas Konsult
May 1992

TR 92-13
Radionuclide solubilities to be used in SKB 91
Jordi Bruno[1], Patrik Sellin[2]
[1]MBT, Barcelona Spain
[2]SKB, Stockholm, Sweden
June 1992